

A SYNTHETIC BIOMATERIALS APPROACH TO THE PREVENTION OF
POSTSURGICAL ADHESIONS IN NEUROSURGERY

by

CHARLES A. FLOREK

A dissertation submitted to the

Graduate School-New Brunswick

Rutgers, the State University of New Jersey

and

The Graduate School of Biomedical Sciences

University of Medicine and Dentistry of New Jersey

In partial fulfillment of the requirements

For the degree of

Doctor of Philosophy

Graduate Program in Biomedical Engineering

Written under the direction of

Joachim Kohn, Ph.D.

And approved by

New Brunswick, New Jersey

October, 2010

© 2010

Charles A. Florek

ALL RIGHTS RESERVED

ABSTRACT OF THE DISSERTATION

A SYNTHETIC BIOMATERIALS APPROACH TO THE PREVENTION OF POSTSURGICAL ADHESIONS IN NEUROSURGERY

By CHARLES A. FLOREK

Dissertation Director:

Joachim Kohn, Ph.D.

In the treatment of spinal stenosis and disc herniation, the lamina and ligamentum flavum are resected to access the spinal canal. When a fibrous scar replaces the surgical defect, the dura or spinal nerves can become tethered to the surrounding tissues. Kuslich et al. and Smyth and Wright demonstrated that light mechanical stimulation of injured spinal nerves induced intraoperative or postoperative sciatic pain similar to the patients' preoperative state [1, 2]. Therefore, adhesive peridural fibrosis contributes to the recurrence of back pain following neurosurgery. In this dissertation, biomaterial membranes are evaluated for the prevention of scar progression to the dura and spinal nerves.

Cell-impermeable, biodegradable tyrosine-derived polycarbonate membranes were fabricated by electrospinning. A degradable surfactant, *trans*-4-hydroxy-L-proline butyl ester HCl, enabled electrospinning from a low toxicity solvent (acetic acid). Anti-adhesion membranes with a 1:1 composition of glassy and rubbery polymers were

fabricated by a dual-spinneret technique, where the composite membrane's suture retention strength, delamination strength, and toughness were greater than conventional electrospun fabrics.

Controlled delivery of an antifibrotic, *cis*-4-hydroxy-L-proline, was achieved through synthesis of drug precursors. Hexyl- and octyl-ester precursors enabled diffusion-controlled release of the antifibrotic over 1 or more weeks, while *cis*-4-hydroxy-L-proline diffused from poly(DTE carbonate) films within 24 hours.

Composite membranes with and without antifibrotic were compared against polymer films and Integra LifeSciences' DuraGen PLUS[®] in a rat laminectomy model. The extent of adhesions was evaluated at 4 and 8 weeks. The fracture of polymeric films permitted scar progression to the dura by 8 weeks, despite inhibition at 4 weeks. The composite membranes did not fracture and reduced the extent of adhesion from 84% (control) to 36%. All adhesions in the composite membrane group formed at the caudal tuck, suggesting that performance could be improved by device fixation. Any effect of *cis*-4-hydroxy-L-proline was obscured by caudal instability. DuraGen PLUS[®] limited the extent of adhesion to 11%, and the adhesions present were comparatively light.

In this dissertation, a synthetic degradable membrane was compared against polymeric films and DuraGen PLUS[®] in peridural adhesion prevention. The membrane possessed inherent barrier properties, superior mechanical properties, and the ability to deliver an antifibrotic. However, the device did not achieve anti-adhesive performance comparable to Integra LifeSciences' DuraGen PLUS[®] in a rat laminectomy model due to the electrospun anti-adhesion membrane's instability within the implantation site.

Acknowledgements

The generous assistance and mentorship of many individuals enabled the completion of this work and my training. Primarily, I must thank Professor Joachim Kohn, whose vision for the New Jersey Center for Biomaterials (NJCBM) created a collaborative environment of diverse expertise and great resources that permits prototype medical devices to progress from conception through commercialization. Furthermore, his mentorship matured my scientific approach and increased my ability to think critically, strategically, and decisively. Professors Wise Young and Martin Grumet are the founding and current directors of the W. M. Keck Center for Collaborative Neuroscience, without whom this project would not have been conceived. I thank them for guidance in understanding the surgical problem, interpreting the results, and for providing the facilities necessary to perform the work. I thank Professor Prabhas Moghe for his mentorship in working in an interdisciplinary environment. His authorship of the NSF-IGERT fellowship on integratively engineered biointerfaces spurred my excitement for Rutgers University and provided the training necessary to take advantage of the opportunities afforded by the NJCBM and collaborations with the Keck Center and his own group.

The development of this project was supported by the National Science Foundation through an Integrative Graduate Education and Research Traineeship on integratively engineered biointerfaces (P.I.: Prabhas Moghe). The work continued under funding from the National Institutes for Health through a Ruth L. Kirschstein predoctoral fellowship, and the studies were concluded with financial support from Trident Biomedical and the

Department of Defense, through the Armed Forces Institute for Regenerative Medicine – Rutgers-Cleaveland Clinic Consortium (P.I.: Joachim Kohn). The financial support and training provided by these fellowships, grants, and partnerships were essential to the completion of this work and to my professional development.

I must also acknowledge the scientific and technical guidance provided by my fellow coworkers in the NJCBM and W. M. Keck Center for Collaborative Neuroscience. Das Bolikal, Ramiro Rojas, Abraham Joy, and Larisa Sheihet provided extensive guidance in the synthetic procedures and characterization methods listed in chapter 4. Polymers were synthesized by Karolina Piotrowska, Larisa Sheihet, Das Bolikal, Matthew Laughland, or Asa Vaughan. Both Jaap Schut and Sanjeeva Murthy provided insights and training related to the materials science aspects of this work. The early animal studies were performed by Sharonda Meade, while the laminectomy studies were performed by Bor Tom Ng and Charlotte Hsu. The collaborative and cooperative environments of these two centers and all of their members provided the resources, experience and encouragement to ensure progression of the work.

I would like to acknowledge special contributions from two members external to Rutgers University. Jean Altus (Stephens) from the Polymer Division of the National Institute of Standards and Technology provided initial training in electrospinning, which allowed me to establish an electrospinning facility at the NJCBM. Many of the innovations that follow in chapter 2 would not have been possible if an external facility provided electrospun materials for this project. Tom Barbolt of TAB Consulting, previously of Ethicon Inc., provided helpful assistance and discussion in interpretation of

the tissue response to implanted biomaterials. Without his expert advice, the biocompatibility of electrospun prototypes could not be adequately discussed.

Finally, I must acknowledge the support and encouragement of my family. My late mother, Carol Ann Florek, and my father, Randolph Florek, encouraged and shaped me over many years. Much of their influence occurred as my mother chauffeured me many miles between Delano and the University of Minnesota, imparting wisdom as the miles passed. My brother, Matt, and uncle, Craig Anderson, are each doctors of a different variety – M.D.s practicing family medicine and ear, nose, and throat surgery, respectively. Their support and prodding (sometimes joking and sometimes serious) helped me to reach the completion of this work. My greatest advocate and greatest source of encouragement was my wife, Olivia Gruber Florek. Her love, affection, cooking, understanding, intermittent dancing, and encouragement supported me in the weakest of days, and for her service I will always feel as though she is part author of this work.

Dedication

To Carol Ann Florek, whose love, faith, endurance, and contentment is an inspiration to
all who knew her.

Table of Contents

Abstract of the dissertation	ii
Acknowledgements.....	iv
Dedication.....	vii
Table of Contents.....	viii
List of Tables	xiii
List of Figures	xv
List of Abbreviations	xxvi
 1 Introduction to the field of adhesion prevention.....	 1
1.1 Clinical background regarding adhesion formation and prevention.....	2
1.1.1 The anatomy of the abdomen prevents tissue adhesion	3
1.1.2 Adhesion formation and complications subsequent to abdominal surgery	4
1.1.3 Medical device strategies for the prevention of abdominal adhesions	5
1.1.4 The anatomy of the spine prevents tissue adhesion.....	9
1.1.5 Disruption of spinal anatomy by surgical intervention	10
1.1.6 Post-surgical adhesions as a cause of failed back surgery syndrome.....	12
1.1.7 The development of post-surgical adhesions in the spine	16
1.1.8 Procedural strategies for the prevention of peridural adhesions.....	17
1.1.9 Medical device strategies for the prevention of peridural adhesions	20
1.1.10 Synthesis of clinical literature review.....	31
1.2 The use of tyrosine-derived polycarbonates in medicine.....	33
1.3 Introduction to the field of electrospinning.....	36
1.4 Introduction to the anti-fibrotic, <i>cis</i> -4-hydroxy-L-proline	43

1.5	Hypotheses	47
2	Materials and Methods	48
2.1	Materials.....	48
2.1.1	Polymers	48
2.1.2	Chemicals for synthesis and fabrication.....	49
2.1.3	Solvents and other materials.....	49
2.1.4	Electrospinning Device.....	50
2.2	Fabrication	50
2.2.1	Solvent cast films.....	50
2.2.2	Compression molded films	51
2.2.3	Electrospinning.....	51
2.3	Characterization	52
2.3.1	Determination of T_g and T_m by differential scanning calorimetry	52
2.3.2	Retention time of hydroxyproline alkyl ester HCl salts by HPLC	53
2.3.3	Controlled release of <i>cis</i> -4-hydroxy-L-proline by ninhydrin assay.....	54
2.3.4	Quantification of fiber diameter by scanning electron microscopy	55
2.3.5	Cell viability with exposure to tHyp alkyl ester HCl salts	55
2.3.6	Cell permeability of electrospun fabrics.....	56
2.3.7	Enzyme linked immunosorbent assay for adsorbed fibronectin.....	57
2.3.8	T-peel delamination strength of electrospun fabrics	57
2.3.9	Tensile strength of electrospun fabrics	58
2.3.10	Suture pull-out evaluation of AAMs, composite films, and collagen foams.....	59
2.4	Animal Studies	60

2.4.1	Sterilization.....	60
2.4.2	Rat subcutaneous implantation.....	60
2.4.3	Rat laminectomy with or without spinal cord injury.....	61
2.4.4	Histology	62
2.4.5	Extent of adhesion	63
2.5	Statistics	63
3	Fabrication of electrospun anti-adhesion membranes	64
3.1	Development of an electrospinning facility	64
3.2	Conventional solvent systems useful for electrospinning TDPCs.....	65
3.3	Low toxicity solvent system for electrospinning TDPCs	70
3.4	Range of polymers useful for electrospinning TDPC.....	74
3.5	Cell interactions with scaffolds of varying fiber diameter and porosity.....	77
3.6	Confirmation of barrier function and effect of chemistry <i>in vivo</i>	82
3.7	Dual-spinneret electrospinning and thermal heat treatments enhance the mechanical properties of electrospun nonwoven fabrics	86
3.8	Electrospun scaffolds impart structural stability to low- T_g polymer films	99
3.9	Sterilization of degradable PEG-containing tyrosine-derived polycarbonates ..	102
3.10	Conclusions regarding the fabrication of anti-adhesion membranes	104
4	Controlled delivery of <i>cis</i> -4-hydroxy-L-proline.....	106
4.1	Exploratory synthesis and characterization of cHyp precursor molecules	106
4.2	<i>cis</i> -4-hydroxy-L-proline lactone	108
4.2.1	Synthesis of <i>cis</i> -4-hydroxy-L-proline lactone	108
4.2.2	Characterization of <i>cis</i> -4-hydroxy-L-proline lactone	109

4.2.3	Utility of <i>cis</i> -4-hydroxy-L-proline lactone HCl	112
4.3	<i>cis</i> -4-hydroxy-L-proline alkyl ester HCl salts	113
4.3.1	Synthesis of <i>cis</i> -4-hydroxy-L-proline alkyl ester HCl salts	113
4.3.2	Characterization of <i>cis</i> -4-hydroxy-L-proline alkyl ester HCl salts	114
4.3.3	Utility of <i>cis</i> -4-hydroxy-L-proline alkyl ester HCl salts	123
4.4	<i>cis</i> -4-hydroxy-L-proline octyl carbonate HCl salt	124
4.4.1	Synthesis of <i>cis</i> -4-hydroxy-L-proline octyl carbonate HCl salt	124
4.4.2	Characterization of <i>cis</i> -4-hydroxy-L-proline octyl carbonate HCl salt	126
4.4.3	Utility of <i>cis</i> -4-hydroxy-L-proline octyl carbonate HCl salt	129
4.5	Subcutaneous screen of <i>cis</i> -4-hydroxy-L-proline octyl ester HCl scaffold	130
4.5.1	Fabrication of <i>cis</i> -4-hydroxy-L-proline-loaded implants	131
4.5.2	Implantation and recovery of <i>cis</i> -4-hydroxy-L-proline-loaded implants	132
4.5.3	Tissue response to <i>cis</i> -4-hydroxy-L-proline-loaded implants	132
4.6	Conclusions regarding the delivery of <i>cis</i> -4-hydroxy-L-proline	134
5	Evaluation of adhesion prevention in the laminectomy site	136
5.1	Exploratory implantation of an electrospun fabric and cHyp microspheres	138
5.1.1	Implantation of fabric and cHyp-loaded microspheres	139
5.1.2	Evaluation of adhesion prevention performance	140
5.1.3	Conclusions of exploratory study	142
5.2	Study #1: non-degradable barrier devices with and without cHyp delivery	143
5.2.1	Materials implanted	144
5.2.2	Implantation and materials handling	146
5.2.3	Evaluation of adhesion prevention performance	147

5.2.4	Summary and corrective measures	152
5.3	Study #2: degradable composite devices versus DuraGen PLUS®.....	153
5.3.1	Materials implanted	154
5.3.2	Implantation and materials handling	155
5.3.3	Evaluation of adhesion prevention performance	157
5.3.4	Biocompatibility of degradable composite devices.....	163
5.3.5	Evaluation of Anti-Adhesion Device Performance	167
5.4	Conclusions regarding anti-adhesion performance in the laminectomy defect .	168
6	Conclusions.....	170
7	References.....	173
	Curriculum Vitae	189

List of Tables

Table 1-1. Procedural statistics for surgical procedures of the spine, as reported by the AANS [64, 65].	12
Table 1-2. Procedural statistics for surgical procedures of the spine, as reported by the U.S. Department of Health and Human Services [66-68].	12
Table 1-3. Solvents of typically used in electrospinning [201, 202] that should be limited due to known or suspected inherent toxicity [216, 218].	41
Table 1-4. polymers electrospun [201, 202] from “solvents with low toxic potential” according to the FDA Guidance for Industry document [216].	42
Table 2-1. Physical properties of polymers used in this dissertation.	48
Table 2-2. Chemicals used for synthesis of cHyp precursors and tHyp alkyl ester HCl salt degradable surfactants	49
Table 2-3. Components of electrospinning device	50
Table 2-4. DSC temperature scans by sample type	53
Table 2-5. HPLC methods utilized to characterize hydrophilic (method #1) and hydrophobic (method #2) molecules.	54
Table 2-6. Cell counting protocols used in NIH ImageJ to count dead and all cells.	56
Table 3-1. Electrospinning parameters for fabrication of electrospun membranes with matched fiber diameter from different polymer chemistries.	67
Table 3-2. Mechanical properties of E1000.5(1k) and 1:1 E1000.5(1k):E0012(1k) composite electrospun Anti-Adhesion Membranes.	94
Table 3-3. Physical characteristics of final electrospun composite AAMs	99

Table 4-1. Inspection of the C=O stretch region (1790-1650 cm ⁻¹) verifies lactone formation.....	110
Table 5-1. Electrospinning parameters for fabrication of electrospun E0000 AAMs with either tHyp BE HCl or cHyp OE HCl from HFIP..	145
Table 5-2. Electrospinning parameters for fabrication of 1:1 E1000.5(1k):E0012(1k) composite AAMs with either tHyp BE HCl or cHyp OE HCl from acetic acid.	154

List of Figures

Figure 1.1. Normal abdominal mesothelium with prominent microvilli. Scale bar: 3.23 μm [11]	4
Figure 1.2. Development of the epidural scar in dogs [7]. At three days, left, a hematoma fills the laminectomy defect. The hematoma is eventually replaced by mature fibrous tissue produced by fibroblasts migrating from the erector spinae muscles, right.....	17
Figure 1.3. Polymerization and resorption of Confluent Surgical's DuraSeal Xact TM , Left [119], and 8-week tissue reaction to DuraSeal Xact TM , Right [120]. At right, DuraSeal Xact TM is represented as clear in this histological section, located above the dura and neo-dura. A layer of vacuolated macrophages borders the gel.	23
Figure 1.4. Scanning electron microscope image of Baxter Healthcare's TISSUDURA..	30
Figure 1.5. Chemical structure of poly(I _{0,2} DTE-co-XX%I _{0,2} DT-co-YY%PEG _{1k} carbonate). The polymer composition is a random distribution of the three monomers, DTE, DT, and PEG _{1k}	34
Figure 1.6. Number of publications per year including "electrospinning" or "electrospun" in the ISI Web of Knowledge database	37
Figure 1.7. The orientation of the hydroxyl group varies between the <i>cis</i> and <i>trans</i> isomers of hydroxy-L-proline	44
Figure 1.8. poly(PEG-Lys-g-cHyp) and its formulation in hyaluronic acid microspheres, as described for the prevention of abdominal adhesions [244].	46
Figure 2.1. Representative image to demonstrate the measurement of extent of adhesion.	
Figure 3.1. The NJCBM Electrospinning apparatus is installed in the center's class 10,000 fume hood (left). The rotating mandrel collector (right) permits collection of 7	

cm by 20 cm sheets of fibroporous fabrics. The gear motor in the center translates the collector for even distribution of fibers, while the variable-speed motor rotates the mandrel.	65
Figure 3.2. The addition of DMF to DCM reduced the average fiber diameter of electrospun mats, thus reducing the interfiber spacing.	66
Figure 3.3. Cell impermeable electrospun nonwoven fabrics with fiber diameter of 0.52 and 0.49 μm (a) and (b) and cell permeable fabrics with fiber diameter of 1.72 and 1.76 μm (c) and (d). Scaffolds have been electrospun from 70/30 THF/DMF and are composed of I ₂ E1000 (a) and (c), and I ₂ E1008(1k) (b) and (d).....	68
Figure 3.4. Electrospinning of E1002(1k) from HFIP to determine preferred electrospinning parameters and solution concentration for a barrier device.	69
Figure 3.5. Schematic of poor stress distribution in beaded fiber constructs, compared to bead-free fiber constructs	70
Figure 3.6. The addition of tHyp octyl ester HCl eliminated beading of fibers during electrospinning of 17% wt/vol E0000 solutions in acetic acid. The sample at top was without surfactant, while the sample at the bottom was electrospun with the a 1:5 loading of tHyp octyl ester HCl per polymer by mass.	71
Figure 3.7. The effect of alkyl chain length and concentration of degradable surfactant in bead formation in acetic acid electrospinning. 3000x (top) and 600x (bottom) SEM images of poly(DTE carbonate) fiber mats electrospun from acetic acid with the addition of surfactant as indicated above.....	72
Figure 3.8. Alkyl chain length of degradable surfactants affected the viability of confluent HDF cultures in serum-free media at 48 hours. No toxicity was noted for either	

surfactant at 0.5 mM, but the octanol-releasing tHypOE was found to be toxic at concentrations ≥ 1.5 mM. Live cells were DAPI-positive, but ED-1 negative, while dead cells were indicated by nuclear binding of ED-1.	73
Figure 3.9. Contraction of electrospun E1008(1k) over 4 hours in PBS at 37 °C	74
Figure 3.10. Observing single fibers in a contracted E1008(1k) scaffold reveals that the fibers have become wider and more tortuous, indicating that the length of each fiber has decreased. The architecture of the I ₂ E1008(1k) scaffold remains similar across storage conditions.....	75
Figure 3.11. Schematic of entropy-driven fiber contracture upon plasticization	75
Figure 3.12. Electrospun scaffolds of I ₂ E10YY(1k) before (top left) and after (bottom left) overnight incubation in PBS at 37 °C.	76
Figure 3.13. Average pore size, $2\bar{r}$, based upon equations following Sampson's derivation of pore size in near-planar fiber networks [253].	77
Figure 3.14. Rat dermal fibroblast interaction with 2.3 ± 0.19 μm (95% C.I., n=60) fiber diameter scaffold at day 5. SEM image (upper left), confocal microscopic image (upper right) and confocal z-stack (bottom)	78
Figure 3.15. Rat dermal fibroblast interaction with 1.0 ± 0.10 μm (95% C.I., n=60) fiber diameter scaffold at day 5. SEM image (upper left), confocal microscopic image (upper right) and confocal z-stack (bottom)	79
Figure 3.16. Rat dermal fibroblast interaction with 0.5 ± 0.04 μm (95% C.I., n=60) fiber diameter scaffold at day 5. SEM image (upper left), confocal microscopic image (upper right) and confocal z-stack (bottom)	80

Figure 3.17. Rat dermal fibroblast interaction with $0.29 \pm 0.03 \mu\text{m}$ (95% C.I., $n=60$) fiber diameter scaffold at day 5. SEM image (upper left), confocal microscopic image (upper right) and confocal z-stack (bottom)	81
Figure 3.18. Two and four week tissue response to I ₂ E1000 and I ₂ E1008(1k) cell permeable nonwoven fabrics (H&E)	83
Figure 3.19. Sketch of remodeled polymer fibers after cell infiltration and proliferation	84
Figure 3.20. Two and four week tissue response to I ₂ E1000 and I ₂ E1008(1k) cell impermeable nonwoven fabrics (H&E)	85
Figure 3.21. Progression of sintering to fusion of electrospun I ₂ E1008(1k) fibers in a vacuum oven.	87
Figure 3.22. Schematic of the Carver press as used to heat treat nonwoven fabrics	88
Figure 3.23. Schematic and photo of the NJCBM dual-spinneret electrospinning apparatus during operation. The mandrel appears white, for it is covered with an accumulating scaffold, while the spinnerets are located at the top and in the right foreground of the photograph.	89
Figure 3.24. The DSC curves obtained for an electrospun 1:1 E1000.5(1k):E0012(1k) composite AAM. Each polymeric fiber was electrospun from acetic acid with a 1:5 loading of tHyp butyl ester HCl, frozen at -80 °C, and freeze dried to remove residual acetic acid. The heat treatment temperatures for the composite (45 °C) and E1000.5(1k) (70 °C) AAMs are highlighted in red.....	90
Figure 3.25. Fracture surface of E1000.5(1k) AAM. Red circles highlight some of the clearly sintered fiber intersections, while the maintenance of device porosity is evident.	91

Figure 3.26. T-peel delamination strength of composite and E1000.5(1k) AAMs plotted on a logarithmic scale.....	92
Figure 3.27. Representative stress-strain curves for E1000.5(1k) and composite AAMs, depicting the determination of key mechanical properties. Experimental data is shown in red, and the line used to determine the 0.2% offset yield strength is blue.....	93
Figure 3.28. Suture pull-out performance of composite AAMs and films, E1000.5(1k) AAMs and DuraGen PLUS®.....	96
Figure 3.29. Failure surfaces of representative loading curves for suture pull-out samples. Note the degree of material deformation in the composite devices, while the E1000.5(1k) sample were cut cleanly by the 5-0 PROLENE suture. In the E1000.5(1k) sample, the extension at failure was identical to the insertion depth, 3 mm, while the deformation of the composite membrane allowed it to resist suture extraction to 7 mm.	97
Figure 3.30. SEM images of (a) E1000.5(1k) AAM, (b) composite AAM with 1:5 tHyp butyl ester HCl, and (c) composite AAM with 1:5 cHyp octyl ester HCL	98
Figure 3.31. Compression molding treatments used to fabricate E1224(1k) films and composite film devices that incorporate E1002(1k) fibers to impart shape stability and suturability.	101
Figure 3.32 Comparison of scaffold architecture following sterilization by high and normal concentrations of ethylene oxide gas or gamma-irradiation. Note the concentration dependence of fusion during ethylene oxide gas sterilization.	102
Figure 3.33. Effect of gamma-irradiation (29 kGy), heat treatment, hydroxyproline alkyl ester HCl salt, and antioxidant loading on device molecular weight. Treatment: as spun (AS), heat treated (HT), or gamma-irradiated (GI); hydroxyproline alkyl ester HCl: tHyp	

butyl ester HCl (tB), cHyp octyl ester HCl (cO); antioxidant: none (No AO), 0.1% vitamin E (VitE), 0.1% butylated hydroxytoluene (BHT).	103
Figure 4.1. Typical and desirable release paradigms for cHyp.....	106
Figure 4.2. Molecules evaluated for the release of cHyp, which vary in hydrophobicity, molecular weight, and susceptibility to hydrolysis.	107
Figure 4.3. Synthetic scheme for producing cHyp lactone HCl	108
Figure 4.4. Formation of lactone confirmed by NMR. The three spectra are for the starting material (red), Z-protected cHyp lactone after flash chromatography (green), and the final product, cHyp lactone HCl (blue).	109
Figure 4.5. Release of cHyp from electrospun E0000 fabrics containing either cHyp or cHyp lactone by HPLC.....	111
Figure 4.6. HPLC chromatograms of cHyp lactone HCl samples prepared in acetonitrile and DI water. Complete hydrolysis of cHyp lactone HCl in water was observed at 5 minutes.	112
Figure 4.7. Synthetic scheme for producing cHyp octyl ester HCl. The same approach was applied for other alkyl ester HCl salts by varying the alcohol in which the synthesis is performed	114
Figure 4.8. ¹ H-NMR spectrum of cHyp octyl ester HCl. No impurity peaks are noted, nor is a COOH peak is present near 12.5 ppm. New Peaks corresponding to the alkyl ester are CH ₃ at 1.0 ppm, CH ₂ at 1.4 ppm, CH ₂ at 1.7 ppm, and the CH ₂ adjacent to the ester bond at 4.3 ppm. The peak at 9.8 ppm is attributed to NH ₂ ⁺ upon formation of the HCl salt.....	115
Figure 4.9. HPLC chromatogram of cHyp octyl ester HCl.....	116

Figure 4.10. HPLC for hydrolysis rate of cHyp octyl ester HCl. The exponent and calculated half-time for hydrolysis for each of the three datasets are: cHyp OE HCl #1, -0.138, 5.0 hours; cHyp OE HCl #2, -0.154, 4.5 hours; and tHyp OE HCl #3, 0.132, 5.3 hours. The average half-time of hydrolysis in PBS is 4.9 hours.....	117
Figure 4.11. Solvent cast films of cHyp alkyl ester HCl salts in E0000 and E1004(1k).	118
Figure 4.12. Loading capacity of cHyp octyl ester HCl was determined via 4 hour release (left) from solvent cast films (right). Air bubbles formed in four of the wells. cHyp release from these wells were excluded from the analysis.....	119
Figure 4.13. Fractional release of cHyp from E0000 films and electrospun fabrics.....	120
Figure 4.14. Fractional release of cHyp as a function of alkyl chain length and polymer chemistry on a time ^{1/2} scale.	121
Figure 4.15. HPLC analysis of eluent indicates cHyp octyl ester HCl diffuses from the polymeric film into the buffer, rather than hydrolyzing to cHyp within the polymer matrix.	122
Figure 4.16. Characterization of larger-scale (2.5 g hydroxyproline) hydroxyproline alkyl ester HCl synthesis.....	124
Figure 4.17. Synthetic scheme for production of cHyp octyl carbonate HCl.....	125
Figure 4.18. Extraction of pyridine and N-boc-cHyp from the intermediate product by ethyl acetate versus DI water separation.	126
Figure 4.19. ¹ H-NMR spectrum of cHyp octyl ester HCl: starting material (red), intermediate products (green), and final product (blue). New Peaks corresponding to the alkyl carbonate are CH ₃ at 0.8 ppm, CH ₂ at 1.2 ppm, and CH ₂ at 1.6 ppm. The pyridine	

impurity in observed in the intermediate product (8.0, 8.5, 8.9 ppm), but not in the final product. The peak at 10.6 ppm is attributed to NH_2^+ upon formation of the HCl salt....	127
Figure 4.20. HPLC of cHyp octyl ester HCl following deprotection and precipitation. The product contains a small impurity of cHyp, 2.2% by peak area.	128
Figure 4.21. elution of cHyp octyl carbonate HCl from E0000 films in comparison to the elution of cHyp and cHyp octyl ester HCl from the same.	129
Figure 4.22. Attempted recovery of tHyp butyl ester HCl after 8 weeks of crystallization in 1:100 ethyl acetate:diethylether at -15 °C. Crystals of product transformed to a viscous state upon attempted isolation.....	130
Figure 4.23. Architecture of E0000 devices implanted in rat subcutaneous screen to screen the effect of cHyp octyl ester HCl.....	131
Figure 4.24. The underside of rat dermis upon recovery of E0000 fabrics with and without cHyp octyl ester HCl loading. Fabrics without cHyp are labeled E0000.....	133
Figure 4.25. One-week rat subcutaneous tissue response to E0000 electrospun fabrics without (left) and with (right) cHyp delivery. In 40x images, the edge of the implant is indicated with a dashed yellow line. Hematoxylin and eosin, 10x (top), 40x (bottom)..	134
Figure 5.1. Diagram of laminectomy and placement of AAMs. A rostral and caudal tuck of AAMs was always attempted, though only consistently achieved in Study #2.	136
Figure 5.2. Electrospun E0000 scaffolds provided by Vipavee Hoven and implanted in the exploratory adhesion prevention study.....	139
Figure 5.3. Gross (top) and detailed (bottom) histological sections of cell-permeable E0000 fabric and fat pad in the laminectomy site. Masson's trichrome.....	140

Figure 5.4. Gross (top) and detailed (bottom) histological sections of cHyp-loaded HA microspheres and fat pad in the laminectomy site. Masson's trichrome.....	141
Figure 5.5. AAMs electrospun from 5.8 %wt/vol E0000 solutions in HFIP with 1:5 loading of either tHyp butyl ester HCl or cHyp octyl ester HCl.....	145
Figure 5.6. Placement of E0000 electrospun AAM and polymer films as an interpositional membrane between the dura and the laminectomy defect.	146
Figure 5.7. Fraction of the laminectomy defect where the dura was adhered to the laminectomy scar.	148
Figure 5.8. Representative 4-week control tissue section, where no interpositional membrane was placed between the dura and laminectomy defect. (H&E, 5x, tiled)	149
Figure 5.9. Representative 4-week film tissue sections, where an E0000 film without (top) or with (bottom) cHyp-delivery was placed on top of the dura before closing the laminectomy defect. (H&E, 5x, tiled).....	150
Figure 5.10. Representative 4-week electrospun AAM tissue sections, where an electrospun E0000 fabric without (top) or with (bottom) cHyp-delivery was placed on top of the dura before closing the laminectomy defect. (H&E, 5x, tiled).....	151
Figure 5.11. Surgical site prior to closure: (a) no intervention, (b) DuraGen PLUS [®] , (c) composite film device, (d) composite AAM.	156
Figure 5.12. Sample recovery 24 hours after trial surgical placement of composite film and composite electrospun AAM devices. At left, the film device was covered with a thick fibrin matrix with some coagulated blood, which could be removed (center). At right, a fibrin gel advances from the margins of the laminectomy defect on the posterior surface of the electrospun AAM.	157

Figure 5.13. Fraction of the laminectomy defect where the dura was adhered to the laminectomy scar at weeks 4 and 8.....	158
Figure 5.14. Representative 4-week (top) and 8-week (bottom) control tissue sections, where no interpositional membrane was placed between the dura and laminectomy defect. (H&E, 5x, tiled).....	158
Figure 5.15. Representative 4-week (top) and 8-week (bottom) composite film tissue sections, where a film composed of E1224(1k) with E1002(1k) fibers was placed between the dura and laminectomy defect. (H&E, 5x, tiled).....	159
Figure 5.16. Variable adhesion prevention performance of cHyp- and non-cHyp-loaded composite AAMs at 8-weeks due to instability at caudal tuck. (H&E, 5x, tiled).....	160
Figure 5.17. Representative 4-week (top) and 8-week (bottom) composite AAM tissue sections, where an 1:1 E1000.5(1k):E0012(1k) membrane was placed between the dura and laminectomy defect. (H&E, 5x, tiled).....	161
Figure 5.18. Representative 4-week (top) and 8-week (bottom) composite AAM + cHyp tissue sections, where an 1:1 E1000.5(1k):E0012(1k) membrane loaded with cHyp octyl ester HCl was placed between the dura and laminectomy defect. (H&E, 5x, tiled).....	162
Figure 5.19. Representative 4-week (top) and 8-week (bottom) DuraGen PLUS [®] tissue sections, where an collagen foam was placed over the dura within the laminectomy defect. (H&E, 5x, tiled).....	163
Figure 5.20. Typical foreign body response to subcutaneous injection of a bolus of poly(D,L-lactide-co-glycolide microspheres at 11 weeks (Left, H&E, 5.6x) and 13 weeks (Right, H&E, 35x) [259]	164

Figure 5.21. Chronic active response to a silk suture that transferred tissue from one rat to the next; histology at 4 weeks (left) and 8 weeks (right). H&E 40x.....	164
Figure 5.22. Foreign body response to a rapidly degrading E1224(1k) film reinforced with E1002(1k) fibers; histology at 4 weeks (left) and 8 weeks (right). H&E 40x.....	165
Figure 5.23. Foreign body response to degradable composite AAM; histology at 4 weeks (left) and 8 weeks (right). H&E 40x.....	166

List of Abbreviations

Greek letters

δ	extension
ε	strain
σ	stress
ϕ	pore fraction
ω	fiber width

Roman letters

AANS	American association of neurological surgeons
ACN	acetonitrile
ANOVA	analysis of variance
ASBO	adhesive small bowel obstruction
BHT	butylated hydroxyl toluene, or 2,6-di-tert-butyl-4-methylphenol
cHyp	<i>cis</i> -4-hydroxy-L-proline
cHyp BE HCl	<i>cis</i> -4-hydroxy-L-proline butyl ester HCl
cHyp HE HCl	<i>cis</i> -4-hydroxy-L-proline hexyl ester HCl
cHyp OE HCl	<i>cis</i> -4-hydroxy-L-proline octyl ester HCl
CLogP	calculated logarithmic octanol water partition coefficient
C.I.	confidence interval
CMC	carboxymethylcellulose
CP	collector potential (units: kV)

CSF	cerebral spinal fluid
D	distance (units: cm)
DCM	dichloromethane, or methylene chloride
DMEM	Dulbecco's modified Eagle's medium
DMF	dimethyl formamide
DSC	differential scanning calorimetry
DT	deaminotyrosyl tyrosine ester carbonate
DTE	desaminotyrosyl tyrosine ethyl ester
DTO	desaminotyrosyl tyrosine octyl ester
ED-1	ethidium homodimer-1
ELISA	enzyme linked immunosorbent assay
ELSD	evaporative light scattering detector
ePTFE	expanded polytetrafluoroethylene
FBGC	foreign body giant cell
FBS	fetal bovine serum
FBSS	failed back surgery syndrome
$^1\text{H-NMR}$	proton-nuclear magnetic resonance
HA	hyaluronic acid
HCl	hydrochloric acid
HDFs	human dermal fibroblasts
H&E	hematoxylin and eosin
HPLC	high performance liquid chromatography
HSD	honestly significant difference

LF	ligamentum flavum
LSD	least significant difference
M_n	number average molecular weight
M_w	weight average molecular weight
MeOH	methanol
MRI	magnetic resonance imaging
MW	molecular weight
n	sample size
N/A	not available
NaOH	sodium hydroxide
NG	needle gauge
NJCBM	New Jersey Center for Biomaterials
NP	needle potential (units: kV)
ORC	oxidized regenerated cellulose
PBS	phosphate buffered saline
PD	polydispersity (M_w/M_n)
PEG	polyethylene glycol
PEG _{1K}	polyethylene glycol, molecular weight 1,000 Da
PGA	poly(glycolic acid)
PLGA	poly(lactic acid-co-glycolic acid)
PLA	poly(lactic acid)
PLLA	poly(L-lactic acid)
Q	flowrate (units: mL/hr)

SEM	scanning electron microscopy
t	time
T9	thoracic vertebra nine
T10	thoracic vertebra ten
TDPC	tyrosine-derived polycarbonate
T _g	glass transition temperature (units: °C)
T _m	melting point (units: °C)
wt	weight
Vit E	Vitamin E, or (±)- α -tocopherol
vol	volume
WAXS	wide angle x-ray scattering
Z	benzyloxy-carbonyl

Units

μl	microliters
μm	micrometers
nm	nanometers
kGy	kilogray (1 kGy = 0.1 Mrad)
M	Molar
MHz	megahertz
mg	milligrams
ml	milliliters
N	Normality

1 Introduction to the field of adhesion prevention

The training of physicians progresses under the maxim, “above all, do no harm” [3, 4]. However, some surgical interventions are beleaguered by the occurrence of serious complications due to subsequent formation of adhesions. Hernia repair surgery and caesarean section surgeries too frequently result in bowel obstructions and infertility, and spinal surgery to relieve pain can leave the patient with similar pain from a new source, fibrous adhesions.

This introduction is organized into three sections. The clinical background will be discussed, followed by a review of the three technologies employed: tyrosine-derived polycarbonates, electrospun membranes, and *cis*-4-hydroxy-L-proline (cHyp) delivery. In the clinical section, the formation and composition of adhesions is reviewed. Then, the body’s adhesion prevention mechanisms, adhesion-related complications and surgical adjuvants for the prevention of post-surgical adhesions will be discussed in the context of both abdominal surgery and the laminectomy defect. Though this dissertation focuses on the prevention of adhesions in spinal surgery, the field of abdominal adhesion prevention will be discussed in brief. A discussion of abdominal adhesion will consider a second biological approach to adhesion prevention and will review a number of technological approaches that have been translated to epidural adhesion prevention.

In the technology sections, the relevance of tyrosine derived polycarbonates, electrospinning, and the anti-fibrotic, *cis*-4-hydroxy-L-proline, will be discussed. Briefly, tyrosine derived polycarbonates are a platform technology that permits access to a broad range of material and biological properties within a library of structurally-related polymers. Electrospinning is an established technology in the air filtration field, but an

emerging technology in the biomedical field. It provides the unique capability to produce nonwoven fabrics with pore sizes that are smaller than the diameter of cell nuclei. Lastly, *cis*-4-hydroxy-L-proline is an imino acid with established antifibrotic activity. Successful delivery of this molecule should enhance adhesion prevention through the reduction of collagen synthesis.

1.1 Clinical background regarding adhesion formation and prevention

Fibrous tissue adhesion results from a series of events that begins with the alteration of normal human anatomy and the presence of extravascular blood following surgical intervention. Anatomical structures that are intended to prevent tissues from adhering to each other are compromised in order to gain access to and repair abdominal and spinal conditions. In the course of surgery, blood accumulates in the surgical field and tissues are injured due to dissection and handling. The blood is diluted by alternating saline and suction, and surgeons strive to achieve meticulous hemostasis prior to surgical closure. However, some fibrinogen forms a fibrin gel matrix intraoperatively [5, 6], and blood may continue to seep from compromised arteries following surgery [7], especially as the patient becomes active. The fibrin gel formed during and following surgery provides a provisional matrix for the migration of neutrophils and the migration and proliferation of fibroblasts, monocytes that differentiate to macrophages, and endothelial cells [8, 9]. Fibrin is degraded in the presence of plasmin and inflammatory cells, which occurs in concert with the synthesis of collagen and proteoglycans in the forming granulation tissue. This granulation tissue remodels to a vascularized, highly organized, collagen-rich scar tissue. The collagen-rich scar tissue can tether tissues together, replacing the anatomical structures meant to ensure independent mobility of these organs.

The adhesive scar replaces apposing monolayers of highly-specialized, serous-fluid secreting mesothelial cells in the abdomen, and in the epidural space, it replaces layers of fat, connective tissue and bone that would have isolated the dura, spinal cord, and spinal nerves from the surrounding musculoskeletal tissue.

1.1.1 The anatomy of the abdomen prevents tissue adhesion

The functions of the abdominal organs, lungs, and heart require movement: the stomach churns, intestines propel food through enteric muscle contractions, the lungs expand with the chest wall, and the heart changes shape with each heartbeat. The peritoneal, pleural, and pericardial cavities allow these organs and the other abdominal organs to perform their functions while shielded from stresses imposed by the musculoskeletal system. The organs roughly conform to the shape of their respective cavities, but relative motion is facilitated by a serosal membrane.

The surface of these serosal membranes is composed of a monolayer of mesothelial cells that are approximately $30\text{ }\mu\text{m}$ in diameter, $3\text{ }\mu\text{m}$ in thickness, and are densely covered with microvilli of $0.1\text{ }\mu\text{m}$ in diameter by $2\text{ }\mu\text{m}$ in length [10]. Mutsaers describes the surface as a “carpet of microvilli” [11], Figure 1.1. The microvilli and entrapped peritoneal fluid yield a high viscosity film at both the visceral and parietal surfaces. The mesothelial cells secrete glycosaminoglycans, mainly hyaluronan, and phosphatidylcholine, and pulmonary surfactant [11]. These components impart lubricative capacity to the peritoneal fluid. Taken together, the mesothelium separates abdominal organs from each other and the abdominal wall by supplying smooth surfaces covered with a viscous film, and separated by peritoneal fluid.

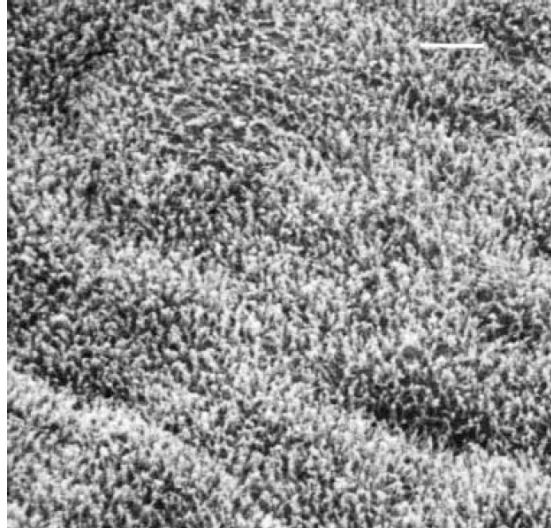


Figure 1.1. Normal abdominal mesothelium with prominent microvilli. Scale bar: 3.23 μm [11]

1.1.2 Adhesion formation and complications subsequent to abdominal surgery

Abdominal adhesions subsequent to laparotomy occur at a rate of greater than 90% [12-16]. Formation follows the general wound-healing response reviewed in Section 1.1, where a fibrin matrix dominates an injured mesothelial surface, and this provisional matrix is remodeled into fibrous tissue, potentially tethering apposing tissues. The incidents proposed to lead to this wound-healing response are diverse and may include “ischemia, surgical trauma, inflammation, hemorrhage, thermal injury, chemical injury, allergic reaction, tissue desiccation, genetic predisposition, and reactions to foreign bodies introduced during the procedure such as glove powder, sutures, and gauze”[15]. The prevalence of abdominal adhesions and the range of potential causes of these adhesions has frustrated the physicians that work in the field [12].

Adhesions cause subsequent complications. The adhesions are fibrous tissue that mature, becoming vascularized and innervated [17], and they contain myofibroblasts [18, 19] that contract the extracellular matrix surrounding them. The presence of adhesions

cause chronic pain to the patient, increase the difficulty of reoperation, and may ultimately result in small bowel obstruction or infertility [20]. Adhesive small bowel obstructions, ASBO, have been observed in 25% of 1500 patients and 15% of 1193 patients at the Cleveland and Mayo Clinics, respectively [12]. Of all incidents of ASBO, 49 to 74% are caused by postsurgical adhesions [14, 21, 22]. Patients operated for ASBO have a high rate of recurrence. Patients with banded or matted adhesions have recurring ASOB of 18 and 24% at 10 years and 24 and 40% at 30 years [23]. Distressingly, the likelihood of reoperation increases with each admission for ASBO [23, 24].

Postsurgical adhesions have significant reproductive implications for women, for constriction of the fallopian tubes may slow or prevent the ovum from reaching the uterus, resulting in either ectopic pregnancies or infertility [5]. It was reported that 15-20% of female infertility is due to the presence of abdominal adhesions [25, 26]. When reconstructive surgery with adhesiolysis was performed, pregnancy rates of 30-52% were achieved [27]. In performance of reconstructive tubal surgery, lysis of adhesions at second-look laparoscopy decreased the occurrence of ectopic pregnancies [28]. Finally, previous pelvic surgery is a significant risk factor for ectopic pregnancy [29]. Due to the occurrence of abdominal adhesions, pelvic operations carry a significant risk of infertility and abnormal pregnancy.

1.1.3 Medical device strategies for the prevention of abdominal adhesions

The medical device approach to adhesion prevention consists of providing a temporary separation of tissues while the patient's mesothelium is functionally restored. Regeneration of the mesothelium begins within 24 hours after injury, and the compromised area is covered with mesothelial cells 7-10 days later [11, 30, 31]. Factors

secreted by macrophages in the wounded mesothelium promotes proliferation of the normally quiescent mesothelial cells [30]. Mesothelial cells may migrate to the defect from areas adjacent to the defect, from the apposed mesothelium, from the peritoneal fluid, or submesothelial precursors may migrate up to the surface [11]. The following barrier devices aim to separate the visceral and parietal surfaces while the mesothelium is regenerated. A discussion of the abilities and limitations of barrier technologies follows.

Genzyme corporation's SeprafilmTM is a hyaluronic acid – carboxymethylcellulose film that hydrates into a gel in 1-2 minutes in saline or within a day *in vivo*, is absorbed within seven days, and is excreted in less than 28 days [32]. The premarket approval states that “reperitonealization occurs within approximately three days after tissue damage,” suggesting that a regenerated serosal membrane will be in place upon absorption of SeprafilmTM [32], though the literature implies that a week or more is necessary [11]. This product provides a hydrogel barrier to adhesion formation while a provisional to mature mesothelium is regenerated. In a multicenter, prospective, randomized double-blind clinical study, SeprafilmTM was able to reduce the incidence of postsurgical adhesions to the midline incision from 94% to 49% in patients scheduled for colectomy and ileal pouch-anal anastomosis with diverting-loop ileostomy [13]. At the 8- to 12-week evaluation performed during ileostomy closure, only 15% of the adhesions in the SeprafilmTM group were considered dense, compared to 58% in the control group. The device's safety profile was determined in a 1,791-patient study under a variety of abdominal operative conditions [33]. The only complication associated with the use of SeprafilmTM was anastomosis leakage, observed at a rate of 6.9% in the SeprafilmTM group, versus 2.4%, when SeprafilmTM was not applied to the anastomosis.

Ethicon Inc.'s Gynecare INTERCEED(TC7) is an absorbable adhesion barrier composed of oxidized regenerated cellulose (ORC). It has been shown to be effective in reducing adhesions in many clinical studies [34-39], with an adhesion-free outcome being 1.5-2.5 times more likely with use of the product than with good surgical technique alone [40]. However, oxidized regenerated cellulose is a procoagulant that is often used in hemostats, for instance, Ethicon Inc.'s Surgicel®. As a provisional fibrin matrix is a capable scaffold for supporting mature scar formation, "meticulous hemostasis" is required before introduction of INTERCEED into the surgical field [41]. Without meticulous hemostasis, the effectiveness of the product is severely diminished [42-44]. The performance of the product in blood-contaminated surgical fields seems to be partially recovered by neutralizing the ORC by forming the sodium salt, increasing the surface pH from pH 2 to pH 5.0 [42].

Gore Medical's ePTFE membrane, PRECLUDE® is a non-degradable, relatively inert, porous polymer membrane made of expanded polytetrafluoroethylene (ePTFE). The pore size is smaller than one micron, so the membrane is a permanent barrier to cell penetration. PRECLUDE® has demonstrated adhesion reduction in gynecological reconstructive surgery, reducing adhesions from 81% to 38% [45]. Similarly, pelvic adhesion occurrence was reduced from 86% to 42% in surgical debulking of epithelial ovarian cancer [46]. In successful surgeries, the implant is typically covered in a thin fibrous capsule [47]. Unlike INTERCEED and Seprafilm™, the Gore-Tex ePTFE membranes require suturing to impart stability to peritoneal (staples or helical tacks are an optional alternative)[48] or pericardial cavity implant site [49].

Covidien's ParietexTM hernia repair device consists of an abdominal wall reinforcement mesh and a collagen-based film barrier for the prevention of postsurgical adhesions [50]. The mesh is composed of knit polyester for tissue integration and reinforcement, and the barrier film is composed of a mixture of oxidized atelocollagen type I, polyethylene oxide (PEO), and glycerol that is gelled around the knit mesh to prevent delamination [50, 51]. ParietexTM has been evaluated in rats, pigs, and in the clinic. In a 21-day comparative rat cecal adhesion study, ParietexTM compared favorably (adhesion occurrence in 1/12 rats) versus ePTFE (5/12 Bard composix E/X; 5/10 Gore-Tex Dual Mesh), Genzyme Sepramesh (11/12 occurrence), and untreated control (10/10 occurrence) [52]. In a 28-day comparative porcine laparoscopic ventral hernia repair model, ParietexTM compared favorably (11% surface area involved in adhesions) versus Ethicon Endosurgery's Proceed (48% area involved) and uncoated polypropylene mesh (46% area involved) [53]. In an 80-patient non-controlled clinical study, 86% of patients were found to be adhesion free according to ultrasound imaging analysis [50]. In a separate study, 77% of patients receiving a non-coated polyester mesh, Ethicon Inc.'s Mersilene mesh, had visceral adhesions at 2.5 years, while 82% of the ParietexTM patients were adhesion free at one year [54]. It is worth noting that the ultrasonic imaging modality is not as conclusive as the second-look laparoscopy used in the clinical studies above. In a 200-patient study of long-term complications and recurrences of laparoscopic repair of incisional hernias, adhesions were not studied directly, but complications due to adhesion were small (only one bowel obstruction at 6 years) [55]. In 11 patients that had recurrence of their incisional hernia, laparoscopic observation of adhesions was possible, and easily-separable film-like omentum-mesh adhesions were observed. ParietexTM is

not specifically indicated for use in adhesion prevention, but the FDA-approved instructions for use indicate that “the absorbable hydrophilic film minimizes tissue attachment to the mesh in case of direct contact with the viscera.”[56]

Barrier devices of various embodiments have either demonstrated or suggested clinical effectiveness in post-surgical adhesion prevention in the abdominal cavity. Though their success rate has not approached 100%, their use has prevented innumerable occurrences of serious complications, such as recurrent small bowel obstruction and infertility. Translation of biomaterial barrier technology from the abdominal cavity to the spine may provide relief to complications of spine surgery.

1.1.4 The anatomy of the spine prevents tissue adhesion

A review of spinal anatomy is necessary to understand the mechanisms by which the body prevents injury and adhesion to the spinal cord and its nerve roots. Below the skin, subcutaneous fat, and erector spinae muscles, lay the vertebrae; each vertebra consists of a vertebral body that bears the compressive loads of the torso and a bony ring that protects the spinal cord. Though it is a single bone, the parts of this ring have individual names: pedicle bones extend from the vertebral body, and laminae bones complete the posterior portion of this ring, connecting at the spinous process, the projection that can be felt in the center of one's back. Beneath the bony skeleton are the ligamentum flavum and the peridural fat [57]. The ligamentum flavum is dense fibrous tissue connecting the central portion of consecutive laminae, and the peridural fat surrounds the dura and nerve roots. These layers provide mechanical isolation of the nerve roots and dura-encased the spinal cord. The cord itself is further protected by the meninges: the dura mater, arachnoid, and pia matter. The dura mater is a tough

connective sheath, which contains the more delicate tissues of the central nervous system. A narrow serous fluid space separates the dura mater from the arachnoid, a looser connective tissue with web-like connections to the pia matter, the richly vascularized outer boundary of the spinal cord. Cerebral Spinal Fluid (CSF) fills the relatively larger space between the arachnoid and pia, suspending the cord in a nearly neutrally-buoyant fluid [57]. The dura matter is joined to the spinal nerves, so protective capabilities of the meninges do not provide isolation to these tissues.

The spinal cord and nerve roots are protected from injury and isolated from adhesion to surrounding tissues by a different mechanism than the heart, lungs, and intestines. Rather than a serous fluid secreting mesothelial cell layer on the surface of all tissues, the spinal anatomy consists of a dense mechanical barrier (lamina and ligamentum flavum), and a cushioning, low cell-permeability layer (peridural fat) to isolate the spinal cord and nerve roots from tethering and irritation by surrounding tissues. Further protection is provided for the crucial and difficult to repair spinal cord by the meninges and CSF. In the following sections, the surgical alteration of these tissues is justified and the consequences of modification are discussed. Then, interventions to prevent peridural adhesion formation are assessed.

1.1.5 Disruption of spinal anatomy by surgical intervention

Surgical modification of the spinal tissues is usually performed for the purpose of relieving pressure on the spinal cord for the treatment of spinal stenosis, or to gain posterior access to an intervertebral disc with herniation into the spinal canal. To treat spinal stenosis, both laminae and the spinous process are typically resected, a laminectomy. In an open discectomy, either a full laminectomy or hemilaminectomy

(removal of one lamina) is typical, while a microdiscectomy, using a microscope and small port or other aids, requires a fenestration, or window, to be made in the lamina – a laminotomy. In all procedures, the ligamentum flavum between the adjacent laminae is typically excised; however, with limited fenestration of the lamina, ligamentum flavum preservation is possible [58-61]. Surgery is reserved for patients that do not respond to more conservative therapy. In comparison to non-surgical therapy, discectomy demonstrates superior pain relief and improvement of function through two to three months, without appreciable differences noted at one or two years, while decompressive laminectomy is superior to non-surgical therapies has been demonstrated over the duration of two years [62].

The American Association of Neurological Surgeons (AANS) surveyed a portion of its membership in 2000 and 2007, reporting the number of United States neurosurgical statistics for 1999 [63] and 2006 [64]. The AANS surveys indicate that a total of 527,310 spinal procedures were performed in 1999 with 1,345,167 being performed in 2006. In 2006, approximately half of spine procedures involving a laminectomy or laminotomy (hereafter, collectively referred to as laminectomies) were intended to gain access the intervertebral disc, while 39% were to decompress the spinal cord in the case of spinal stenosis, with the remaining 12% of laminectomies intended to gain access to the cord and surrounding tissues, Table 1-1. The majority (83%) were performed at the lumbar level, 2.5% were performed at the thoracic level, and 15% were performed at the cervical level [64]. To verify the accuracy of the AANS estimates, the U.S. Department of Health and Human Services database of inpatient and ambulatory procedures was utilized. Detailed reports documenting the procedures of interest were available for 1994 [65],

1995 [66], and 1996 [67], see Table 1-2. The average number of applicable procedures performed in 1994-1996 is 424,000. Excluding the 37% of disc surgeries that are performed by a lateral or anterior approach [63], the U.S. Department of Health and Human Services data indicates that approximately 307,000 laminectomies were performed per year. Laminectomies were performed at a rate of 240,000 to 300,000 procedures per year in the late 1990's with approximately 420,000 being performed in the United States in 2006.

Table 1-1. Procedural statistics for surgical procedures of the spine, as reported by the AANS [63, 64].

Year	Spine (total)	Laminectomy (total)	Decompressive Laminectomy for Stenosis	Discectomy involving laminectomy	Laminectomy (other)
1999	527,310	241,588	85,876	141,620	14,062
2006	1,345,167	422,080	165,008	205,966	51,106

Table 1-2. Procedural statistics for surgical procedures of the spine, as reported by the U.S. Department of Health and Human Services [65-67].

Procedure	ICD-9-CM code	1994	1995	1996
• Reopening of the laminectomy site	3.02	6,000	5,000	3,000
• Exploration and decompression of the spinal canal	3.09	85,000	102,000	122,000
• Excision or destruction of intervertebral disc	80.5	333,000	293,000	324,000
Total:		424,000	400,000	449,000

1.1.6 Post-surgical adhesions as a cause of failed back surgery syndrome

Hundreds of thousands of laminectomies are being performed in the United States each year, but 10-30% of these surgeries fail to relieve the patient's chronic pain, with failure being attributed to a diverse set of surgical and non-surgical etiologies [68-71]. The broadly defined diagnosis for these cases is termed Failed Back Surgery Syndrome

(FBSS). Reintervention due to FBSS is necessary in 5-18% of primary open discectomy case and 7-15% of microdiscectomies [70], causing significant pain to patients and a significant cost to the healthcare system. Peridural fibrosis is indicated as the cause of FBSS at a consistent rate of 14-15% of FBSS cases [68, 69, 72]. Furthermore, peridural fibrosis significantly complicates revision surgeries, for the scar binds the distinct tissues together, eliminating the natural planes of dissection [73].

The attribution of chronic pain in FBSS to peridural fibrosis is a controversial subject [74], but one which has the support of a clinical study and two experimental studies. Ross et al. demonstrated correlation between recurrent sciatic pain and the extensiveness of peridural scarring observed by MRI in 197 patients undergoing discectomy with or without the use of an adjuvant (ADCON-L, Gliatech Inc.) intended to reduce peridural scarring [75]. Study-wide, patients with extensive scarring were 3.2 times more likely to experience recurrent sciatic pain at 6 months (16.7%, 14/84 versus 5.3%, 6/113; $p=0.009$). In the control group, a patient was 3.7 times more likely to have recurrent sciatic pain at 6 months (22% versus 6%; $p=0.034$). The results of this clinical study demonstrate correlation of postsurgical sciatic pain to peridural fibrosis, but do not elucidate the causation of FBSS.

The experimental findings of Kuslich et al. and Smyth and Wright demonstrated that light mechanical stimulation of previously injured spinal nerves will induce intraoperative or postoperative sciatic pain similar to the patient's preoperative state [1, 2]. From 1987 to 1990, Kuslich, Ulsrom, and Michael operated on 193 consecutive patients using "progressive local anesthesia" during spinal decompression or discectomy, permitting the patients to be fully awake or only lightly sedated during the operation.

The patient was able to describe the relative intensity and similarity to preoperative pain in response to the application of mild force to the spinal tissues with blunt surgical instruments. The authors' major finding follows:

“Stimulation of the compressed or stretched nerve root consistently produced the same sciatic distribution pain as the patient had experienced preoperatively. In spite of all that has been written about other tissues in the spine causing leg pain, we were never able to reproduce the patient's sciatica except by finding and stimulating a stretched, compressed, or swollen nerve root. Sciatica could be produced by either pressure or stretch on the caudal dura, on the nerve root sleeve, on the ganglion, or on the nerve distal to the ganglion depending on the site of compression. ... This pain could always be eliminated by the injection of 0.5 cm³ of 1% xylocain via a 30-gauge needle beneath the nerve sleeve proximal to the site of compression” [1].

In the study, 166 of 167 compressed nerve roots produced pain, and 90% of the pain was found to have the same intensity and distribution of sciatic pain that the patient had experienced pre-operatively. Lower back pain was associated with the annulus fibrosus, though the relationship was not as resolute. It is important to note that the normal, uncompressed, unstretched nerve roots were completely insensitive to pain. Smyth and Wright's 1958 study corroborate these findings [2]. Nylon threads were passed under the involved nerve root, healthy nerve root, and other tissues of the spine and made accessible at the skin surface. Either 1, 10, or 14 days after the surgery, each thread was pulled lightly, generating contact but not traction, and sharp sciatic pain was induced immediately when stimulating the involved spinal nerve, while neighboring spinal nerves were much less sensitive [2]. Taken together, these two studies demonstrate hypersensitivity of spinal nerves with a history of compression to minor mechanical stimuli, resulting in the reproduction of the patient's previous sciatic pain. If these spinal nerves become tethered to the surrounding musculoskeletal tissues by peridural fibrosis,

the patient's movements and posture will produce traction on the involved nerve, inducing recurrent sciatica, which contributes to the frequent occurrence of FBSS.

Further evidence for the clinical significance of epidural scarring as a cause for FBSS is provided by the effectiveness of epidural adhesiolysis for relief of low back pain [76]. Epidural adhesiolysis with hypertonic saline (10% NaCl), provides immediate pain relief, with sustained relief in 72, 93, or 92% of patients at 6 months, but falling to 52, 47, or 73% of patients at one year [77-79]. The effectiveness of adhesiolysis was found to be superior to epidural steroid injections in 2009, with 73 versus 12% patients experiencing significant pain relief at one year [79]. Non-endoscopic adhesiolysis was found to be superior in performance and value to endoscopic adhesiolysis [77]. A year of pain relief was found to cost \$2,080 in the first study [77], and \$2,693 in the second study [78].

The findings reviewed above indicate that FBSS positively correlates with the presence of peridural scar tissue, that light mechanical manipulation of hypersensitive spinal nerves will reproduce a patient's sciatic pain, and that lysis of the peridural adhesions provides extended pain relief for many FBSS patients. Manipulation of the dura, nerve root sleeve, or ganglion also induced sciatic pain, likely due to their mechanical attachment to the spinal nerves [1]. Taken together, these findings provide strong motivation to produce a medical device that can prevent the epidural scar from bridging to the dura, nerve roots sleeve, ganglia, or spinal nerves, for the epidural scar would tether these sensitive, pain-inducing tissues to the musculoskeletal system. Based upon the cost of epidural adhesiolysis, a device capable of preventing fibrosis-induced FBSS could be valued as high as \$2,000 to \$2,700 per year of effectiveness. Assuming a product cost of \$1000 and a 20% adoption rate for application in surgeries involving

laminectomy, \$84 million in revenue could be generated in the US per year. Integra LifeSciences' is evaluating DuraGen Plus® as an adhesion barrier matrix in a clinical trial, and estimates the worldwide market for spinal adhesion inhibition to exceed \$300 million [80].

1.1.7 The development of post-surgical adhesions in the spine

To prevent the invasion of fibrous tissue to the spinal canal, one must understand the mechanisms through which it is formed. In 1974, LaRocca and Ian described a “laminectomy membrane” as a fibrotic scar that “fills the surgical defect and has posterior attachments to the erector spinae muscle mass and anterior attachments within the spinal canal, where it adheres to the dura and nerve roots” [7]. The authors followed the progression of scar formation by histological staining in dogs at 3 days and 1, 2, 6, 9, and 12 weeks after operation. The closely spaced timepoints provided insight into the development of an epidural adhesion. On day three, the laminectomy defect was filled with a hematoma, Figure 1.2. By day seven, fibroblasts were seen to migrate from the erector spinae muscles towards the defect, producing a collagenous scar as they migrated from lateral to medial. At subsequent time points, the fibrosis reached the dura and the scar matured, with increasing density of fibrous tissue.

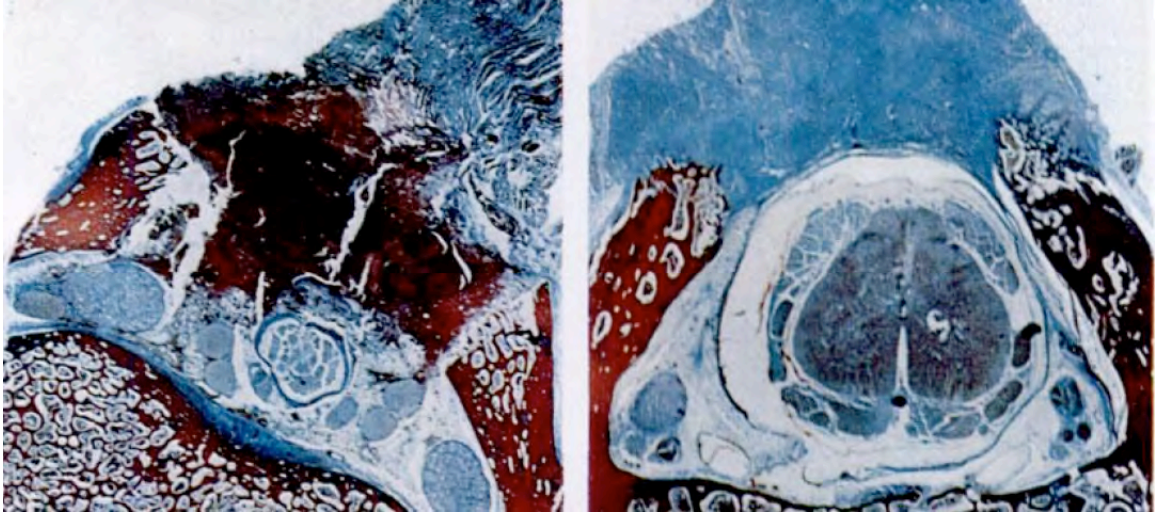


Figure 1.2. Development of the epidural scar in dogs [7]. At three days, left, a hematoma fills the laminectomy defect (Masson's trichrome, original magnification 0.7x). The hematoma is eventually replaced by mature fibrous tissue produced by fibroblasts migrating from the erector spinae muscles, right (Masson's trichrome, original magnification 3x).

With an understanding of peridural adhesion formation, scientists and physicians have taken measures to prevent two events from occurring: formation of a provisional fibrin matrix between the laminectomy defect and the dura, and migration of inflammatory cells from the musculoskeletal tissues to the epidural space. In the following sections procedural and device-oriented strategies will be discussed. Meticulous hemostasis is an obvious goal; autologous free fat transplantation and ligamentum flavum preservation are reviewed. Then, a number of hydrogel-, viscous biopolymer solution-, synthetic biomaterial barrier-, and collagen matrix-approaches are discussed.

1.1.8 Procedural strategies for the prevention of peridural adhesions

Autologous free fat transplantation is an attractive strategy for the prevention of peridural adhesions, but its use resulted in mixed clinical outcomes. Autologous fat transplantation was described as early as 1912 [81-83]. Subsequent studies have

supported the use of free fat transplantation, demonstrating the presence of viable fat in the laminectomy site months to years after the initial surgery via CT scan, MRI, or myelogram [84-88]. The fat transplant decreases in size over time [89-91] but is effective in producing an operative plane of dissection if revision surgery is necessary. Though autologous free fat transplantation is regarded as a safe and competent for preventing fibrous infiltration into the spinal canal, a 1995 156-patient clinical study of Gelfoam versus free-fat graft versus no interpositional membrane demonstrated no clinical or radiological differences between treatment groups at 1 year [92]. A more focused, 186-patient, prospective, double-blind, randomized study of patients undergoing their first surgery for lumbar disc herniation with and without autologous fat graft found no significant differences in clinical outcome, pain, or activities of daily living at a median 24.2 month follow-up [93]. In fact, the fat transplantation patient population was prone to degeneration of reflexes involving the nerve roots. A third clinical study involving 99 patients undergoing laminectomy and discectomy verified that free fat autografts did not have an effect on clinical outcome, pain, or daily activities at a mean of 2.6 years follow-up [94]. (In this study, reflex response was similar between groups.) Four reoperations were necessary, two from each group; only one could be attributed to the presence or absence of a free fat autograft. A description of the complication is included, for similar complications associated with autologous fat transplantation have been encountered in the clinic [95-97]:

“The second patient from group A had been operated on for a right-sided L4-5 lumbar disc herniation in 1995. An L4-5 discectomy via partial hemilaminectomy was performed, and the right L5 root and dura were wrapped in a free autofat graft measuring 2×1×2 cm. The postoperative course was uneventful, and the patient recovered well. In 1999, he started getting the same sciatic pain he had suffered before surgery. An SLR [straight leg raising] test was positive at 45° on

the right side. The patient had weakness in dorsiflexion of the feet and decreased sensation in the L5 dermatome. An MRI showed a doubtful lesion compressing and surrounding the left L5 radix at the level of L4-5. In the second operation, this radix was compressed with a piece of a free autfat graft in the foramen which had been used during the first operation. It had dimensions of 2×0.5×1 cm. Histopathological evaluation showed vascularized, irregular fat tissue surrounded by fibromyelin tissue (Resim 2). Postoperatively, the patient was relieved of pain just after the operation, and neurological deficits gradually disappeared. For 3 years, follow-up examination was uneventful” [94].

The lack of clinical efficacy of autologous fat autografts may be due to the quality of fat, rather than the presence or absence of fatty tissue. In biopsy specimens, Kanamori et al. demonstrated that transplanted fat does not maintain its normal structure; rather, fat globule size becomes highly varied (10/18 cases), varied with some vacuolar degeneration of fat (5/18 cases), or prominent vacuolar degeneration of fat cells (3/18 cases) [98]. Fat tissue has relatively low vascularity, but a degree of nutrient transport and waste removal is still required. The slow rate of revascularization of fatty tissue results in fat necrosis in the central portion of the graft [91]. Necrotic fat cells release their fat droplets to the extracellular space, recruiting macrophages and inciting an inflammatory reaction that leads to the eventual production of fibrous tissue and fatty cysts [90, 99]. The variable fraction of fat cells that are not adequately maintained following free fat transplantation leads to various degrees of fibrous tissue deposition within the free fat autograft as observed in the clinic [88-90, 98, 100]. Evaluation of the quality of fat and presence or absence of fine fibrous tissue cannot be adequately resolved by CT scan or MRI but may have clinical significance.

Rather than the addition of fat to the laminectomy defect, the preservation of the ligamentum flavum (LF) has been investigated for the prevention of peridural fibrosis and sciatic pain. Park, Kim, and Chung describe their attraction to the technique:

“Preservation of the natural barrier is the safest and most effective way to reduce the extent of peridural fibrosis. The prevention or inhibition of the invasion of fibroblasts from the muscle layer is an important factor in reducing the extent of scar formation. We believe that preservation of the ligamentum flavum not only reduces scar formation but also helps the surgeon to locate the anatomical plane at reoperation” [58].

In 2000, Song and Park describe microdiscectomy through a limited fenestration of the lamina, thinning of the LF, then access through a 2-2.5 cm longitudinal incision with ligament retraction [61]. In 2002, Park et al. analyzed their clinical experience after 377 procedures [58]. Remarkably, 84% of patients reported all of the following: no or minimal pain; work was not adversely affected; no use of narcotic medication; satisfied with the procedure. Though this study was not controlled, two independent studies in Turkey demonstrated the effectiveness of a three-sided flap method of LF preservation [59, 60]. In a 600 patient study, the LF-preserving technique resulted in an increase of patient satisfaction at 4 weeks (96.75% versus 81.5%), a decrease in the incidence of peridural fibrosis (18% versus 37%), and a decrease in the 8-year reoperation rate (4.5% versus 9%) [60]. A 20-patient study demonstrated that the LF-preserving technique significantly reduced epidural scarring [59]. In this small study, pairwise comparisons of clinical outcomes show non-statistical superiority in pain and Oswestry Disability Index improvement and a statistical superiority in improvement of straight leg raising ability ($p = 0.012$). At present, LF preservation is the surgical technique with the best clinical evidence for the reduction of peridural fibrosis and reoperation rate.

1.1.9 Medical device strategies for the prevention of peridural adhesions

The only product to have been approved for use in the U.S. to inhibit postsurgical peridural fibrosis was Gliatech Incorporated’s adhesion preventing gel, ADCON-L. The device was approved through a premarket approval mechanism on May 27th, 1998 [101].

The gel formulation was based upon the observation that proteoglycans, and more specifically, the carbohydrate portion of the proteoglycans, could prevent the migration of fibroblasts. Combining the selected carbohydrate polymer with gelatin produced a gel that was deemed capable of inhibiting epidural adhesions [101-103]. ADCON-L has been counterindicated for use in the presence of dural nicks, for it may hinder healing of the dura and exacerbate CSF leakage [104, 105]. In a nine-month period, Lee Hieb, MD, performed 57 surgeries that were candidates for ADCON-L [105]. Twenty-seven patients were treated with the adhesion barrier, and five developed CSF leakage. None of the other 30 patients treated in that time period developed CSF leakage, and this surgeon only encountered one other development of CSF leakage in his previous ten years of treating spinal stenosis. In addition to these complications, a 357-patient clinical trial in Germany failed to demonstrate any improvement in patient-oriented endpoints in 2001 [106]. That definitive study has been affirmed by three other clinical studies [107-109]. Due to CSF leakage, scarce clinical efficacy, FDA scrutiny of questionable data recording practices, and aluminum particles in raw materials, Gliatech ceased distribution of ADCON-L and declared bankruptcy on May 9, 2002 [110]. After ADCON-L was removed from the market, no adhesion prevention product was available for clinical use in spinal surgery, and some studies ceased because they were considered unethical without the availability of an adhesion barrier [111].

Following the removal of ADCON-L from the market, a gel composed of carboxymethylcellulose (CMC) and PEO, FzioMed Inc.'s Oxiplex/SP, was evaluated for reduction of peridural fibrosis and postsurgical leg pain. Oxiplex/SP is an interpenetrating network of PEO and CMC polymers, in which the CMC is stabilized by

ionic calcium crosslinking [112]. The PEO preferentially leaves the gel network; the authors believe that this creates a protein-repellent shell around the tissue-adherent CMC core [112]. However, the length of effectiveness may be questioned, for 25% of the PEO was released into room temperature phosphate buffered saline (PBS) within an hour, and the CMC was sufficiently swollen at 1 hour to permit onset of its dissolution [112]. Oxiplex/SP failed to demonstrate differences in clinical outcome or MRI in two clinical trials [113, 114]. Despite no study-wide significance in the 35-patient pilot study, an 18-patient subgroup with baseline leg pain ≥ 40 received some statistical relief of symptoms compared to control groups at 30 days [113, 115]. Similarly, in the second, 352-patient clinical trial, the sponsor identified a subgroup with baseline pain ≥ 63 , where Oxiplex/SP was able to provide a statistical improvement in leg pain relief at 6 months [114]. The Orthopaedic and Rehabilitation Devices Panel found the device to be “not approvable” on July 15th, 2008 due to the lack of study-wide effectiveness; the panel also found the intraoperative patient assignment performed by the sponsor to be inappropriate [114]. Despite poor clinical results in the U.S., the product continues to be used in 49 countries outside the U.S., and a 70-patient clinical study had demonstrated both improvements in leg pain and a reduction in Oswestry disability index at 3 years [116].

An *in situ* crosslinking approach with adhesion-prevention potential has been approved by the FDA for use as an adjuvant to sutured repair of the dura during spine surgery for the intetion of providing watertight closure [117]. Covidien’s DuraSeal XactTM is based upon similar technology to Confluent Surgical’s SprayGelTM adhesion barrier for abdominal surgeries (Confluent Surgical was purchased by Covidien). Both products are *in situ* crosslinking poly(ethylene glycol) (PEG) gels. The gel forms when

two solutions are simultaneously sprayed onto the surgical field. The first part is an aqueous solution of N-Hydroxysuccinimide-terminated PEG and a blue dye, and the second solution is a trilycine borate buffer at pH 10.01-10.37 [117]. Upon application, the gel has water content in excess of 90%. The PEG chains contain ester bonds that hydrolyze, permitting dissolution of water-soluble degradation products that are cleared through the kidneys [117]. Though this device is approved only as an adjuvant to sutured closure of the spinal dura, the application of similar technology for adhesion prevention, quotes from the company's website, and a white paper entitled "A Unique Dual-Function Device: A Dural Sealant with Adhesion Prevention Properties" [118] all imply to the surgeon that the use of this "adjuvant" may prevent peridural adhesions.

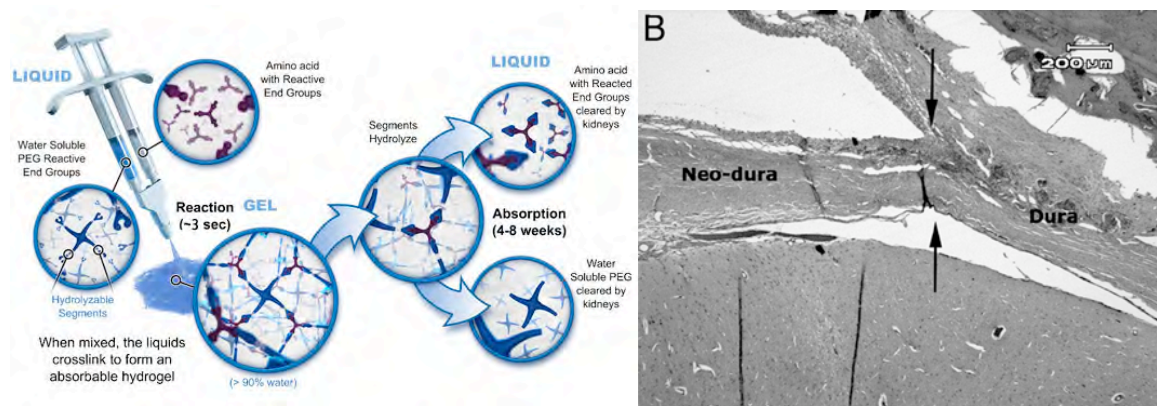


Figure 1.3. Polymerization and resorption of Confluent Surgical's DuraSeal XactTM, Left [119], and 8-week tissue reaction to DuraSeal XactTM, Right [120]. At right, DuraSeal XactTM is represented as clear in this histological section, located above the dura and neo-dura. A layer of vacuolated macrophages borders the gel.

DuraSeal XactTM is competent in significantly increasing resistance to CSF leakage in canine craniotomy models with either a loosely sutured dural incision [121], or as an adjuvant to DuraGen or Durepair onlay repair of a 1.5 cm circular defect [120]. As an adjuvant to onlay repair, DuraSeal XactTM dramatically reduced the adhesion of the cranial bone flap to the dural repair site [120]. In all three studies, a boundary of

vacuolated macrophages was observed around the hydrogel [118, 120, 121]. The FDA contraindicated the use of the device in confined, bony structures, for the device may swell up to 50% [117]. Complications associated with swelling have been noted in two case studies. The swelling induced cervicomedullary compression following the treatment of Chiari malformation [122]. Additionally, cauda equina compression following discectomy and nerve root decompression was encountered in South Africa [123]. These studies reinforce the FDA's contraindication for use in confined bony structures. Confluent Surgical's DuraSeal Xact™ shows promise for the prevention of adhesions on the posterior of the dura, but does not realize the potential protection that a gel or viscous liquid may provide to the spinal nerves due to swelling and the potential for compression. It may not be expressly used for the prevention of postsurgical adhesions in the U.S., for it has only been approved to seal dural defects, which are carefully avoided in discectomy and spinal decompression surgeries – surgical interventions that are performed more frequently than spinal durotomies.

An *in situ* crosslinking product derived from hyaluronic acid is being evaluated for adhesion prevention in the spine. Fidia Advanced Biopolymers initiated a clinical trial on July 14th, 2009 to evaluating Hyalospine™ in a US clinical trial for post-surgical fibrosis and adhesions following laminectomy for spinal stenosis or disc herniation [124]. Patient recruitment for this trial began May 28th 2010. Fidia Advanced Biopolymers' technology relies upon modifying the hyaluronic acid biopolymer so that it auto-crosslinks under physiological conditions [125]. A similar products from this Fidia Advance Biopolymers, Hyaloglide® was shown to improve functional recovery from revision flexor tendon repairs in hand surgery in a 45-patient, multicenter, prospective

clinical trial in Italy [126]. The results suggest that the product inhibited the reformation of adhesions that caused the first surgery to fail. Further, the device has been shown to be effective in reducing the incidence and severity of adhesions in a rabbit fibro-adhesive knee surgery model [127]. A rat peripheral nerve model was less convincing [128].

Abdominal adhesion prevention devices have been evaluated for application in the prevention of peridural adhesion, most successfully, the Gore-Tex ePTFE membrane. Gore-Tex ePTFE membranes limited peridural fibrosis in a 12-week canine laminectomy model, while control and fat grafts resulted in dense scar tissue formation in the laminectomy site [129]. The ePTFE membrane was evaluated in a 66 patient clinical trial, where it covered the decompressive laminectomy or hemilaminectomy defect and was sutured to the capsule of the adjacent facets [130]. The treatment group had a lower incidence of both peridural fibrosis (25 versus 3 patients with no peridural fibrosis) and radicular pain (3 versus 14) than the control group. Seroma formation was more prevalent in the treatment group (27 versus 12), but no clinical problems were associated with seroma formation. These results are the most convincing clinical results demonstrated by a synthetic device, but the technology does not seem to be pursued by W.L. Gore and Associates, Inc. The requirement to suture this device, as with their abdominal device, may limit its use in the confined operating field during microdiscectomy.

Less convincingly, Genzyme's Seprafilm™ and Ethicon Inc.'s Gynecare Interceed TC7 have been evaluated in rat laminectomy and hemilaminectomy studies. These studies are included in this review strictly for completeness. A 2004 report compared Seprafilm™ and Gore-Tex in an 8-week rat total laminectomy model,

indicating that each membrane created a dissection plane and provided a reduction in the amount of tissue adhering to the dura matter [131]. However, the scoring system is called into question, for figure 3A illustrates extensive or moderate adhesion to the dura, while the caption states that no dural adhesion was observed. Figure 3B's caption states that the tissue section is from the Seprafilm™ group, but a membrane, likely Gore-Tex ePTFE, is seen in the section. Seprafilm™ is excreted by four weeks [32], so it should not be present in an eight-week tissue section. Recently, Seprafilm™ and Interceed TC7 were evaluated in an adult rat hemilaminectomy study, demonstrating less dural adhesion and spinal cord retraction than in the no-intervention group [132]. This study is not clinically relevant, for the drilled hemilaminectomy defect in a rat model can be no larger than 2 mm². Seprafilm™ and Interceed TC7 may have potential in peridural adhesion prevention following spinal surgery, but these studies do not provide sufficient evidence to support that conclusion.

Bioresorbable polymer films have been evaluated for application in epidural adhesion prevention. Unlike ePTFE, a resorbable device will not permanently reside in the surgical site, reducing the risk of chronic foreign body response. In 2002, Welch, et al. investigated the use of MacroPore Biosurgery Inc.'s 70:30 poly(L-lactide-co-D,L-lactide) films in ovine laminotomy windows and canine hemilaminectomies [133]. Both 200µm films anchored to the posterior of a lamina, covering the laminotomy, and 20µm films placed between the dura and laminae were able to reduce the scar volume in the laminotomy site. However, 20µm films were encapsulated upon gross excision and were folded in histological sections. The authors believed that the film was insufficiently tucked under the laminae. The mechanism of action proposed by the authors was that the

encapsulated implants created an organized fibrous tissue dissection plane. In 2004, the same group re-evaluated the 20 μ m film in an ovine laminectomy model, placing an oval film between the dura and laminae [134]. At eight weeks, three of six polymer film sites had scar tissue that consisted of thin membranous threads, two required some blunt dissection, with sharp dissection only required at one site. Comparatively, only one control site could be dissected with mild blunt dissection, four required some sharp dissection, with one animal requiring extensive sharp dissection. MacroPore Biosurgery Inc. was acquired by Kensey Nash in June of 2007 [135], and this technology does not appear to be pursued by Kensey Nash.

The group that evaluated MacroPore's poly(lactide film) has evaluated a different bioresorbable epidural adhesion barrier from Biomet, Inc. [136]. Three films were evaluated in ovine laminectomy model: 20 μ m and 40 μ m 88:12 poly(lactide-co-glycolide) films, and a 40 μ m poly(lactide-co-caprolactone) film, Mesofol®. At eight weeks, the Mesofol® barrier film had superior results, where two of five animals had no adhesions present, two more had thin membranous threads, and one required blunt dissection to separate the laminectomy scar from the dura. In contrast, only one of seven control animals had scar adhesion composed of thin membranous threads, two required some blunt dissection, one required some sharp dissection, and three of seven required sharp dissection. In 2007, Mesofol® received 510k approval as a surgical sheet to reinforce soft tissues where weakness exists [137]. In Europe, this device is used to separate muscle tissue from other muscles, tendons, and nerves following surgery.

Collagen-based products designed for rapid dural repair may surprisingly be used for peridural adhesion prevention through a converse mechanism to the adhesion barriers

described above. Though these devices are used to accelerate the synthesis of a collagenous tissue to reinforce a compromised dura, Integra LifeSciences is evaluating the use of DuraGen Plus® for adhesion prevention following spine surgery [138]. The proposed mechanism of action has not been discussed in the literature, but one could conceive that the guided and rapid production of fibrous tissue above the peridural fat could approximately regenerate a ligamentum flavum-like tissue, protecting the fat. Zerris et al. evaluated the tissue response to DuraGen, a low density crosslinked collagen foam, Medtronic Neurosurgery's Durepair®, a high density non-crosslinked collagen product, and Bio-Vascular Inc.'s Dura-Guard Dural Repair Patch, a high density crosslinked collagen matrix [139]. The highly porous, low-density, crosslinked, collagen foam of DuraGen promotes rapid infiltration of host cells, predominantly fibroblasts, without accumulation and proliferation of macrophages [139, 140]. At one month, the non-crosslinked, suturable, collagen fiber matrix of Durepair® is populated with host fibroblasts and neovasculature without the proliferation of inflammatory cells. By three months, three of the five Durepair® matrices were completely vascularized, with complete vascularization and collagen remodeling observed at six months [139]. In contrast, the similarly dense, glutaraldehyde-crosslinked Dura-Guard device had insignificant cell infiltration through six months, and most of the permeating cells were inflammatory cells. Furthermore, an inflammatory response was observed at the surface of the dural graft [139].

The results of Zerris et al [139] imply that either low density and crosslinked or higher density and non-crosslinked collagen matrices have good potential to regenerate a ligamentum flavum-like tissue with minimal inflammatory response. The minimal

inflammatory response may be attributed to the highly conserved structure of collagen across species [141-144]. The low potential for immune-mediated rejection of a collagen-based device and the potential biofunctionality of such a device has promoted many investigations of decellularized tissues for wound repair and tissue engineering applications [145, 146].

Integra LifeSciences is evaluating the use of DuraGen Plus® for adhesion prevention following spine surgery in a US clinical trial [138]. This product received the CE mark for use in Europe in 2004 [147], so some clinical data has been accumulated regarding its performance. A 115-patient retrospective study in Italy demonstrated a significant reduction in peridural fibrosis, post-operative pain, and reoperation rate [148]. These trends were consistent as the patient population grew to 430 patients [149]. The excellent biocompatibility suggested by the highly conserved structure of collagen [141-144], demonstrated by Zerris et al. [139], and established by its safety history in more than 450,000 patients [150] may lead to rapid clinical acceptance of this product if adhesion prevention is demonstrated in the US clinical trial. However, the highly porous device lacks inherent barrier function.

Baxter International Inc. seems poised to offer a competing device that exploits this weakness, as evidenced by their recent, Feb 4th, 2010, patent application for a “non-porous, microscopically multilayered collagen foil biomatrix” [151], Figure 1.4. Preliminary data provided in the application indicates that the directed in-growth of repair cells is 10-15 times higher parallel to these microscopic layers compared to penetration through the microscopic layers. Unlike the Integra LifeSciences product, this device is not chemically crosslinked; rather, it is stabilized by “natural” crosslinking. This

“natural” crosslinking is enabled by an enzyme, likely lysyl oxidase [152], which converts lysine and hydroxylysine residues to aldehydes: allysine and hydroxyallysine [153]. These lysine derivatives are responsible for the physiological crosslinking of naturally produced collagen and are therefore more easily remodeled by the host than glutaraldehyde-crosslinked collagen devices. One would expect that this dense collagen device would have a mild tissue reaction with gradual integration with the host tissue.

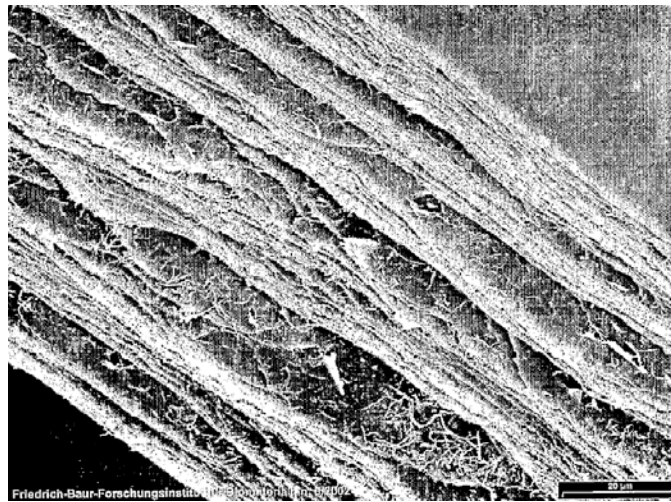


Figure 1.4. Scanning electron microscope image of Baxter Healthcare's TISSUDURA.

The safety and efficacy of the device as a cranial dura patch was evaluated in two recent clinical studies with good results [154, 155]. The substitute was used primarily in an underlay fashion with sutured margins sealed with fibrin glue. In the second study, a patient underwent a second surgery for schwannoma, permitting histological evaluation of the dural graft. Fibroblasts had grown into the multilayered construct by 40 days, and some neovascularization was present [154]. Perivascular accumulation of a moderate number of lymphocytes and foreign body giant cells (FBGCs) was evident. This multilayered collagen foil biomatrix has inherent barrier properties and is expected to uneventfully incorporate into the body through the physiological remodeling.

1.1.10 Synthesis of clinical literature review

Postsurgical adhesions compromise both abdominal surgery and neurosurgery. In the neurosurgical procedures of discectomy and decompressive laminectomy, peridural fibrosis tethers the dura and spinal nerves to musculoskeletal tissues. Mechanical stimulation of the spinal nerves or dura through these adhesions can reproduce sciatic pain similar to the pain experienced by the patient prior to their neurosurgical procedure. Reintervention is required in 5-18% of neurosurgical procedures. Reoperation and pain-relieving operations, such as epidural adhesiolysis, are a significant cost to the health care system. Patient discomfort and healthcare costs could both be reduced if a surgical technique or medical device was competent to reduce peridural adhesion formation subsequent to neurosurgery.

Postsurgical adhesions form after spinal surgery when a hematoma fills the laminectomy site, fibroblasts migrate from the erector spinae muscles, and the provisional fibrin matrix is remodeled to an adhesive scar. The most successful surgical technique to address peridural adhesion is to preserve the ligamentum flavum when approaching the peridural space. The LF is sutured closed, conserving one of the biological barriers to the expansion of the postsurgical hematoma, migration of fibroblasts, and formation of adhesive tethering. This technique shows promise, but a pivotal, multi-center, controlled clinical trial reporting direct analysis of radicular pain has not yet been proven the technique's effectiveness.

The effectiveness of the Gore-Tex ePTFE membrane has been demonstrated in a 66-patient clinical trial published in 1999. As the occurrence of peridural fibrosis was reduced from 91% to 24%, a reduction in the occurrence of radicular pain from 42% to

9% was observed. Though effective, FDA approval for peridural adhesion prevention does not seem to have been pursued, perhaps due to device permanence or the necessity of sutured fixation. Early clinical results of Integra LifeScience's DuraGen PLUS® demonstrate reductions in peridural fibrosis, pain, and reoperation rate. A U.S. clinical study is scheduled for completion in December of 2010, and if successful, Integra LifeScience's device may gain rapid clinical acceptance due to Neurosurgeons' familiarity with the product's use as a dural regeneration matrix.

With the removal of ADCON-L from the market in 2002, many approaches have been pursued, but each has a shortcoming. Of the products with clinical results, Integra LifeScience's DuraGen PLUS® is animal derived, cross-linked, fragile, and does not have inherent barrier properties, and Gore-Tex's ePTFE membrane is permanent and requires suturing. Other devices have been investigated but do not yet have clinical results. Baxter International Inc.'s TISSUDURA has barrier properties, but requires fixation and is animal-derived. Fidia Advanced Biopolymers' HyaloSpine® may not have sufficient duration in the implant site for this application. Biomet Inc.'s Mesofol® poly(lactide-co-caprolactone) film has demonstrated promising pre-clinical results, but previous film approaches have had poor implant site stability. Covidien's DuraSeal Xact™ PEO hydrogel may have promise in adhesion prevention, but its use is contraindicated in confined bony spaces, where swelling may compress the spinal cord or spinal nerves.

A successful alternative to DuraGen PLUS® in the prevention of epidural adhesion prevention must be as effective and additionally have inherent barrier properties, superior mechanical properties, and be synthetic and resorbable. To compete

with the rest of the developing technologies, the synthetic device should have superior conformance to underlying tissues than demonstrated by the MacroPore polylactide film, not swell, like Covidien's DuraSeal Xact™, and have tunable degradation and erosion properties, enabling the selection of an optimal resorption time.

In this dissertation, an electrospun, tyrosine-derived polycarbonate fabric will be evaluated for peridural adhesion prevention. The process of electrospinning is capable of producing nonwoven mats with pore sizes sufficiently small to exclude fibroblast penetration, yielding inherent barrier properties. The use of tyrosine-derived polycarbonates allows a broad range of device resorption times, mechanical properties, and thermal properties that will be leveraged throughout this work. Additionally, *cis*-4-hydroxy-L-proline will be delivered from the implant to directly inhibit the secretion of collagen near the device. The effectiveness of refined prototypes is evaluated against Integra LifeScience's DuraGen PLUS® in a rat laminectomy model.

1.2 The use of tyrosine-derived polycarbonates in medicine

Tyrosine-derived polycarbonates (TDPC) are an emerging category of structurally-related amorphous polymers that provide tunable degradation rate, water uptake, stiffness, and protein adsorption. The generalized formula for the polymer library is poly(I_{0,2}DTR-co-XX%I_{0,2}DT-co-YY%PEG_{MW} carbonate), where DT is desaminotyrosyl tyrosine, R represents the length of the alkyl ester pendent chain (e.g., E = ethyl ester, B = butyl ester, H = hexyl ester, O = octyl ester ...) [156]. The utility of a subset of this polymer library is investigated for the fabrication of an anti-adhesion device for neurosurgery. In this dissertation, ethyl ester pendent chains are utilized, and PEG molecular weight was fixed at 1000 (PEG_{1k}). The chemical structure of

poly(I_{0,2}DTE-co-XX%I_{0,2}DT-co-YY%PEG_{1k} carbonate) is depicted in Figure 1.5. The chemical formula is abbreviated I_{0,2}EXXY(1k), where XX represents the mol% of DT and YY represents the mol% of PEG_{1k} in random terpolymers of DTE, DT, and PEG_{1k}.

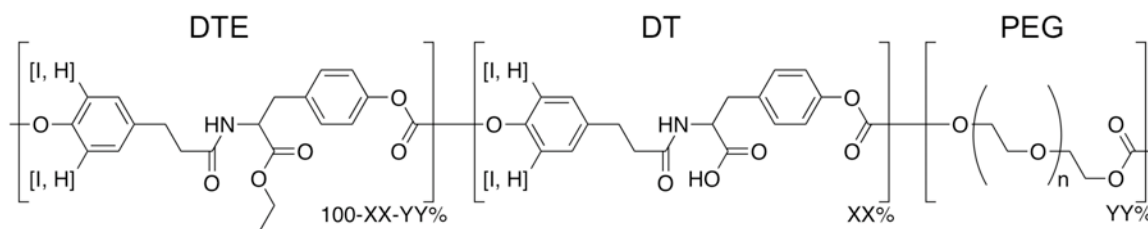


Figure 1.5. Chemical structure of poly(I_{0,2}DTE-co-XX%I_{0,2}DT-co-YY%PEG_{1k} carbonate). The polymer composition is a random distribution of the three monomers DTE, DT and PEG_{1k}.

TDPCs offer an alternative to the polyesters commonly used in biomedical applications (e.g., poly(lactic acid), poly(glycolic acid), poly(ϵ -caprolactone), polydioxanone and block, segmented, or random copolymers thereof). The listed homopolymers and copolymers offer a useful range of degradation rate, glass transition temperature, and stiffness. However, they do not possess the broad range of water uptake and protein repellency obtained by PEG-containing copolymers.

The terpolymer TDPC library permits tuning of physical and biological properties through varying the ratio of monomers and macromers during synthesis. Degradation rate and water content is elevated by increasing the mol% DT [157], increasing the mol% PEG_{1k} [158, 159], or reducing the alkyl ester pendent chain length [160]. Glass transition temperature is decreased with increasing mol% PEG_{1k} [156, 158, 159] and alkyl ester pendent chain length [161]. Surface hydrophobicity, as indicated by air-water contact angle, decreases with increasing mol% DT [161] and PEG_{1k} [159, 162-164]. And, Khan demonstrated that drug elution can be expedited through increasing PEG-content [158].

The physical characteristics of the polymers impact the biological response at the cell-biomaterial and protein-biomaterial interface. Tzampazis et al., Weber et al., Johnson et al., and Macario et al. each demonstrated that protein adsorption could be inhibited through copolymerization with PEG [162-165]. Marked reductions in cell attachment were observed and cell migration rate was sensitively modulated [162, 164]. However, iodine content and free carboxylic acid groups ($XX \neq 0$), complicated the effect of PEG [162, 163]. PEG copolymerization can also influence cell fate, as PEG_{1k} copolymerization at 0 or 3 mol% enhanced the osteogenic differentiation of human mesenchymal cells compared the 5 mol% PEG_{1k}. Finally, alkyl ester pendent chain length influenced the bone apposition versus fibrous encapsulation response to bone pins over a three year period [166].

The platform technology of the I₂EXXYY(1k) series of TDPCs offers a range of biological and physical properties to be leveraged in the evaluation of an anti-adhesion device for neurosurgery. The protein repellency effect of PEG_{1k} will be evaluated for its ability to modulate the inflammatory response to electrospun nonwoven fabrics. The modulation of polymer T_g through PEG_{1k} copolymerization will be utilized to fabricate flexible and tough prototypes with good shape retention properties.

1.3 Introduction to the field of electrospinning

Electrospinning is a fabrication technique capable of producing a nonwoven mat of ultrafine polymeric fibers from a polymer solution or melt that is accelerated through an electric field. These polymeric fabrics have been studied in the fields of tissue engineering and medical devices because of their high surface area to present biological cues, their architectural similarity to extracellular matrix, and the ease of incorporating drug delivery functionality to the devices [167, 168].

The fabrication technique of electrospinning is not new, but its application to medical device fabrication could only be considered recently. Anton Formhals described the “electrical spinning” of a continuous fiber band from a solvent in 1934 [169]. The device depicted in this US patent used a serrated spinning wheel to draw polymer solution from a bath and electrostatically spin it to a collector for winding into a fiber. His 1938 patent featured the more recognizable spinning from metallic nozzles to which polymer solution was advanced from a reservoir [170]. In 1943, Fred Manning described the direct fabrication of a non-woven mat from electrostatically spun fibers, rather than winding filaments into a fiber [171]. The technology didn’t find application in medical device research until the Reneker group demonstrated the electrospinning of more than 20 polymers into fibers with diameters ranging from 40 nm to 5 μ m and suggested the medical application of a wound dressing [172, 173]. Those papers were published in 1995 and 1996, and the number of publications has expanded dramatically since then [174], see Figure 1.6. The widespread interest in research laboratories is likely due to the low device cost (< \$5,000) and the size and shape similarity of the electrospun fibers with collagen fibrils (10-500 nm) and fibers (1-20 μ m) [175]. This architectural similarity is

attractive, for the presentation of biological cues on biomimetic scaffolds enhances the cells' sensitivity to those cues [167, 176].

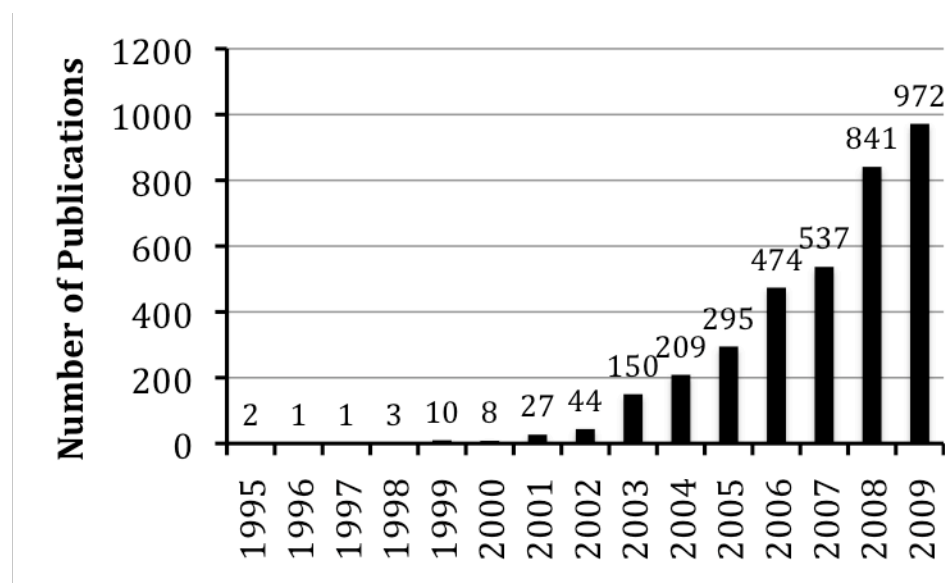


Figure 1.6. Number of publications per year including “electrospinning” or “electrospun” in the ISI Web of Knowledge database

The medical device industry may be prepared for the release of a commercial electrospun product. The dramatic expansion of publications noted above has built a substantial body of theoretical [177-181] and empirical [182-190] knowledge regarding electrospinning. Most of the publications related to electrospun fibers are for their exploration as tissue engineering scaffolds, small molecule and biological delivery devices, wound dressings, tissue-engineered vascular grafts, and abdominal adhesion devices as summarized in a number of reviews [168, 191-202]. In addition to the wealth of knowledge on the production and application of these nonwoven mats, the ability to fabricate them on a large scale has emerged through interactions with either Donaldson Company Inc. or Zeus Incorporated. Donaldson Company Inc. produces over 10,000 m² of electrospun fibers for the air filtration industry [203], and they partnered with SurModics Inc. to launch a synthetic extracellular matrix, Ultra-Web®, for the

biomedical engineering field in 2006 [204]. Additionally, bioabsorbable and fluoropolymer extrusion supplier Zeus Inc. has presented electrospun samples at Society for Biomaterials Conference exhibitions and is interested in cooperatively developing electrospun fabrics for medical applications [205]. The emergence of large-scale manufacturing capabilities may enable the commercialization of successful electrospinning-based research endeavors.

Two prominent research groups have attempted to bring electrospun products to the market. The Reneker group has developed a wound dressing that releases nitric oxide to aid the healing of diabetic wounds or to treat cutaneous leishmaniasis, and the Chu and Hsiao group has developed an antibiotic-releasing membrane for the prevention of abdominal adhesions. The Reneker technology consists of poly(ethylenimine) electrospun fibers that are modified to have diazeniumdiolate functionality on their surface, such that they release nitric oxide at a half life from 6-30 hours at pH 7.4 and 37°C [206-208]. The technology was found to be “not effective enough” in treating cutaneous leishmaniasis, prematurely terminating a phase III clinical trial [209]. However, the therapy is continuing to be evaluated in a phase III clinical trial for the treatment of diabetic foot ulcers [210]. The ability to bring an electrospun material to a phase III clinical trial means that the group was able to find a partner to manufacture the product in a reproducible and traceable way, according to current good manufacturing practices. The group’s Coalescence Filtration Nanomaterials Consortium’s membership consists of five filtration companies: Ahlstrom, Donaldson Company, Cummins Filtration, Parker Hannifin Corporations, and MemPro Ceramics [211].

Benjamin Chu and Benjamin Hsiao have attempted to commercialize an abdominal adhesion prevention device through a Stony Brook University's startup company STAR Bioscience, previously STAR Inc. [212]. They demonstrated that an electrospun membrane composed of 85:15 PLGA, PEG-b-PLA diblock copolymer, and an antibiotic (Cefoxitin Sodium) was capable in preventing abdominal adhesions in a rat abraded-cecum abdominal adhesion model [213]. Across three studies, adhesions occurred at a rate of 78% in control animals, 45% of PLGA membranes, 28% of PLGA membranes with PEG-b-PLA, and 25% of animals treated with PLGA membranes plus the drug [213]. The membranes reduced the occurrence of adhesions to zero of twelve rats when the antibiotic was combined with the block copolymer in the PLGA membranes [213, 214]. The presence of the copolymer reducing the drug's burst-release from 70% to 50% and extended the delivery of the therapeutic to one week [215]. Though a 2002 news article reports that a reduction in the occurrence and severity of abdominal adhesions had been demonstrated in 200 rats [212], I have not been able to identify any clinical trials for this material.

The success of the Chu group in preventing abdominal adhesions is promising for the application of a similar technology in the prevention of peridural adhesions. The market of abdominal adhesion prevention may be more difficult to enter, for there are already products with established performance for that application, notably Genzyme Corporation's SeparafilmTM. Since there are no FDA-approved adhesion prevention devices for discectomies or decompressive laminectomies, a new peridural adhesion prevention device may be easier to introduce. Additionally, the inhibition of peridural adhesions may be more attainable because the site is more confined, there is less relative

motion of the tissues, the device does not need to facilitate regeneration of a mesothelium, and the peridural fat will assist in inhibiting the progression of fibrous tissue to the dura and spinal nerves.

There are two significant difficulties to be overcome in introducing an electrospun membrane: manufacturing the devices in large batches under cGMP conditions, and removing the residual solvents utilized in solution electrospinning. This dissertation will address the presence of residual solvents in fabricated polymer samples. The topic of manufacturability will be discussed in the final recommendations, but the actual scale up is considered outside the scope of the work. The success of Reneker's group in reaching the clinic and the demonstrated collaborative efforts of Donaldson Company and Zeus Inc. indicate that electrospun medical devices are attainable.

The removal of residual solvents is significant, and it will be addressed in this dissertation. Most electrospun medical device prototypes are produced by solution spinning, rather than melt spinning. A preference for solution spinning is likely due to the room-temperature processing conditions, which ease the incorporation of drugs, peptides, and proteins, and the lower costs associated with prototype fabrication at the laboratory scale. However, the solvents used in solution spinning are often toxic, see Table 1-3. The FDA Guidance for Industry recommends that these solvents be present in concentrations in the hundreds of PPM or less [216]. Reducing the level of residual solvents to this level may be difficult, for most of the solvents listed in Table 1-3 can hydrogen bond with the device constituents, and dimethylformamide, pyridine, and dioxane are particularly high-boiling solvents. Chu's group fabricated their adhesion-prevention device from dimethylformamide (DMF) with removal of residual solvent by

exposing the device to vacuum at room temperature for one week [215, 217]. Thermogravimetric Analysis (TGA) was used to confirm removal of DMF, but this method is not sensitive enough to detect residual solvents at the 100 ppm level. It would be preferable to use a solvent that is considered to have low toxic potential.

Table 1-3. Solvents of typically used in electrospinning [201, 202] that should be limited due to known or suspected inherent toxicity [216, 218]. *THF is listed as a solvent with “low toxic potential,” but when mixed with DMF, the solvent system contains “solvents to be limited.” [216] Abbreviations: DCM, dichloromethane; THF, tetrahydrofuran; DMF, N,N-dimethylformamide; HFIP, 1,1,1,3,3,3-hexafluoroisopropanol; TFE, 2,2,2-trifluoroethanol; PCL, poly(ϵ -caprolactone); PPC, poly(propylene carbonate); PLA, poly(lactic acid); PGA, poly(glycolic acid); PLGA, poly(lactide-co-glycolide); PHBV, poly(3-hydroxybutyrate-co-3-hydroxyvalerate); PEG-b-PLA, poly(ethylene glycol)-b-poly(lactic acid) diblock copolymer; PLCL, poly(lactide-co- ϵ -caprolactone); HA, hyaluronic acid; PEO, poly(ethylene oxide); PDO, poly(dioxanone); PEUU, poly(ester urethane)urea.

Solvent	Polymers	Permitted Daily Exposure [mg]	Concentration [ppm]
Chloroform	PCL, PPC, PLA, PLGA, PHBV, PEG-b-PLA, PLA/PCL	0.6	60
DCM	PLA, PLGA, PLCL, PCL, poly(DTE carbonate), poly(ϵ -caprolactone-co-ethyl ethylene phosphate)	6	600
THF/DMF*	PLGA	8.8 (DMF)	880 (DMF)
DMF	Zein, HA, PLA, PLGA, PCL, PEO, poly(ethylene glycol-co-lactide)	8.8	880
HFIP	Collagen, Elastin, Gelatin, Fibrinogen, Chitin, Chitosan, HA, PLA, PGA, PLGA, PCL, PLCL, PDO, PEUU	Unknown, Reduced respiration rate to 50% at 165 ppm in rats [218]	
TFE	Collagen, Gelatin, Chondroitin Sulfate, PCL	Unknown, Reduced respiration rate to 50% at 11,000-23,000 ppm in rats [218]	
Methanol	PCL, Silk fibroin	30	3000
Pyridine	PLA	2	200
Dioxane	PLA	3.8	380

The reviews of Xie et al. and Sill et al. identified some polymers that can be electrospun from solvents of low toxic potential, Table 1-4 [201, 202, 216]. Of the polymers on this list, only poly(ethylene-co-vinyl alcohol) and poly(lactide-co- ϵ -caprolactone) are organic, water-insoluble, synthetic polymers, making them candidate materials. When exposed to humidity, poly(ethylene-co-vinyl alcohol) and poly(lactide-co- ϵ -caprolactone) have T_g s well below body temperature (-10 to -60 °C) [219, 220], so devices fabricated from these polymers would have poor dimensional stability due to polymer chain mobility. A poly(ethylene-co-vinyl alcohol) or poly(lactide-co- ϵ -caprolactone) electrospun mat's fine features may change during ambient storage, the device could adhere to itself or its packaging, and it could permanently deform under routine handling. There is a need to find a method for electrospinning high- T_g polymers – polymers would remain glassy under physiological conditions – from solvents with low toxic potential.

Table 1-4. polymers electrospun [201, 202] from “solvents with low toxic potential” according to the FDA Guidance for Industry document [216].

Polymer(s)	Solvent(s)
poly(ethylene-co-vinyl alcohol)	Isopropanol/water
Collagen/poly(ethylene oxide)	10 mM HCl pH 2.0
poly(lactide-co- ϵ -caprolactone)	Acetone
poly(ethylene oxide)	Water or ethanol
Dextran	Water
Chitosan	90% Acetic acid
Chitosan/poly(vinyl alcohol)	Acetic acid
Chitosan/poly(ethylene oxide)	Acetic acid/dimethyl sulfoxide
Gelatin	Formic acid
Gelatin/poly(vinyl alcohol)	Formic acid
Gelatin/siloxane	Acetic acid/ethyl acetate/water
Sodium alginate/poly(ethylene oxide)	Water

The technique of electrospinning has promise for producing a barrier to scar progression and adhesion formation following laminectomy. Electrospun membranes

with antibiotic delivery have prevented rat abdominal adhesions in a cecal adhesion model, and the Reneker group has brought a device to clinical trials for two different indications. Zeus Inc. and Donaldson Company represent potential industrial partners to scale up prototypes that perform well in the laboratory. This dissertation will draw upon the body of theoretical and empirical knowledge of electrospinning to create a synthetic, biodegradable, electrospun, tyrosine-derived polymeric fabric with inherent barrier properties and sufficient mechanical properties. The electrospinning of tyrosine-derived polycarbonates and their barrier functionality will be described. The use of biodegradable surfactants to enable electrospinning from acetic acid is discussed, and the superior mechanical properties of composite electrospun devices will be illustrated.

1.4 Introduction to the anti-fibrotic, *cis*-4-hydroxy-L-proline

The laminectomy scar is primarily composed of collagen, which is synthesized and remodeled by fibroblasts and macrophages during the wound-healing response [8, 9]. To directly inhibit collagen synthesis, an antifibrotic, *cis*-4-hydroxy-L-proline (cHyp), will be delivered locally. The process of collagen synthesis, destabilizing effect of cHyp, and historical application of cHyp are discussed below.

The collagen molecule is composed of three polypeptide strands, pro- α chains, which form left-handed helical domains. Each pro- α chain contains approximately 1000 amino acids, and the triple-helical domain of the protein follows a X-Y-Glycine repeating structure, where approximately one-third of the X positions are proline and one-third of the Y positions are hydroxyproline [221]. Hydroxyproline residues result from the posttranslational modification of proline by hydroxylases in the rough endoplasmic reticulum [221, 222]. These hydroxyproline residues are essential to the stability of the

collagen triple helix [223]. Rosenbloom et al. found the melting temperature of collagen synthesized by chick embryonic tendon cells to be slightly above body temperature, 37.9 °C [224]. When proline hydroxylase was inhibited by α,α' -dipyridyl, conversion of proline to hydroxyproline decreased from 44% to <1% and the melting temperature decreased to 23.5 °C.

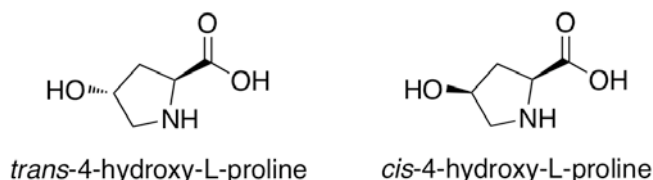


Figure 1.7. The orientation of the hydroxyl group varies between the *cis* and *trans* isomers of hydroxy-L-proline

The presence of *trans*-4-hydroxy-L-proline, tHyp, in the Y position favors the *trans* conformation of peptide bonds, which is required for triple helix formation [225]. The equilibrium constant, $K_{trans/cis}$, is 6.1 for tHyp, 4.6 for proline, and only 2.4 when cHyp is substituted in the Y position [225]. Proline can obtain either an *UP* or *DOWN* pucker, introducing some greater conformational flexibility, while tHyp strongly favors the *UP* conformation, and cHyp favors the *DOWN* conformation [226]. When Vitagliano et al. surveyed 478 protein chains from the Protein Data Bank, they found 178 proline residues where the peptide bond with the preceding residue was in the *cis* conformation; 145 of these proline residues assumed the *DOWN* pucker conformation [227]. Taken together, these studies indicate that tHyp favors the *trans* conformation of peptide bonds that stabilizes triple helix formation, while cHyp favors the *cis* conformation of peptide bonds, which destabilizes triple helix formation. This “inductive effect,” driven by the electronegativity of the hydroxyl group or a substituted fluorine, has been convincingly

demonstrated by the Raines laboratory at the University of Wisconsin [225, 228-230], causing theories of stabilization by a hydrogen bonding network to fall out of favor [231].

When the triple-helical conformation of collagen is disrupted, collagen secretion is decreased and its degradation is enhanced. Collagen pro- α chains are secreted from two intercellular pools, where ~70% is secreted at a half time of 14 minutes, while the remainder is secreted at a half time of 115 minutes [232]. When 1.53 mM cHyp was present in the media, the entire population of collagen pro- α chains was secreted at a half-time of ~130 minutes [233]. These kinetics were indistinguishable from those observed when 0.3 mM α,α' -dipyridyl was used to inhibit triple helix formation through inhibition of prolyl hydroxylase. The results suggest that non-helical collagen is secreted at one-tenth the rate of triple-helical collagen. The “defective” collagen accumulates in the rough endoplasmic reticulum [234] and is degraded intracellularly by lysosomal proteases [235]. Non-helical collagen is susceptible to degradation by general proteases intracellularly and extracellularly, while helical collagen are highly resistant to general proteases (e.g., pepsin), for their peptide bonds are located in the interior of the helix [223].

Because cHyp can decrease secretion of collagen and enhance the degradation of any secreted collagen, it has been used as an antifibrotic agent. It has been used to inhibit vitreoretinopathy in a rabbit model through either direct injection (20 or 60 μ g doses every two days for the first week) [236] or through delivery from two PLGA scleral plugs (3.0 mg cHyp total) [237]. The Kohn laboratory has synthesized a poly(PEG-Lysine) carrier for cHyp, where cHyp is grafted to Lysine by either amide or ester bonds [238, 239]. Both poly(PEG-lysine-g-cHyp ester) and poly(PEG-lysine-g-cHyp amide) were

competent to inhibit the proliferation of fibroblasts and smooth muscle cells on uncoated tissue culture plates, and poly(PEG-lysine-g-cHyp amide) reduced collagen accumulation in a poly(vinyl alcohol) sponge by 33% in a rat subcutaneous pocket at two weeks [240]. The same polymers also inhibitive pulmonary fibrosis in rats exposed to hypoxic conditions for 7 days [241, 242]. Impressively, 0.6 mg poly(PEG-lysine-g-cHyp) delivered from an osmotic minipump was able to partially reverse pulmonary hypertension after 7-day exposure to hypoxia [242]. Eventhough cHyp can modify the structure of proteins, liver toxicity was not noted in a clinical anticancer study at doses of 8 grams cHyp per day, 4 days per week, over three weeks [243]. The doses used to obtain a local antifibrotic effect are significantly lower.

Delivery of cHyp was used to prevent lyzed abdominal adhesions from reforming in an adult rabbit model [244]. Poly(PEG-Lys-g-cHyp) was delivered to the lyzed adhesion site via incorporation into hyaluronic acid microspheres, which were loaded into a PEG-b-PLA phase separated gel, Figure 1.8. In control animals, 88% of lyzed adhesions reformed at three weeks. In PEG-b-PLA treated animals, 83% of lyzed adhesions reformed, while only 14% of lyzed adhesion reformed in animals treated with cHyp-loaded gels. This study demonstrates that controlled delivery of cHyp can enhance adhesion prevention.

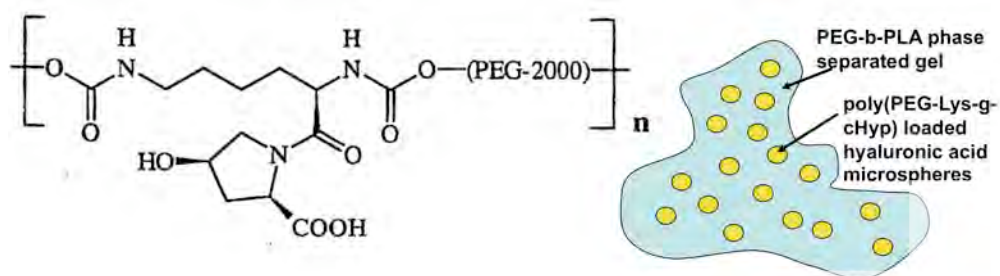


Figure 1.8. poly(PEG-Lys-g-cHyp) and its formulation in hyaluronic acid microspheres, as described for the prevention of abdominal adhesions [244].

1.5 Hypotheses

In the development of an anti-adhesion device for neurosurgery, the following hypotheses were evaluated:

- (1) Cell-impermeable nonwoven fabrics can be fabricated through electrospinning
- (2) PEG_{1k} incorporation will reduce protein adsorption to biomaterial surfaces and reduce the inflammatory response to implanted biomaterials
- (3) *cis*-4-hydroxy-L-proline delivery from polymeric implants can be controlled through precursor molecules
- (4) Cell-impermeable nonwoven fabrics provide superior adhesion prevention, compared to polymer films.
- (5) Controlled delivery of *cis*-4-hydroxy-L-proline enhances the adhesion prevention performance of anti-adhesion devices for neurosurgery.

2 Materials and Methods

2.1 Materials

2.1.1 Polymers

The polymers used in this dissertation were synthesized by members of the New Jersey Center for Biomaterials, Table 2-1. The polycondensation reaction of diphenols and PEG_{1k} progressed by triphosgene in the presence of pyridine in dichloromethane (DCM), consistent with the recent publication of Magno et al. [245].

Table 2-1. Physical properties of polymers used in this dissertation. T_g was determined by differential scanning calorimetry at a heating rate of 10 °C/min. The weight-average molecular weight was determined by gel permeation chromatography in DMF+0.1% trifluoroacetic acid relative to polystyrene standards

Polymer	Code	Lot #	T_g	MW [kDa]	PD
poly(DTE carbonate)	E0000	Isochem 052	95	210	1.5
poly(DTE-co-10%DT-co-8%PEG _{1k} carbonate)	E1008(1k)	LS072905-09-80	46	171	1.4
poly(I ₂ DTE-co-10%I ₂ DT carbonate)	I ₂ E1000	KP083105-02-05	141	221	1.4
poly(I ₂ DTE-co-10%I ₂ DT-co-8%PEG _{1k} carbonate)	I ₂ E1008(1k)	LS080105-09-82	86	185	1.4
poly(I ₂ DTE-co-10%I ₂ DT-co-12%PEG _{1k} carbonate)	I ₂ E1012(1k)	KP090105-02-09	57	216	1.5
poly(DTE-co-10%DT-co-0.5%PEG _{1k} carbonate)	E1000.5(1k)	MDL052909n7p49	95	245	1.7
poly(DTE-co-12%PEG _{1k} carbonate)	E0012(1k)	MDL-043007n2p94	33	225	1.4
poly(DTE-co-12%DT-co-24%PEG _{1k} carbonate)	E1224(1k)	MDL-092308n6p8	-4	153	1.5

Additionally, a polymer of PEG and Lysine grafted with cHyp, poly(PEG-Lys-g-cHyp), in Hyaluronic acid (HA) microspheres was provided by James Pachence of Vectramed Inc. The HA microspheres (Lot V125A) had a 10-60 µm diameter, and 30% of the lysines were activated with cHyp. These microspheres were used in an exploratory rat laminectomy study to test the effect of cHyp alone.

2.1.2 Chemicals for synthesis and fabrication

Table 2-2. Chemicals used for synthesis of cHyp precursors and tHyp alkyl ester HCl salt degradable surfactants

Molecule	Catalog number	Supplier	Location
Z-cHyp	C-3200	BACHEM	King of Prussia, PA
cHyp	F-1025	BACHEM	King of Prussia, PA
N-Boc- <i>cis</i> -Hyp	654019-1G	Aldrich	St. Louis, MO
N-Boc- <i>trans</i> -Hyp	04-12-0104	EMD Chemicals	Gibbstown, NJ
1-butanol	537993-4L	Aldrich	St. Louis, MO
1-hexanol	H13303-4L	Aldrich	St. Louis, MO
1-octanol	11261-5	Aldrich	St. Louis, MO
thionyl chloride	320544-2.5L	Aldrich	St. Louis, MO
butyl chloroformate	184462-100G	Aldrich	St. Louis, MO
octyl chloroformate	252808-5G	Aldrich	St. Louis, MO
Pyridine	P368-500	Fisher Scientific	Fair Lawn, NJ
dimethylaminopyridine (DMAP)	14827-1000	Acros Organics	Morris Plains, NJ
dicyclohexylcarbodiimide (DCC)	D80002-100G	Aldrich	St. Louis, MO
Palladium on Barium Sulfate	195060500	Acros Organics	Morris Plains, NJ
4 N HCl in dioxane	345547-100ML	Aldrich	St. Louis, MO

2.1.3 Solvents and other materials

The following solvents were utilized for electrospinning, synthesis, or high performance liquid chromatography (HPLC): DCM, acetic acid, ethyl acetate, HPLC grade methanol, and diethyl ether (Fisher Scientific, Fair Lawn, NJ); chloroform, trifluoroacetic acid (TFA), and HPLC grade water (Acros Organics, Morris Plains, NJ); HFIP, HPLC grade acetonitrile, HPLC grade water + 0.1% TFA and dimethyl sulfoxide- d_6 (Aldrich, St. Louis, MO); and DMF and THF (EMD Chemicals, Gibbstown, NJ). Additionally, a ninhydrin assay for hydroxyproline content was performed. cHyp was eluted into PBS (Dulbecco's PBS, Aldrich, St. Louis, MO), and the eluent was evaluated with a working solution containing ninhydrin (Aldrich, St. Louis, MO), ethylene glycol (Fisher Scientific, Fair Lawn, NJ), tin(II) chloride (Acros Organics, Morris Plains, NJ), and sodium acetate (Aldrich, St. Louis, MO).

2.1.4 Electrospinning Device

An electrospinning facility was established at the NJCBM. The critical electrospinning components are listed in Table 2-3. Additionally, the collector frame was fabricated from ½” lexan sheet, steel and aluminum plate, threaded rods, ball bearing slides, a ball bearing conveyor roller, pulleys and a belt drive. The device was installed in a class 10,000 cleanroom to minimize contamination of electrospun nonwoven fabrics.

Table 2-3. Components of electrospinning device

Component	model	Supplier	City
High voltage power supply	DS30PN-5W	Gamma High Volgate Research	Ormond Beach, FL
Variable voltage DC power supply	1627A	BK Precision	Yorba Linda, CA
Pittman 24 V DC motor	14204S005	Pittman	Harleyville, PA
1 Hz 115 V AC gear motor	6142K51	McMaster Carr	Robbinsville, NJ
Syringe pumps	780100	KD Scientific	Holliston, MA
5 mL Sterile luer-lock disposable syringes	NORM-JECT	Henke Sass Wolf	Tuttlingen, Germany
Blunt tipped stainless steel needles (19 and 23 gauge)	91019 and 91023	Hamilton company	Reno, NV
20 gauge x 3' Teflon tubing	86510	Hamilton company	Reno, NV
Male luer lock to male luer lock connector	86511	Hamilton company	Reno, NV

2.2 Fabrication

2.2.1 Solvent cast films

Polymer films containing either cHyp or cHyp precursors were fabricated by solvent casting from HFIP. The polymer solutions were 2-3% wt/vol E0000, I₂E1008(1k), or E1004(1k) in HFIP with a 1:5 loading of cHyp or cHyp precursor per polymer mass. The polymer solution was poured into a 60 cm Teflon dish and allowed to evaporate in the fume hood overnight. The film was demolded from the dish and dried in a vacuum oven for 12 hours at 40 °C.

2.2.2 Compression molded films

Compression molded films were pressed from either as-synthesized polymer powders or films (E1224(1k)) or electrospun scaffolds. A press temperature, T_p , is chosen based upon the T_g of the polymer, typically ~ 40 °C above T_g . The carver press (model 4122, Carver Inc. Wabash, IN) and custom-designed steel mold (REVA mold) are preheated to T_p for at least 45 minutes. The polymer was placed between steel plates lined with 12 μm thick Teflon films (American Durafilm, Holliston, MA). Steel shims between 50 and 150 μm in thickness were also placed between these Teflon films. The steel plates and polymer were placed into the REVA mold, and the following pressing protocol was performed: T_p no pressure, 5 minutes; ramp 15,000 lbf, 1 minute; hold 15,000 lbf, 1 minute; release pressure; remove steel plates and film; cool on benchtop; release film from mold. This procedure consistently produced high quality films of uniform thickness. Any deviation or modification of the procedure is noted in the subsequent text.

2.2.3 Electrospinning

Solution electrospinning was performed using the custom-designed apparatus described in sections 2.1.4 and 3.1. A concentrated, typically 5-25% wt/vol, polymer solution was prepared in specified solvent(s). Solution viscosity is the primary factor in determining scaffold architecture, so efforts were made to ensure accuracy of solution preparation: Solvent addition to a 20 mL scintillation vial was performed gravimetrically to prevent underestimation of solvent volume when using high vapor pressure solvents. Polymer was weighed to within 0.5% accuracy and transferred to the vial. It was determined that concentrated polymer solutions may not reach equilibrium until 6 hours,

so polymer solutions were allowed to equilibrate at room temperature with agitation for a minimum of 12 hours. The solution was removed from agitation for a minimum of 2 hours before electrospinning.

The polymer solution was transferred to a NORM-JECT syringe and advanced through the tubing, connector, and stainless steel needle. The solution flowrate (Q , typically 0.1-6 ml/hr) was controlled via syringe pump, and the electrical potential of the needle (NP, typically 6 - 30kV) and mandrel collector (CP, typically -6 - 0 kV) was regulated by the high voltage power supply. Fibers were spun over a distance of 10 - 24 cm, and a nonwoven fabric was collected on an aluminum foil wrapped collector. A mass of 200 - 300 mg was typically electrospun into a 7 x 13 cm fabric. The fabric was left on the aluminum backing and packaged in sterilization pouches (Fisher Scientific, Fair Lawn, NJ). After vacuum degassing, the electrospun fabric was either heat treated or sterilized.

2.3 Characterization

2.3.1 Determination of T_g and T_m by differential scanning calorimetry

Polymers, electrospun fabrics, and synthesized surfactants and precursors were characterized by differential scanning calorimetry (DSC); a DSC 823e (Mettler Toledo, Columbus, OH) with autosampler was utilized for sample analysis. Approximately 5 mg samples were transferred to aluminum sample pans (Mettler Toledo, Columbus, OH), crimp sealed, and pierced. The autosampler loaded the test pans and executed the appropriate temperature scan, Table 2-4. In polymer-containing samples, the T_g was measured on the second heating curve the ASTM midpoint method. When samples contained both polymer and hydroxyproline alkyl ester HCl salts, the first heating did not

surpass the T_m of the surfactant or drug precursor. The T_m of hydroxyproline alkyl ester HCl salts were indicated by the peak of the melting curve.

Table 2-4. DSC temperature scans by sample type

Polymeric sample		Polymer + hydroxyproline alkyl ester HCl salt		Hydroxyproline alkyl ester HCl salt	
1	equilibrate at -25 °C	1	equilibrate at -25 °C	1	equilibrate at 25 °C
2	ramp to 160 °C an 10 °C/min	2	ramp to 115 °C an 10 °C/min	2	ramp to 200 °C at 10 °C/min
3	equilibrate at 160 °C	3	equilibrate at 115 °C		
4	ramp to -25 °C at -10 °C/min	4	ramp to -25 °C at -10 °C/min		
5	equilibrate at -25 °C	5	equilibrate at -25 °C		
6	ramp to 200 °C at 10 °C/min	6	ramp to 200 °C at 10 °C/min		

2.3.2 Retention time of hydroxyproline alkyl ester HCl salts by HPLC

The characterization of cHyp precursor starting materials, intermediate products and final products was performed by HPLC. The instrument consisted of a Waters 2695 HPLC unit with a Waters Atlantis® T3 3 μ m 4.6x100mm column (Part 18003728, Waters, Milford, MA), Waters 2487 dual wavelength UV/Vis absorbance detector, and a Sedex evaporative light scattering detector (ELSD, model 75, Sedex Inc., Sedex, France). Two methods were used, each with a flowrate of 0.8 mL/hr. The first method was used to quickly evaluate more hydrophilic molecules, such as cHyp and cHyp lactone, and the second method was used to more completely resolve hydrophobic molecules.

Table 2-5. HPLC methods utilized to characterize hydrophilic (method #1) and hydrophobic (method #2) molecules. All gradients are linear. Mobile phase A is HPLC grade water + 0.1% TFA; mobile phase B is acetonitrile + 0.1% TFA

Method #1		Method #2	
0-2 minutes	100% A	0-2 minutes	100% A
2-6 minutes	gradient to 100% B	2-10 minutes	gradient to 100% B
6-8 minutes	100% B	10-14 minutes	100% B
8-9 minutes	gradient to 100% A	14-15 minutes	gradient to 100% A
9-10 minutes	100% A	15-16 minutes	100% A

2.3.3 Controlled release of *cis*-4-hydroxy-L-proline by ninhydrin assay

cHyp was eluted from solvent cast films and electrospun fabrics into PBS. The hydroxyproline content of the eluent was analyzed by a microplate ninhydrin assay adapted from Starcher [246]. Three solutions were prepared separately to comprise the working reagent: (A) 200 mg ninhydrin in 7.5 mL ethylene glycol, filtered; (B) 30 mg tin(II) chloride in 300 μ L ethylene glycol, filtered; (C) 16.4 grams sodium acetate in 10 mL acetic acid, addition of deionized water up to a volume of 50 mL. The working reagent consisted of 7.5 mL of solution A, 250 μ L of solution B, and 2.5 mL solution C.

Samples were analyzed by absorbance at 440 nm in a spectrophotometer (PowerWaveX spectrophotometer, Bio-Tek Instruments, Winooski, VT). 100 μ L of eluent was transferred to a well of a 96-well microtiter plate (Corning[®] Costar[®], Lowell, MA). Once all samples were transferred to the plate, 100 μ L of working reagent was transferred and mixed in each well of the microtiter plate by multichannel pipette. The Carver press was used to heat the plate to 100 °C for 8 minutes, which deviates from Starcher, who floated the plate on boiling water [246]. The plate was removed, allowed to cool for 10 minutes, and absorbance at 440 nm was evaluated. This method was useful over a range of 0.05 – 1.0 mg/mL hydroxyproline in PBS.

2.3.4 Quantification of fiber diameter by scanning electron microscopy

The fiber diameter of electrospun fabrics was quantified from scanning electron microscopy (SEM) images. Samples were mounted on aluminum studs, sputter coated with gold and palladium at 30 mA for 120 seconds (Blazers SCD 004 sputter coater), and imaged on an AMRAY 1830i at a 20 kV acceleration potential. Digital images were imported into NIH ImageJ and either 60 or 100 fiber widths were measured in pixels and converted to microns through measurement of the image's scalebar. The fiber diameter was expressed as mean \pm 95% C.I., unless otherwise noted. Where cell-laden fabrics were imaged by SEM, the cells were first fixed in 4% paraformaldehyde in PBS, rinsed with copious volumes of DI water, blotted dry with a Kimwipe[®], and dried under vacuum at room temperature.

2.3.5 Cell viability with exposure to tHyp alkyl ester HCl salts

Confluent human dermal fibroblasts (HDFs) (passage 8-11) were propagated in Dulbecco's modified eagle's medium (DMEM) with 10% fetal bovine serum (FBS) and 100 units penicillin and 0.1 mg streptomycin per mL. To rapidly obtain confluent cultures, HDFs were seeded into 96-well plates at 30,000 cells per well or $\sim 100,000$ cells/cm² in serum-free media consisting of DMEM supplemented with 50 μ g/mL L-ascorbic acid and antibiotics. All cell-culture reagents were supplied by Sigma-Aldrich (St. Louis, MO). At 24 hours, the medium was changed to the test media, which consisted of the serum-free media plus 0.5, 1.5, or 4.0 mM tHyp butyl ester HCl or tHyp octyl ester HCl. 48 hours later, "dead cells" were stained with 4 μ M ethidium homodimer-1 (Molecular Probes, Eugene, OR) for 30 minutes at room temperature.

Cells were fixed with 4% paraformaldehyde, permeablized with 0.1% triton X-100, and cell nuclei were stained with 1 µg/mL DAPI (Molecular Probes).

Viability of confluent cell cultures was evaluated by counting the number of cell nuclei positive for ED-1, “dead cells” versus the number of nuclei positive for DAPI, “all cells”. A Nikon Eclipse TE-2000-S microscope was used to obtain digital images, which were quantified using NIH imageJ. Cells were counted using the protocols outlined in Table 2-6.

Table 2-6. Cell counting protocols used in NIH ImageJ to count dead and all cells.

“dead” cells, Ethidium Homodimer-1 positive		“all” cells, DAPI positive	
1	despeckle	1	despeckle
2	subtract background (rolling ball radius 10 pixels, disable smoothing)	2	unsharp mask (sigma 2.0, mask weight 0.9)
3	remove bright outliers (radius 5, threshold 5)	3	despeckle
4	convert to 8-bit grayscale image	4	subtract background (rolling ball radius 40 pixels, sliding paraboloid)
5	threshold at intensity of 25	5	convert to 8-bit grayscale image
6	analyze particles with area > 8 pixels with any circularity	6	threshold at intensity of 40
		7	analyze particles with area > 8 pixels with any circularity

2.3.6 Cell permeability of electrospun fabrics

Transgenic GFP rat dermal fibroblasts were obtained from Joanne Babiarz of the Keck Center for Collaborative Neuroscience. Using 24-well plates, the fibroblasts were plated at 10,000 cells/cm² onto electrospun fabrics in DMEM with 10% FBS and 100 units penicillin and 0.1 mg streptomycin per mL. At 5 days, the cells were fixed with 4% paraformaldehyde for 15 minutes at room temperature. Stacks of images were obtained using a Leica TCS SP2 confocal microscope (Exton, PA). The cells were imaged using the 488 nm laser, detecting fluorescence emission in the 500-535 nm range, while the fabric was imaged in reflectance mode, using the 594 nm laser and detection in the 590-600 nm band.

2.3.7 Enzyme linked immunosorbent assay for adsorbed fibronectin

An enzyme linked immunosorbent assay (ELISA) for adsorbed fibronectin was performed following Bae et al. [247]. Polymer films were coated onto 15 mm coverslips by spin coating a 2.5% wt/vol polymer solution in DCM or THF. The coverslips were held at the bottom of a 24-well plate using silicone o-rings. Fibronectin adsorption to the polymer films was performed by incubating the films with 200 μ L 40 μ g/mL human plasma fibronectin (Sigma, St. Louis, MO) in PBS for 2 hours at 37 °C. The wells were then rinsed 3x with DPBS. The assay for adsorbed fibronectin progressed as follows:

- Apply 300 μ L 3% dry milk DPBS blocking solution, incubate 2 hrs, 37 °C
- Rinse 3 times with 300 μ L DPBS
- Apply 200 μ L 1:10,000 Rabbit anti-human fibronectin antibody (Millipore, Billerica, MA), incubate 1 hr, 37 °C
- Rinse 4 times with 200 μ L DPBS
- Apply 200 μ L 1:40,000 Goat anti-rabbit conjugated with horseradish peroxidase (Millipore, Billerica, MA), incubate 1 hr, 37 °C
- Rinse 4 times with 200 μ L DPBS
- Remove O-ring with tweezers
- Apply 400 μ L of OPD solution (SigmaFast kit, Sigma, St. Louis, MO) to each well and wrap plate with aluminum foil to protect from light, incubate 20 minutes at room temperature
- Stop reaction with 100 μ L 3M H₂SO₄
- Transfer 300 μ L of solution from each well to a 96-well microtiter plate
- Read absorbance at 492 nm on PowerWaveX spectrophotometer (Bio-Tek Instruments, Winooski, VT)

2.3.8 T-peel delamination strength of electrospun fabrics

T-peel specimens were prepared by laminating the test specimen between two pieces of 3M Transparent Tape[®] (Model 600, 3M, St. Paul, MN). The electrospun samples were 21 mm wide or greater, while the tape was 19 mm wide. T-peel specimens were prepared simultaneously in pairs as follows: A 30 cm piece of transparent tape was secured, glue side up, to the benchtop. The electrospun sample was adhered to the center of the tape. Folded Kimwipes[®] were adhered lateral to the T-peel sample with the fold

butting up against the electrospun sample. A second piece of transparent tape was adhered to the top of the electrospun sample and to the top sheet of the folded Kimwipe[®]. The construct was cut in half, and the Kimwipes and electrospun scaffold were trimmed to the tape width, and the graspable tape-Kimwipe[®] ends were trimmed to approximately 4 cm. This process yielded two T-peel specimens that were stabilized by a Kimwipe[®].

The T-peel specimens were evaluated on the MTS Sintec 5/d materials tester (MTS, Eden Prairie, MN) with a 10 N load cell at 100 mm/min. One of the graspable ends was clamped in the top grip, the crosshead was lowered, and the other end of the T-peel specimen was secured in the lower grip. The crosshead was carefully raised to remove slack from the system and specimen alignment was checked. At this point, the stabilizing Kimwipe[®] was cut with a razor blade to prepare the sample for evaluation. The load and extension were set to zero, and the test began, collecting load and extension data at 10 Hz.

The load versus extension curve quickly ramps to a plateau value and roughly maintains this value while the sample was delaminating. The delamination force was averaged over this 55-60 mm plateau, and delamination strength was calculated from the average force divided by the 19 mm specimen width, reported in N/cm.

2.3.9 Tensile strength of electrospun fabrics

Tensile test specimens were cut from candidate AAMs (approximately 8 x 20 mm). Approximately 4 mm of the each end of the sample was laminated between two layers of 3M transparent tape[®] to prevent failure at the grip surface. The length and width of the center of the test-specimen were measured to within 0.5 mm by ruler, and

the thickness was measured to 1 μm by digital micrometers (Model 293-344, Mitutoyo, Japan).

The tensile test specimens were evaluated using the MTS Sintec 5/d materials tester with a 100 N load cell at 10 mm/min. One end of the specimen was clamped in the top grip, the crosshead was lowered, and the other end of the tensile test specimen was secured in the lower grip. The crosshead was carefully raised to remove slack from the system and specimen alignment was checked. At this point, the load and extension were set to zero, and the test began, collecting load and extension data at 10 Hz.

The load, P , versus extension, δ , data was imported into Microsoft Excel and converted to stress, σ , versus strain, ε , using the width, W , thickness, t , and length, L as follows:

$$\sigma = \frac{P}{W \cdot t} \quad (2.1)$$

$$\varepsilon = \frac{\delta}{L} \quad (2.2)$$

Calculation of subsequent mechanical properties are outlined in section 3.7.

2.3.10 Suture pull-out evaluation of AAMs, composite films, and collagen foams

Rectangular suture pull-out specimens were prepared such that a 5 mm x 5 mm sample of AAM, composite film, or DuraGen PLUS[®] was exposed above the support of 3M transparent tape[®]. The sample was pierced 3 mm from its edge with a 5-0 PROLENE suture (Ethicon Inc. Sommerville, NJ). The sample was clamped in locking forceps, which were subsequently clamped in the lower grip of the MTS Sintec 5/d materials tester. The suture ends were clamped in the upper grip, and the load cell was set to zero. The slack was carefully removed from the system, and the extension was set

to zero. Suture pull-out evaluation proceeded at 100 mm/min with data collected at 10 hz by a 100 N load cell. Data is presented as load versus extension.

2.4 Animal Studies

2.4.1 Sterilization

Samples for cell culture or implantation were sterilized by either ethylene oxide gas or gamma irradiation. Ethylene oxide gas sterilization was executed using an Anderson Products AN-74i benchtop sterilizer and AN-71 ethylene oxide ampules (Anderson Products, Haw River, NC). Following sterilization, samples were degassed under vacuum at 40 °C for 12 hours and room temperature for an additional 36 hours.

For the second laminectomy study, materials were sterilized by gamma irradiation (Sterigenics, Rockaway, NJ). Samples were packaged in nitrogen-purged heat-sealable foil pouches (Foil-O-Rap, Ludlow Coated Products, Columbus, GA). A dose window of 25-40 kGy was specified, and an actual dose of 28.9-32.0 kGy was observed. These samples were immediately ready for implantation.

2.4.2 Rat subcutaneous implantation

Rat subcutaneous implantation of electrospun fabrics proceeded according to Rutgers University animal protocol 94:048. Briefly, adult Sprague Dawley rats were anesthetized by intraperitoneal injection of ketamine (40-75 mg/kg) and xylazine (5-12 mg/kg). The rat's back was clipped and disinfected, alternating chlorhexiderm scrub and 70% isopropanol alcohol. Two midline dorsal thoracic incisions were made, and four subcutaneous pockets were made by blunt dissection, two pockets lateral to each incision.

One pocket was left empty to evaluate the tissue response to the creation of a subcutaneous pocket, and experimental samples were implanted into the other three.

The incisions were closed with staples, and a topical antibiotic was applied to incision line. Following surgery, Baytril (5-15mg/ml) was administered by intraperitoneal injection, and Buprenorphine (0.01-0.05mg/kg 2-3 times daily as needed) was administered for post-operative pain and distress. Animals were sacrificed by CO₂ inhalation at specified timepoints (e.g., 1, 2, 4 weeks) to evaluate the tissue response to the experimental materials.

2.4.3 Rat laminectomy with or without spinal cord injury

Rat laminectomy surgeries progressed according to Rutgers University animal protocol 98:028. Adult (~74 days) female Sprague Dawley rats were anesthetized by isofluorane inhalation administered by a nosecone. The rat's back was clipped and disinfected by betadine solution and 75% ethanol. A 4 cm incision was made along the midline of the back over the ninth thoracic vertebra (T9). Sharp dissection was used to remove a portion of the erector spinae musculature, expose the spinous process, and gain access to the laminae. The spinous processes were removed from thoracic vertebrae nine and ten using ronguers. The laminae were completely removed at T10 and partially resected at T9, see Figure 5.1. Bleeding was controlled using cotton balls and gauze.

In laminectomy study #2, contusive cord injury was performed, while in laminectomy study #1, the anti-adhesion membranes were immediately implanted. A contusive spinal cord injury was created via 10 mg weight drop from a height of 12.5 mm. The weight drop was controlled and monitored by the multicenter animal

spinal cord injury study impactor. Hemostasis was achieved and the rats were returned for placement of experimental materials for the prevention of postsurgical adhesions.

Following a saline rinse, the prototype membranes were apposed to the dura and tucked between the dura and lamina rostral and caudal to the implant site using Dumostar #3 and #5 forceps. If caudal tuck could not be achieved, the rostral tuck was considered sufficient and the membrane was left in apposition to the dura. The surgical site was closed in layers, suturing the erector spinae muscles with two interrupted stitches using silk sutures and the incision line was closed with staples. All rats received cephalozolin, and antibiotic (25 mg/kg daily) for 7 days after injury. At either 4 or 8 weeks, the rats were sacrificed by decapitation following deep anesthetization by intraperitoneal pentobarbital (45 mg/kg). Animal tissues were fixed by cardiac perfusion with 4% paraformaldehyde in PBS, and the spinal column was removed *en bloc* to continue fixation in a 50 mL centrifuge tube filled with 4% paraformaldehyde in PBS.

2.4.4 Histology

External parties performed histological slide preparation. The Hematoxylin and Eosin (H&E) stains of subcutaneous studies were performed by either Goode Histolab (New Brunswick, NJ), section 3.6, or Kathleen Roberts, department of pharmacology and toxicology (Piscataway, NJ), section 4.5. Rat spinal columns were larger than standard histological cassettes, so decalcification, paraffin embedding, and sectioning of spinal tissues was performed by Neuroscience Associates (Knoxville, TN). Neuroscience associates cut three serial 6 μm sagittal sections at 100 μm intervals near the centerline of the spinal cord. In the exploratory study, the slides were stained according to the Mallory trichrome staining procedure, which stains connective tissue (blue) and cytoplasm (red).

In the larger laminectomy studies, H&E staining was deemed sufficient to evaluate the extent of adhesion and observe the tissue response to the implant.

2.4.5 Extent of adhesion

The extent of adhesion was measured by analysis of tiled 5x images of histological sections. A single central histological slide was chosen for evaluation. The presence or absence of nerve roots posterior to the spinal cord indicated the slide position. Lateral sections contained nerve roots, while the central slide(s) did not. Adhered regions were indicated by penetration of peridural fat by collagenous tissue, creating a continuous scar from the dura to the laminectomy scar. The primary statistic used in evaluation was the fraction of adhesion, calculated as the length of adhered regions in pixels divided by the length of laminectomy defect in pixels, Figure 2.1



Figure 2.1. Representative image to demonstrate the measurement of extent of adhesion.

2.5 Statistics

Unless otherwise noted, all statistics are expressed as an arithmetic mean \pm 95% confidence interval. Where single comparisons were made, a t-test was employed at $\alpha = 0.05$ and equal variance between sample sets. A single-tailed t-test was used where the expected outcome was known and hypothesized, while a two-tailed t-test was employed where the expected outcome was not hypothesized. Where multiple comparisons were evaluated, an analysis of variance was performed. If study-wide

significance was established, $p \leq 0.05$, then Tukey's honestly significant difference (HSD) was applied to test the significance of a pairwise comparison of means.

3 Fabrication of electrospun anti-adhesion membranes

Candidate anti-adhesion membranes (AAMs) were fabricated by electrospinning. Cell-impermeable barrier devices were fabricated by solution spinning from conventional organic solvents, and a low-toxicity solvent system was devised to limit the potential toxicity of electrospun prototypes. A useful range of PEG_{1k} content (T_g) was identified, and a dual-spinneret technique was utilized to fabricate AAM prototypes with superior mechanical properties.

3.1 Development of an electrospinning facility

Electrospinning training was provided by Jean Altus (Stephens) at the Polymer Division of the National Institute for Standards and Technology. Having observed the technology, an electrospinning facility was established at the New Jersey Center for Biomaterials (NJCBM), Figure 3.1. One or more syringe pumps were used to advance the polymer solution through Teflon tubing to a stainless-steel blunt-ended needle. The needle spinneret potential was maintained at 6-30 kV by a dual-polarity high-voltage power supply. The negative terminal of the power supply was used to maintain the collector potential at -6 to 0 kV. A custom fabricated mandrel collector was insulated from the benchtop by a lexan frame. The mandrel was rotated by a 24V DC motor and a variable power supply, and translation of the mandrel was achieved through the use of a gear motor and connecting rod. The apparatus was installed in a class 10,000 cleanroom

to limit the amount of dust, pyrogens, and bioburden accumulated in the device during fabrication.

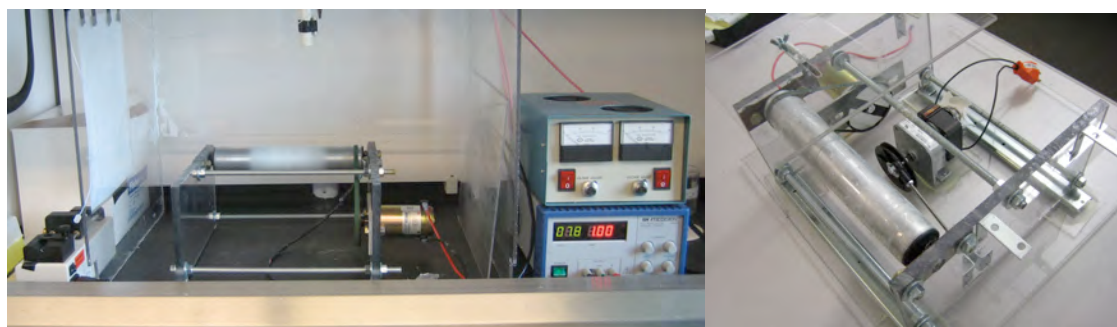


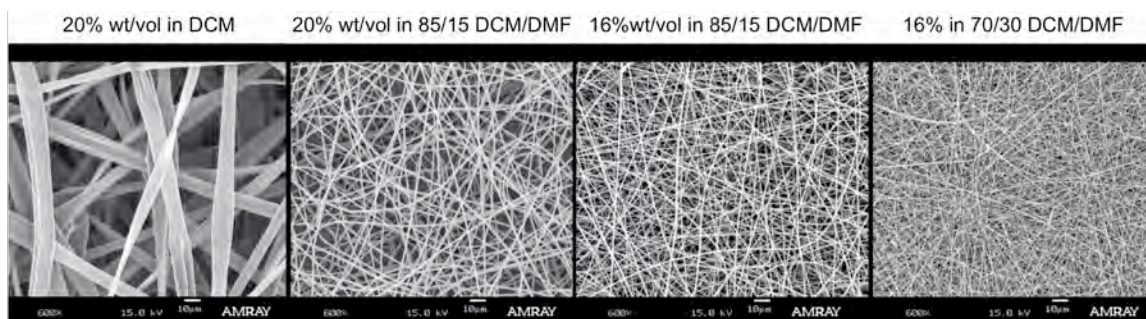
Figure 3.1. The NJCBM Electrospinning apparatus is installed in the center's class 10,000 fume hood (left). The rotating mandrel collector (right) permits collection of 7 cm by 20 cm sheets of fibroporous fabrics. The gear motor in the center translates the collector for even distribution of fibers, while the variable-speed motor rotates the mandrel.

3.2 Conventional solvent systems useful for electrospinning TDPCs

Tyrosine-derived polycarbonates can be electrospun from a variety of organic solvents, similar to those tabulated in Table 1-3. Kohn-group collaborators have electrospun E0000 and E2000 from solvent mixtures of DCM and methanol, ranging from 100% DCM to 50/50 DCM/methanol [248]. The addition of a cosolvent permitted the electrospinning of finer diameter fibers, reducing the fiber diameter from 1.6 μm to 0.8 μm . Jarusuwannapoom et al. found that solvent systems with greater conductivity and dipole moment aided in electrospinning ultrafine fibers [249]. In comparison to DCM's dipole moment of 1.6 Debye and conductivity of 0.6 $\mu\text{S}/\text{cm}$ [248], the dipole moment and conductivity of DMF are 3.82 Debye and 10.9 $\mu\text{S}/\text{cm}$ [249]. These properties of DMF have made it a prevalent solvent for use in electrospinning, table 1-3.

The effective use of DMF as a cosolvent in electrospinning E0000 from DCM/DMF solutions is depicted in Figure 3.2. Progressive addition of DMF resulted in progressively smaller diameter fibers. The use of a DMF as a cosolvent enabled 0.23 μm

fibers to be electrospun from 16 %wt/vol E0000 in 70/30 DCM/DMF. The ultrafine fibers reduced the interfiber spacing from tens of microns to single microns. Fine diameter fibers are required for the fabrication of cell-impermeable devices. Without the use of a cosolvent, progressively diluted solutions of E0000 in DCM resulted in the formation of beaded fibers that produced a brittle fabric.



Electrospinning E0000 from DCM/DMF

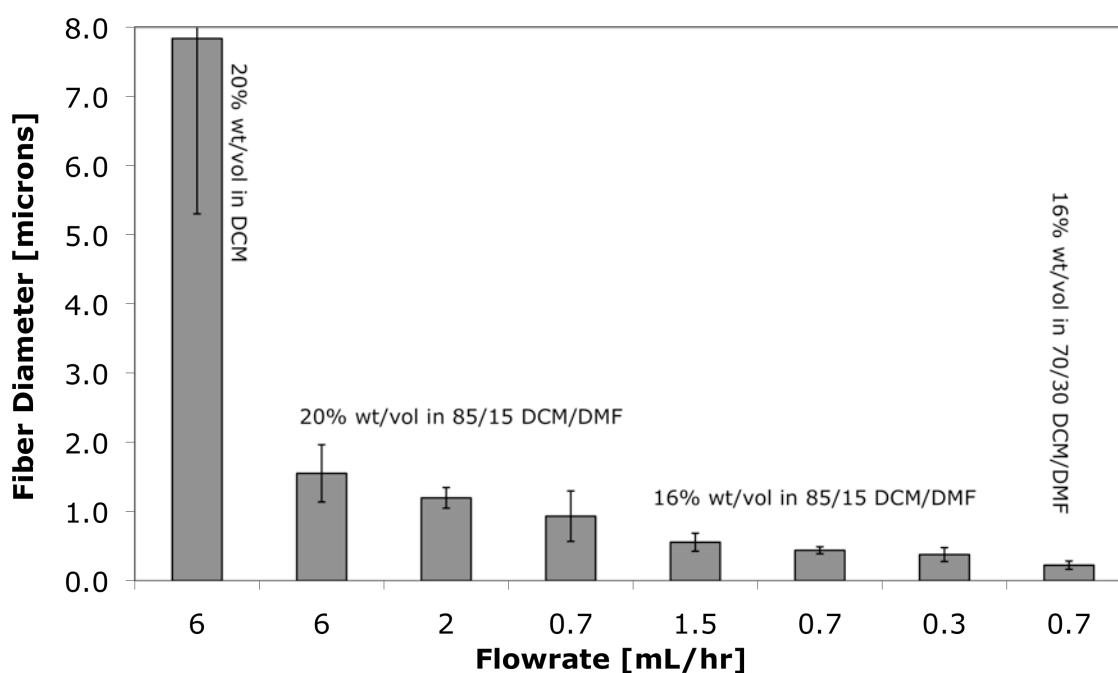


Figure 3.2. The addition of DMF to DCM reduced the average fiber diameter of electrospun mats, thus reducing the interfiber spacing.

In the electrospinning of DT-containing TDPCs, Tetrahydrofuran was substituted for DCM. The substitution of solvents was made because DT-containing polymers were

not perfectly soluble in DCM, and THF is a solvent of low toxic potential [216]. This solvent system was used extensively for the electrospinning of I_{0,2}EXXY(1k) polymers. A ratio of 70/30 THF/DMF was found to permit fabrication of electrospun constructs over the greatest range of architectures.

With sufficient experience in electrospinning TDPCs from 70/30 THF/DMF, architecture-matched electrospun nonwoven fabrics could be fabricated across polymer chemistries. McKee et al. and Gupta et al. noted that the primary parameter to control fiber diameter was solution concentration (viscosity), and they observed a power-law relationship between solution concentration and fiber diameter, with exponents of 2.6 and 3.1, respectively [182, 183]. The fiber diameter of I₂E10000 and I₂E1008(1k) fabrics were matched by electrospinning a concentration series of polymer solutions in 70/30 THF/DMF, fitting a power curve, and calculating the desired concentration to produce fibers of 0.5 μ m and 1.8 μ m diameter. The fabrics' average fiber diameters were indistinguishable, Table 3-1 and Figure 3.3. These electrospun fabrics were implanted in subcutaneous pockets for 2 and 4 weeks to observe the effects of device architecture and chemistry on cell penetration and inflammatory response, section 3.6.

Table 3-1. Electrospinning parameters for fabrication of electrospun membranes with matched fiber diameter from different polymer chemistries. Key: polymer concentration, C; needle potential, NP; distance, D; needle gage, G; flowrate, Q; solvent system, SS; fiber diameter, FD; and confidence interval, CI.

Polymer	C [% wt/vol]	NP [kV]	D [cm]	G	Q [mL/hr]	SS	FD [μ m]	95% CI (n=60) [μ m]
I ₂ E1000	20.9	12	18	19	0.1	70/30 THF/DMF	0.52	0.04
I ₂ E1008(1k)	31.2	12	18	19	0.1	70/30 THF/DMF	0.49	0.03
I ₂ E1000	43.7	21	18	23	1.5	70/30 THF/DMF	1.72	0.17
I ₂ E1008(1k)	57.5	21	18	23	1.5	70/30 THF/DMF	1.76	0.09

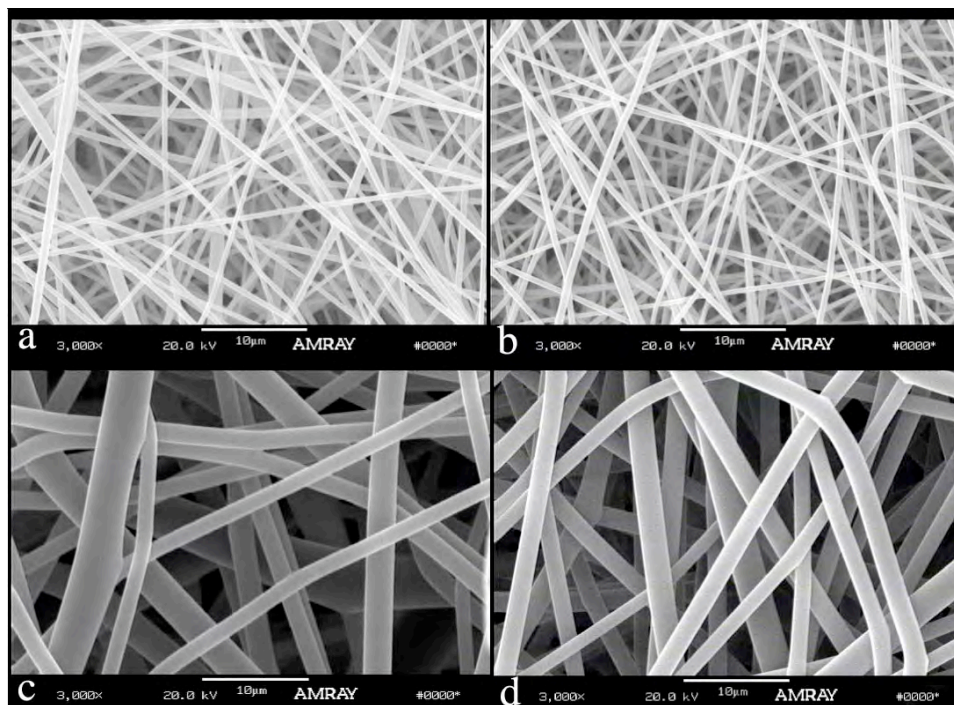


Figure 3.3. Cell impermeable electrospun nonwoven fabrics with fiber diameter of 0.52 and 0.49 μm (a) and (b) and cell permeable fabrics with fiber diameter of 1.72 and 1.76 μm (c) and (d). Scaffolds have been electrospun from 70/30 THF/DMF and are composed of I₂E1000 (a) and (c), and I₂E1008(1k) (b) and (d).

Though effective, the THF/DMF solvent system had a number of shortcomings. Very low flowrates (0.1 to 0.3 mL/hr) were necessary to prevent dripping during fabrication of fine fiber diameter fabrics, Table 3-1. These flowrates were impractical for the fabrication of large polymer fabrics from dilute solutions. Additionally, a small variation in the ratio of DMF content can dramatically affect the morphology of fibers, Figure 3.2. In recent years, HFIP has been used extensively as an electrospinning solvent, for it is a polar organic solvent with versatile solubility. It has been used to electrospin a wide range of biopolymers and synthetic polymers, Table 1-3, and its use does not introduce variability of preparing a mixed solvent system.

Polymer solutions 12, 15, and 20% wt/vol E1002(1k) were electrospun from HFIP. The 20% wt/vol solution produced ribbon-like fibers under all conditions, and was

not considered for further investigation. Fabrics electrospun from 12% and 15% wt/vol solutions at varying flowrate and needle potential included in Figure 3.4.

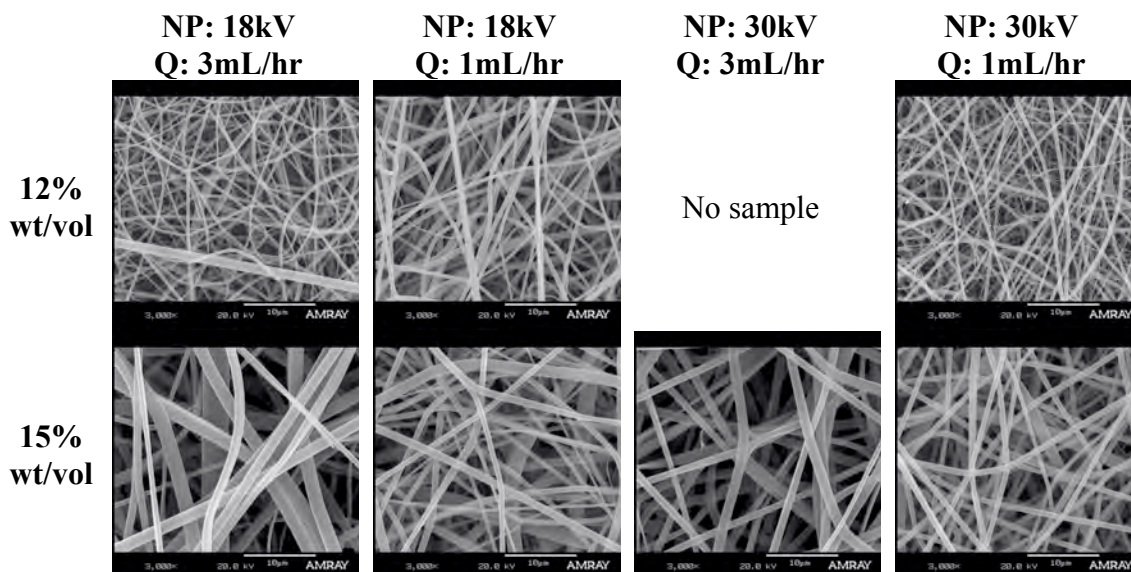


Figure 3.4. Electrospinning of E1002(1k) from HFIP to determine preferred electrospinning parameters and solution concentration for a barrier device.

The best conditions to electrospin E1002(1k) were 30 kV and 1 mL/hr, due to the more uniform fiber diameter and reduced fusion of fibers during fabrication. At 30 kV and 1 mL/hr, the 15 % wt/volume solution produced fibers of $0.68 \pm 0.05 \mu\text{m}$ diameter, with a standard deviation of $0.27 \mu\text{m}$, and the 12% wt/vol solution produced $0.28 \pm 0.03 \mu\text{m}$ diameter fibers with a standard deviation of $0.15 \mu\text{m}$. The fabric spun from the 12% wt/vol solution was composed of sufficiently fine fibers for the production of a barrier device.

The use of HFIP is prevalent in the field of electrospinning. However, Nielson et al. noted a 50% reduction of the respiration rate of mice at a concentration of 165 ppm [218]. The TDPCs and their degradation products are generally regarded as safe. Rather than adding an organic solvent with known toxicity to the device, a low-toxicity solvent system was pursued.

3.3 Low toxicity solvent system for electrospinning TDPCs

Polymers of the NJCBM TDPC terpolymer library are soluble in acetic acid. Traditional electrospinning requires organic solvents that may pose a threat to human health. To prevent the irritation of tissue adjacent to the device, acetic acid has been pursued as a solvent for electrospinning. Electrospinning E0000 from acetic acid produced brittle constructs with beaded fibers, Figure 3.6. The beaded structures concentrate the polymer mass in the near-spherical fibers, where it does not efficiently contribute to bearing loads in the final construct, Figure 3.5. Furthermore, the intersection between the fine fibers and spherical beads produces a stress concentration, further weakening the construct.

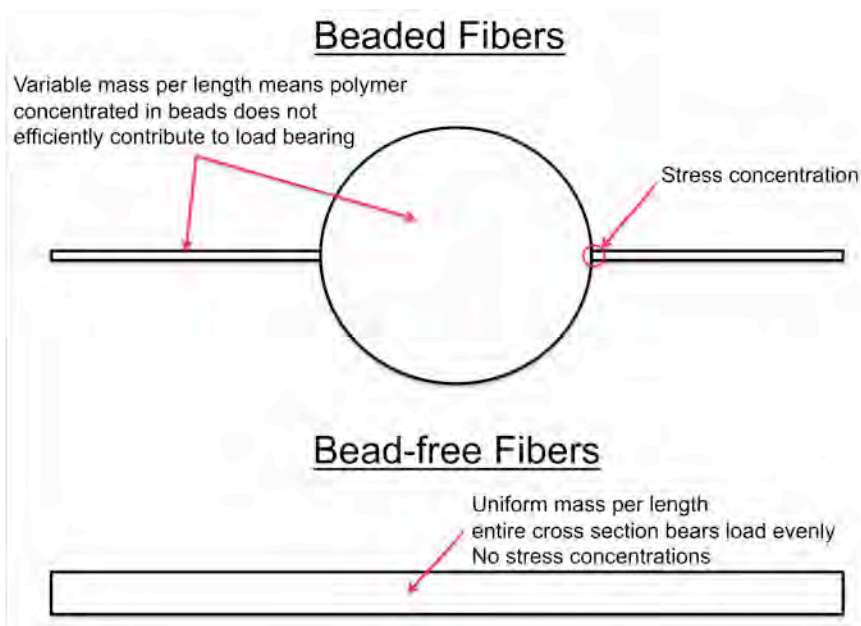


Figure 3.5. Schematic of poor stress distribution in beaded fiber constructs, compared to bead-free fiber constructs

Beaded fibers form during electrospinning as the surface tension acts to reduce the surface area of the electrospun jet. To reduce beading, either the drawing tension in the fiber can be increased (e.g., increase viscosity, increase charge density) or the surface

tension can be decreased. Through the incorporation of surfactant molecules in the polymer solution, the surface tension of the solution, onset voltage of electrospinning, presence of beading, average fiber diameter, and variance of fiber diameter were all reduced [250-252]. Surfactants must either be used in low concentrations or they must lose their effectiveness under physiological conditions, for surfactant molecules cause toxicity through disruption of cell membranes.

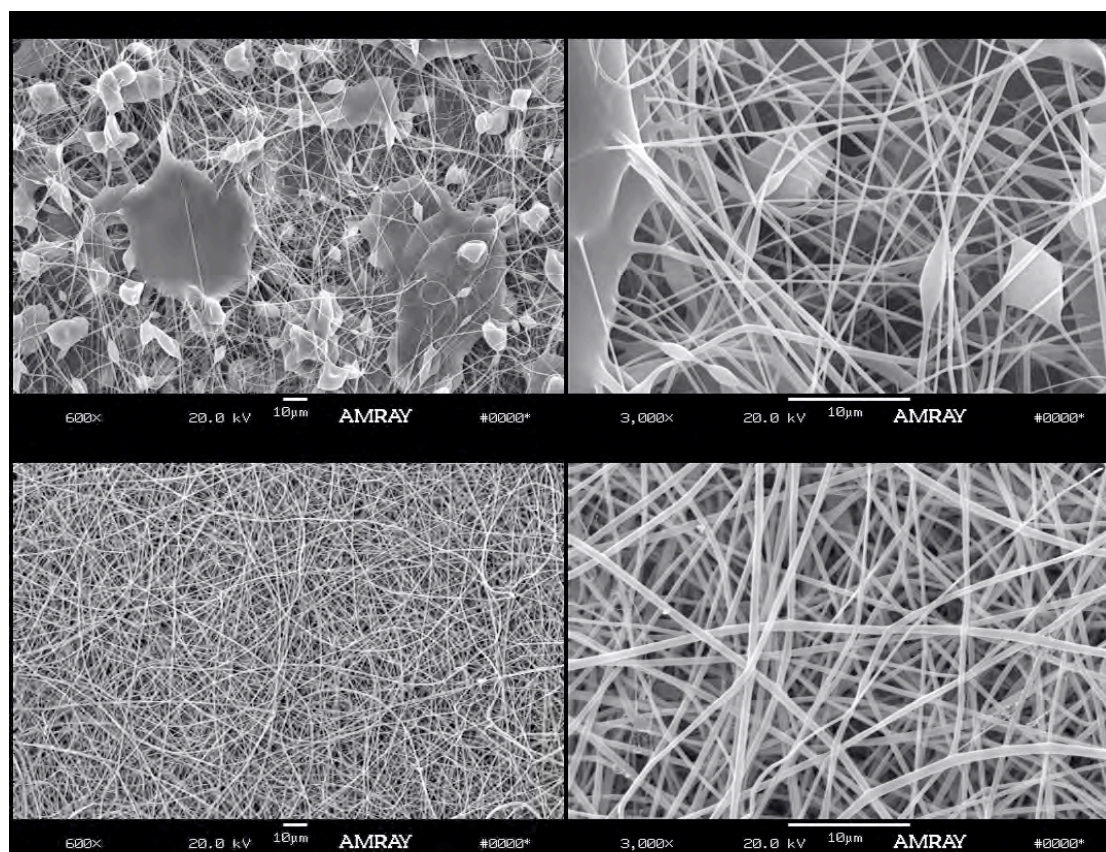


Figure 3.6. The addition of tHyp octyl ester HCl eliminated beading of fibers during electrospinning of 17% wt/vol E0000 solutions in acetic acid. The sample at top was without surfactant, while the sample at the bottom was electrospun with the a 1:5 loading of tHyp octyl ester HCl per polymer by mass.

A series of degradable weak surfactants were synthesized and evaluated. An ester bond between the hydrophilic and hydrophobic portions of the molecule hydrolyzes under physiological conditions, releasing trans-4-hydroxy-L-proline (tHyp) and either

butanol or octanol. Synthesis and characterization of tHyp butyl ester HCl and tHyp octyl ester HCl are discussed in detail alongside the delivery of cHyp, section 4.3. Their ability to reduce beading and enable electrospinning from acetic acid follows.

A 1:5 loading of tHyp octyl ester HCl per polymer mass eliminated beading when electrospinning 17% wt/vol E0000 solutions from acetic acid, Figure 3.6. The effectiveness of tHyp butyl ester HCl was explored, for 1-butanol is a solvent of “low toxic potential,” while octanol is not [216]. Both degradable surfactants were capable of reducing beading at a 1:5 loading. However, only the octyl ester was capable of preventing beading at a 1:25 loading, Figure 3.7. As octanol is a degradation product of TDPCs containing DTO, its use may be permissible. To evaluate the toxic potential of both surfactants, their effect on cell viability was examined.

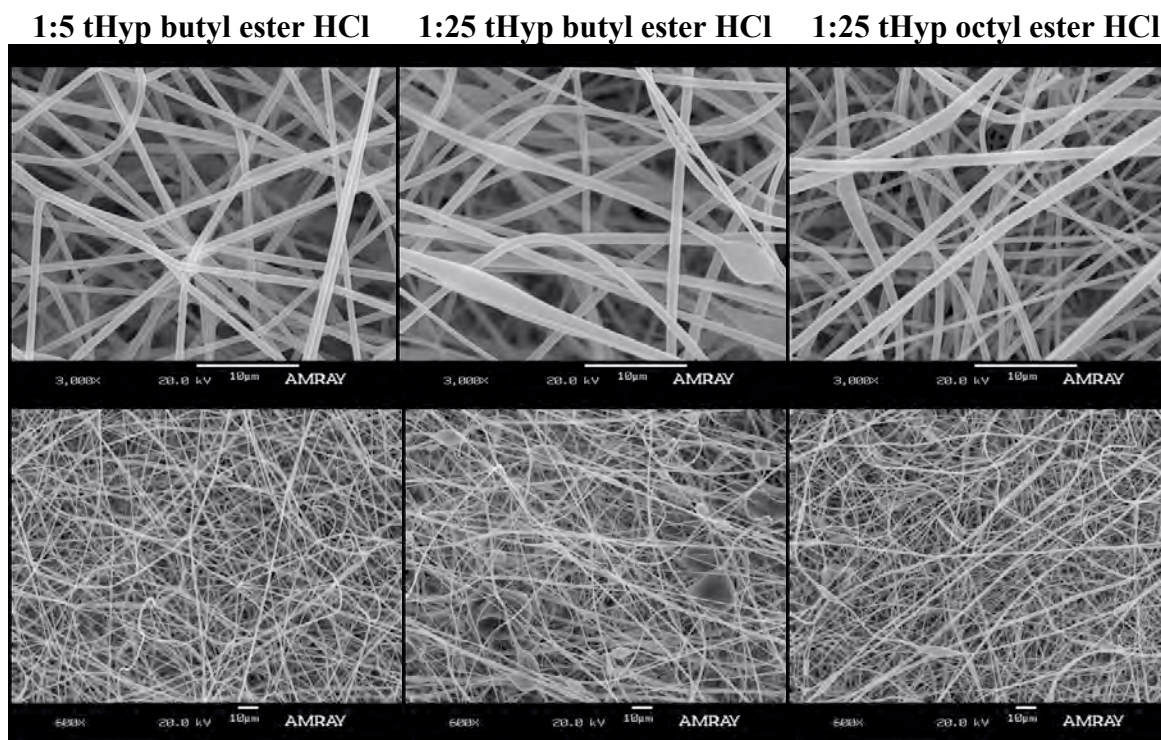


Figure 3.7. The effect of alkyl chain length and concentration of degradable surfactant in bead formation in acetic acid electrospinning. 3000x (top) and 600x (bottom) SEM images of poly(DTE carbonate) fiber mats electrospun from acetic acid with the addition of surfactant as indicated above.

The toxicity of tHyp alkyl ester HCl surfactants was evaluated on a culture of confluent human dermal fibroblasts (HDFs) in serum-free media. At 48 hours, dead cells were indicated by ethidium homodimer-1 positive nuclei, while viable cells stained positively for DAPI, but not ethidium homodimer-1 (ED-1). The toxicity of surfactants is depicted in Figure 3.8. tHyp octyl ester HCl demonstrated cytotoxicity at 1.5 mM while no toxicity was noted for tHyp butyl ester HCl at concentrations up to 4.0 mM.

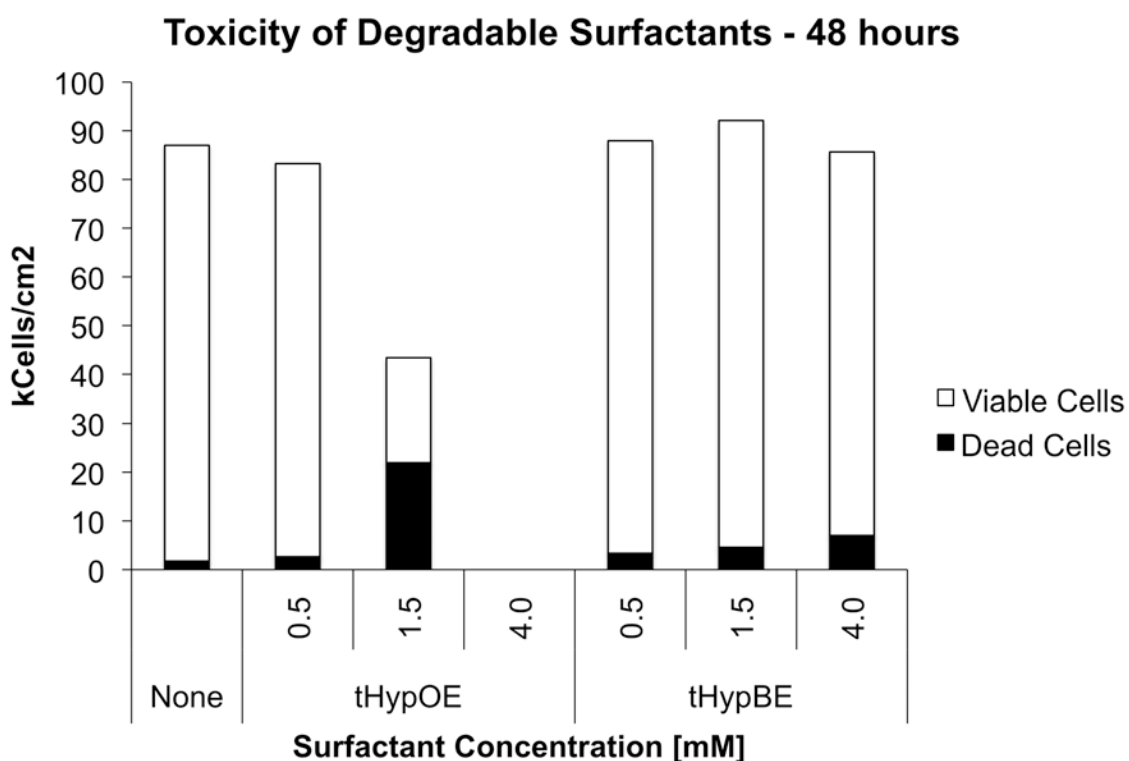


Figure 3.8. Alkyl chain length of degradable surfactants affected the viability of confluent HDF cultures in serum-free media at 48 hours. No toxicity was noted for either surfactant at 0.5 mM, but the octanol-releasing tHypOE was found to be toxic at concentrations ≥ 1.5 mM. Live cells were DAPI-positive, but ED-1 negative, while dead cells were indicated by nuclear binding of ED-1.

tHyp butyl ester HCl was less cytotoxic in these experiments, and butanol is characterized as less toxic than octanol [216], so tHyp butyl ester HCl was selected for to electrospinning TDPCs from acetic acid.

3.4 Range of polymers useful for electrospinning TDPC

Not all polymers are suitable for electrospinning. In particular, catastrophic changes in scaffold shape occurred when the polymer fibers were glassy at room temperature but transitioned to rubbery upon swelling with water under physiological conditions. This was first noticed when characterizing a degradable, PEG-containing, electrospun fabric composed of E1008(1k) ($T_g = 46$), Figure 3.9.

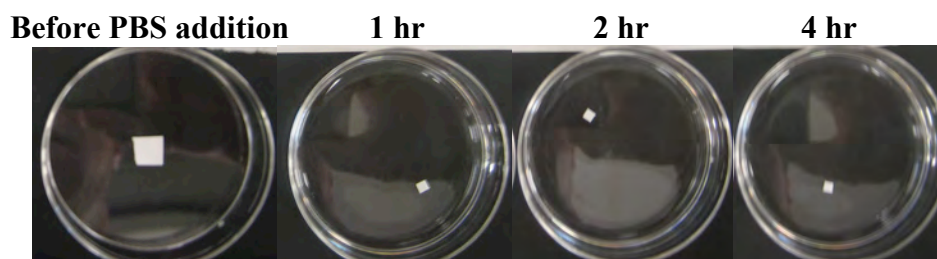


Figure 3.9. Contraction of electrospun E1008(1k) over 4 hours in PBS at 37 °C

SEM images demonstrated the changes in the fabric microarchitecture that led to fabric contraction. The fibers of the E1008(1k) fabric became much thicker and tortuous, Figure 3.10. The covalently-bound iodine present in I₂E1008(1k) increased the glass transition temperature versus E1008(1k), 46 °C vs 86 °C, respectively. I₂E1008(1k) did not present any obvious macroscopic or microscopic signs of shrinkage after 24-hour immersion in PBS at 37 °C, Figure 3.10.

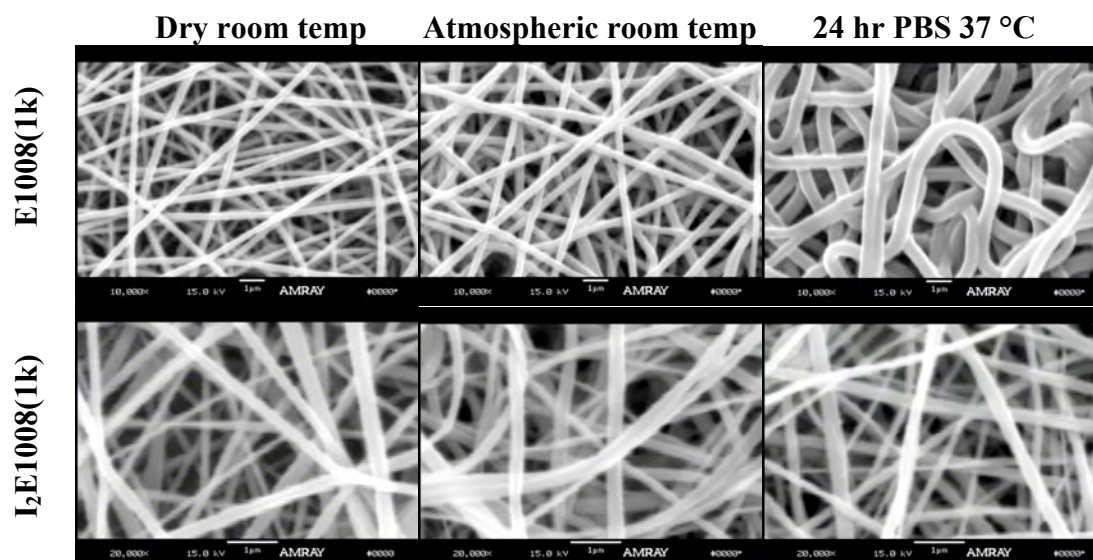


Figure 3.10. Observing single fibers in a contracted E1008(1k) scaffold reveals that the fibers have become wider and more tortuous, indicating that the length of each fiber has decreased. The architecture of the I₂E1008(1k) scaffold remains similar across storage conditions.

When heated above their glass transition temperature, a polymer's individual chains have significant mobility relative to one another. If the initial state of the polymer chains was ordered, a loss in this order would contract the material in the direction of chain alignment, and cause expansion in the direction perpendicular to chain alignment, as depicted in Figure 3.11. The polymer chains are partially aligned due to fiber drawing during electrospinning. If the polymer becomes rubbery upon immersion in physiological fluids due to the increase in temperature and the plasticization of water uptake, the loss of chain alignment will result in the contraction observed in Figure 3.10.

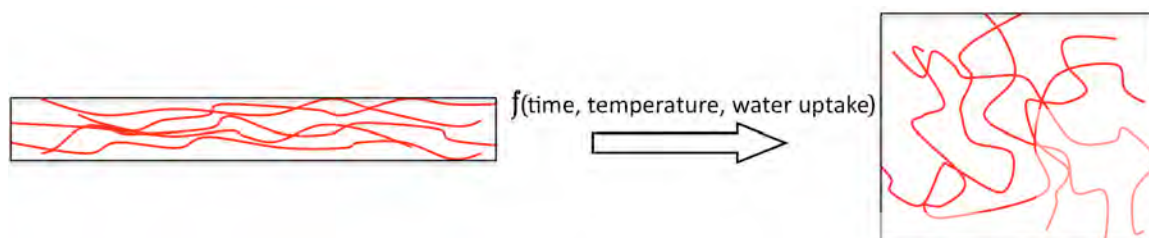


Figure 3.11. Schematic of entropy-driven fiber contracture upon plasticization

Iodine-containing polymers were surveyed to observe the permissible range of PEG_{1k} content before catastrophic contraction would occur. The degree of contraction of I₂E1000(1k), I₂E1008(1k), and I₂E1012(1k) electrospun mats was evaluated. The area, in pixels, was compared to that of a 25-cent coin in photographs before and after overnight incubation at 37 °C in PBS. The square root of the ratio of area before and after incubation was used to calculate the %(*L/L*) contraction:

$$\% (L/L) = 100 \cdot \left(1 - \sqrt{\frac{Area_f}{Area_i}} \right) \quad (3.1)$$

The images and resulting contraction ratio are pictured in Figure 3.12.

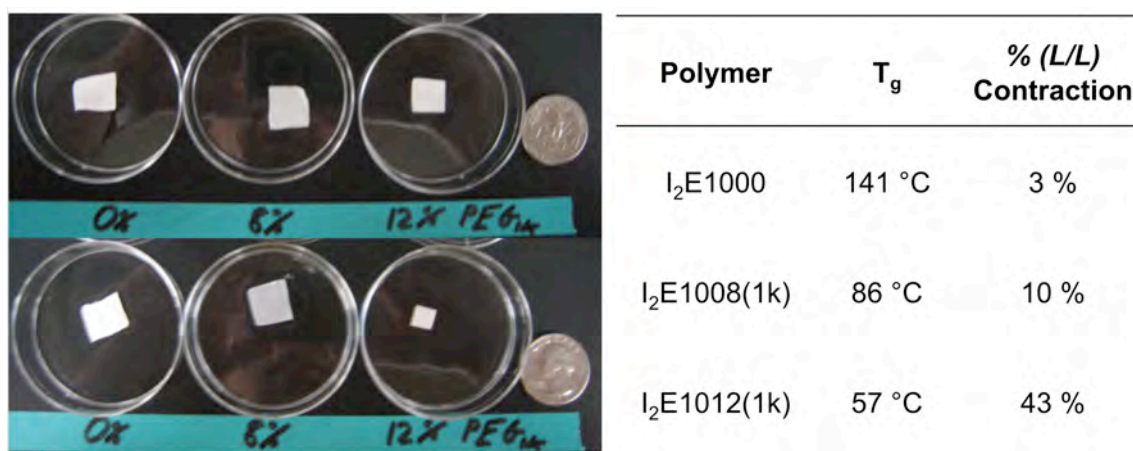


Figure 3.12. Electrospun scaffolds of I₂E10YY(1k) before (top left) and after (bottom left) overnight incubation in PBS at 37 °C. The %(*L/L*) contraction is tabulated at right.

Up to 8 mol% PEG_{1k} can be incorporated into polymers of the I₂E10YY(1k) family without catastrophic contracture. Beyond that level of PEG incorporation, the scaffold's area would shrink appreciably. When implanting a barrier device between the dura and laminectomy scar, such contracture would result in an instantaneous failure.

3.5 Cell interactions with scaffolds of varying fiber diameter and porosity

In the creation of a barrier device, cell permeability is of primary importance. Cell infiltration can be achieved by size-excluding cell nuclei from entering the construct. In electrospun scaffolds, size-exclusion is achieved by reducing the fiber diameter and subsequently, the interfiber spacing. It is intuitive to note that the finer the fibers of a nonwoven mesh, the more closely they pack together. However, the pore size of a fibroporous mesh is not easy to define. In 2003, Sampson derived a mathematical definition for the mean pore radius, \bar{r} , in isotropic near-planar fiber networks [253]:

$$\bar{r} = -\frac{\sqrt{\pi}}{4} \left(1 + \frac{\pi}{2 \ln(\phi)} \right) \omega \quad \text{for } e^{-\pi/2} \leq \phi \leq 1 \quad (3.2)$$

where ϕ is the pore fraction and ω is the fiber width. In two-dimensional projection, the fiber width is identical to the fiber diameter. The pore size, $2\bar{r}$, of electrospun materials with typical fiber diameter and pore fraction is presented in Figure 3.13.

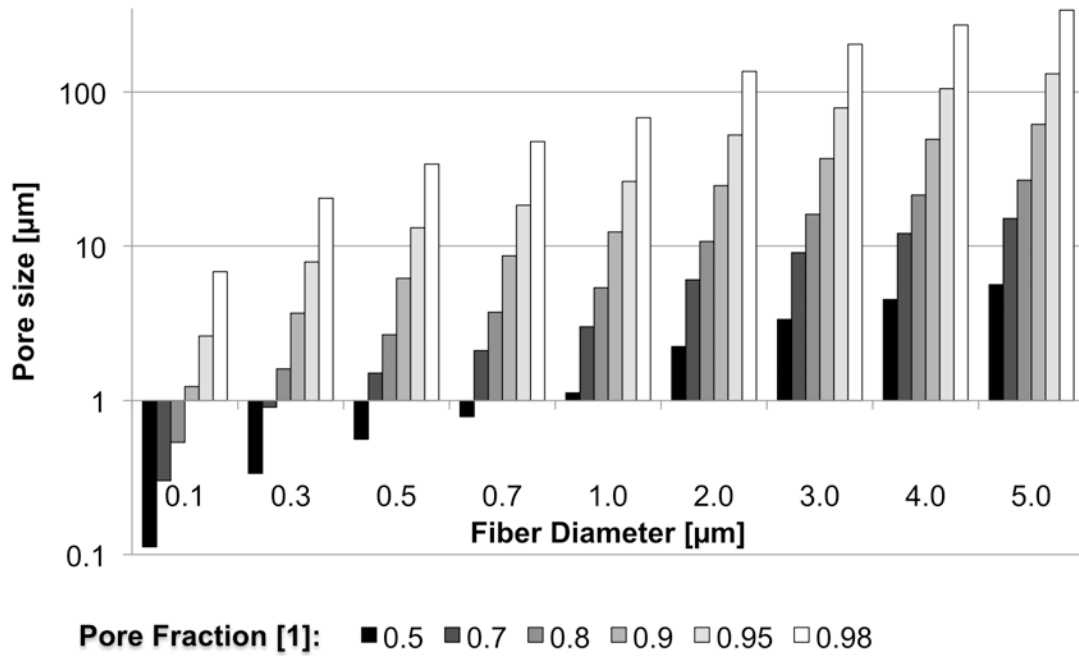


Figure 3.13. Average pore size, $2\bar{r}$, based upon equations following Sampson's derivation of pore size in near-planar fiber networks [253].

These calculations offered guidance on how to pursue in fine-tuning pore size, but only cell culture or animal experimentation could reveal whether the fabrics are barriers to cell penetration. Electrospun E0000 fabrics of varying diameter were cultured with transgenic GFP-expressing rat dermal fibroblasts for 5 days. The cells were fixed and confocal microscopy images were taken to assess fibroblast penetration of the fibroporous mats. To verify the confocal images, a second set of scaffolds was fixed, washed with copious volumes of deionized water, blotted dry with a kimwipe, dried under vacuum, and imaged by SEM. The cell-scaffold interaction will be described one fiber diameter at a time.

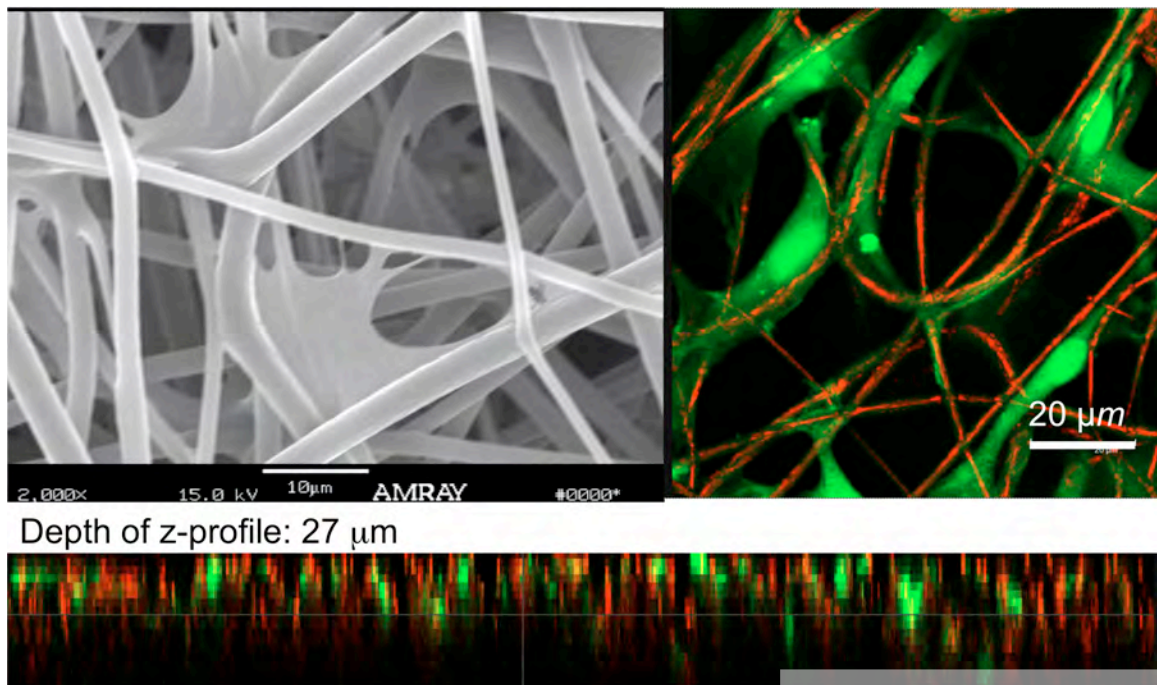


Figure 3.14. Rat dermal fibroblast interaction with $2.3 \pm 0.19 \mu\text{m}$ (95% C.I., $n=60$) fiber diameter scaffold at day 5. SEM image (upper left), confocal microscopic image (upper right) and confocal z-stack (bottom)

Rat dermal fibroblasts freely penetrated the $2.3 \mu\text{m}$ fiber diameter fabric, Figure 3.14. The large interfiber spacing forced cells to attain an elongated morphology, spreading along the fibers. Cell nuclei were commonly located at the intersections of

crossing fibers, while the processes extended along the electrospun fibers. Fabrics of this configuration are suitable for tissue culture scaffolding and have been applied to the support of human dermal skin equivalents and the expansion of pluripotent human embryonic stem cells.

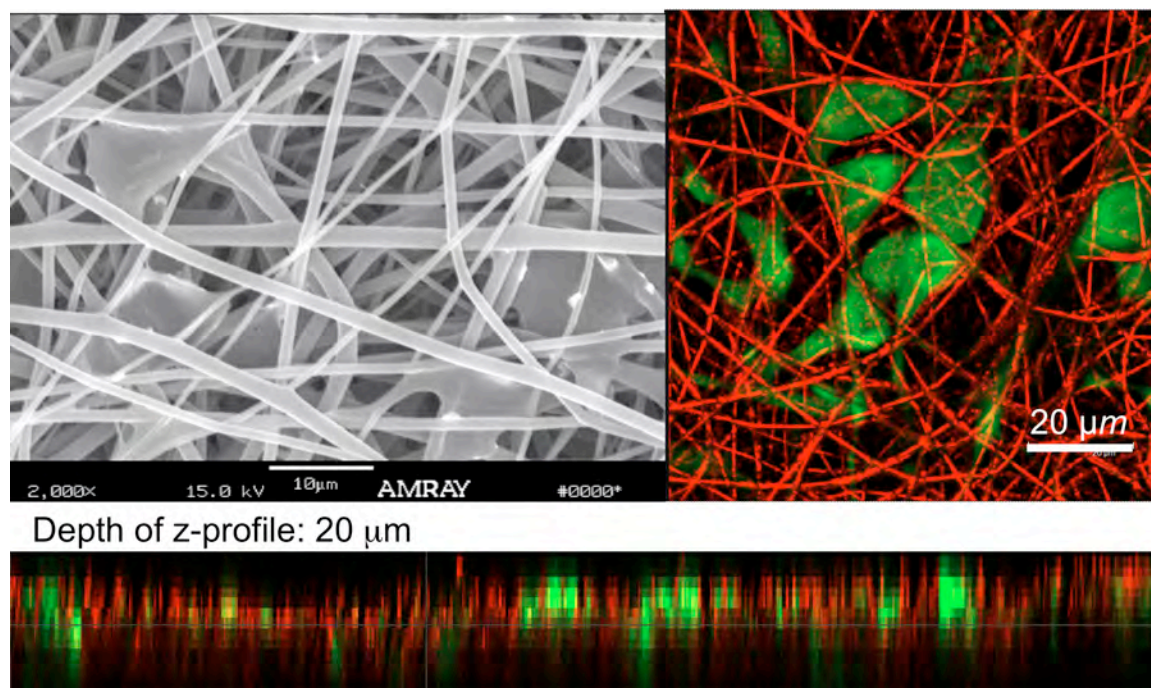


Figure 3.15. Rat dermal fibroblast interaction with $1.0 \pm 0.10 \mu\text{m}$ (95% C.I., $n=60$) fiber diameter scaffold at day 5. SEM image (upper left), confocal microscopic image (upper right) and confocal z-stack (bottom)

In the $1.0 \mu\text{m}$ scaffold, the cells were able to penetrate the network of fibers, as in the $2.3 \mu\text{m}$ scaffold, but the nature of the cell's interaction was different. One observes that the fibroblasts interacted with a “pocket” of fibers that formed a pore around the cell, Figure 3.15. A comparison of cells cultured in these two environments may prove interesting, for the architecture of the scaffold dramatically influences cell morphology. Though fibroblasts were seen below the top layer of fibers, the cell infiltration rate into this fabric is likely lower than the rate into the $2.3 \mu\text{m}$ fiber diameter fabric.

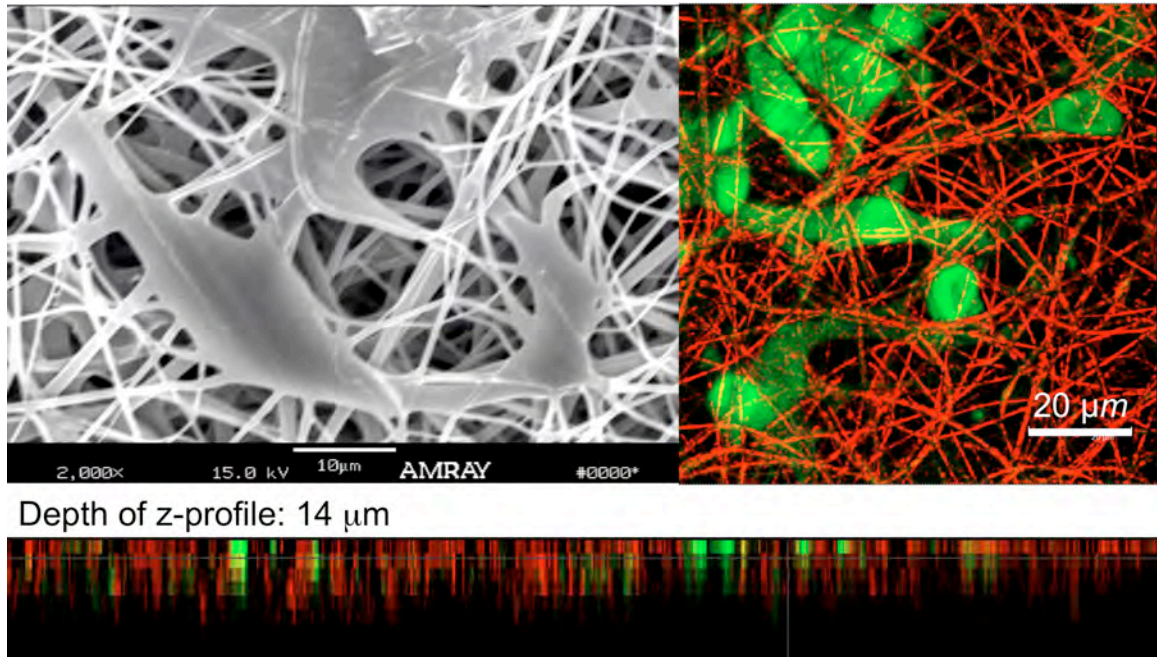


Figure 3.16. Rat dermal fibroblast interaction with $0.5 \pm 0.04 \mu\text{m}$ (95% C.I., $n=60$) fiber diameter scaffold at day 5. SEM image (upper left), confocal microscopic image (upper right) and confocal z-stack (bottom)

Cell penetration into $0.5 \mu\text{m}$ scaffolds was limited by the multiple layers of closely-spaced fibers. At this pore fraction, complete barrier function is inconclusive Figure 3.16. However, with compression of the adjacent fiber layers, the pore fraction could be reduced and cell-impermeable membranes could be fabricated from $0.5 \mu\text{m}$ fiber diameter nonwoven fabrics. The fibroblasts cultured on this matrix assumed a dominantly round morphology, as in the $1.0 \mu\text{m}$ fiber diameter fabrics. However, on $0.5 \mu\text{m}$ fiber diameter fabrics, the cell nuclei and cell bodies are even more compact, as the interfiber spacing is narrower.

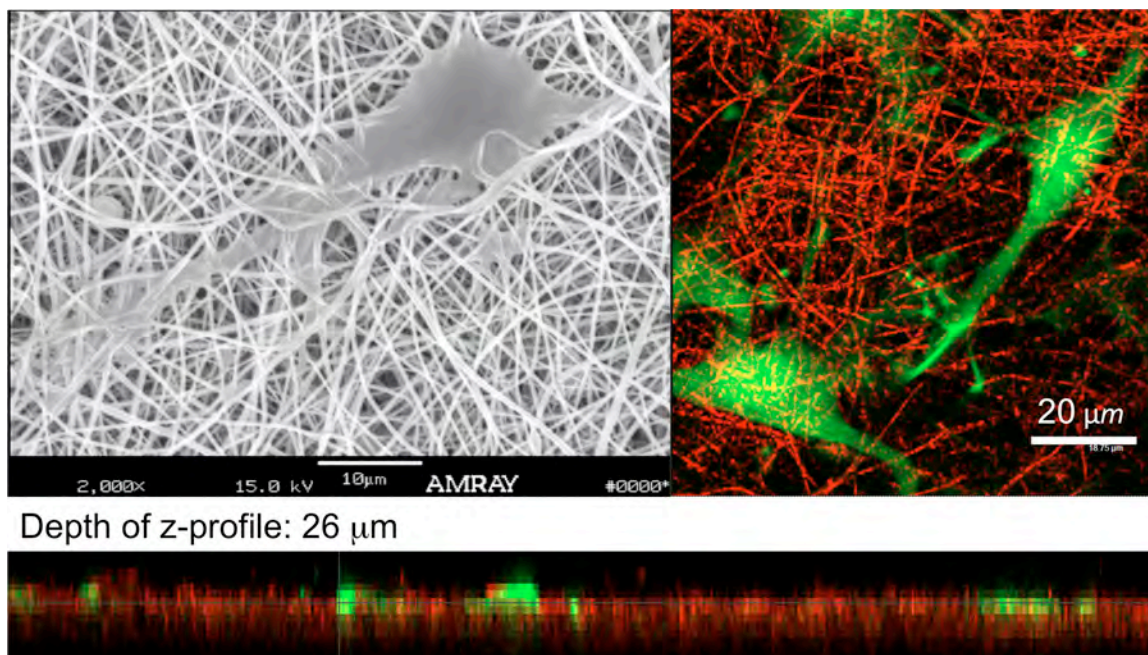


Figure 3.17. Rat dermal fibroblast interaction with $0.29 \pm 0.03 \mu\text{m}$ (95% C.I., $n=60$) fiber diameter scaffold at day 5. SEM image (upper left), confocal microscopic image (upper right) and confocal z-stack (bottom)

When the fiber diameter of electrospun mats was reduced to $0.29 \mu\text{m}$, the fabrics were cell-impermeable, for the nuclei were too large to penetrate the fiber network. The confocal z-stack clearly shows cell nuclei on top of the electrospun membrane. On the $0.5 \mu\text{m}$ fabrics, the cells could nearly obtain the shape of a pore outlined by fibers, but the fibroblasts can not nearly obtain the dimension of a pore between the $0.29 \mu\text{m}$ fibers. Rather, the fibroblasts interacted with a textured surface, which induced a highly spread morphology.

The observation of cell penetration is highly consistent with the pore size predicted by Sampson's calculations [253], Figure 3.13. Though not measured for these specific scaffolds, a pore fraction of approximately 0.85 is typical for electrospun TDPCs. At that pore fraction, 0.29 , 0.5 , 1.0 , and $2.3 \mu\text{m}$ fiber diameter nonwoven fabrics have pore diameters of 2.2 , 3.8 , 7.7 , and $17.7 \mu\text{m}$, equation 3.2. Considering that cell

nuclei have a diameter of $\sim 6\text{-}8\text{ }\mu\text{m}$, Sampson's calculations have predictive value for estimating the pore size and cell permeability of electrospun nonwoven fabrics.

3.6 Confirmation of barrier function and effect of chemistry *in vivo*

The effects of device chemistry and device permeability were evaluated in a subcutaneous pocket to evaluate barrier function and severity of inflammatory response. In section 3.4, the greatest accessible range of PEG-content in degradable tyrosine-derived ter-polymers was found to occur between I₂E1000 and I₂E1008(1k). In section 3.5, electrospun nonwoven fabrics with fiber diameter $\geq 1.0\text{ }\mu\text{m}$ were determined to be cell permeable, while those with fiber diameter $\leq 0.5\text{ }\mu\text{m}$ were cell-impermeable. Cell permeable and cell impermeable electrospun scaffolds were fabricated from I₂E1000 and I₂E1008(1k), Figure 3.3 and Table 3-1, for implantation in a subcutaneous pocket.

The electrospun fabrics were placed in a subcutaneous pocket created by blunt dissection. The progression of cell infiltration and severity of inflammatory reaction were observed at 2 and 4 weeks. Samples were recovered *en bloc* and fixed by diffusion, so patent blood vessels were indicated by red blood cells. Hematoxylin and eosin histological images are presented in Figure 3.18 and Figure 3.20.

The histological slides demonstrated that cells could grow into the bulk of an electrospun device and survive. Interestingly, different rates of cell infiltration were observed despite indistinguishable device architecture. While the I₂E1008(1k) device had fully swollen with inflammatory cells at 2 weeks, cells only migrated 40-60 μm into the I₂E1000 fabric. Johnson et al. observed the same ranking of smooth muscle cell migration on films of these polymers *in vitro* [162]. Some neovasculature was noted at two weeks in the I₂E1008(1k) device, while a similar amount of angiogenesis was only

noted at 8 weeks in the I₂E1000(1k) fabric. At eight weeks, more mature vascularity was noted within fabrics of I₂E1008(1k).

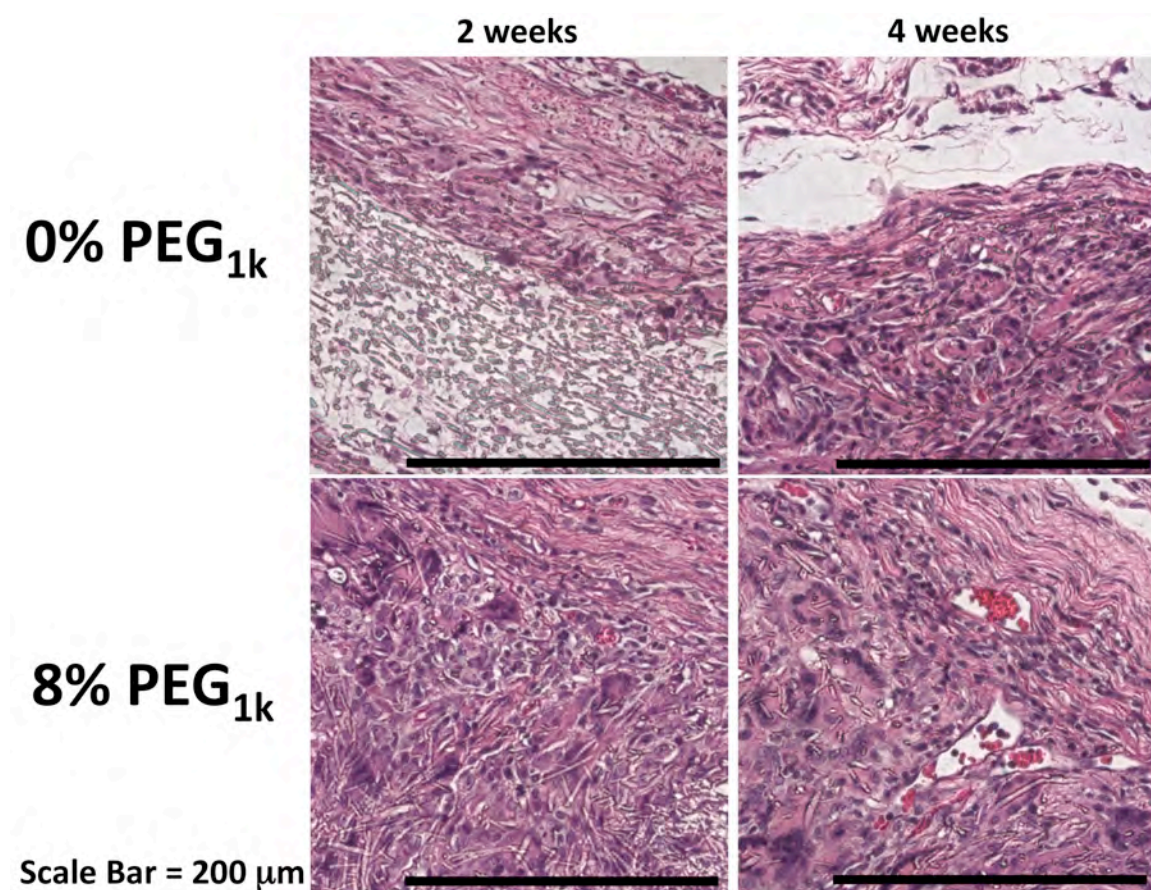


Figure 3.18. Two and four week tissue response to I₂E1000 and I₂E1008(1k) cell permeable nonwoven fabrics (H&E)

Both cell-permeable devices were completely swollen with cells by four weeks, and prominent fusion of macrophages into FBGCs had occurred. Monocytes migrating from newly patent vasculature were evident. Cell-permeable fabrics must be avoided for anti-adhesion device prototypes, for these devices were swollen with inflammatory cells. Fabric swelling is noted by the orientation of polymer fibers in these fabric cross-sections, Figure 3.19. If the thickness of the device had not expanded, the fibers would present round fiber cross-sections and parallel elliptical fibers. However, the fabric was expanded in the thickness direction, resulting in reorientation of the device fibers.

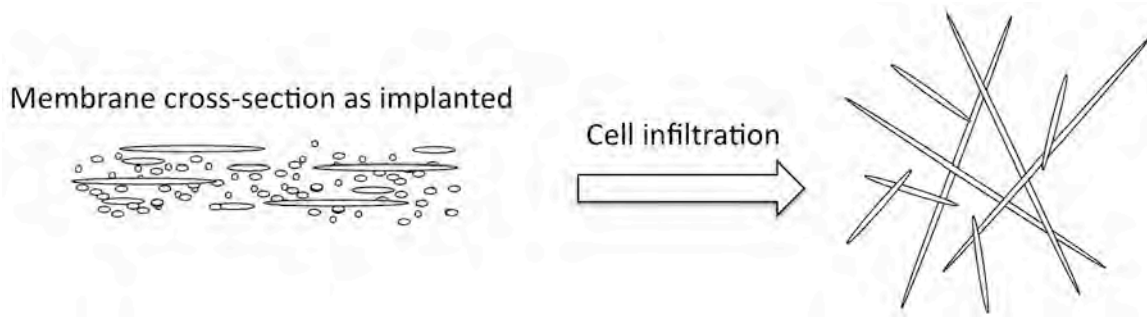


Figure 3.19. Sketch of remodeled polymer fibers after cell infiltration and proliferation

The $0.5\ \mu\text{m}$ fiber diameter fabrics were largely cell-impermeable over the four-week period. However, inflammatory cells penetrated the outer $30\text{--}40\ \mu\text{m}$ of the I₂E1000 scaffolds at two and four weeks, and similar penetration was observed at four weeks in the I₂E1008(1k) scaffolds, Figure 3.20. The inflammatory cells did not bridge the thickness of the scaffolds, so a continuous scar would not have been formed. However, due to the semi-permeability observed in these $0.5\ \mu\text{m}$ fiber diameter scaffolds, a preferable electrospun anti-adhesion device would be composed of finer fibers, have a lower pore fraction, or both.

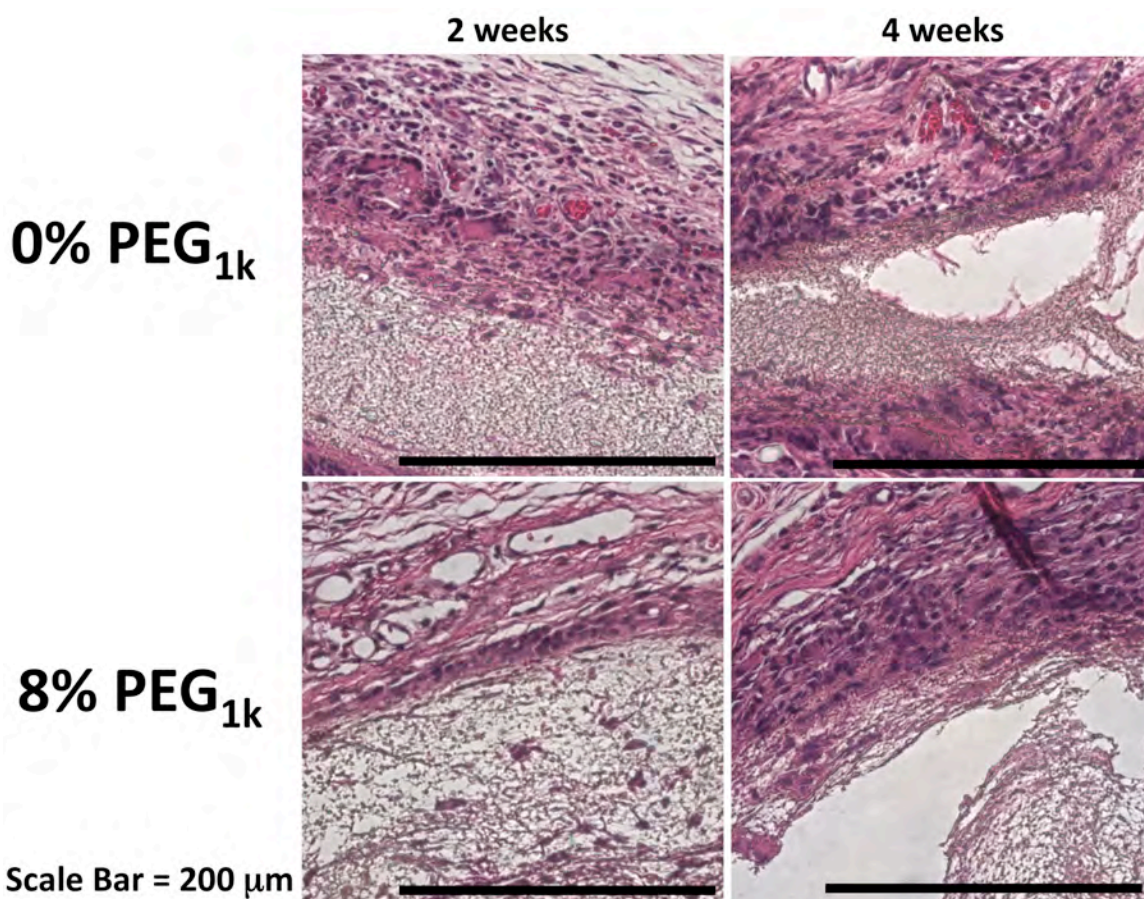


Figure 3.20. Two and four week tissue response to I₂E1000 and I₂E1008(1k) cell impermeable nonwoven fabrics (H&E)

In these studies, the only PEG-effect noted was the increased migration rate into cell-permeable fabrics. Intermediate levels of protein adsorption are known to increase cell migration rate [164]. Tziampazis et al. reduced protein adsorption, cell attachment and motility at 8 mol% PEG_{1k} in a series of E00YY(1k) polymers [164]. However, Macario et al. and Johnson et al. demonstrated that either iodination or DT incorporation diminished the protein repellency of PEG-containing materials [162, 163]. In Johnson et al.'s investigation, I₂E1008(1k) was insufficient to decrease protein adsorption or cell attachment compared to E0000, while smooth muscle cell migration rate was highest with 8 mol% PEG_{1k} in a series of I₂E10YY(1k) polymers [162].

Variation in polymer chemistry was no longer pursued for the anti-adhesion project, for neither the literature nor these experiments offered any positive biological effect within the range of tyrosine-derived polycarbonates that produce stable electrospun fabrics. Polymer selection will be made upon the criteria of degradation and drug delivery. Regarding shape stability under physiological conditions, minimal PEG-content is desirable. As low copolymerization with PEG_{1k} is desirable, the use of iodinated polymers can be circumvented as well. It is desirable to avoid iodinated polymers due to the low solubility of degradation products.

3.7 Dual-spinneret electrospinning and thermal heat treatments enhance the mechanical properties of electrospun nonwoven fabrics

Conventional electrospun nonwoven fabrics are stabilized through bonding of fiber-fiber intersections. This bonding occurs either upon deposition of fibers during fabrication or through sintering in a post-electrospinning heat treatment. If the polymeric fibers are swollen with solvent upon deposition, the plasticizing effect of the solvent allows subsequent layers of fibers to fuse together during fabrication. This approach is poorly controlled, for minor changes in electrospinning distance, room temperature, or humidity can alter the degree of fiber-to-fiber bonding. Post-electrospinning heat treatment can be effective, but the temperature control of vacuum ovens is relatively poor, the process is time consuming, and the lack of support in the *x-y* plane allows the polymeric fabric to contract. In this section, the enhancement of mechanical properties through use of dual spinneret electrospinning and rapid heat treatment with compression in a carver press will be discussed.

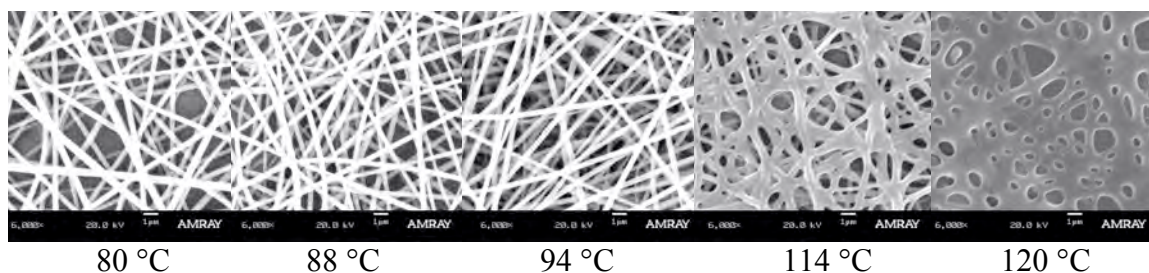


Figure 3.21. Progression of sintering to fusion of electrospun I₂E1008(1k) fibers in a vacuum oven.

Conventionally, an electrospun membrane is heated in a vacuum oven to sinter the fiber intersections. In Figure 3.21, the progression of fiber-to-fiber sintering is demonstrated for an I₂E1008(1k) electrospun fabric, $T_g=85\text{ }^{\circ}\text{C}$. Here, the oven temperature was roughly ramped from $80\text{ }^{\circ}\text{C}$ to $120\text{ }^{\circ}\text{C}$ over one hour. The goal is to produce a scaffold where fiber intersections are bonded, but the rest of the fiber architecture is not compromised, similar to the $94\text{ }^{\circ}\text{C}$ sample. In practice, desirable sintering can be achieved by heat treatment at a temperature near the onset of glass transition ($\sim 20\text{ }^{\circ}\text{C}$ below the midpoint T_g) for two hours. However, the adjustment of oven temperature is error prone, and fluctuations in oven temperature can result in the destruction of the sample, see the $114\text{ }^{\circ}\text{C}$ sample.

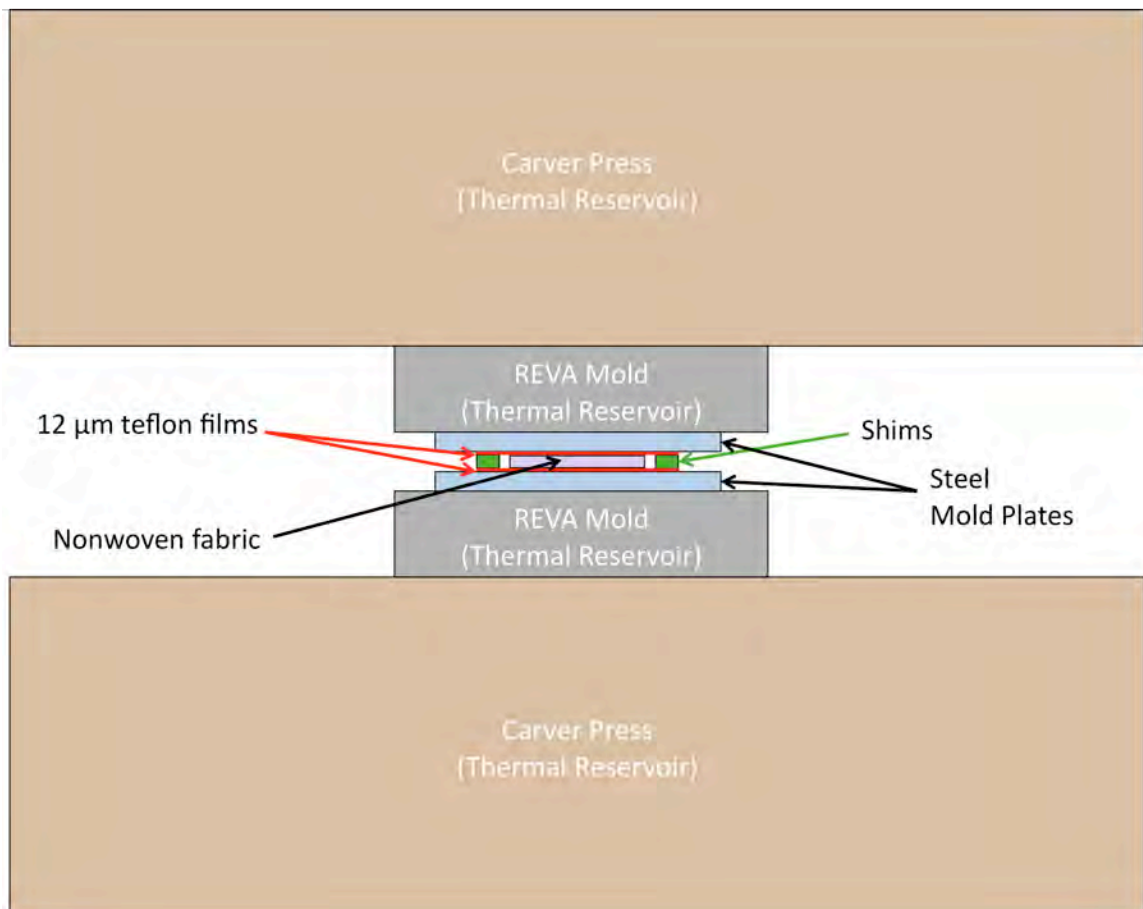


Figure 3.22. Schematic of the Carver press as used to heat treat nonwoven fabrics

Heat treatment by Carver press provides tightly controlled temperature and porosity. The large thermal reservoirs of the platens and REVA mold rapidly heat the steel plates of the mold and the nonwoven mat, Figure 3.22. The shims provide controlled compression of the fibers, apposing fiber-fiber intersections to promote sintering. Samples were prepared for heat treatment by assembling shims and nonwoven fabric between steel plates lined with 12 μm thick Teflon films. The plate assembly was placed into the preheated press, and 1,000 lbf was applied for 10 minutes. Shims were selected to achieve a target pore fraction of 0.50. In the compression of 30 electrospun anti-adhesion membranes, the initial pore fraction of 0.810 ± 0.005 was reduced to

0.587 ± 0.011 . Heat treatment by carver press increased the rate of heat treatment, enhanced temperature control, and permitted control of pore fraction.

Multilayered electrospinning was described by Kidoaki, Kwon, and Matsuda in 2005 [254]. The authors rapidly translated a collector horizontally beneath two adjacent spinnerets, such that the central portion of the collected mat was composed of alternating layers of fibers of each composition. At the New Jersey Center for Biomaterials, an electrospinning apparatus was constructed such that two spinnerets were arranged circumferentially around a rotating mandrel, Figure 3.23. This apparatus was first used to prevent the burst-release of mupirocin when delivering both mupirocin and lidocaine HCl from a single implant [255]. A similar device was used by Hong et al. to deliver antibiotics in a soft tissue reinforcement graft [256]. Here, the device will be used to improve the reproducibility of heat treatment and create nonwoven fabrics with superior delamination strength, suture-retention strength, and toughness.

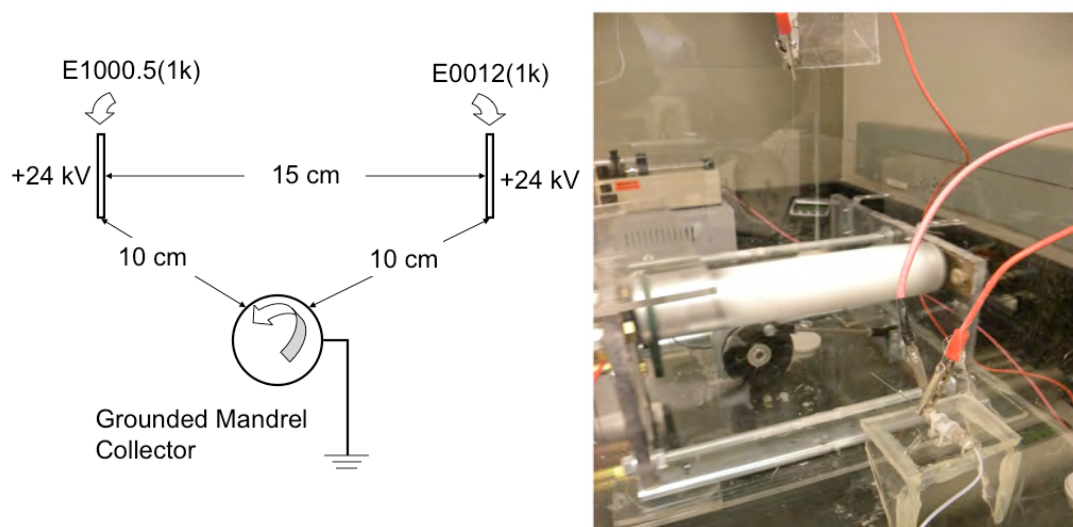


Figure 3.23. Schematic and photo of the NJCBM dual-spinneret electrospinning apparatus during operation. The mandrel appears white, for it is covered with an accumulating scaffold, while the spinnerets are located at the top and in the right foreground of the photograph.

As depicted in Figure 3.23, E1000.5(1k) and E0012(1k) were simultaneously electrospun at a 1:1 ratio into a single polymeric nonwoven fabric. The interpenetrating network of a glassy polymer ($T_g=88\text{ }^{\circ}\text{C}$) with a rubbery polymer ($T_g=35\text{ }^{\circ}\text{C}$ – before water uptake) resulted in a composite device where the E1000.5(1k) fibers provided structural stability, while the E0012(1k) fibers increased the compliance of the construct. In the following paragraphs, the heat treatment and subsequent properties composite and E1000.5(1k) anti-adhesion membranes are discussed.

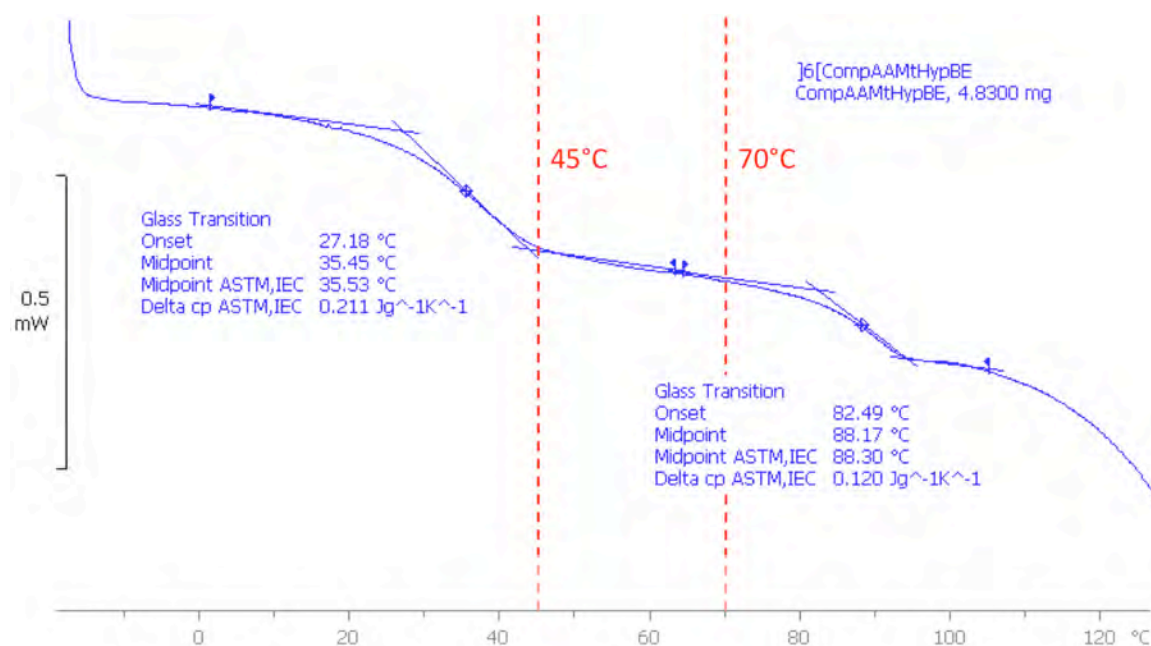


Figure 3.24. The DSC curves obtained for an electrospun 1:1 E1000.5(1k):E0012(1k) composite AAM. Each polymeric fiber was electrospun from acetic acid with a 1:5 loading of tHyp butyl ester HCl, frozen at $-80\text{ }^{\circ}\text{C}$, and freeze dried to remove residual acetic acid. The heat treatment temperatures for the composite ($45\text{ }^{\circ}\text{C}$) and E1000.5(1k) ($70\text{ }^{\circ}\text{C}$) AAMs are highlighted in red.

The E1000.5(1k) AAM was heat treated using at $70\text{ }^{\circ}\text{C}$ to soften the polymer and allow fiber-fiber intersections to bond under the compression to 0.50 pore fraction in the carver press. If temperatures within the glass transition range ($80\text{--}95\text{ }^{\circ}\text{C}$) were used, the fibers became too soft and melted. The t-peel delamination data and failure surfaces reveal that heat treatment at $70\text{ }^{\circ}\text{C}$ for 10 minutes under compression is sufficient to

sinter the fiber-fiber intersections, Figure 3.25. Composite AAMs could be heat treated at 45 °C, making the E0012(1k) component totally flowable, while the E1000.5(1k) component was well within its glassy range. Low temperature heat treatment prevents disruption of the oriented polymer chains in the electrospun E1000.5(1k) fibers and would permit the inclusion of enzymes or other bioactive molecules that may be sensitive to thermal degradation.

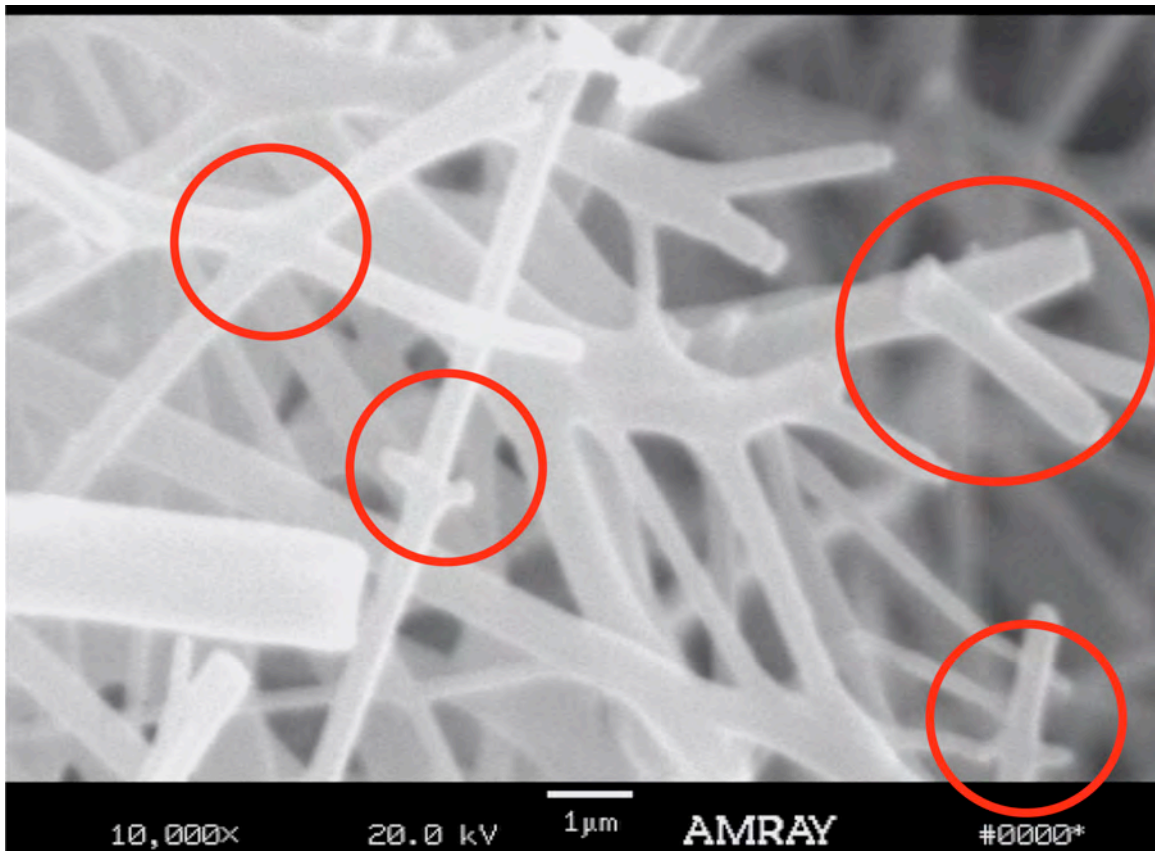


Figure 3.25. Fracture surface of E1000.5(1k) AAM. Red circles highlight some of the clearly sintered fiber intersections, while the maintenance of device porosity is evident.

Heat treated E1000.5(1k) and composite AAMs were evaluated by T-peel delamination, suture pull-out, and tensile strain. The first generation of AAMs implanted in the laminectomy site failed due to delamination, inciting an unacceptable inflammatory response in areas of delamination, section 5.2.3. The primary criterion for this second-

generation device was therefore to have superior delamination strength. Significant toughness and strain-to-failure is necessary to endure handling with sharp forceps (Dumostar #3 and #5), so maximum delamination strength is not the only criterion. Finally, the most successful synthetic membrane for peridural adhesion prevention, Gore-Tex ePTFE membrane, was sutured to the facet capsule to impart stability [130], so candidate AAMs were subjected to suture pull-out evaluation.

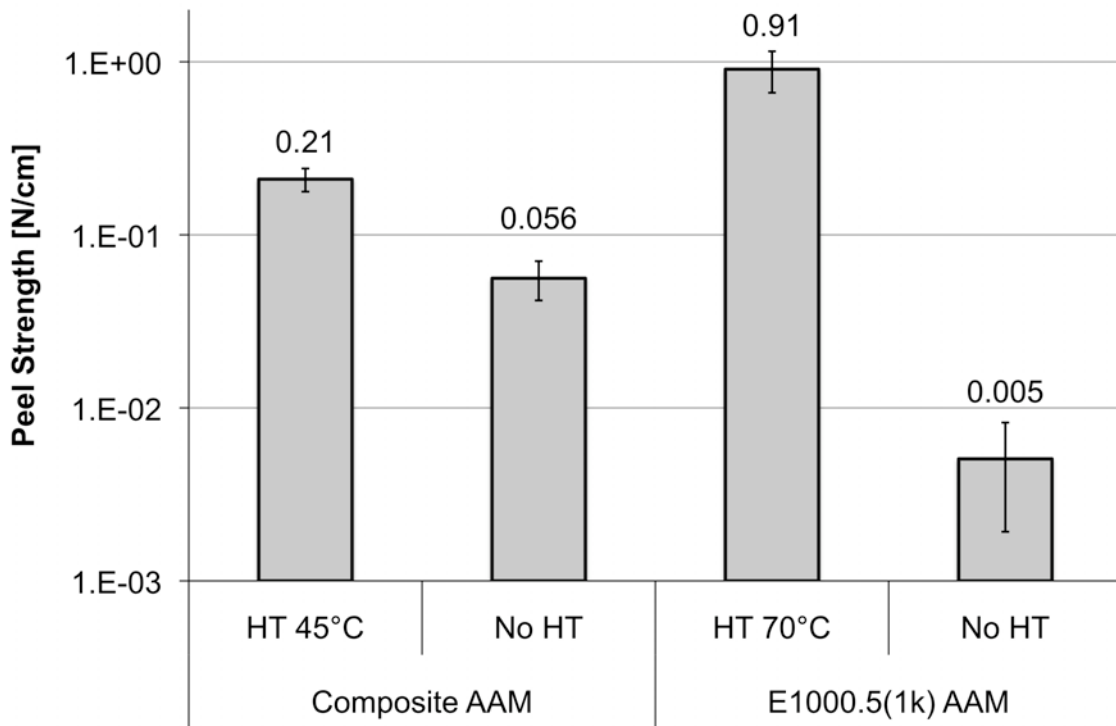


Figure 3.26. T-peel delamination strength of composite and E1000.5(1k) AAMs plotted on a logarithmic scale.

When electrospun from acetic acid, E1000.5(1k) AAMs possessed a delamination strength that was hardly distinguishable from the load cell baseline, while the composite AAMs possessed 10-times greater delamination strength, Figure 3.26. Upon their respective heat treatments, the E1000.5(1k) AAMs had 4.3-times greater delamination strength than the composite counterparts. The E1000.5(1k) AAMs had a network of glassy fibers that were fused at fiber intersections, while the E1000.5(1k) fibers within

the composite AAMs were unaffected by heat treatment at 45 °C. Rather, adjacent fiber layers within composite AAMs were adhered with the softer E0012(1k) polymer fibers. Additionally, only half the mass of composite AAM fibers participated in inter-layer sintering, while the entire fiber population within E1000.5(1k) membranes could bond adjacent fiber layers. The composition and thermal history of E1000.5(1k) AAMs yielded superior delamination strength.

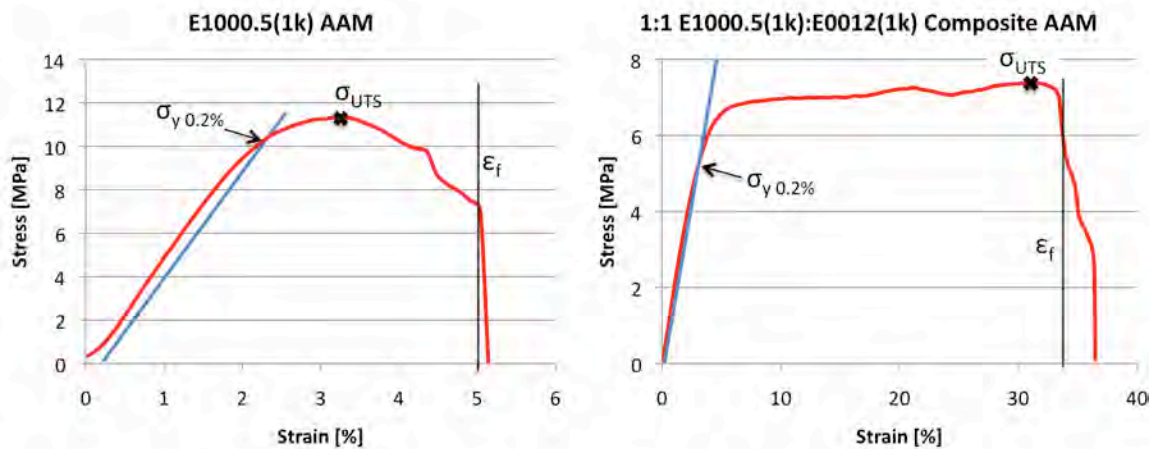


Figure 3.27. Representative stress-strain curves for E1000.5(1k) and composite AAMs, depicting the determination of key mechanical properties. Experimental data is shown in red, and the line used to determine the 0.2% offset yield strength is blue.

Following tensile evaluation at 10 mm/min, stress, σ , versus strain, ϵ , curves were plotted, and mechanical properties were calculated as follows. The modulus, E , of each curve was calculated as the slope of the linear portion of the stress-strain curve at low strain. The strain-to-failure, ϵ_f , was defined as the strain at the point where the specimen fails – the point where the load borne by the sample rapidly decreased. Yield strength, $\sigma_{y 0.2\%}$, was defined by the intersection of the stress-strain curve and a straight line with slope equivalent to the E , which has an x-axis intersection at 0.2% strain – often referred to as the offset yield point. This definition is used, for it is mathematically defined, rather

than subjective. The ultimate tensile strength, σ_{UTS} , is defined as the maximum stress endured by the specimen during the tensile test.

The toughness was also calculated. The toughness of a material can be understood as the energy per unit volume required to cause the device to fail. The toughness was calculated by integrating the stress-strain curve as follows:

$$T = \int_0^{\varepsilon_f} \sigma d\varepsilon \quad (3.3)$$

where T is toughness in Pascals, as ε is dimensionless. The units of T are equivalent to work per volume, as one Joule is equivalent to 1 N-m, so a J/m^3 is equivalent to 1 N/m^2 , or a Pascal. An estimate of the sample toughness was calculated by stepwise integration of the stress-strain curves, equation 3.4.

$$T = \sum_{i=1}^{n-1} \left(\frac{\sigma_{i+1} + \sigma_i}{2} \right) \cdot (\varepsilon_{i+1} - \varepsilon_i) \quad (3.4)$$

The tensile test results are summarized in Table 3-2.

Table 3-2. Mechanical properties of E1000.5(1k) and 1:1 E1000.5(1k):E0012(1k) composite electrospun Anti-Adhesion Membranes.

Property	E1000.5(1k) AAM		Composite AAM		T test	Ratio
E [MPa]	468	± 44	141	± 19	0.010	3.3:1
ε_f [%]	5.1	± 2.0	36	± 11	0.005	1:7.2
$\sigma_{y \ 0.2\%}$ [MPa]	10.8	± 1.2	5.6	± 1.3	0.005	1.9:1
σ_{UTS} [MPa]	12.1	± 1.4	6.8	± 1.1	0.012	1.8:1
Toughness [MPa]	2.4	± 1.3	0.47	± 0.12	0.028	1:5.2

Under tensile evaluation, the composite membranes had a lower modulus of elasticity, yield strength, and ultimate tensile strength. In the composite device, each of these properties decreases to approximately one-half the value observed in E1000.5(1k) devices. The reason for this difference is because the stiffer E1000.5(1k) fibers bear the mechanical loads placed upon the device, while the E0012(1k) fibers are highly

compliant and ductile, transferring loads between adjacent E1000.5(1k) fibers. Since only half of the mass of the composite device is composed of the stiff, load-bearing fibers, such a decrease in these properties is expected. The decreased modulus of the device is beneficial, for the composite device would more easily conform to tissue surfaces during placement and after implantation.

The composite AAMs have superior strain-to-failure, ϵ_f , and toughness. Impressive 7-fold and 5-fold improvements in ϵ_f and toughness mean that composite devices would have superior resistance to damage when handled with sharp objects during surgery. The dramatic improvement in ϵ_f is due to the low T_g polymer's ability to transfer load between adjacent high T_g fibers. In a thermally-bonded single-material electrospun mat, the polymer fibers are rigidly anchored together. When the longitudinally-oriented fibers yield then fail, the other randomly-aligned fibers are not able to reorient in the matrix and bear the load, so a defect propagates across the mat over a small change in strain. In contrast, the composite mat's E1000.5(1k) fibers are adhered by the more compliant E0012(1k), permitting E1000.5(1k) fibers to reorient in response to the longitudinally-oriented fibers' yielding and failure. The load transfers to newly longitudinally-aligned fibers as the strain increases up to ϵ_f , resulting in a long plateau at high σ from the onset of yield to ϵ_f , Figure 3.27. Despite having only half the $\sigma_{y\ 0.2\%}$ and σ_{UTS} of E1000.5(1k) AAMs, composite AAMs are 5 times tougher.

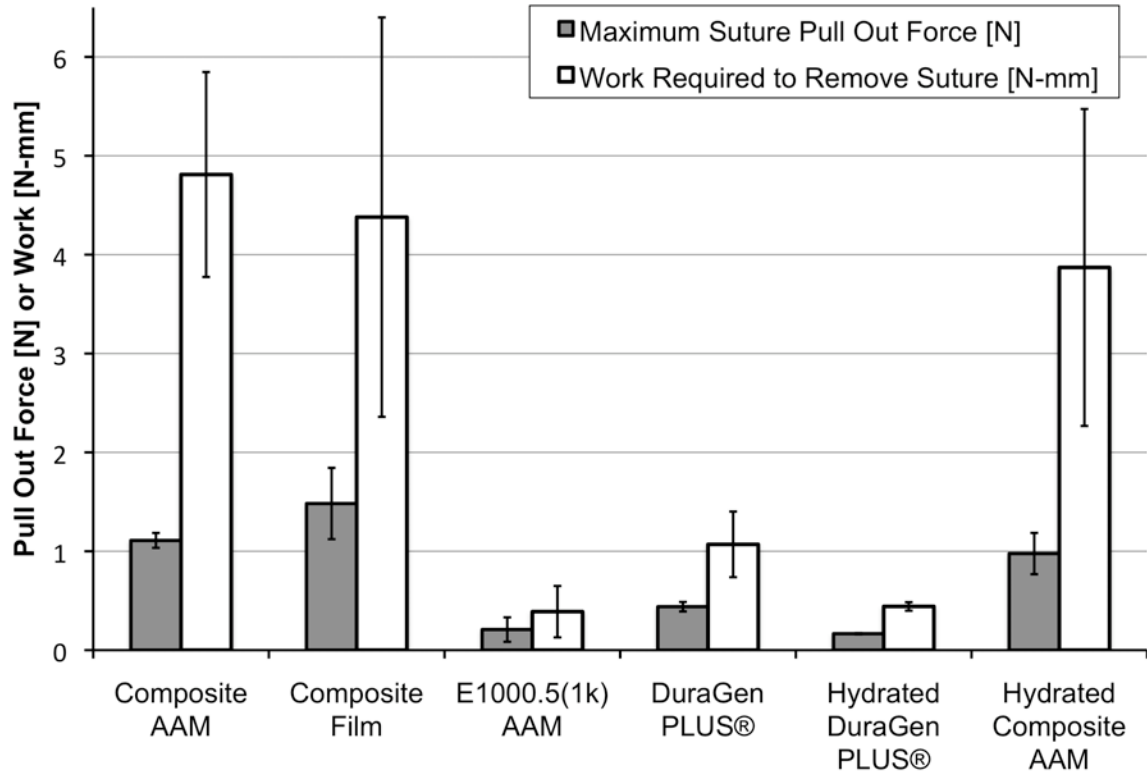


Figure 3.28. Suture pull-out performance of composite AAMs and films, E1000.5(1k) AAMs and DuraGen PLUS®.

The greater compliance and toughness of composite AAMs produced superior suture pull-out performance than E1000.5(1k) AAMs and the comparator device, DuraGen PLUS®. The suture pull out force and work of composite AAMs and composite films were statistically indistinguishable ($p = 0.28$, $p = 0.75$), while the suture pull out performance of composite AAMs was greater than both E1000.5(1k) AAMs and DuraGen PLUS® ($p < 0.001$ in all cases). Integra LifeSciences does not consider DuraGen PLUS® to be suturable, other than the optional presence of tensionless stay sutures. Upon hydration, the superiority of the composite AAM to DruaGen PLUS® was more dramatic. While DuraGen PLUS® lost 59 and 61% of its suture retention strength and work upon hydration, the suture pull out force and work of composite AAMs decreased only 12 and 20%.

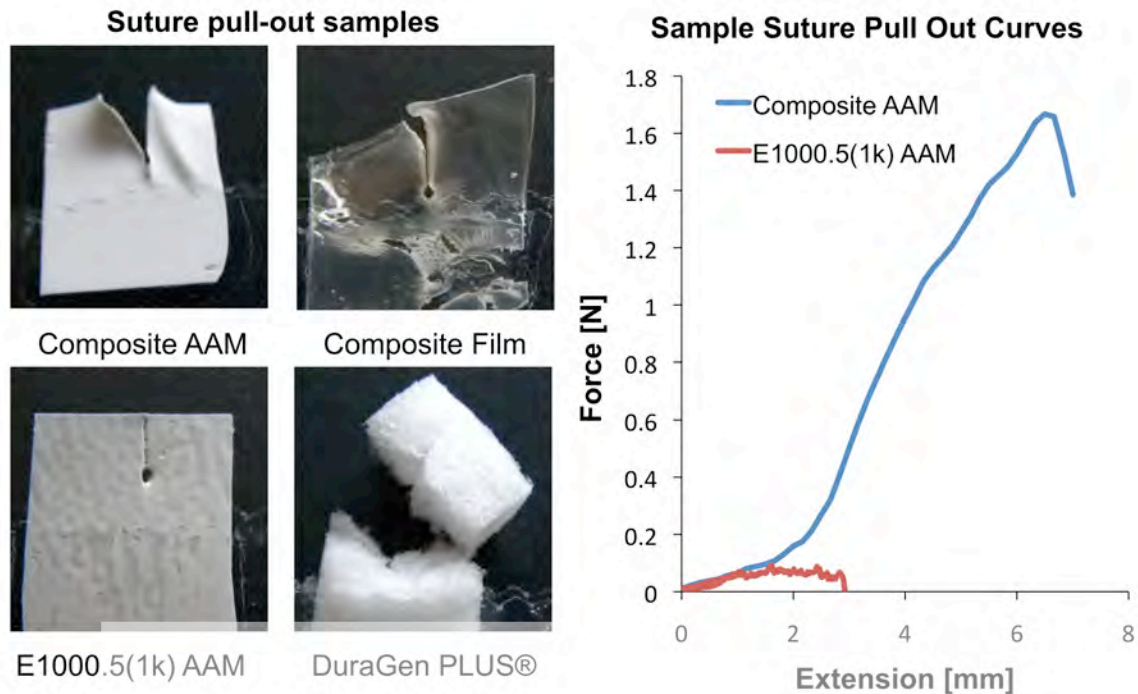


Figure 3.29. Failure surfaces of representative loading curves for suture pull-out samples. Note the degree of material deformation in the composite devices, while the E1000.5(1k) sample were cut cleanly by the 5-0 PROLENE suture. In the E1000.5(1k) sample, the extension at failure was identical to the insertion depth, 3 mm, while the deformation of the composite membrane allowed it to resist suture extraction to 7 mm.

The interpretation of increased E1000.5(1k) fiber recruitment was confirmed by inspection of the recovered samples and force versus extension curves, Figure 3.29. In both the E1000.5(1k) and composite membrane curves, the load in the suture increased from 0 to 0.9 mm extension as the curvature of the suture loop was reduced. Beyond 0.9 mm, the E1000.5(1k) AAM curve reached a plateau, where the withdrawing suture was met with a consistent amount of resistance from fracturing fibers. In contrast, the composite membrane's resistance to suture withdrawal increased significantly beyond 1.6 mm. At that point, the fibers behind the suture had fractured and the load was transferred laterally, recruiting additional fibers up to the point of failure, which dramatically increased the work required to remove the suture.

The use of composite electrospun construction yielded the required improvement in delamination strength and resulted in dramatic enhancement of device toughness and suture pull-out strength. Delamination strength was increased by adhering E1000.5(1k) fibers to each other in a sparse web of E0012(1k) fibers during compression molding at a temperature above the T_g of E0012(1k), but well below the T_g of E1000.5(1k). The delamination strength of heat-treated E1000.5(1k) electrospun AAMs was superior to the composite membrane, but the highly fused structure of these membranes was a detriment to their compliance, strain-to-failure, toughness, and suture pull-out strength. The rigid structure of the heat treated E1000.5(1k) membranes did not permit load transfer between fibers. In contrast, the highly compliant E0012(1k) material within the composite membranes permitted load sharing amongst E1000.5(1k) fibers that realigned to resist the applied loads.

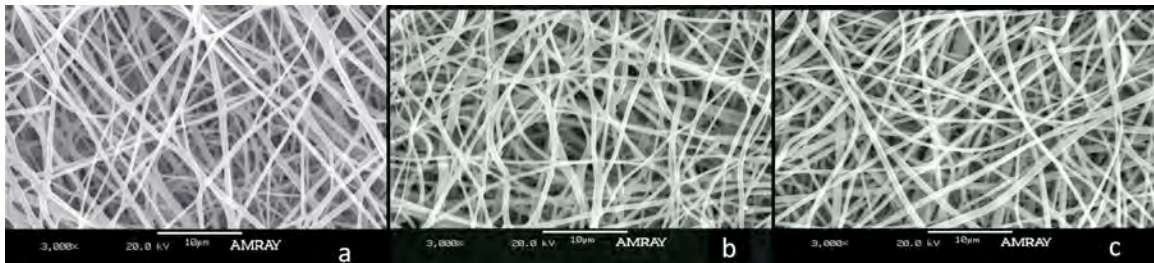


Figure 3.30. SEM images of (a) E1000.5(1k) AAM, (b) composite AAM with 1:5 tHyp butyl ester HCl loading, and (c) composite AAM with 1:5 cHyp octyl ester HCl loading

The porous architecture of the fibroporous mats was maintained following heat treatment in the carver press, Figure 3.30. SEM images confirm that the compression did not close the pores, and fluid permeability tests confirmed the potential for nutrient transport across the device. At a pressure of 50 cm H₂O, PBS would flow through the finished membranes at a rate of ~0.6 mm/s, which varied according to pore fraction (PBS flux @ 50 mmH₂O = $0.27\phi - 0.10$, for $0.53 \leq \phi \leq 0.67$). Analysis of the SEM images

revealed that each of the three mats had a fiber diameter of approximately 0.4 μm , Table 3-3. Thickness and mass per unit area measurements taken during heat treatment revealed that the composite AAMs had pore fraction of approximately 0.6, while the E1000.5(1k) materials had a pore fraction of 0.5, identical to the target pore fraction. Using Sampson's mathematical calculation of pore radius, equation 3.2, pore diameters were calculated based upon average and 95% confidence values of pore fraction and fiber diameter. In all three nonwoven fabrics, the average pore diameter was less than 1 μm . For comparison, the non-heat treated, 0.29 μm fiber diameter, cell impermeable nonwoven fabric in Figure 3.17 has an estimated pore diameter of 2.2 μm .

Table 3-3. Physical characteristics of final electrospun composite AAMs

Device	Fiber Diameter [μm]	Pore Fraction [1]	Average pore diameter [μm]		Thickness [μm]
			Central Estimate	High Estimate	
E1000.5(1k) AAM	0.40 \pm 0.03	0.49 \pm 0.06	0.43	0.62	66 \pm 8
Composite AAM tHypBE HCl	0.38 \pm 0.03	0.57 \pm 0.03	0.60	0.75	82 \pm 4
Composite AAM cHypOE HCl	0.43 \pm 0.04	0.61 \pm 0.01	0.83	0.95	91 \pm 4

Both the E1000.5(1k) and composite AAMs are candidate materials for the prevention of epidural adhesion, but the 1:1 E1000.5(1k):E0012(1k) composite membranes were selected for the final animal model due to their superior toughness and suture retention strength. The composite AAMs were competitively evaluated against DuraGen PLUS® for peridural adhesion prevention following laminectomy, section 5.3.

3.8 Electrospun scaffolds impart structural stability to low- T_g polymer films

As noted in sections 5.2.2 and 5.2.4, the stiffness of E0000 films created difficulties during implantation and permitted film fracture during the implantation period. A more compliant and tougher film could be fabricated from a polymer with a T_g

well below body temperature. The compliance of a low- T_g material would permit the implant to flex with the animal's movements without inducing high tensile and compressive stresses that lead to fracture.

The drawback of low- T_g materials is that they have poor shape retention – the exact property that imparts fracture resistance. As a consequence, the materials are difficult to handle and their shape may change upon hydration. When dry, E1224(1k) adhered to surgical instruments, causing difficulty in trimming or especially suturing, Figure 3.31. In suturing, the film adheres to the needle and resists piercing. The film is drawn to a cone or tube surrounding the needle. However, by incorporating E1002(1k) fibers into a matrix of E1224(1k), a suture is easily passed through the composite film device. The E1002(1k) fibers were first laminated between E1224(1k) films under minimal pressure, imparting suturability, Figure 3.31 method #1. However, by slowly increasing the compression force, a more homogenous composite film device was fabricated, Figure 3.31 method #2.

E1224(1k) film - 80 μm thick

Compression of films:

70 $^{\circ}\text{C}$, slowly advance platens without significant pressure for 9 minutes

70 $^{\circ}\text{C}$, ramp to 15,000 lbf, in 1 minute

hold 15,000 lbf 1 minute

release pressure over 30 seconds

Two E1224(1k) films with E1002(1k) electrospun fabric

Composite compression method #1:

70 $^{\circ}\text{C}$, contact only, 30 minutes

Two E1224(1k) films with E1002(1k) electrospun fabric

Composite compression method #2:

70 $^{\circ}\text{C}$, contact only, 10 minutes

70 $^{\circ}\text{C}$, 1,000 lbf, 10 minutes

70 $^{\circ}\text{C}$, ramp to 10,000 lbf in 1 minute

hold 10,000 lbf 4 minutes

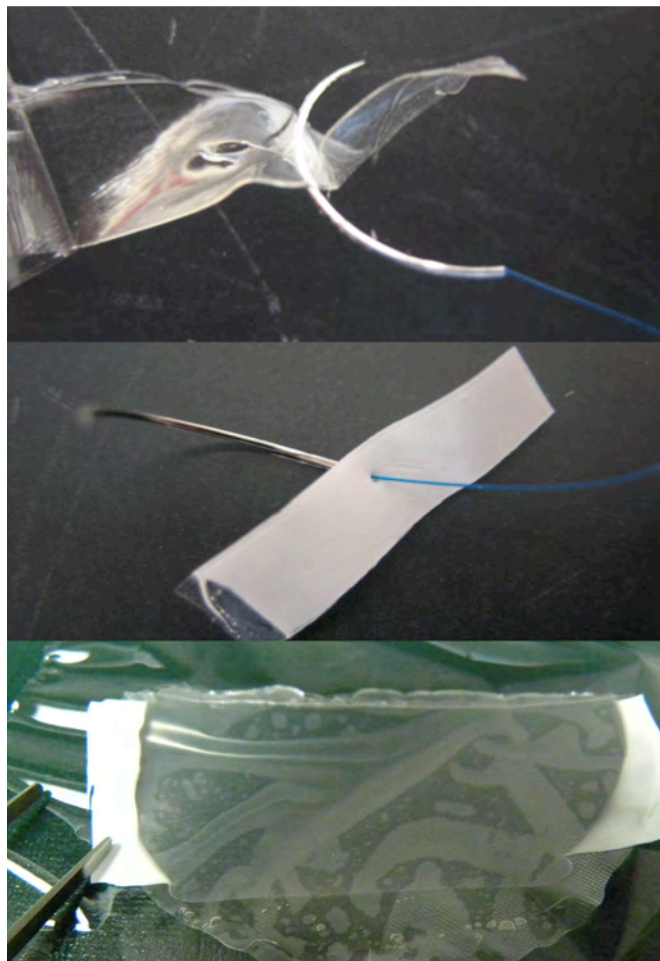


Figure 3.31. Compression molding treatments used to fabricate E1224(1k) films and composite film devices that incorporate E1002(1k) fibers to impart shape stability and suturability.

Composite film devices fabricated by method #2 consisted of a matrix of E1224(1k) reinforced with E1002(1k) fibers. The E1002(1k) fibers remained a unique phase while the E1224(1k) flowed into the fabric's void space. E1002(1k) fabrics remained opaque white when subjected to the same 70 $^{\circ}\text{C}$ compression procedure. Additionally, the margins adjacent to the composite film were opaque white, and a clear delineation existed between the transparent E1224(1k) film and the translucent E1002(1k) composite film. The translucent nature of the composite film indicated that an

interface between the two phases exists. Finally, a film composed primarily of E1224(1k) could not have retained its shape during suture pull-out evaluation without a distinct phase of a glassy polymer, Figure 3.29. This highly-flexible composite film device circumvented shape instability and handling shortcomings of Low- T_g polymer films, and served as the degradable fracture-resistant replacement for E0000 in the final laminectomy study, section 5.3.1.

3.9 Sterilization of degradable PEG-containing tyrosine-derived polycarbonates

PEG-containing TDPC electrospun fabrics would contract upon sterilization by ethylene oxide gas. When E1000.5(1k) electrospun scaffolds were sterilized as part of a large sterilizer load, a length per length contraction of 17% was observed (31% by area). Additionally, the sterilized scaffolds had higher flexural rigidity. The contraction and changes in handling properties were due to fiber fusion during sterilization, and these changes were more severe at greater concentrations of ethylene oxide, Figure 3.32.

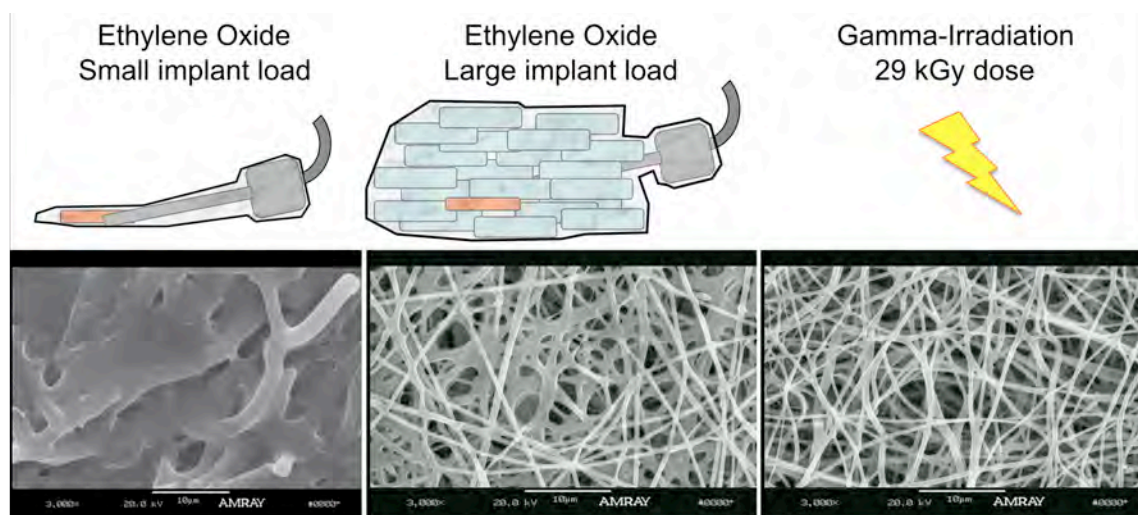


Figure 3.32. Comparison of scaffold architecture following sterilization by high and normal concentrations of ethylene oxide gas or gamma-irradiation. Note the concentration dependent fusion of polymer fibers during ethylene oxide gas sterilization.

Sterilization by gamma-irradiation did not affect the scaffold architecture, nor did it cause contraction of the scaffold. However, gamma-irradiation did reduce polymer molecular weight, as previously demonstrated for TDPCs [257]. Figure 3.33 depicts the effect of anti-oxidant loading, and hydroxyproline alkyl ester HCl salt on the molecular weight of composite AAMs as spun, after heat treatment, or after gamma-irradiation (29 kGy). The only statistically significant effect was gamma-irradiation ($p < 0.01$). Electrospun composite AAMs lost 25% molecular weight, while the composite film devices decreased 17% in molecular weight. Gamma-irradiated composite AAMs and films without antioxidant loading were used in the comparator rat epidural adhesion prevention study, section 5.3.

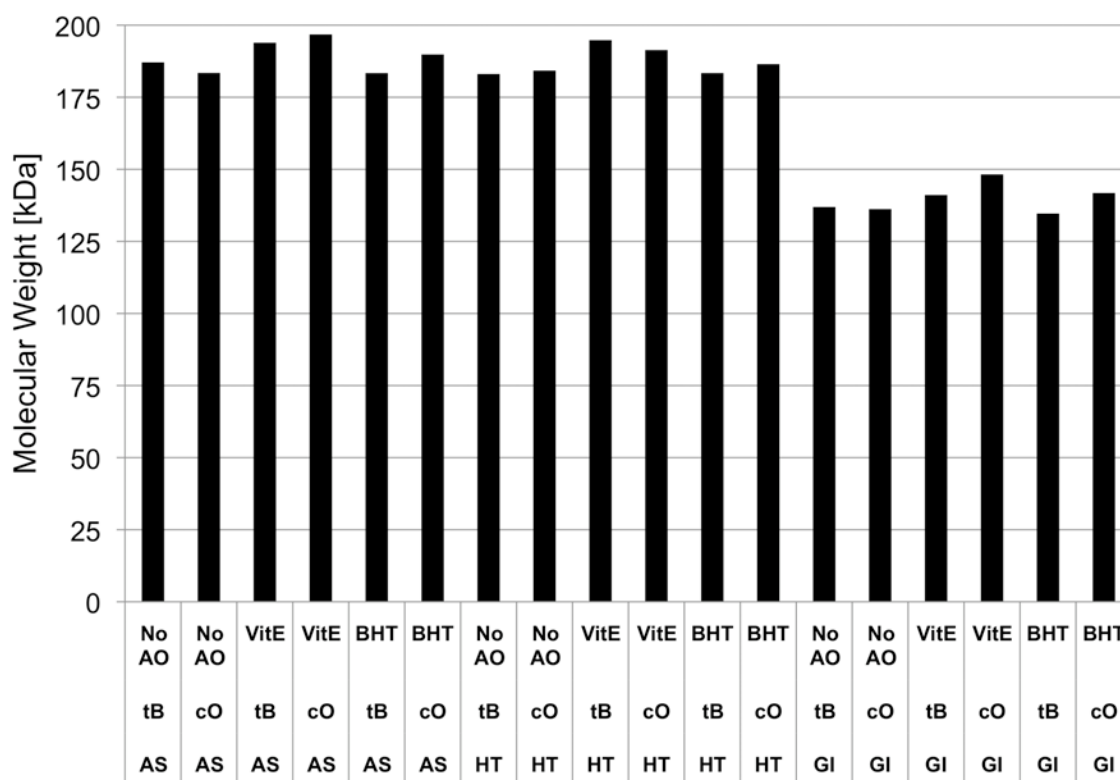


Figure 3.33. Effect of gamma-irradiation (29 kGy), heat treatment, hydroxyproline alkyl ester HCl salt, and antioxidant loading on device molecular weight. Treatment: as spun (AS), heat treated (HT), or gamma-irradiated (GI); hydroxyproline alkyl ester HCl: tHyp butyl ester HCl (tB), cHyp octyl ester HCl (cO); antioxidant: none (No AO), 0.1% vitamin E (VitE), 0.1% butylated hydroxytoluene (BHT).

3.10 Conclusions regarding the fabrication of anti-adhesion membranes

The establishment of an electrospinning facility at the NJCBM enabled creative expansion of the conventional technique to leverage the synthetic expertise of the group and broad thermal and mechanical properties of TDPCs. While acquiring electrospinning expertise, cell-impermeable and cell-permeable fabrics were electrospun from conventional solvent systems (e.g., DCM/DMF, THF/DMF, and HFIP).

The laboratory's synthetic capabilities were utilized to synthesize degradable weak surfactants that enabled bead-free electrospinning from acetic acid, a solvent of low toxic potential. tHyp octyl ester HCl was effective in preventing bead formation at a 1:25 surfactant : polymer loading. tHyp butyl ester HCl demonstrated the least toxicity, yet was capable of inhibiting bead formation at a 1:5 surfactant : polymer loading.

Polymer T_g governed the range of amorphous TDPCs useful in electrospinning. If a polymer transitioned from glassy to rubbery upon exposure to physiological buffer, the relaxation of polymer chain alignment resulted in catastrophic contraction of the devices. The contraction of an anti-adhesion device for neurosurgery would thwart their intended barrier function, so such polymers were excluded. The greatest range of PEG_{1k}-incorporation was provided by iodinated polymers, for their T_g s were approximately 40 °C higher than the corresponding non-iodinated polymers. Up to 8 mol% PEG_{1k} content was obtained without catastrophic contraction.

Subcutaneous implantation of cell-permeable and cell-impermeable fabrics demonstrated enhanced cell penetration in I₂E1008(1k) fabrics versus I₂E1000(1k) fabrics, consistent with cell motility data observed in vitro [162]. As polymer compositions containing I₂ or DT suppress the non-fouling performance of copolymers

containing PEG_{1k} and no PEG-effect was observed in cell-impermeable fabrics, polymers with low PEG-content were chosen for use in the anti-adhesion device for neurosurgery.

A Dual spinneret technique enabled the fabrication of an interpenetrating network of high- T_g and low- T_g fibers. Heat treated scaffolds of a 1:1 composition of E1000.5(1k) and E0012(1k) had superior suture retention strength, compliance, strain-to-failure, and toughness in comparison to conventional E1000.5(1k) devices. While E1000.5(1k) devices heat treated by compression molding at 70 °C had greater delamination strength, the composite film device's delamination strength was 40-times greater than a non-heat treated E1000.5(1k) fabric.

Composite AAMs electrospun from acetic acid solutions were superior candidates for implantation in a laminectomy defect, for they had lower toxic potential, better handling properties, and greater mechanical integrity than conventional electrospun fabrics.

4 Controlled delivery of *cis*-4-hydroxy-L-proline

The imino acid *cis*-4-hydroxy-L-proline is a well-known antifibrotic agent, but controlled delivery of the molecule has proven challenging. The molecule's small molecular weight and hydrophilic nature prevent retention in common polymeric materials, [237]. Rather than directly incorporating cHyp into the polymeric matrix, more hydrophobic cHyp precursor molecules were designed, synthesized and evaluated. The aim of the work was to create a system that would slowly release cHyp to areas of fibrosis surrounding the implant, Figure 4.1. The synthesis and remodeling of granulation tissue occurs over a period of weeks [8], so four weeks was chosen as a target timeframe for the delivery of cHyp. In this chapter, I hypothesize that precursors to cHyp provide a tunable system to modulate sustained release of cHyp from degradable polymeric implants.

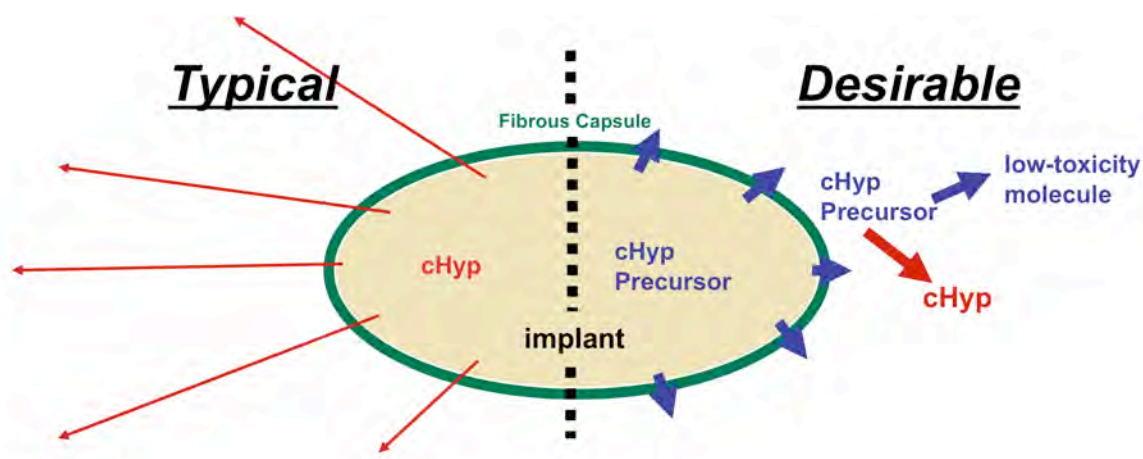


Figure 4.1. Typical and desirable release paradigms for cHyp

4.1 Exploratory synthesis and characterization of cHyp precursor molecules

The approach to delivering cHyp was to increase retention in the polymer matrix by creating a precursor to cHyp that is more hydrophobic, similar to the polymeric

materials commonly used in medical devices. A calculated octanol-water partition coefficient, ClogP, was used as the primary predictor of the retention potential of precursor molecules. Hydrolysis was chosen as the preferred method of releasing cHyp, for body pH and temperature are tightly regulated.

The molecules evaluated in this chapter range in hydrophobicity, molecular weight, and susceptibility to hydrolysis, Figure 4.2. Hydrophobicity is indicated by CLogP values, for CLogP is the estimation of $\text{Log}_{10}(C_{\text{octanol}}/C_{\text{water}})$ if a separation were performed of the test molecule against octanol and water. Greater hydrophobicity and molecular weight should each promote greater retention. CLogP varies from -1.91 for cHyp and 2.67 for cHyp octyl ester HCl. As cHyp rapidly diffuses from polymeric implants, it is essential for the hydrolytically active bond to remain stable in the polymer for at least one week and up to the targeted delivery period of four weeks. The bond types investigated were (in decreasing order of hydrolytic susceptibility): lactone, carbonate, and ester bonds.

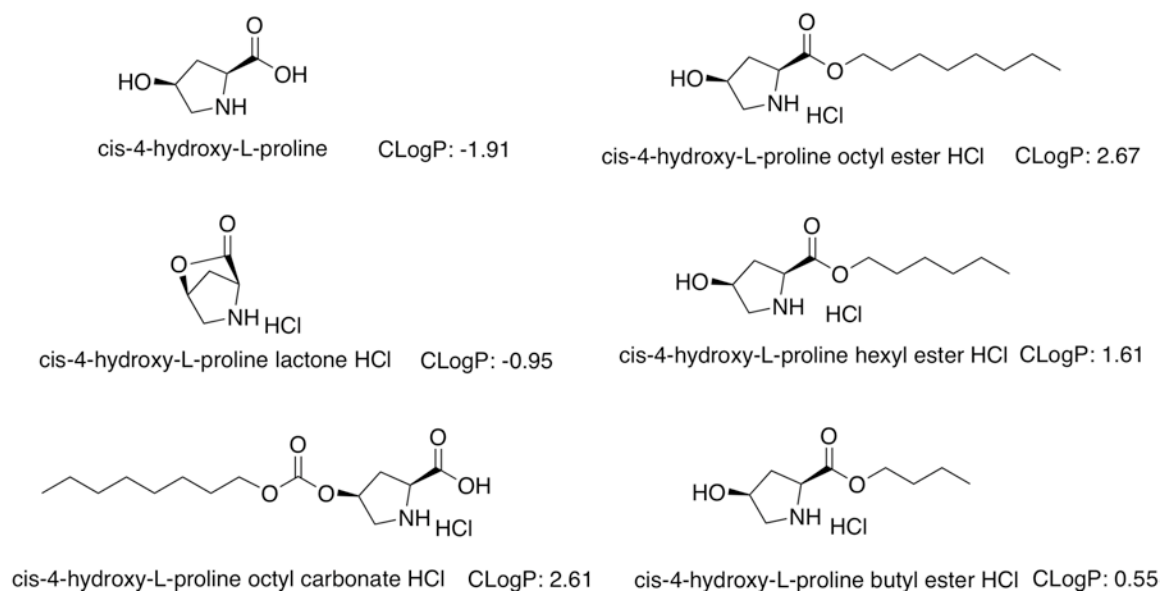


Figure 4.2. Molecules evaluated for the release of cHyp, which vary in hydrophobicity, molecular weight, and susceptibility to hydrolysis.

The rationale, synthesis, characterization, and evaluation of each of these candidate precursors are evaluated in the following sections. A preferred precursor was selected, its toxicity was screened in a rat subcutaneous pocket, and the degradation of final polymer-precursor electrospun nonwoven mats was evaluated.

4.2 **cis-4-hydroxy-L-proline lactone**

The lactone precursor was pursued first, for cHyp is recovered upon hydrolysis. In comparison to cHyp, cHyp lactone has a 10-fold greater preference to distribute into octanol versus water, so the formation of this cyclic bond has potential to control the release of cHyp. No additional molecules would be incorporated into the implant, circumventing additional toxicological evaluation.

4.2.1 **Synthesis of cis-4-hydroxy-L-proline lactone**

The synthetic scheme to synthesize cHyp lactone HCl was adopted from Poiani et al., who generated cHyp lactone as an intermediate to tether cHyp to a water-soluble polymer [240]. The scheme follows their synthetic steps VII through IX, substituting Benzyloxy-carbonyl (Z) protection of the secondary amine for Boc-protection, and subsequently replacing deprotection by hydrogenolysis instead of acidolysis.

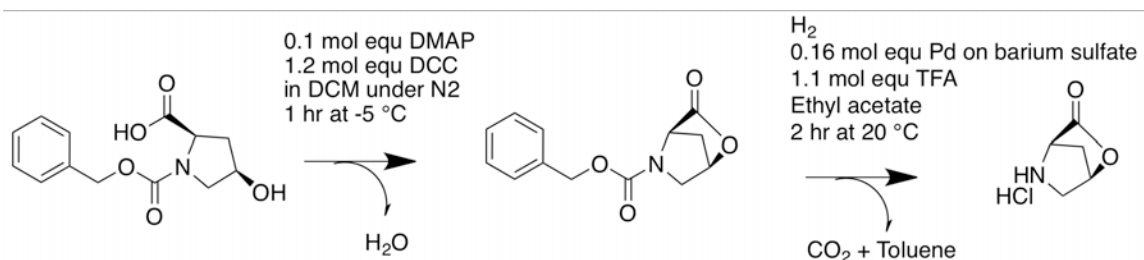


Figure 4.3. Synthetic scheme for producing cHyp lactone HCl

4.2.2 Characterization of *cis*-4-hydroxy-L-proline lactone

The formation of the lactone bond was confirmed by both ^1H -NMR and FTIR. In formation of the lactone, the proton corresponding to the carboxylic acid disappears (12.5 ppm), Figure 4.4. Additionally, the integration of the peak near 4.5 ppm, decreased in integration from 2.16 protons to 0.90 protons, corresponding to the loss of the hydroxyl group. In the deprotection step, the aromatic peaks at 7.3 ppm and the CH_2 peaks at 5.1 ppm both disappear as expected. However, an impurity with low chemical shifts appears to be present in the final product. Before further purification, the molecule was evaluated for its potential to control the release of cHyp.

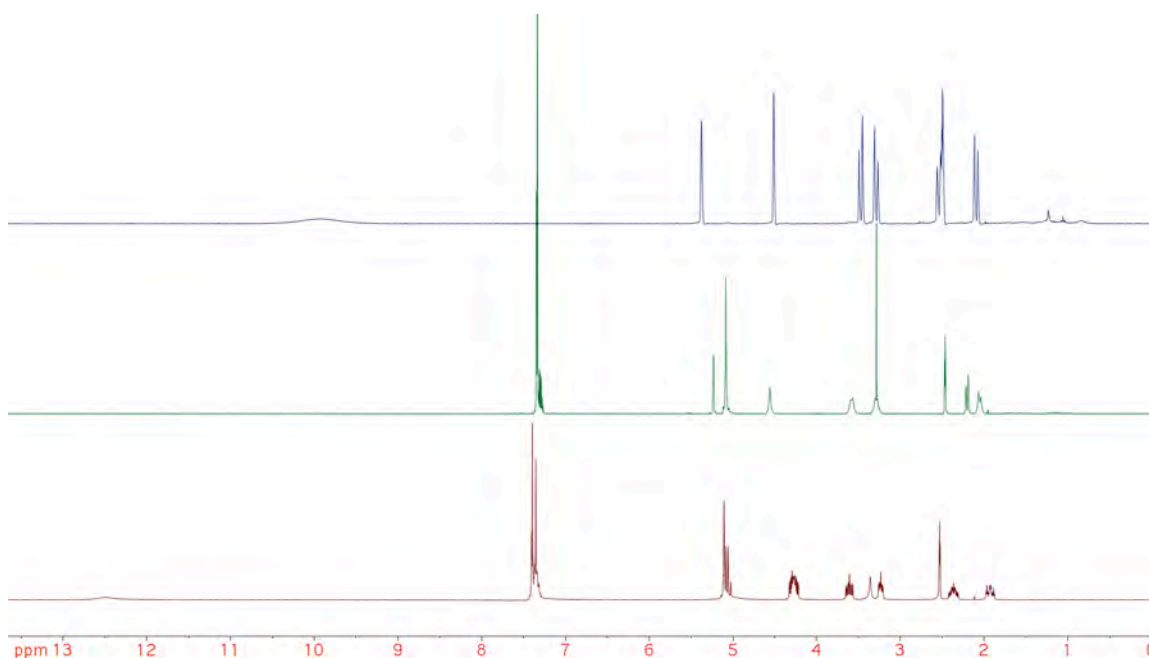


Figure 4.4. Formation of lactone confirmed by NMR. The three spectra are for the starting material (red), Z-protected cHyp lactone after flash chromatography (green), and the final product, cHyp lactone HCl (blue).

Fourier transform infrared (FTIR) spectroscopy was used to corroborate the ^1H -NMR results and verify lactone formation. The $\text{C}=\text{O}$ stretch region ($1790\text{--}1650\text{ cm}^{-1}$) was monitored for a new peak, corresponding to the lactone, and the disappearance of a peak

due to the carboxylic acid. In this region, a new, high wavenumber peak appeared at 1799, which was attributed to the formation of the lactone. The C=O stretch corresponding to the carboxylic acid (1751 cm^{-1}) remained in the impure intermediate, but following purification, no infrared absorbance peak remained near 1750 cm^{-1} . Verifying conversion of the carboxylic acid to the lactone.

Table 4-1. Inspection of the C=O stretch region ($1790\text{-}1650\text{ cm}^{-1}$) verifies lactone formation.

molecule	peak assignment	Wavenumber [cm^{-1}]	Intensity
Z-cHyp	Protecting group	1684	1.87
	Carboxylic acid	1763	1.33
Z-cHyp lactone	Protecting group	1708	1.47
before flash	Carboxylic acid	1751	0.88
chromatography	Lactone	1799	1.01
Z-cHyp lactone	Protecting group	1688	0.90
after flash	Lactone	1797	0.84
chromatography			

cHyp lactone HCl did not provide controlled delivery of cHyp lactone from electrospun E0000. Both cHyp lactone HCl and cHyp were electrospun into E0000 fibers at a loading of 1:5 precursor : polymer. Release kinetics into DI water were evaluated by HPLC. In cHyp lactone HCl scaffolds, the average release reached the 49% study-wide average at 1 hour. To investigate the recovery of cHyp from the lactone, 2.10 mg cHyp lactone was added to an HPLC vial with 1 mL DI water. From 1 hour to 10 hours, 1.07 ± 0.07 mg cHyp was recovered. This measurement confirmed that the cHyp lactone product contained ~50% impurity by mass. This impurity is likely due to palladium on barium sulfate. Palladium is dense (12 g/cm^3), and some of the particles were very fine and difficult to filter. At this small synthetic scale a small amount of palladium translated into a large fraction of impurity. Correcting the acquired release curves to compensate for the impurity level results in immediate burst release of 100% of cHyp from the E0000 fibers.

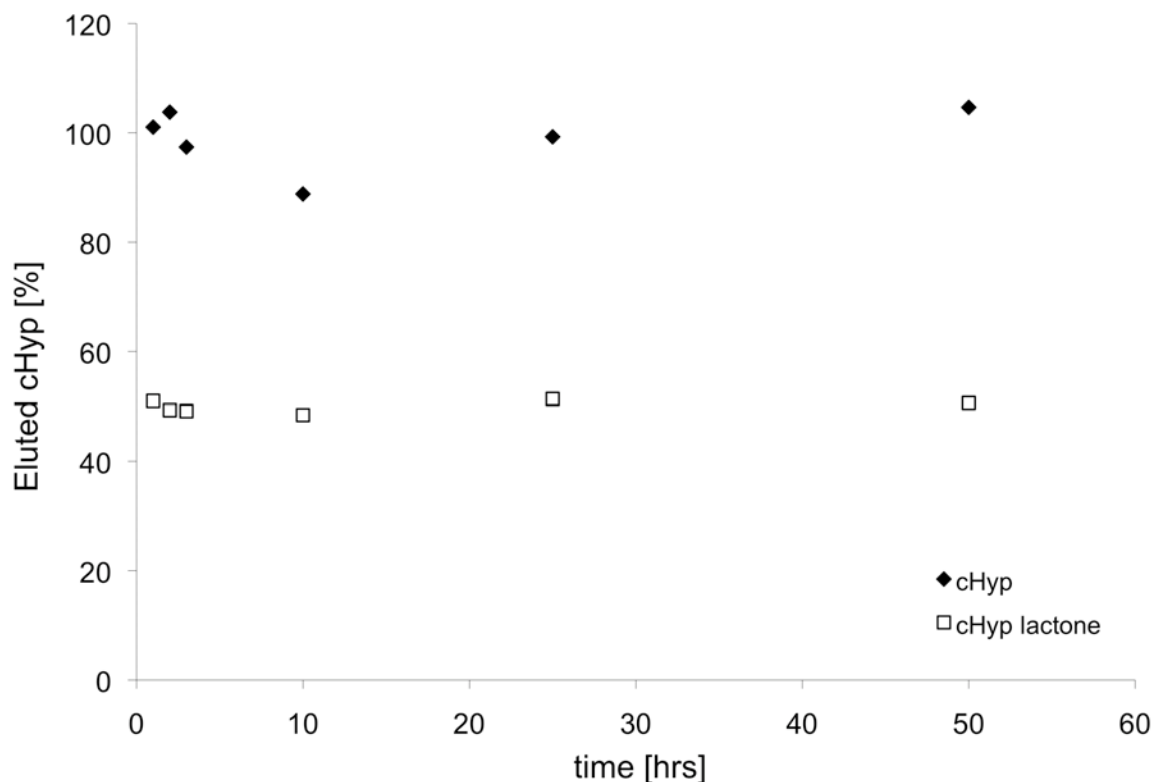


Figure 4.5. Release of cHyp from electrospun E0000 fabrics containing either cHyp or cHyp lactone by HPLC.

The hydrolytic sensitivity of cHyp lactone was highlighted when preparing cHyp lactone HCl samples for HPLC in either HPLC grade water or acetonitrile. The cHyp lactone HCl water sample was immediately injected for analysis, followed by the sample prepared in acetonitrile. The chromatograms demonstrate that cHyp lactone HCl hydrolyzed within five minutes of exposure to water, Figure 4.6. Furthermore, the sample prepared in acetonitrile contains cHyp, indicating that cHyp lactone HCl will hydrolyze during storage at 4 °C.

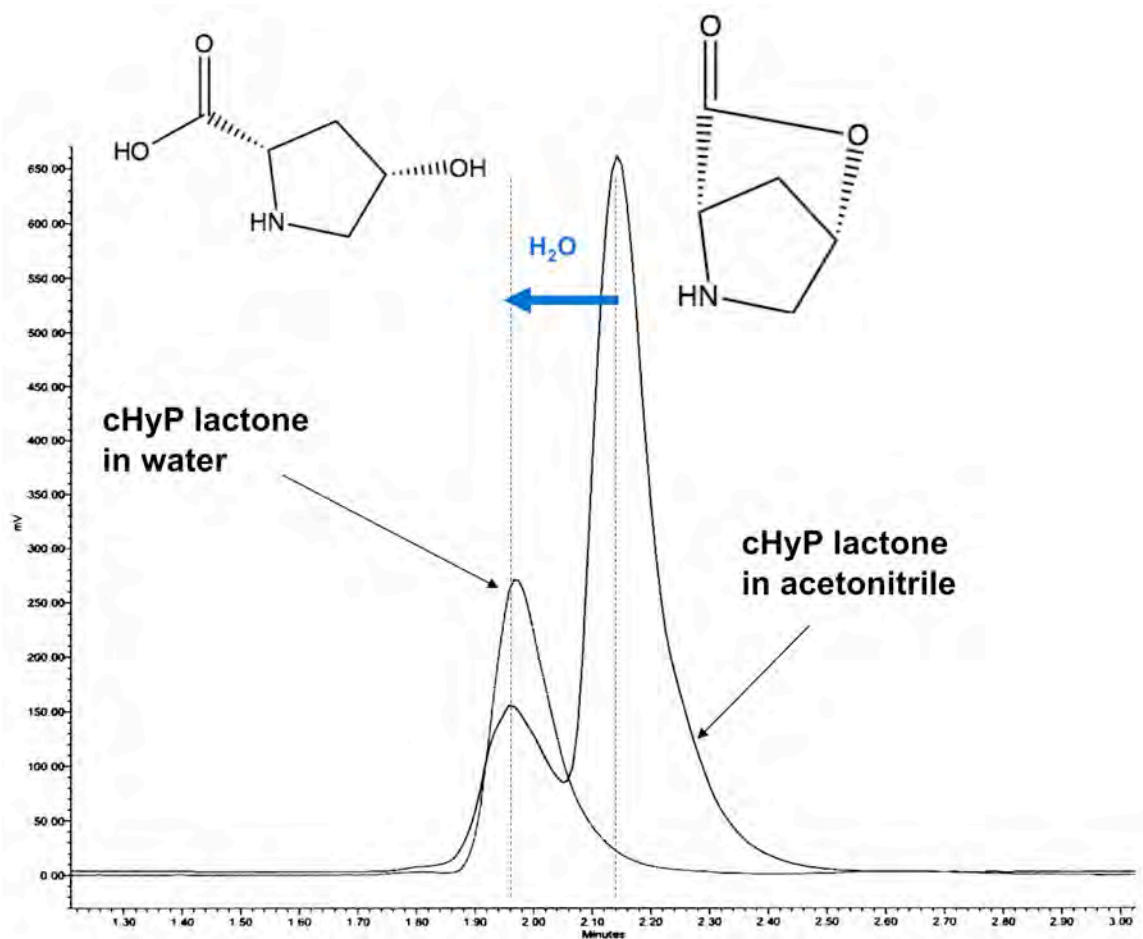


Figure 4.6. HPLC chromatograms of cHyp lactone HCl samples prepared in acetonitrile and DI water. Complete hydrolysis of cHyp lactone HCl in water was observed at 5 minutes.

4.2.3 Utility of *cis*-4-hydroxy-L-proline lactone HCl

cHyp lactone HCl is not a suitable cHyp precursor molecule. The product is so hydrolytically unstable that it hydrolyzes within 5 minutes of contact with water, and significant hydrolysis occurred during 7 weeks of storage at 4 °C. Inclusion of the molecule in a matrix of E0000 did not slow its hydrolysis, as 100% of the cHyp load was delivered within 1 hour of the implant's immersion in DI water. The observed release kinetics for cHyp lactone HCl were indistinguishable from those of cHyp. Therefore, this molecule had no utility for this project was abandoned.

4.3 *cis*-4-hydroxy-L-proline alkyl ester HCl salts

A series of cHyp alkyl ester molecules was chosen for inspection, for the ester bonds explored here are significantly more stable to hydrolysis than the strained, cyclical ester bonds found in cHyp lactone HCl. Schoenmakers et al. demonstrated that ester bonds could be used to release drugs through hydrolysis with 50% delivery observed at either 5 or 16 days [258]. That range of hydrolytic activity was consistent with the aim of sustained cHyp delivery over four weeks. Alkyl esters of cHyp were pursued, for the alcohol degradation products are part of the polymer library. The pendent chains of the DTR monomers vary from ethyl through octyl esters, [160]. Ethanol and Butanol are considered solvents of “low toxic potential,” while the higher MW alkyl alcohols are not [216]. As the Kohn laboratory continues to pursue products containing DTO, the inclusion of octanol into an anti-adhesion device for neurosurgery would not enlarge the NJCBM catalog of degradation products.

4.3.1 Synthesis of *cis*-4-hydroxy-L-proline alkyl ester HCl salts

The synthetic strategy for production of cHyp alkyl ester HCl salts was adapted from an NJCBM laboratory protocol for monomer synthesis REF. The reaction is performed in the alcohol of interest. The reaction vessel with alcohol is cooled to -5 °C in a saturated NaCl ice bath. 1.2 mol equivalents of thionyl chloride were added dropwise to the alcohol while stirring. The thionyl chloride activates the octanol, producing octyl chloride, Figure 4.7. After alcohol activation, cHyp is added to the reaction vessel. Upon addition, cHyp is insoluble in the alcohol. The vessel is slowly heated to 90 °C; the reaction proceeds at this temperature for four hours. During either the slow heating or 4-hour reaction time, the solution becomes clear, indicating that the

ester has formed. The product's alkyl ester facilitates dissolution in the respective alcohol.

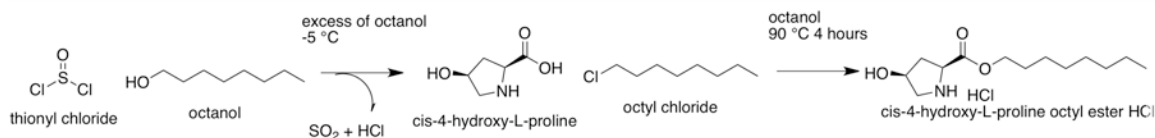


Figure 4.7. Synthetic scheme for producing cHyp octyl ester HCl. The same approach was applied for other alkyl ester HCl salts by varying the alcohol in which the synthesis is performed

The product is isolated through precipitation in -15 °C diethyl ether and filtration. The precipitated product is then transferred to a scintillation vial and dried under vacuum. This synthetic scheme is less time consuming than the lactone synthesis, as neither separations or flash chromatography are necessary to obtain the desired product.

4.3.2 Characterization of *cis*-4-hydroxy-L-proline alkyl ester HCl salts

The ¹H-NMR spectrum for cHyp octyl ester HCl is shown in Figure 4.8. The progression of the synthesis is confirmed by the absence of a COOH peak at 12.5 ppm, and the appearance of four peaks associated with the alkyl ester. The terminal CH₃ is located at 1.0 ppm, ten CH₂ protons are represented at 1.4 ppm, the CH₂ β to the ester oxygen appear at 1.7 ppm, and the CH₂ peak α to the ester oxygen is identified at 4.3 ppm. An HCl salt forms at the secondary amine, as in the lactone deprotection; the broad peak at 9.8 ppm is attributed to the NH₂⁺. This peak was additionally present in the ¹H-NMR spectrum of cHyp lactone only after deprotection. The baseline of the spectrum is very clean and no impurity peaks are noted, with the exception of solvent peaks from DMSO (2.6 ppm) and water (3.3 ppm, superimposed with one of the two peaks associated with the CH₂ adjacent to the secondary amine).

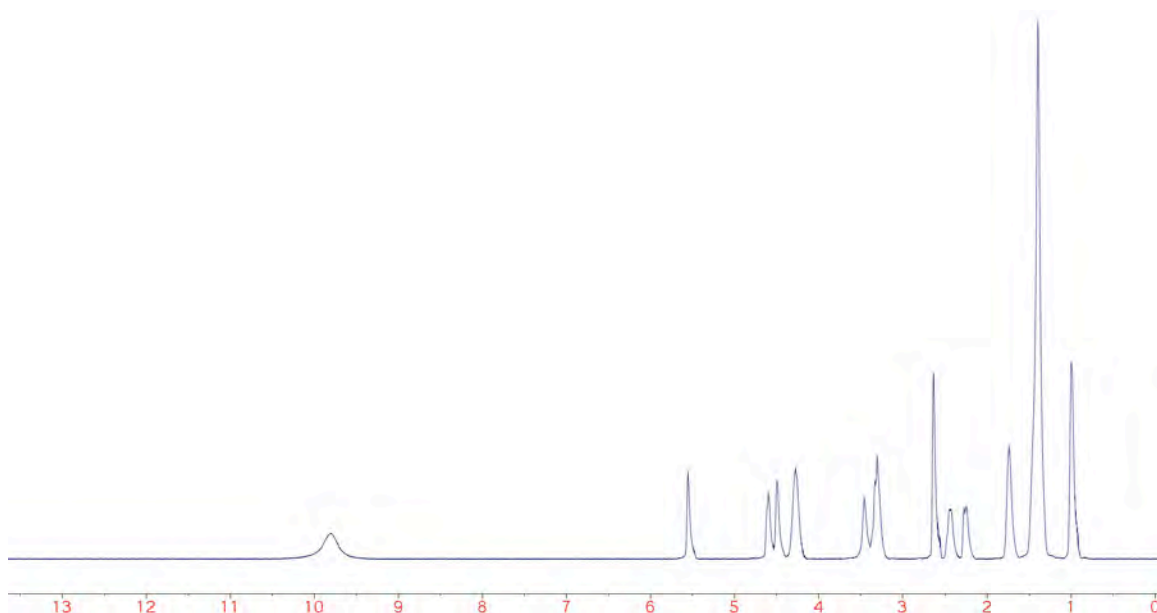


Figure 4.8. ^1H -NMR spectrum of cHyp octyl ester HCl. No impurity peaks are noted, nor is a COOH peak is present near 12.5 ppm. New Peaks corresponding to the alkyl ester are CH_3 at 1.0 ppm, CH_2 at 1.4 ppm, CH_2 at 1.7 ppm, and the CH_2 adjacent to the ester bond at 4.3 ppm. The peak at 9.8 ppm is attributed to NH_2^+ upon formation of the HCl salt.

As suggested by the ^1H -NMR spectrum, HPLC of the final product indicates high purity. The chromatogram, Figure 4.9, has does not demonstrate and ELSD peaks in addition the the cHyp octyl ester HCl peak at 9.79 minutes. As the ELSD detector must be used to detect these non UV-absorbent molecules, any solid impurities would be identified. Any unreacted cHyp would have eluted at 1.95 minutes, Figure 4.6. The baseline drifts as the percentage of acetonitrile in the mobile phase increases, but no distinct peaks are noted. This synthetic strategy is straightforward to perform and yields a product of high purity.

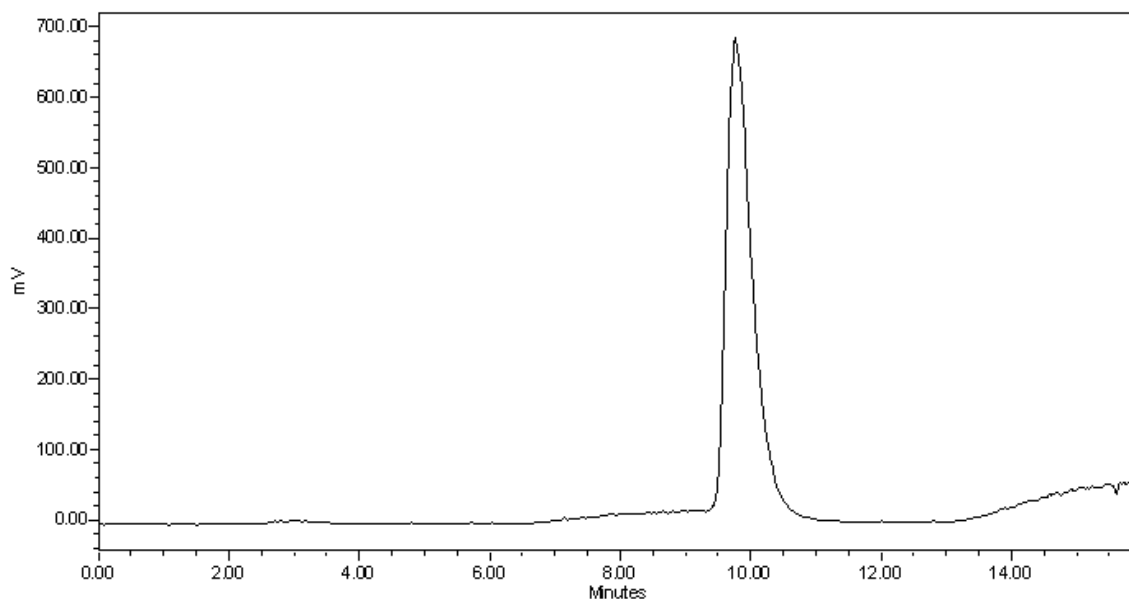


Figure 4.9. HPLC chromatogram of cHyp octyl ester HCl

The hydrolysis rate was characterized by incubating cHyp octyl ester HCl (cHyp OE HCl) in an HPLC vial in PBS at 37 °C. Periodically, the vial contents would be injected, and the disappearance of the cHyp OE HCl peak at 9.19 minutes was monitored. Due to the necessity of the ELSD, the appearance of a cHyp peak could not be monitored, for the early elution from the column was masked by buffer salts. Both *cis* and *trans* isomers of hydroxyproline octyl ester HCl salts hydrolyzed with a half time of 4.9 ± 0.6 hours. The observed hydrolysis rate is 1-2 orders of magnitude faster than the hydrolysis rates observed by Schoenmakers et al. [258]. A faster hydrolysis rate may not inhibit the performance of this drug precursor, for hydrolysis within the polymer matrix is expected to be slower than hydrolysis under physiological conditions.

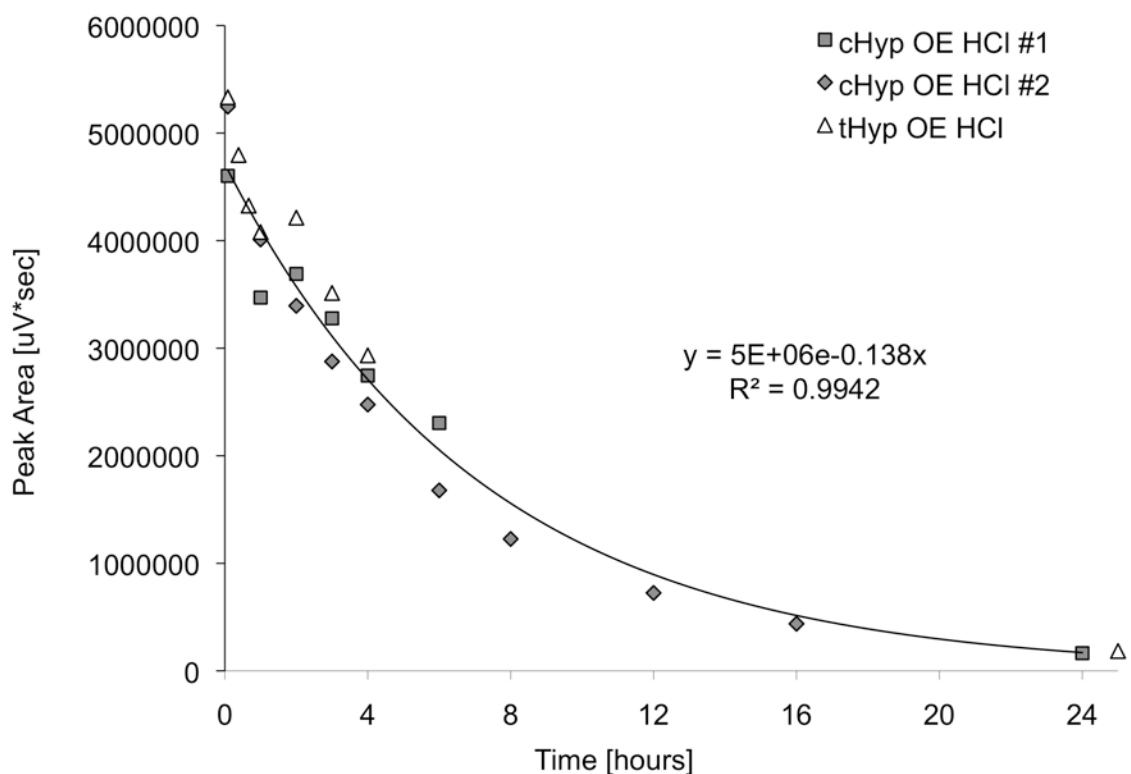


Figure 4.10. HPLC for hydrolysis rate of cHyp octyl ester HCl. The exponent and calculated half-time for hydrolysis for each of the three datasets are: cHyp OE HCl #1, -0.138, 5.0 hours; cHyp OE HCl #2, -0.154, 4.5 hours; and tHyp OE HCl #3, 0.132, 5.3 hours. The average half-time of hydrolysis in PBS is 4.9 hours.

The hydrolysis rate of cHyp alkyl esters within polymeric films of different equilibrium water content was evaluated. Films with 1:5 loading of cHyp alkyl ester HCl salt : polymer were solvent cast from HFIP into Teflon dishes. E0000 was chosen as the low water content polymer, and E10004(1k) was chosen as the high water content polymer. Non-iodinated TDPCs containing more than 4 mol% PEG_{1k} were not useful for electrospinning, so they were excluded. The octyl and hexyl ester precursors made uniform films, but cHyp butyl ester HCl phase separated from the polymer matrix and crystallized, Figure 4.11. The calculated octanol-water partition coefficients were separated by one order of magnitude for each addition of CH₂-CH₂, as the CLogP values for butyl, hexyl, and octyl esters were 0.55, 1.61, and 2.67, respectively. The cHyp butyl

ester HCl's relative hydrophilicity reduced its solubility in the polymer matrix, resulting in separation and crystallization of the cHyp precursor. Note that the more hydrophilic polymer, E1004(1k), induced less phase separation and crystallization of cHyp butyl ester HCl. cHyp butyl ester HCl was excluded from further investigation as a precursor to cHyp.

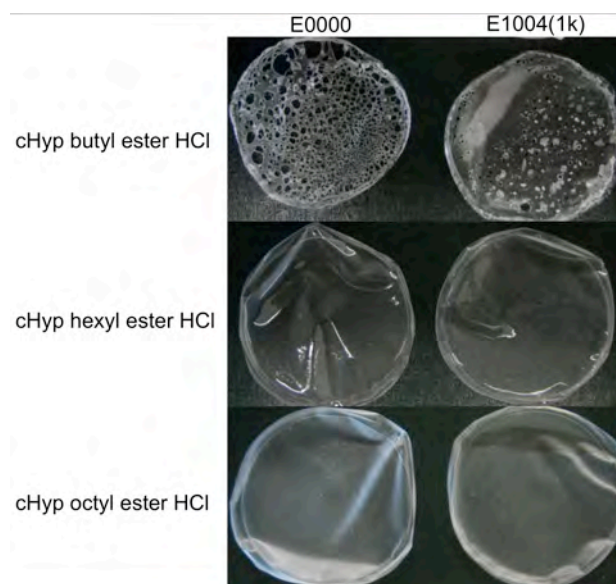


Figure 4.11. Solvent cast films of cHyp alkyl ester HCl salts in E0000 and E1004(1k)

The maximum loading capacity of solvent cast films was determined via loading E0000 films with varying ratios of cHyp octyl ester HCl per polymer by mass, Figure 4.12. The ninhydrin assay adapted from Startcher [246] was used to quantify the amount of cHyp released from solvent cast films at 4 hours. At four hours, the quantity of cHyp released from films of up to 1:3 precursor : polymer loading were statistically indistinguishable, while a 1:2 loading increased burst release. The relative cloudiness of 1:2- and 1:3-loaded films indicates that a degree of micro phase separation has occurred at these loadings. The maximum capacity of E0000 for cHyp octyl ester HCl was in the

range of 1:5 to 1:3 precursor : polymer. Kinetic release at these loading was evaluated in films and electrospun nonwoven fabrics.

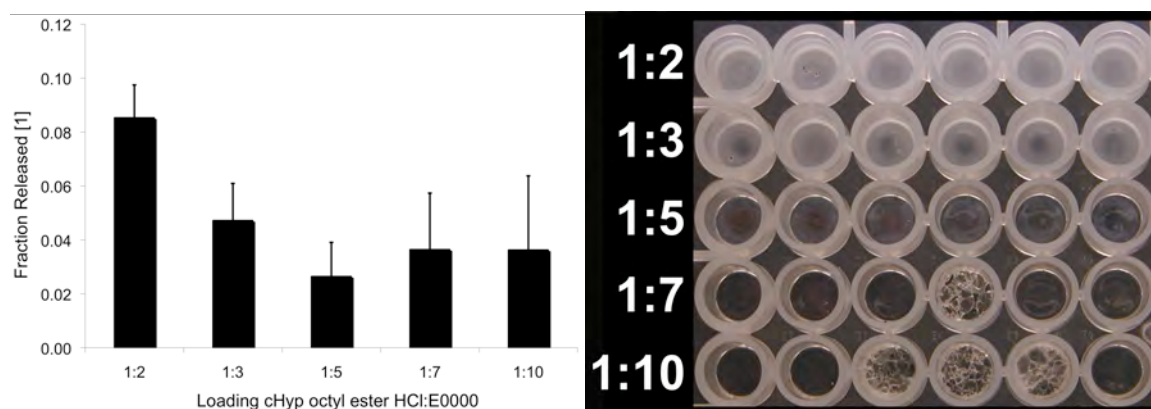


Figure 4.12. Loading capacity of cHyp octyl ester HCl was determined via 4 hour release (left) from solvent cast films (right). Air bubbles formed in four of the wells. cHyp release from these wells were excluded from the analysis.

Elution of cHyp from 1:3 precursor : polymer E0000 films and electrospun fabrics was evaluated over 5 ½ weeks. After the first 48 hours, the release rates were comparable, but the electrospun fabrics demonstrated a burst release of 20% of the cHyp load, Figure 4.13. To avoid this burst release, the loading was reduced to 1:5 cHyp octyl ester HCl : polymer. To maintain the same cHyp content at a 1:5 loading, the total device mass must increase by 50%.

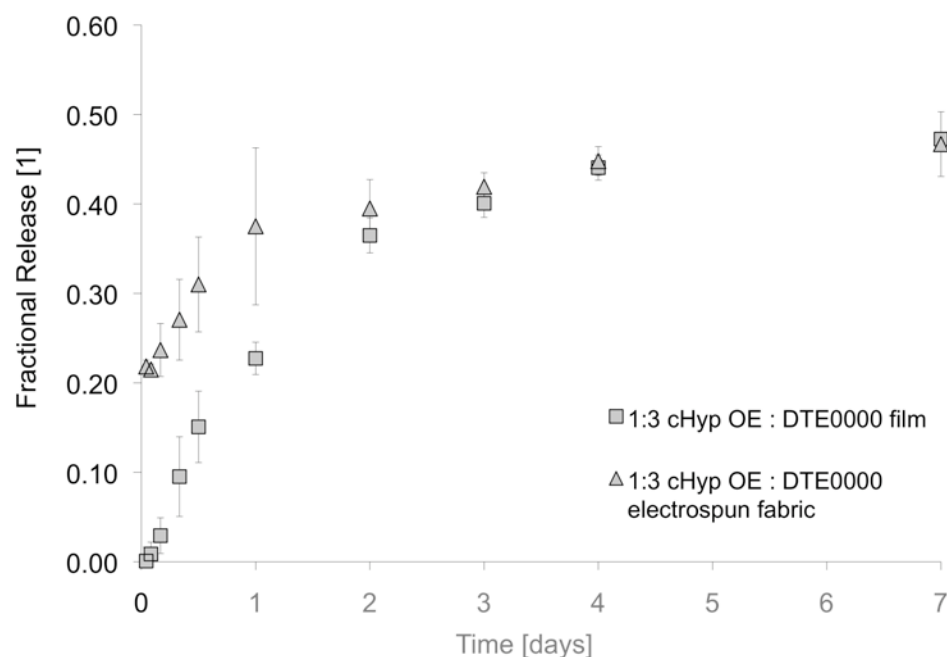


Figure 4.13. Fractional release of cHyp from E0000 films and electrospun fabrics

The release of cHyp as a function of alkyl chain length and polymer chemistry in 1:5 precursor : polymer films was evaluated over five weeks, Figure 4.14. Both the octyl and hexyl ester precursor molecules successfully controlled the release of cHyp from the polymer matrix. The hexyl ester released 18% of cHyp in the first hour of incubation, while no burst release was noted when the octyl ester precursor was used. Excluding delivery in the first hour, the octyl ester precursor released 25% and 37% of cHyp from E0000 and E1004(1k). Comparatively, the hexyl ester released 44% and 49% of cHyp loading. From week 1 to 5, the hexyl ester released 5% and 13% cHyp from E0000 and E1004(1k), while the octyl ester released 13% and 8% over the same duration. The release kinetics of cHyp could be tailored to emphasize elution in the first week of implantation through use of cHyp hexyl ester HCl, or cHyp release could be sustained at over five weeks through use of cHyp octyl ester HCl.

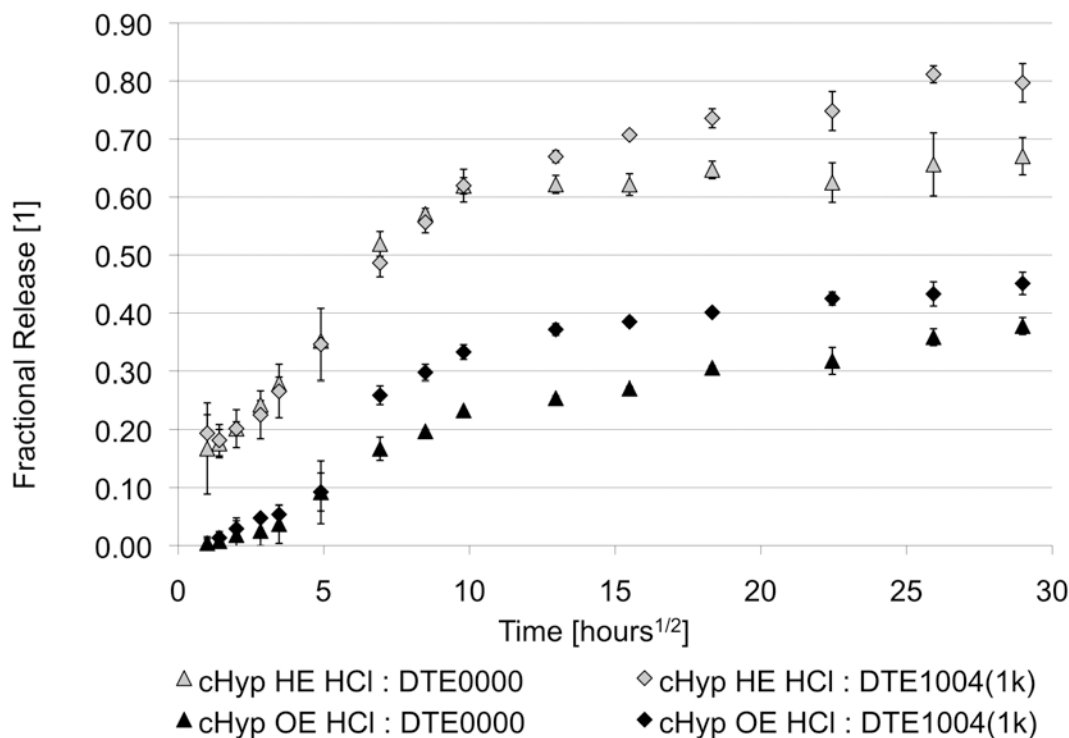


Figure 4.14. Fractional release of cHyp as a function of alkyl chain length and polymer chemistry on a time^{1/2} scale. Each of five weeks occurs at 13, 18, 22, 26, and 29 hours^{1/2}.

To attempt to inhibit collagen secretion during the remodeling of granulation tissue, one should focus on antifibrotic delivery over multiple weeks [8]. Films containing cHyp hexyl ester HCl delivered 62% and 67% of cHyp in the first week, so an insufficient amount of cHyp was available for delivery in the following weeks. In E0000, cHyp octyl ester HCl delivered one-fourth of the cHyp load in the first week with an additional 13% in the following four weeks. Due to enhanced polymer erosion by enzymatic and mechanical activity, the drug release rates may be enhanced in animal models. From the same series of polymers, Khan observed that voclosporin release doubled (2.1 ± 0.3) in the first four weeks of implantation in a rat subcutaneous pocket [158]. Due to the cHyp reservoir remaining after 25% delivery in one week and the potential for enhanced drug release *in vivo*, cHyp octyl ester HCl was chosen as the preferred ester-based precursor to cHyp.

On time^{1/2} axes, the release kinetics of cHyp each precursor appears linear, with two different release rates – one that governs the first week, and a second, slower rate that governs cHyp release in weeks two through five. Khan noted similar behavior when releasing voclosporin from TDPCs; however, he noted a transition in diffusive drug release rate at two weeks, rather than one [158]. The kinetics of drug release appear to be diffusion controlled, rather than controlled by ester bond hydrolysis. HPLC analysis of eluents demonstrated the presence of cHyp octyl ester HCl. In an earlier study, I₂E1008(1k) films were unable to prevent burst release of cHyp octyl ester HCl. The *apparent* hydrolysis rate was slower than the 4.9 hours observed in Figure 4.10; rather, a half-time of 5.5 hours was observed, Figure 4.15. The *apparent* rate was slower because cHyp octyl ester HCl continued to diffuse from the films into the buffer. Diffusive release of cHyp octyl ester HCL from E0000 films was observed at 48 hours.

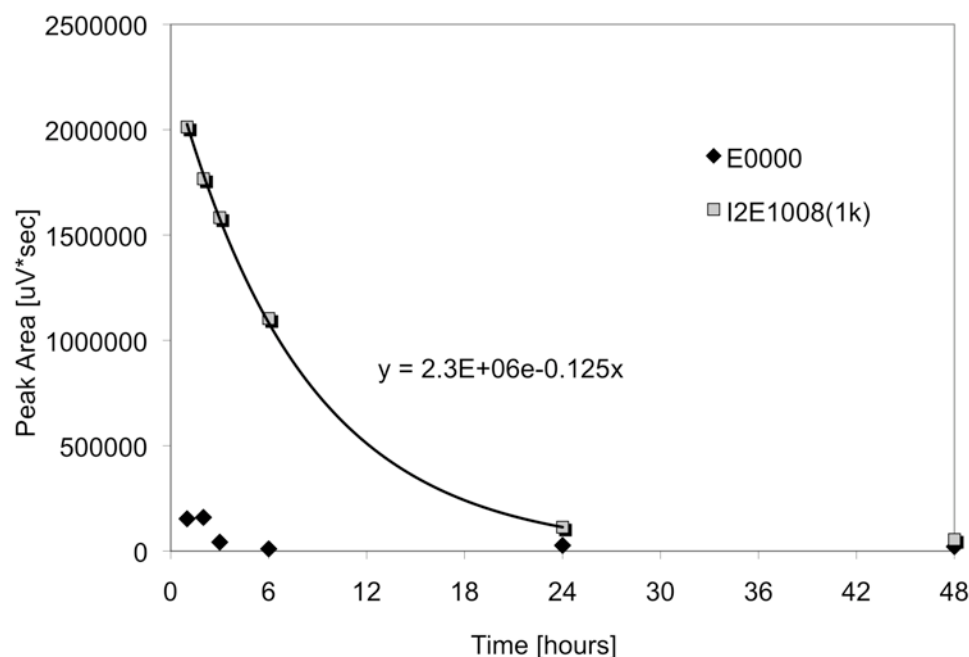


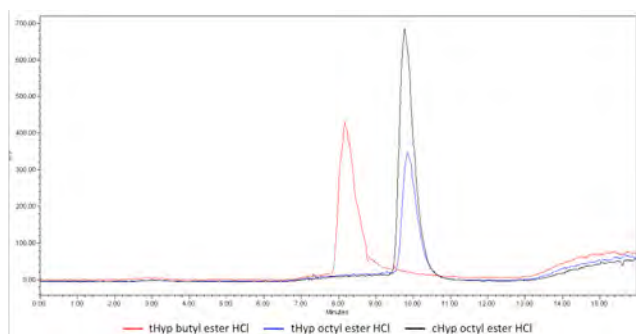
Figure 4.15. HPLC analysis of eluent indicates cHyp octyl ester HCl diffuses from the polymeric film into the buffer, rather than hydrolyzing to cHyp within the polymer matrix.

The evidence for diffusive release of cHyp octyl ester HCl from TDPC films suggests that cHyp delivery may be enhanced in weeks 2-5 through increasing the hydrolytic susceptibility of the labile bond. It has been demonstrated that TDPCs do not retain cHyp, so the hydrolysis of the tethering bond would release the cHyp.

4.3.3 Utility of *cis*-4-hydroxy-L-proline alkyl ester HCl salts

cis-4-hydroxy-L-proline alkyl ester HCl salts provide a tunable diffusive release system for cHyp from TDPC materials. While cHyp butyl ester HCl crystallized in the solvent-casting process, cHyp alkyl esters with chain lengths ≥ 6 can be used to modulate cHyp release. cHyp hexyl ester enhanced release during the first week of incubation. cHyp octyl ester demonstrated potential for releasing 25% of cHyp in the first week, while the majority of the cHyp reservoir was retained for potential release in subsequent weeks. The mechanical, cellular, and enzymatic processes encountered *in vivo* are likely to increase release in weeks 2-5 beyond the 13% observed *in vitro*.

For the inhibition of epidural scarring, cHyp octyl ester HCl shows the most promise, so this molecule was scaled up for further investigation. Additionally, tHyp butyl ester HCl and tHyp octyl ester HCl were synthesized for use as a low toxicity surfactant for electrospinning and an inactive control molecule. Performing the synthesis at a 2.5 gram hydroxyproline scale was straightforward and produced a high yield of pure product, Figure 4.16.



Molecule	Yield [%]	Retention Time [min]	Melting Point [°C]
tHyp BE HCl	95	8.17	148
tHyp OE HCl	89	9.87	126
cHyp OE HCl	92	9.79	141

Figure 4.16. Characterization of larger-scale (2.5 g hydroxyproline) hydroxyproline alkyl ester HCl synthesis.

4.4 *cis*-4-hydroxy-L-proline octyl carbonate HCl salt

To potentially enhance cHyp delivery in weeks 2-5, cHyp octyl carbonate HCl was pursued. As with cHyp octyl ester HCl, the only degradation products are the antifibrotic imino acid and octanol. While the ester was formed at the carboxylic acid of cHyp, the carbonate was formed at the hydroxyl group.

4.4.1 Synthesis of *cis*-4-hydroxy-L-proline octyl carbonate HCl salt

The synthetic strategy was adapted from Stjerndahl and Holmberg, who created a degradable surfactant using octyl chloroformate to form a carbonate bond between tetra(ethylene glycol) and a $(\text{CH}_2)_7\text{CH}_3$. The carbonate bonds of NJCBM TDPCs are formed using triphosgene. Triphosgene chemistry could not be used here, for carbonate bonds could form between cHyp and itself, octanol and itself, and cHyp and octanol. The use of octyl chloroformate circumvented this complication. Due to the potential formation of an anhydride bond at the carboxylic acid, 2.2 mol equivalents of octyl chloroformate were added dropwise to a 2.6 %wt/vol solution of N-boc-cHyp in DCM,

Figure 4.17. If the anhydride bond formed, it hydrolyzed during acidic deprotection, while carbonate bonds are relatively stable to hydrolysis under acidic conditions.

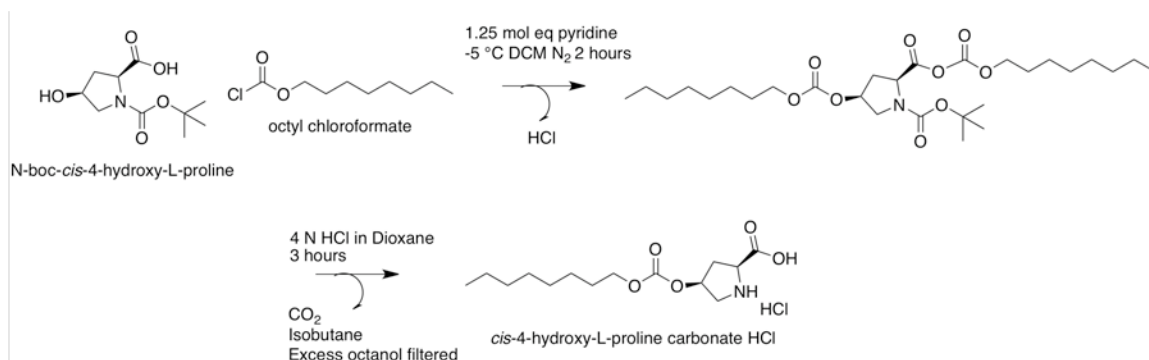


Figure 4.17. Synthetic scheme for production of cHyp octyl carbonate HCl

To obtain pure product, unreacted starting material and pyridine were extracted from the intermediate products by ethyl acetate versus DI water separation, Figure 4.18. The final product partitioned into the aqueous phase of DI water versus chloroform, DCM, or ethyl acetate separations, so this purification step must be performed on the intermediate products. Deprotection proceeded in 4N HCl in dioxane, terminated by evaporation under N₂. The product was precipitated in diethyl ether and filtered, rinsing with diethyl ether. The product was transferred to a scintillation vial and dried under vacuum. After drying, the product was stored at -15 °C. A yield above 47% was observed – the calculation did not include the material utilized for trial extractions. Due to the excessive starting material present in the aqueous extracts, greater yield could be achieved through optimization of the reaction conditions.

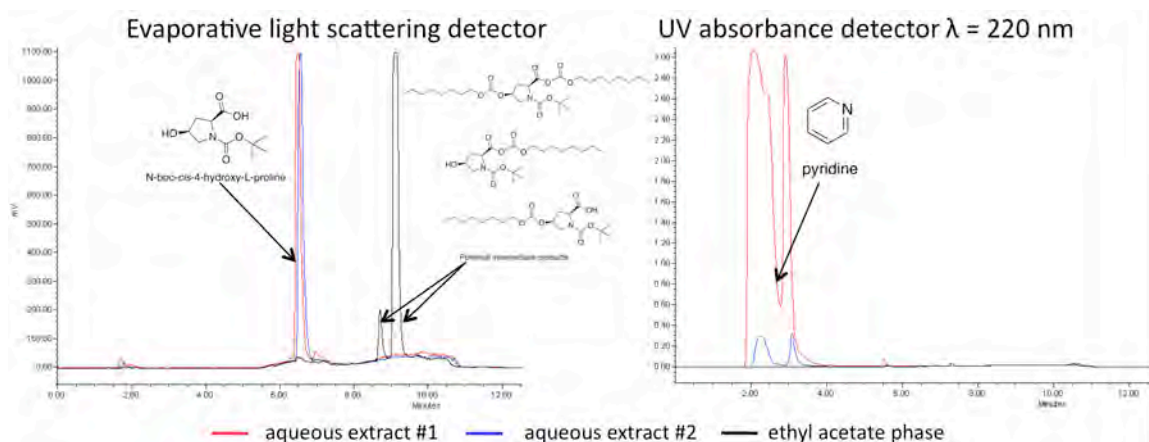


Figure 4.18. Extraction of pyridine and N-boc-cHyp from the intermediate product by ethyl acetate versus DI water separation. HPLC chromatograms demonstrate the presence of pyridine and N-boc-cHyp in the first two aqueous extracts, but not the organic phase.

4.4.2 Characterization of *cis*-4-hydroxy-L-proline octyl carbonate HCl salt

^1H -NMR demonstrated the formation of cHyp octyl carbonate HCl and removal of the pyridine impurity, Figure 4.19. The alkyl carbonate's CH_3 peak was observed at 0.8 ppm, while a ten-hydrogen CH_2 peaks was observed observed at 1.2 ppm, the CH_2 β to the carbonate oxygen appeared at 1.6 ppm, and the CH_2 α to the carbonate oxygen was present at 4.4 ppm. Peaks attributed to pyridine (8.0, 8.5, 8.9 ppm) were present in the intermediate product, but the final product's spectrum did not present any of these features. Upon deprotection, a peak at 10.6 ppm was observed, which is attributed to the secondary amine.

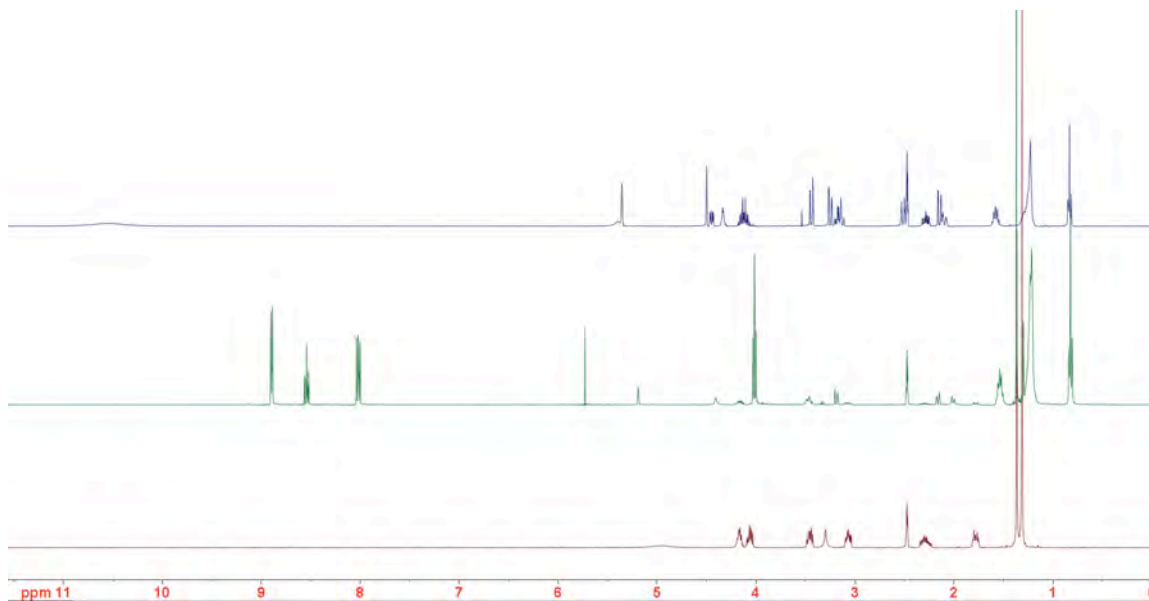


Figure 4.19. ^1H -NMR spectrum of cHyp octyl ester HCl: starting material (red), intermediate products (green), and final product (blue). New Peaks corresponding to the alkyl carbonate are CH_3 at 0.8 ppm, CH_2 at 1.2 ppm, and CH_2 at 1.6 ppm. The pyridine impurity is observed in the intermediate product (8.0, 8.5, 8.9 ppm), but not in the final product. The peak at 10.6 ppm is attributed to NH_2^+ upon formation of the HCl salt.

The final product purity was characterized by HPLC with detection by ELSD. cHyp octyl carbonate HCl eluted at 8.89 minutes, and a small cHyp peak (2.2% by area) was present at 1.99 minutes. Though a small cHyp peak is present, this material was suitable for exploratory evaluation for controlled delivery of cHyp. In comparison to cHyp octyl ester HCl, cHyp octyl carbonate HCl has two additional oxygen atoms, which provide partial negative charges due to the electronegativity of oxygen and its lone pairs of electrons. The more polar character of cHyp octyl carbonate HCl results in a lower CLogP (2.61 versus 2.67) and shorter retention time during HPLC (8.98 versus 9.79 minutes).

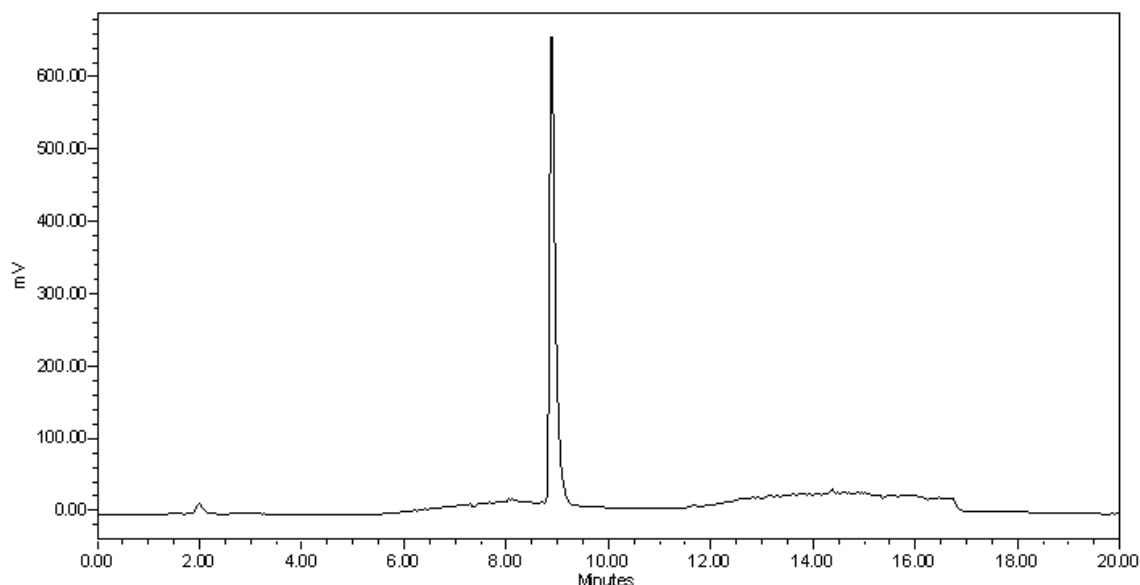


Figure 4.20. HPLC of cHyp octyl ester HCl following deprotection and precipitation. The product contains a small impurity of cHyp, 2.2% by peak area.

The release of cHyp from cHyp octyl carbonate HCl loaded films was compared to release from cHyp and cHyp octyl ester HCl loaded films. Solvent cast films with a 1:5 loading of cHyp octyl carbonate HCl : E0000 did not phase separate. Upon immersion in PBS, the first six hours of cHyp-elution was identical between cHyp octyl carbonate HCl and cHyp loaded films, Figure 4.21. The octyl carbonate precursor did not provide controlled release. Rather, the carbonate bond was too sensitive to hydrolysis, such that cHyp was liberated from the hydrophobic alkyl chain before the alkyl chain could provide any retention. The cumulative fraction of cHyp release became greater than 1, for the cHyp impurity in cHyp octyl carbonate HCl resulted in an underestimation of the mol-content of cHyp within the film. The presence of a cHyp impurity in the final product eluded to high hydrolytic susceptibility of cHyp octyl carbonate HCl.

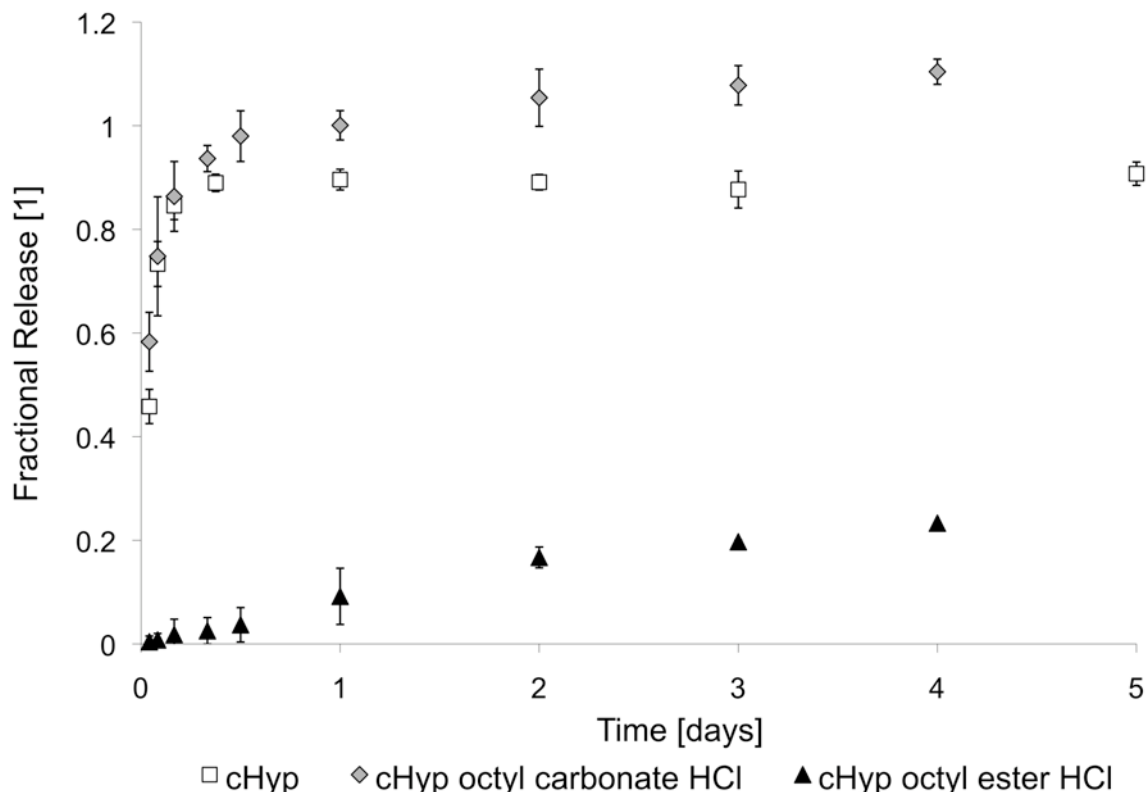


Figure 4.21. elution of cHyp octyl carbonate HCl from E0000 films in comparison to the elution of cHyp and cHyp octyl ester HCl from the same.

4.4.3 Utility of *cis*-4-hydroxy-L-proline octyl carbonate HCl salt

cHyp octyl carbonate HCl is too hydrolytically unstable to increase the retention of cHyp in TDPC films. The increased rate of hydrolysis versus cHyp octyl ester HCl was intended to increase cHyp release after one-week of implantation. However, the immediate hydrolysis prevented any retention of cHyp for delivery in the second week.

While cHyp octyl carbonate HCl was not useful for controlled delivery of cHyp, tHyp butyl carbonate HCl could potentially be the ideal degradable surfactant to enable electrospinning from acetic acid. The molecule should provide similar surfactant performance as tHyp butyl ester HCl. Due to the immediate hydrolysis upon immersion in physiological buffers, no potential for surfactant toxicity could be associated with tHyp

butyl carbonate. The molecule was therefore pursued thoroughly, but purification of the final products could not be achieved. Precipitates were not formed in DCM:diethylether, or chloroform:diethylether. A very fine precipitate formed in ethyl acetate:diethylether, but upon filtration a viscous gel formed. A precipitate in 200 mL of 1:100 ethyl acetate:diethylether was allowed to crystallize at -15 °C for 8 weeks. As above, a viscous product was deposited on the filter and the crystals formed on the flask wall become a viscous gel upon drying under vacuum, Figure 4.22. If the product was isolated, its handling would be problematic, so this degradable surfactant was abandoned.



Figure 4.22. Attempted recovery of tHyp butyl ester HCl after 8 weeks of crystallization in 1:100 ethyl acetate:diethylether at -15 °C. Crystals of product transformed to a viscous state upon attempted isolation

4.5 Subcutaneous screen of *cis*-4-hydroxy-L-proline octyl ester HCl scaffold

A subcutaneous screen of cHyp octyl ester HCl-loaded E0000 electrospun AAMs was performed to evaluate any potential toxicity of the cHyp precursor. Because octanol is not a solvent of “low toxic potential,” [216] list, and tHyp octyl ester HCl

demonstrated cytotoxicity at concentrations ≥ 1.5 mM, a subcutaneous screen of candidate AAMs was necessary before progressing to the laminectomy study.

4.5.1 Fabrication of *cis*4-hydroxy-L-proline-loaded implants

Nonwoven fabrics of DTE0000 were electrospun at a concentration of 7% wt/vol in HFIP with or without a 1:3 loading of cHyp octyl ester HCl. The prototypes were sterilized by the ethylene oxide gas method, allowed to degas under vacuum, and were then heat treated under vacuum at 40°C for 12 hours, Figure 4.23. The non-drug-containing fabrics were composed of 300 nm fibers with some beading. However, the beading was not so extensive that the fabrics were brittle. The surfactant effect of cHyp octyl ester HCl permitted bead-free electrospinning of 280 nm E0000 fibers from HFIP. Subsequent studies included tHyp butyl ester HCl to prevent beading within electrospun nonwoven fabrics.

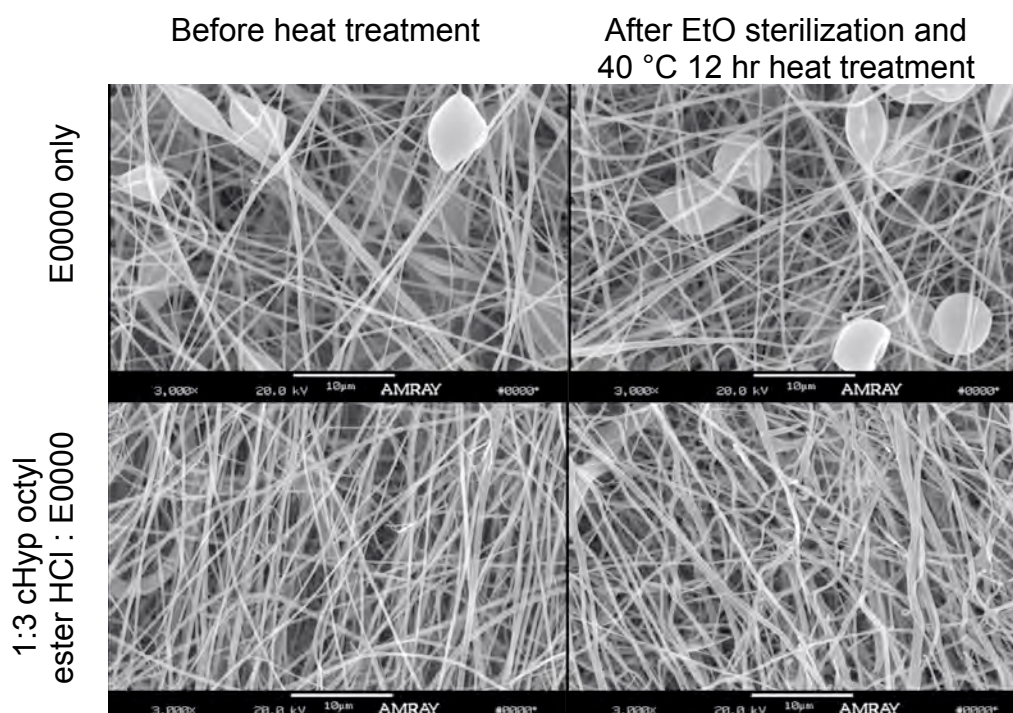


Figure 4.23. Architecture of E0000 devices implanted in rat subcutaneous screen to screen the effect of cHyp octyl ester HCl.

Over seven days, this cHyp-loaded fabric delivered 47% of its cHyp capacity, with 18% being delivered in a burst-release fashion, Figure 4.13.

4.5.2 Implantation and recovery of *cis*4-hydroxy-L-proline-loaded implants

Fabric implants (approximately 15 mm square) were implanted into subcutaneous pockets on the back of a rat. The subcutaneous pockets were formed via blunt dissection. Three fabrics were implanted via two incisions. One sample was placed in the incision closer to the head and two additional samples were placed in the incision towards the rat's tail. In each of three rats, two cHyp-loaded fabrics and one non-loaded fabric were implanted. In concern over whether the hydrophobic, small pore size fabric would become hydrated upon implantation, one of the two cHyp-loaded fabrics per rat was pre-wet in a 0.1% PEG_{1k} PBS solution. Fabrics from each of the three experimental groups were rotated between implantation sites in subsequent rats.

4.5.3 Tissue response to *cis*4-hydroxy-L-proline-loaded implants

At one week, the implants were recovered and inspected. The E0000 fabrics without cHyp loading were contracted, while the cHyp-loaded scaffolds maintained their shape, Figure 4.24. The membranes did not contract due to thermal relaxation of polymer chain alignment, as in section 3.4, for electrospun E0000 fabrics do not contract *in vitro*. Rather, the E0000 fabrics must have been contracted by cellular traction on the granulation tissue adjacent to the implant. Interestingly, the cHyp octyl ester HCl fabrics were not contracted by the host tissues of the subcutaneous pocket. Additionally, the cHyp-loaded implants were loosely associated with the tissue. The histologist had

difficulty cutting cross-sections of tissue including the implant without the tissue delaminating.

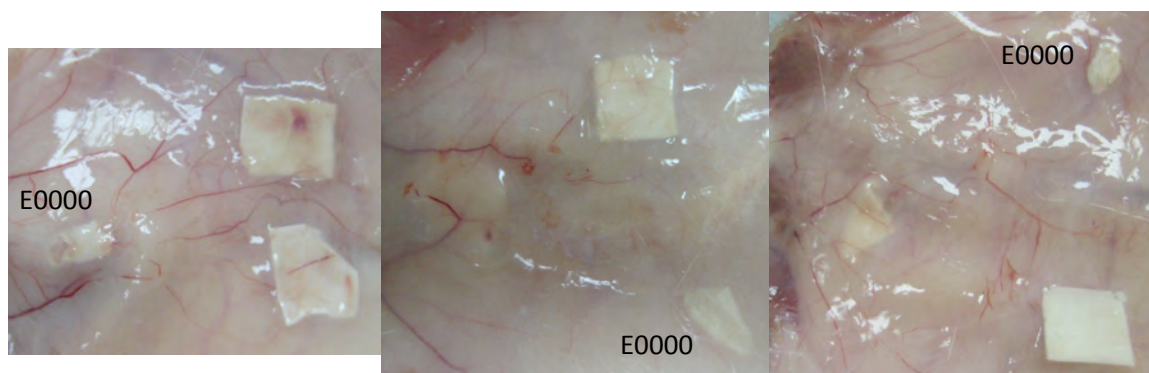


Figure 4.24. The underside of rat dermis upon recovery of E0000 fabrics with and without cHyp octyl ester HCl loading. Fabrics without cHyp are labeled E0000.

The physical observations following implantation were promising, but histological staining revealed that both cHyp-loaded and non-loaded fabrics were surrounded by granulation tissue, Figure 4.25. Both fabrics prevented cell penetration through the device, though cells penetrated the outer 20 μ m of the non-drug loaded implant at one week. The difference in cell penetration is likely due to the difference in device architectures, rather than cHyp delivery. Though the fiber diameter of both fabrics was indistinguishable, the beading of the non-drug-loaded membranes reduced the density of fibers, increasing the effective pore diameter.

The cHyp-loaded E0000 fabrics did not demonstrate signs of toxicity at the implant site. Inflammatory cells were present at the tissue-implant interface with a thickness of only 2 cell layers. If the device were eluting a compound that compromised cell viability, a much thicker layer of phagocytotic cells would be observed along with a number of dead cells. Rather, a mild inflammatory response is observed here. The absence of any apparent toxicity permits cHyp octyl ester HCl loaded fabrics to be implanted into the laminectomy defect for evaluation as a barrier to epidural adhesion.

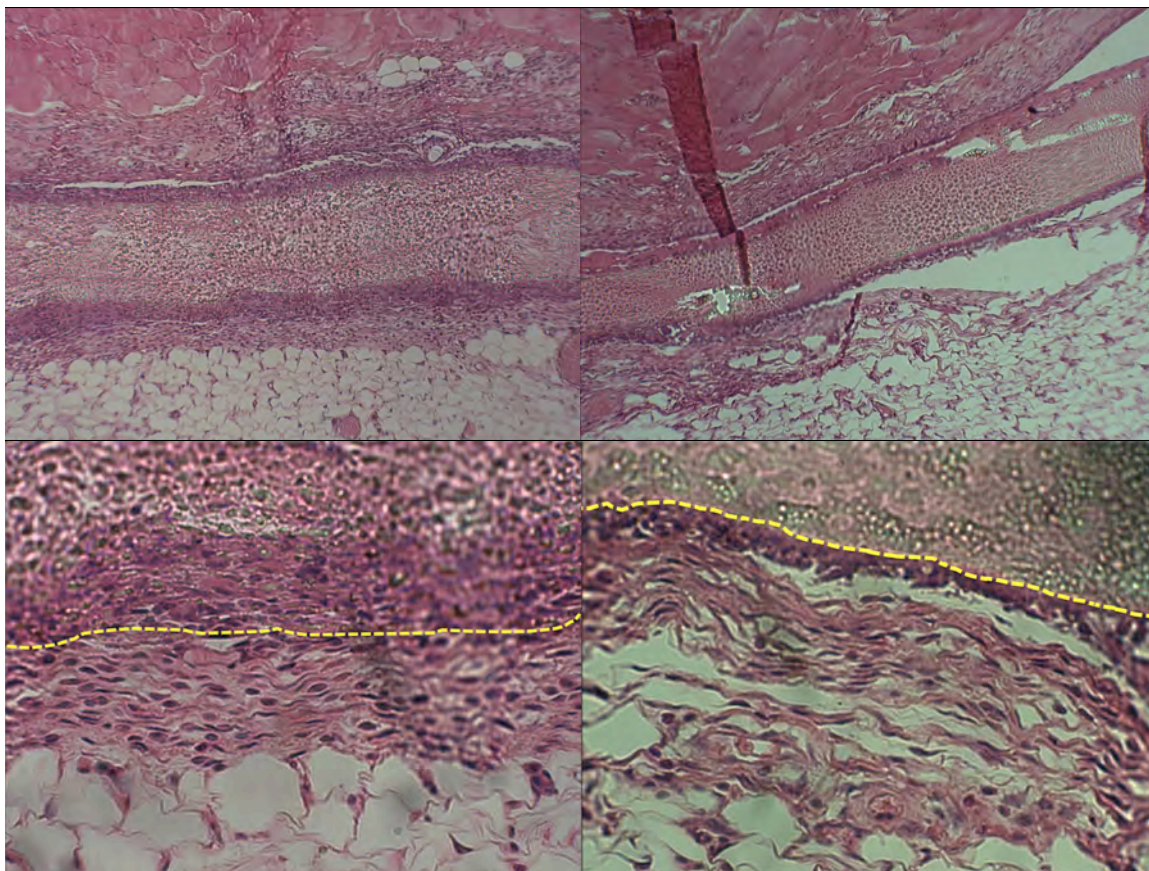


Figure 4.25. One-week rat subcutaneous tissue response to E0000 electrospun fabrics without (left) and with (right) cHyp delivery. In 40x images, the edge of the implant is indicated with a dashed yellow line. Hematoxylin and eosin, 10x (top), 40x (bottom).

4.6 Conclusions regarding the delivery of *cis*-4-hydroxy-L-proline

The delivery of cHyp from polymer matrices is challenging, for cHyp is a very small and hydrophilic molecule. As the relatively hydrophobic polymer swells with even modest amounts of water, the small molecule rapidly elutes out of the matrix. Retention in the polymer matrix was achieved through synthesis of a series of hydrolytically degradable cHyp precursors. Lactone and carbonate precursors were too susceptible to hydrolysis, releasing cHyp in the first hours of incubation. However, cHyp alkyl ester HCl salts were stable to hydrolysis in the polymer matrix and controlled the release of cHyp through diffusion. Because these precursors released cHyp from the polymer

through diffusion, rather than hydrolysis in matrix, the alkyl chain length was used to modulate release. cHyp hexyl ester HCl provided excellent delivery characteristics for one week, while cHyp octyl ester HCl delivered 25% in week one and 13% in weeks 2-5. cHyp octyl ester HCl was selected for use *in vivo*, for polymer and precursor degradation may be enhanced *in vivo*, releasing additional cHyp in weeks 2-5. After diffusion from the polymer matrix, the diffused alkyl esters degrade at a half-time of 4.9 hours at physiological temperature and pH.

Trial implantation of cHyp octyl ester HCl E0000 fabrics did not present signs of toxicity at one week. Rather, a mild inflammatory response was present. The generalized soft-tissue response to a benign implant is fibrous encapsulation [8]. The fibroblasts within the capsule produce traction against the extracellular matrix. As a result of this traction, the E0000 fabric contracted in the absence of cHyp loading (3/3), while the E0000 fabrics with cHyp delivery did not contract (0/6). Collagen fibers and elongated fibroblasts were observed in histological sections. This is anecdotal, rather than direct, evidence of a cHyp effect. Furthermore, it is confounded by a difference in the microscopic architecture of the fabric. However, a well-defined boarder between the host tissue and the bead-free E0000 fabric demonstrated barrier performance at one week. Cell-impermeable fabrics that release cHyp at a controlled rate have been demonstrated and may be evaluated for the prevention of peridural adhesion.

5 Evaluation of adhesion prevention in the laminectomy site

Anti-adhesion membrane prototypes were evaluated for adhesion prevention in a adult female Sprague Dawley rat laminectomy model with or without spinal cord injury. The laminectomy was performed at thoracic vertebrae nine and ten, exposing approximately 5 mm of the dura. The inclusion of spinal cord injury was meant to simulate handling of the spinal cord and surrounding tissues during discectomy, the most common surgery involving a laminectomy, Table 1-1. The MASCIS weight drop instrument was used to impart a consistent injury to the dura, dropping a 10-gram rod 12.5 mm onto the exposed dura. Spinal cord injury via weight drop was excluded from Study #1 to minimize the injury imparted to test animals.

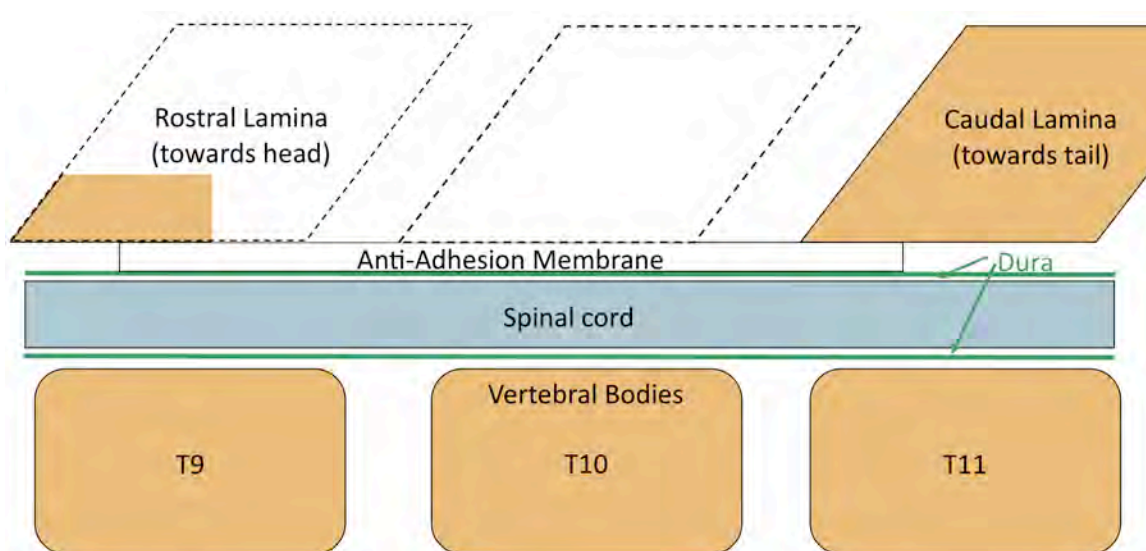


Figure 5.1. Diagram of laminectomy and placement of AAMs. A rostral and caudal tuck of AAMs was always attempted, though only consistently achieved in Study #2.

In the progression of the surgery, a 4 cm incision was made along the midline of the back over the ninth thoracic vertebra. Sharp dissection was used to remove some of the erector spinae musculature, expose the spinous process, and gain access to the

laminae. The spinous processes were removed from thoracic vertebrae nine and ten using ronguers. The laminae were completely removed at T10 and partially resected at T9, Figure 5.1. Bleeding was controlled using cotton balls and gauze. The cord was rinsed with saline, the spinal cord injury was performed, and bleeding was again controlled with cotton. The prototype AAMs were apposed to the dura and tucked between the dura and lamina rostral and caudal to the implant site using Dumostar #3 and #5 forceps. If caudal tuck could not be achieved, the rostral tuck was considered sufficient and the membrane was left in apposition to the dura. The surgical site was closed in layers, suturing the erector spinae muscles with two interrupted stitches using silk sutures and stapling the incision line.

Adhesion prevention was measured histologically. The histological approach is not as rapid as MRI, and it doesn't supply qualitative or quantitative data on the tenacity of adhesion, as surgeon observation or mechanical testing does. However, histological images provide a detailed representation of the tissue response near the implant. Such information provided useful insights into the design of subsequent prototype generations. In histological evaluation of the extent of dural adhesion, sagittal sections were imaged and the extent of adhesion was quantified. Adhered regions were indicated by the penetration of peridural fat by collagenous tissue. The primary statistic used in evaluation was the fraction of adhesion, calculated as the length of adhered regions in pixels divided by the length of laminectomy defect in pixels.

Three studies are presented in this chapter. An exploratory study is briefly discussed to describe the laminectomy site's response to cell-permeable scaffolds, fat pads, and cHyp-loaded hyaluronic acid microspheres, which were not represented in the

subsequent studies of AAM prototypes. Second, the first formal study is discussed. The first formal study explored the factors of device architecture (films versus electrospun fabrics) and cHyp delivery (with or without). E0000 was used in the first formal study, which can be considered non-degradable over a 4-week implantation period. In the second formal study, refined degradable composite films and composite AAMs were compared against DuraGen PLUS[®], a material currently in clinical trials for the prevention of peridural adhesion prevention [138].

5.1 Exploratory implantation of an electrospun fabric and cHyp microspheres

At the beginning of the development of an anti-adhesion device for neurosurgery, an exploratory study was performed to observe the tissue response in the laminectomy defect following spinal cord injury and to observe the tissue response to electrospun E0000 fabrics and to cHyp. Electrospun E0000 fibers were provided by Vipavee Hoven of Chulalongkorn University, Bangkok, Thailand, a member of the first group to electrospin TDPCs [248]. The average fiber diameter of the provided fibers was $3.0 \pm 0.3 \mu\text{m}$, Figure 5.2. According to Sampson's model for pore size [253], assuming a typical pore fraction of 0.85, the average effective pore diameter of these electrospun mats was $23 \mu\text{m}$. According to those calculations and the *in vitro* cell experiments performed in section 3.5, the E0000 fabrics provided by Vipavee Hoven were highly cell permeable.

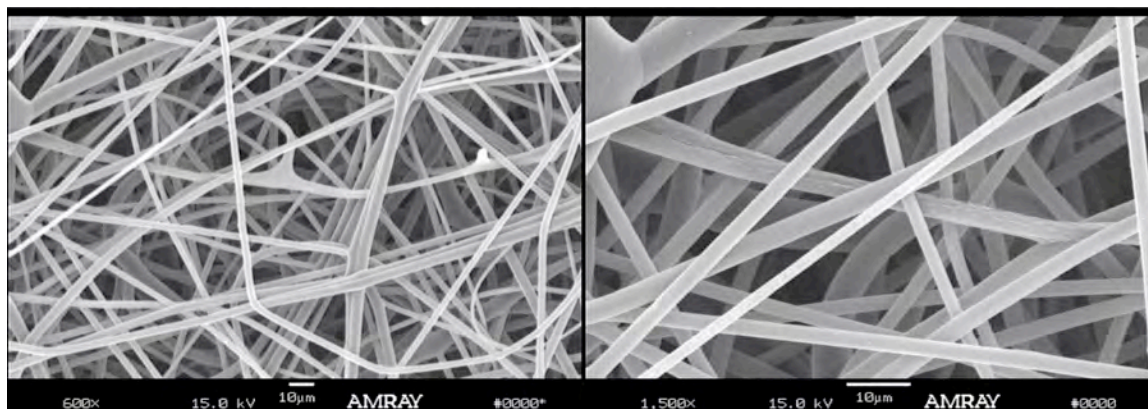


Figure 5.2. Electrospun E0000 scaffolds provided by Vipavee Hoven and implanted in the exploratory adhesion prevention study.

cHyp-loaded hyaluronic acid (HA) microspheres were provided by James Pachence of VectraMed Inc. The HA microspheres were 10-60 μ m in diameter and contained 30% active poly(PEG-Lys-g-cHyp), Figure 1.8. These microspheres utilize the same technology outlined in VectraMed's patent for abdominal adhesion prevention [244], However, in the PEG-PLA hydrogel was not used in this study. Rather, 1.5 mg of HA microspheres was placed on top of the dura with a spatula.

5.1.1 Implantation of fabric and cHyp-loaded microspheres

One animal each was used to survey the surgical site response to TDPC fabrics and cHyp-loaded hyaluronic acid (HA) microspheres. An ethylene oxide gas sterilized E0000 cell-permeable electrospun fabric was intraoperatively cut to the size of the laminectomy defect and laid on top of the dura. The polymeric fabric was not tucked beneath the rostral or caudal laminae. The cHyp-loaded HA microspheres were weighed into a microcentrifuge tube (1.5 mg). The HA microspheres were placed on the dura using a fine spatula. In both cases, a fat pad was placed on top of the experimental materials to stabilize their placement and inhibit the migration of inflammatory cells.

5.1.2 Evaluation of adhesion prevention performance

At two weeks, significant adhesion with involvement of the spinal cord was noted in both rats, Figure 5.3.

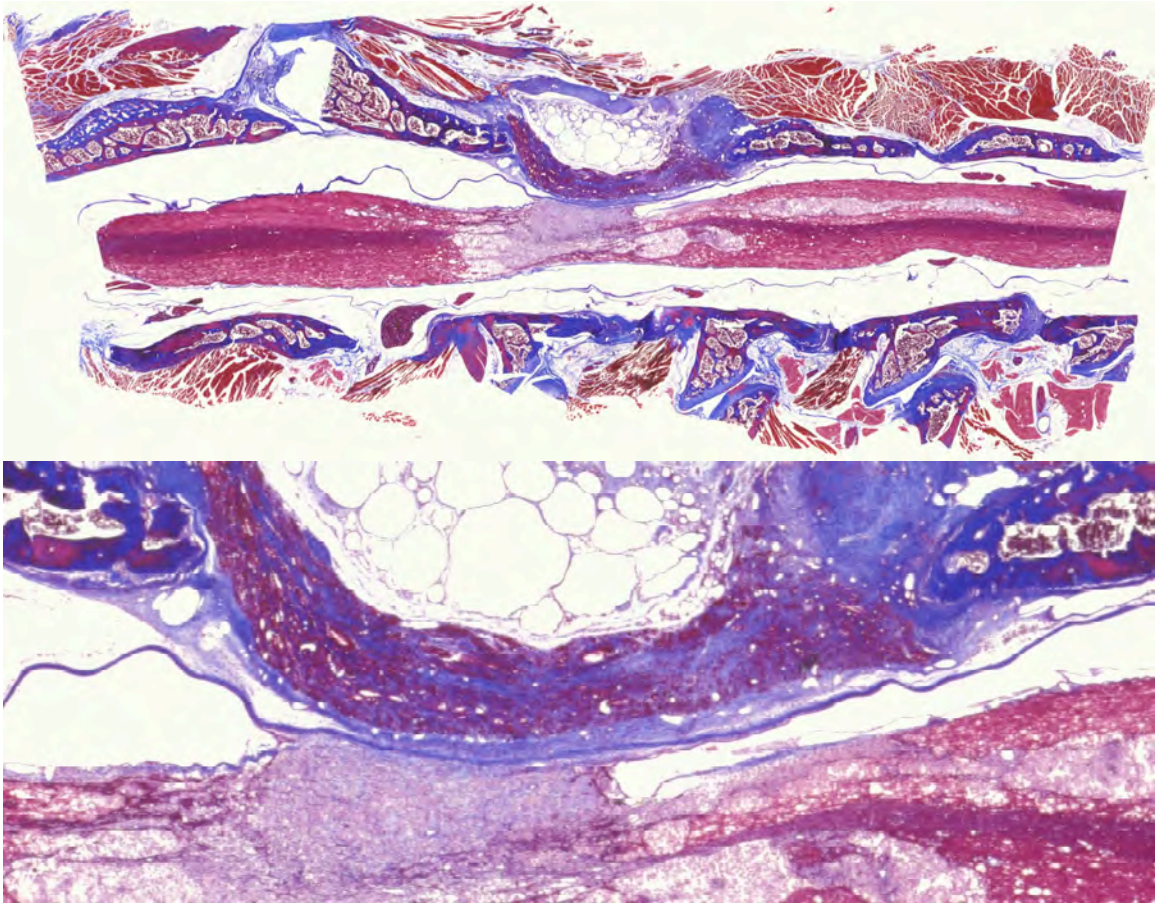


Figure 5.3. Gross (top) and detailed (bottom) histological sections of cell-permeable E0000 fabric and fat pad in the laminectomy site. Masson's trichrome

The E0000 fabrics were fully infiltrated with cells (pink), swelling to a thickness of 1-1.5 mm. Newly synthesized connective tissue (blue) was present throughout and surrounding the implant. The fat pad and cell-swollen fabric intruded into the spinal canal and compressed the dura against the injured spinal cord. This compression, in conjunction with the wound-healing response in the spinal cord, caused sub-dural adhesion in addition to peridural adhesion to the laminectomy scar. The dura (dark blue

line) adhered to the cell-laden implant through connective tissue along the length of the laminectomy membrane. The fat pad prevented the accumulation of collagen within its bulk, but connective tissue and inflammatory cells were clearly able to migrate and proliferate around and below the pad. Furthermore, even at 2 weeks, the fat pad started to become compromised. Collagenous tissue had infiltrated into the posterior portions of the fat pad.

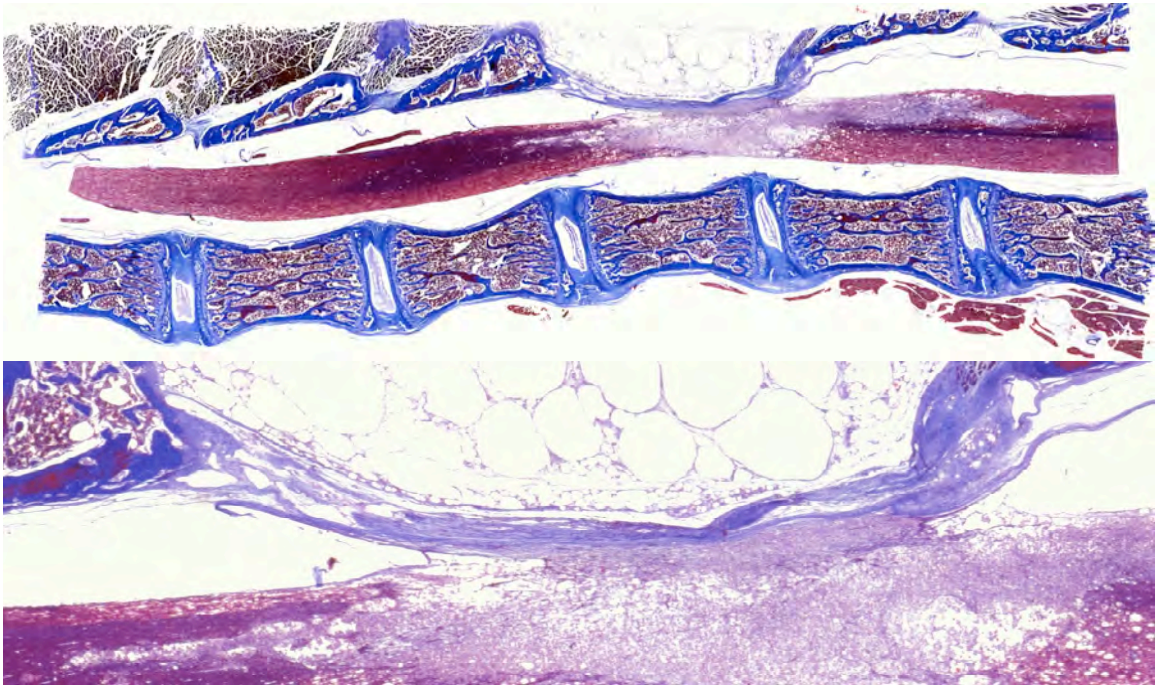


Figure 5.4. Gross (top) and detailed (bottom) histological sections of cHyp-loaded HA microspheres and fat pad in the laminectomy site. Masson's trichrome

The HA microspheres with cHyp delivery were insufficient to prevent scar progression to the dura. Connective tissue was observed at both the rostral and caudal margins of the laminectomy site. Despite the delivery of cHyp, collagenous scar tissue was observed posterior to the dura across the length of the defect. Perhaps, the collagen secreted observed here had less mechanical integrity, but it clearly tethered the dura to laminae at each end of the laminectomy site. The fat pad in this section does not appear to have been compromised, however it did compress the dura onto the spinal cord.

5.1.3 Conclusions of exploratory study

The exploratory rat laminectomy study provided a number of insights for the design of experiments and AAM prototypes. The use of a fat pad was eliminated from subsequent studies. Though the fat pad was able to reduce the density of fibrosis in the center of the laminectomy, it did not inhibit adhesive tethering of the dura to the margins of the laminectomy site. Inflammatory cells were able to migrate around the pad and secrete connective tissue between the dura and laminae. This observation supports the clinical observations that autologous free fat transplantation can reduce density of fibrosis and provide a surgical plane [84-88]. The inability of a fat pad to inhibit adhesive scarring at the margins of the laminectomy site offers an explanation of the lack of patient-oriented outcomes in fat transplantation groups [92-94]. This small exploratory study demonstrated the degradation of autologous fat [88-91, 98, 100] and demonstrated intrusion into the spinal canal – similar to cauda equina observed in clinical autologous fat transplantation [94-97]. Autologous fat pads were not used in subsequent studies, for fat transplantation can cause intrusion into the spinal canal, enhancing adhesive involvement of the spinal cord. A successful anti-adhesion membrane would be able to prevent adhesive tethering without the assistance of autologous fat.

Anti-adhesion membrane prototypes must function as a barrier to fibrin matrix deposition and cell migration from the region of the erector spinae muscles. To supersede the performance of fat transplantation, the successful membrane would provide barrier function at the margins of the implant site in addition to the center. The cell-permeable synthetic device caused inflammatory cells to proliferate in response to the abundant foreign body surface area, as observed in Figure 3.18. Cell-impermeable

devices expose a smaller foreign body surface area, and incite less inflammatory cell proliferation in soft tissue, Figure 4.25 and Figure 3.20. Finally, it appears that cHyp must be delivered from a barrier device to be effective. In the prevention of reformation of lysed abdominal adhesions, the HA microspheres were embedded in a PEG-b-PLA phase-separated gel, [244]. Technology to control the release of cHyp from AAMs, section 4.3, was utilized in the subsequent formal rat laminectomy studies.

5.2 Study #1: non-degradable barrier devices with and without cHyp delivery

Anti-adhesion membranes (AAMs) and polymer films were evaluated in a four-week rat laminectomy study with three replicates per experimental group. To limit the pain and suffering inflicted upon the rats, spinal cord injury was omitted from this study. The two factors compared in this study were device architecture (films versus electrospun AAMs), and antifibrotic delivery (none versus controlled cHyp delivery)

Polymer films were compared to the electrospun AAMs to test the whether a porous device will have a less severe inflammatory response due to the increased nutrient, waste, and biological-signaling transport around the device. A polymer film creates a barrier to both cells and nutrient transport. Waste and biological cues, such as cytokines, are concentrated at the device surface, for one-half of their potential diffusion path is been blocked by the presence of the solid implant. In contrast, highly porous electrospun AAMs allow these cues to diffuse into the device, as well as into the surrounding tissue, reducing their concentration at the device-host interface. This porosity also allows nutrients to diffuse from one side of the device to the other, so healing can occur on the either side of the AAM, even if one side is isolated from the

vasculature. The unique pore size achieved by an electrospun device permits nutrients to transport, while cell nuclei are size-excluded from migrating through this barrier device.

The second effect evaluated in this study was anti-fibrotic delivery. cHyp was delivered in precursor form from the polymer implants. The precursor, cis-4-hydroxy-L-proline octyl ester HCl greatly increases the temporal window of drug delivery from hours to weeks, section 4.3. The delivery of cHyp is expected to reduce the severity of adhesion through inhibiting collagen synthesis [233-235] and promotion of collagen degradation by general proteases [221, 223]. Both polymer films and electrospun AAMs were loaded with 20% cHyp octyl ester HCl per polymer mass.

5.2.1 Materials implanted

Electrospun AAMs were fabricated in a class 10,000 cleanroom. Solutions of 5.8% wt/vol E0000 with 1:5 loading of cHyp octyl ester HCl or tHyp buytl ester HCl were prepared in HFIP. Electrospinning progressed under the conditions in Table 5-1. Fiber diameter was well matched between tHyp BE HCl and cHyp OE HCl loaded scaffolds: $0.28 \pm 0.02 \mu\text{m}$ and $0.29 \pm 0.02 \mu\text{m}$, respectively. Using Sampson's calculations [253] and assuming a typical pore fraction of 0.85 (pore fraction of these scaffolds was not measured directly), equation 3.2 predicts an effective pore diameter of $2.2 \mu\text{m}$. The estimated pore diameter and the barrier performance demonstrated during the subcutaneous screen, section 4.5.3, suggest that these scaffolds would function as barrier devices.

Table 5-1. Electrospinning parameters for fabrication of electrospun E0000 AAMs with either tHyp BE HCl or cHyp OE HCl from HFIP. Key: polymer concentration, C; needle potential, NP; collector potential, CP; distance, D; needle gage, G; flowrate, Q; fiber diameter, FD; and confidence interval, C.I.

Materials	C [% wt/vol]	NP [kV]	CP [kV]	D [cm]	G	Q [mL/hr]	FD [μ m]	95% C.I. (n=60) [μ m]
1:5 tHyp BE HCl:E0000	5.8	18	-6	18	23	0.5	0.28	0.02
1:5 cHyp OE HCl:E0000	5.8	18	-6	18	23	0.5	0.29	0.02

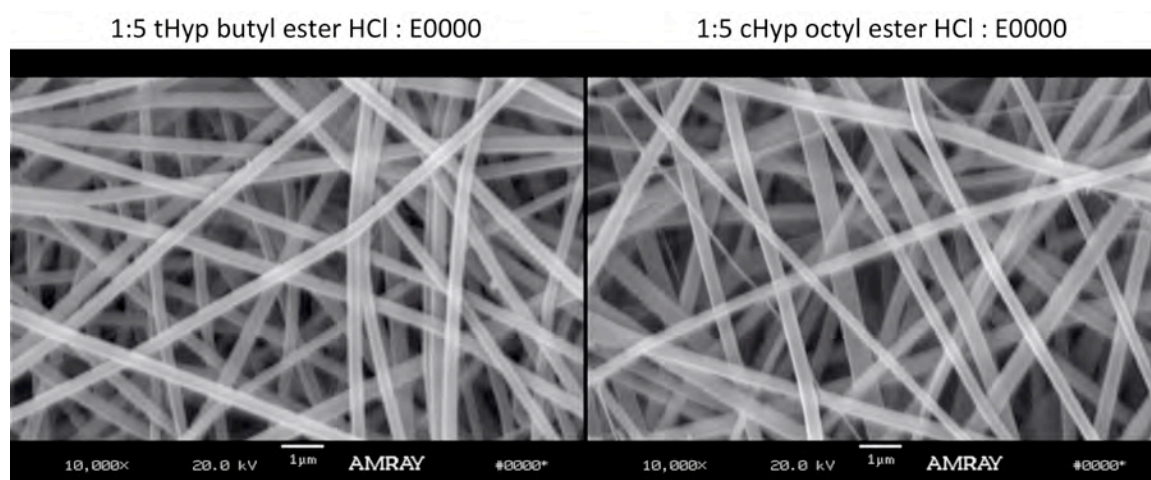


Figure 5.5. AAMs electrospun from 5.8 %wt/vol E0000 solutions in HFIP with 1:5 loading of either tHyp butyl ester HCl or cHyp octyl ester HCl

The comparator film devices were fabricated by compression molding using the REVA mold with a 50 μ m shim stack. E0000 films were pressed from polymer powder using the following protocol: 130 °C no pressure, 5 minutes; ramp 15,000 lbf, 1 minute; hold 15,000 lbf, 1 minute; release pressure, cool on benchtop, and release film from mold. cHyp-loaded films were fabricated from 45 mg sample of the electrospun AAM by compression molding at 115 °C, using the same sequence as above. Both films measured 50 μ m in thickness.

All samples were packaged in sterilization pouches and sterilized by the ethylene oxide gas sterilization method. Degassing proceeded at 40 °C under vacuum for 12 hours

followed by 36 hours of vacuum at room temperature. Karolina Piotrowska showed that this degassing method reduced EtO in electrospun E0000 fabrics from 196 ppm to undetectable levels by ^1H -NMR (Chemical shift: 2.21 ppm).

5.2.2 Implantation and materials handling

Bor Tom Ng, of the W. M. Keck Center for Collaborative Neuroscience, implanted the electrospun AAMs and polymer films into the laminectomy defect, attempting to tuck the prototype between the laminae rostral and caudal to the defect. A rostral tuck of 0.5-1 mm was achieved with all materials. However, the caudal tuck proved challenging. To achieve a caudal tuck, a fibro-membranous tissue was resected, and the edges of the implant were advanced between the lamina and dura.

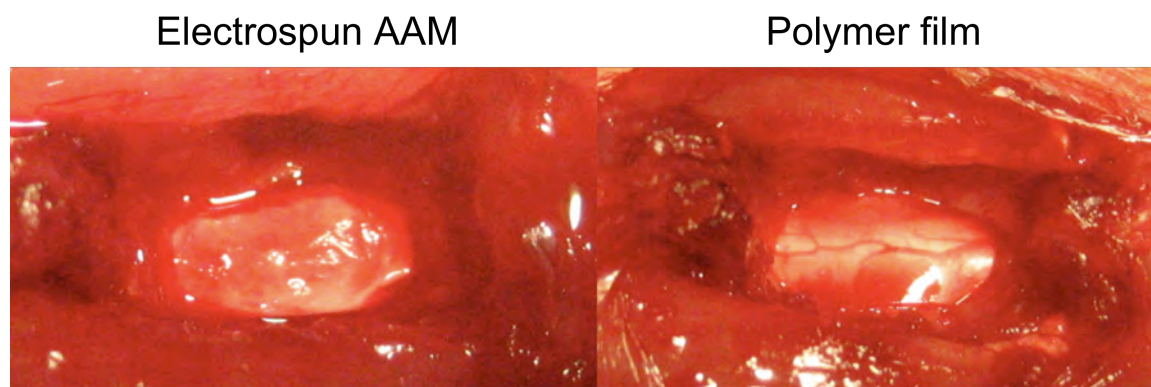


Figure 5.6. Placement of E0000 electrospun AAM and polymer films as an interpositional membrane between the dura and the laminectomy defect.

Intraoperative observation demonstrated that the E0000 films were too stiff, and the E0000 electrospun fabrics were too flexible. During the attempted caudal tuck, the E0000 films would obtain a convex shape and spring flat when the forceps were released. This behavior made permitted placement of the first corner under the rostral lamina, but lack of flexibility posed challenges when guiding the second corner under the caudal lamina. As a result, the implantation of the membrane took too long and caused too

much bleeding. Some convex flexion remained in the polymer films upon final placement, and blood was often trapped between the film and the dura, Figure 5.6. In contrast, the electrospun AAMs would fold over on themselves too easily when attempting the caudal tuck. The forceps could be placed near the edge of the implant, advancing the implant underneath the caudal lamina, but the leading edge of the implant would fold over on the forceps. When the forceps were removed, the implant was either released from the lamina or the corners remained in place with a fold present in the center of the fabric. Three of six electrospun AAMs obtained a partially successful caudal tuck, while the film devices achieved a caudal tuck at the four corners, while the film butted against the caudal lamina at the centerline.

The flexural stiffness of E0000 films was too great to conform to the tissue and permit placement of the device without inciting excessive bleeding. In contrast, the flexural stiffness of the E0000 electrospun fabrics was too low to maintain the fabric's shape while advancing the membrane between the lamina and dura. The flexural compliance of the electrospun AAM imparted excellent apposition to the dura and incited minimal bleeding. Complete rostral tucks of 0.5-1 mm were achieved with all materials, while partial caudal tucks were achieved in six-of-six films and three-of-six AAMs. In the other three AAMs, the fabric was laid on top of the caudal lamina.

5.2.3 Evaluation of adhesion prevention performance

The four-week extent of adhesion as a fraction of the laminectomy defect is presented in Figure 5.7. The delivery of cHyp did not have an effect on the extent of adhesion. Pooling the experimental groups to control (n=3), film (n=6), and electrospun AAMs (n=6), only the E0000 film devices were able to reduce the extent of adhesion

versus control animals: 0.62 versus 0.20 ($p = 0.007$). Other comparisons did not reach statistical significance. In this section, the interpretation of histological sections highlights the causation for the experimental group's respective adhesion prevention performance.

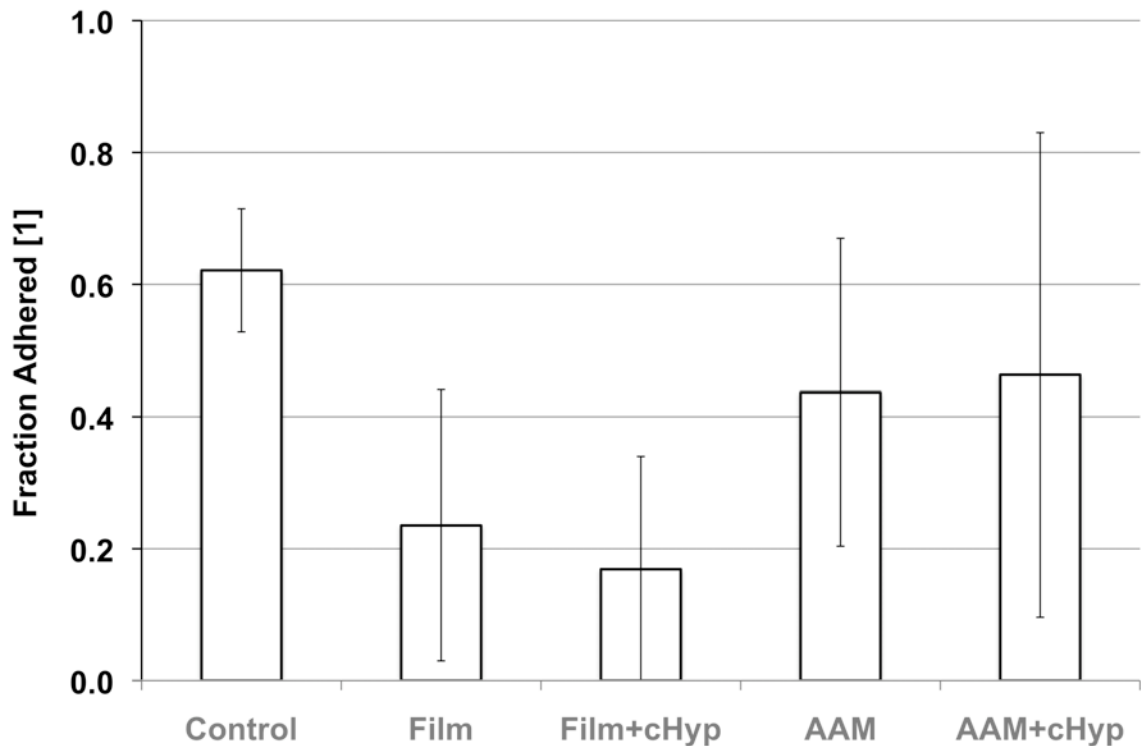


Figure 5.7. Fraction of the laminectomy defect where the dura was adhered to the laminectomy scar.

Where laminectomy was performed and the site was closed without any intervention to prevent peridural adhesion, the extent of adhesion was observed to be 0.78, 0.28, and 0.80. A representative histological section is presented in Figure 5.8. The spinal cord is present at the bottom of the figure. The fine pink horizontal line is the dura, and the large less-organized tissue above the dura is the laminectomy scar. At the extreme right and left of the image, the rostral and caudal lamina appear as dense, organized bony tissue. Due to trimming at the rostral end of the laminectomy site, some bone remodeling is observed there. Without the use of an interpositional membrane, the

laminectomy defect was filled with granulation tissue. At four weeks, the granulation tissue has become more organized, as it is being remodeled into scar tissue. At the rostral (left) end of Figure 5.8, a margin of white remains. At this location, the peridural fat was not compromised by connective tissue. The aim of the anti-adhesion devices is to preserve this white margin across the entire length of the laminectomy defect. The rightmost 80% of the dura has been tethered to the laminectomy scar.

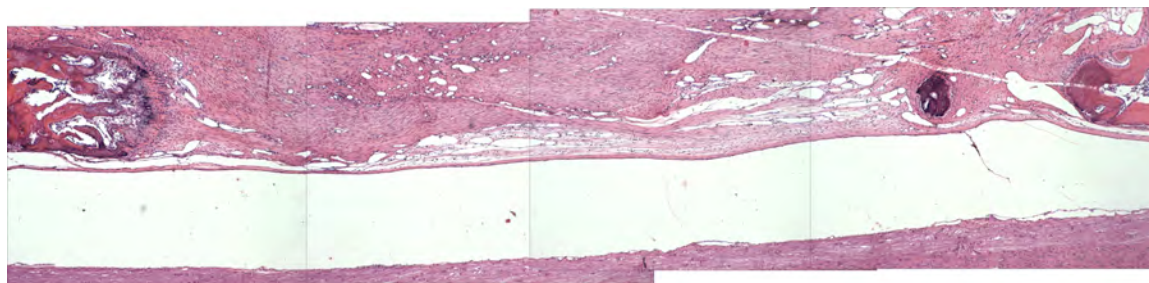


Figure 5.8. Representative 4-week control tissue section, where no interpositional membrane was placed between the dura and laminectomy defect. (H&E, 5x, tiled)

When the dura was covered with E0000 films before closure of the laminectomy defect, 0.33, 0.11, and 0.27 of the dura was adhered to the wound-healing scar. When cHyp was delivered from polymer films, statistically-indistinguishable performance was observed: 0.09, 0.30, and 0.12 extent of adhesion. Though 5 of 6 films fractured and 3 of 6 films were displaced from the peridural fat, the extent of adhesion was significantly reduced, Figure 5.9. The gaps between the film fragments offer a route for scar progression to the dura. If the inflammatory response were to remain quiescent, the scar may not progress farther. However, solid E0000 devices degrade slowly and do not erode under physiological conditions for over three years [166]. Minimal inflammatory activity at an implant site can only be expected once the device has been eroded, for the local inflammatory response is heightened during resorption as phagocytotic cells are recruited to process the degradation products.

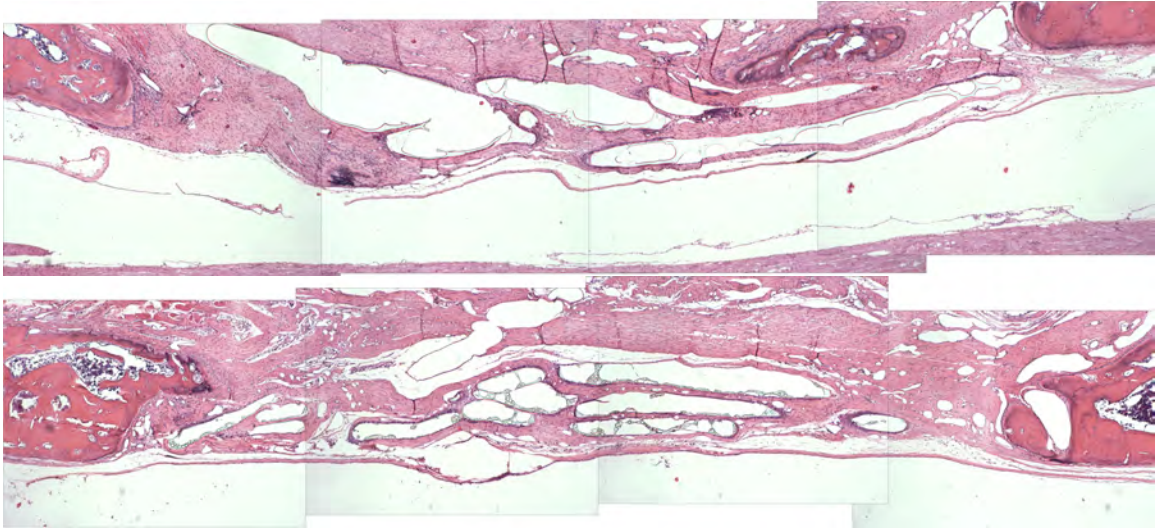


Figure 5.9. Representative 4-week film tissue sections, where an E0000 film without (top) or with (bottom) cHyp-delivery was placed on top of the dura before closing the laminectomy defect. (H&E, 5x, tiled)

When the dura was covered with electrospun E0000 AAM prototypes before closure of the laminectomy defect, 0.22, 0.91, and 0.18 of the dura was adhered to the wound-healing scar. When cHyp was delivered from electrospun AAM prototypes, statistically-indistinguishable performance was observed: 0.15, 0.69, and 0.54 extent of adhesion. The average extent of adhesion across these six samples was 0.45, which was not significantly different than the control group ($p = 0.23$). The performance of the AAM prototypes was compromised by delamination of the fabric and the subsequent inflammatory response to the abundance of foreign polymeric fibers at the site of implantation. The delamination was especially prevalent at the caudal end of the device, where the membrane was handled extensively in attempts to achieve a tuck between the caudal lamina and dura.

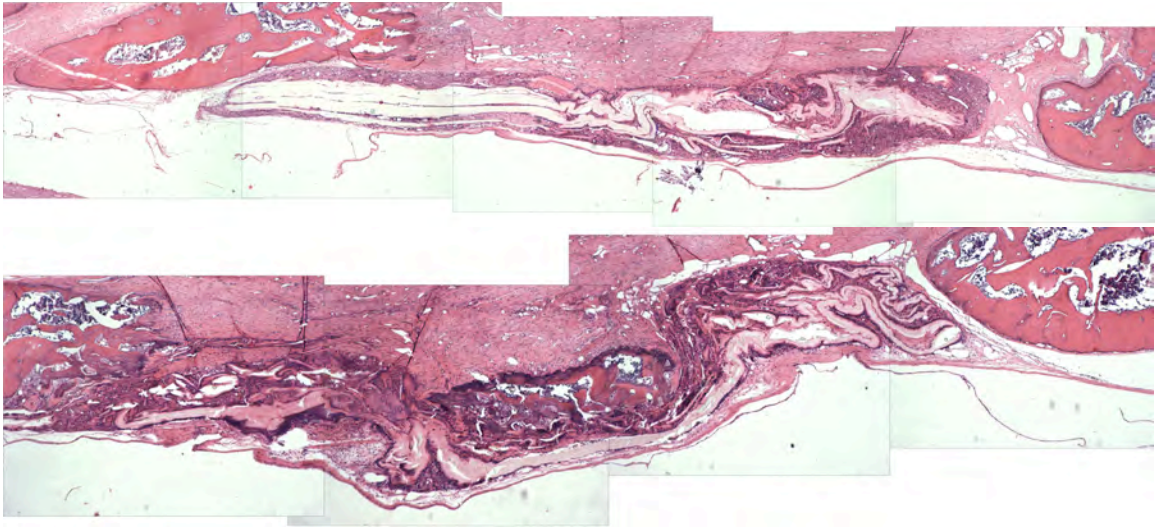


Figure 5.10. Representative 4-week electrospun AAM tissue sections, where an electrospun E0000 fabric without (top) or with (bottom) cHyp-delivery was placed on top of the dura before closing the laminectomy defect. (H&E, 5x, tiled)

Where a severe foreign body response is present, inflammatory cells will continue to recruit inflammatory cells, resulting in a chronic active response until the foreign body has been removed. Macrophages moderate this response through the secretion of “proteases, chemotactic factors, arachidonic acid metabolites, reactive oxygen metabolites, complement components, coagulation factors, growth-promoting factors, and cytokines” [8]. The presence of macrophages and foreign body giant cells (FBGC) at the implant interface is a typical feature of normal foreign body response. A chronic active response can be distinguished from an acceptable foreign body response by the presence of an abundance of neutrophils and continuously-recruited monocytes. The delaminated regions of AAMs produced such a response. At the conclusion of this study, electrospun AAMs were not candidates for peridural adhesion prevention; they would only become candidates if shortcomings in implant delamination and the subsequent chronic active inflammatory response were surmounted.

5.2.4 Summary and corrective measures

Four weeks after rat laminectomy, adhesions formed over more than half the defect length in the absence of an interpositional membrane. Effectively non-degradable E0000 films were difficult to place in the implant site and incited excess bleeding, but the films were effective barriers to scar progression at four weeks. The displacement and fracture of the majority of films invites suspicion of their ability to resist adhesion formation through device erosion. However, E0000 compression-molded films have proven the concept that polymeric films can prevent epidural adhesion. A veterinary medicine group at Colorado State University has already demonstrated that slowly-degrading polymer films can prevent peridural adhesion [133, 134, 136]. The field has not demonstrated inhibition of peridural adhesion through device resorption.

Composite polymer films of E1224(1k) with a minor phase of E1002(1k) fibers were fabricated, section 3.8. The high PEG-content of the composite films increased their compliance and fracture resistance, while simultaneously increasing device degradation and resorption rates. The composite film devices were intended to overcome shortcomings in device handling and attempt to advance the field of peridural adhesion prevention through investigation of a rapidly-degrading polymeric film. High PEG-content films are not suitable for delivery of cHyp, for they do not retain the cHyp octyl ester HCl, Figure 4.15. cHyp has not yet demonstrated an adhesion prevention effect, so it will only be evaluated in the AAM group in study #2.

The delamination of electrospun E0000 AAMs resulted in the recruitment of an abundance of inflammatory cells at four weeks. The chronic active inflammatory response and loss of barrier function resulted in device failure. The first priority for a

second-generation AAM was increased delamination strength. Rapid, high-consistency heat treatment methods were developed, which provided consistent fusion of fiber-fiber intersections and control over pore fraction, and thus pore diameter, section 3.7. Composite AAM construction provided increased toughness, strain-to-failure, compliance, and greater suture retention strength. These properties were intended to increase the scaffold's resilience to handling with sharp instruments, but they could also enable suture fixation of the device. Additionally, the potential toxicity of the fibers was reduced by electrospinning the composite devices from acetic acid, rather than HFIP. The data presented in section 3.7 was sufficient to warrant inclusion of electrospun AAMs in the final comparator study versus DuraGen PLUS®.

A cHyp effect was not demonstrated in this study. The intensity of inflammatory response in electrospun AAMs and the fracture of polymeric films compromised the performance of the respective devices. The mechanical function of the anti-adhesion device for neurosurgery was intended to supply the primary adhesion prevention effect. The delivery of cHyp was meant to enhance an effective physical barrier device. The shortcomings of a defective barrier would likely mask any cHyp effect. As the physical nature of each device was compromised, cHyp delivery will be included in one group in study #2, for its performance is yet to be disproven.

5.3 Study #2: degradable composite devices versus DuraGen PLUS®

The characterization of TDPC anti-adhesion devices performed in sections 3.7 and 3.8 demonstrated that the shortcomings of the first generation devices have been surmounted. Due to the DT and PEG_{1k} content of the second-generation devices, the effects of polymer degradation were evaluated in study #2. In this comparator study, the

performance of bioerodible prototypes was benchmarked against the performance of Integra LifeSciences' DuraGen PLUS[®], which has seen success in Europe [148, 149], and is under investigation in the US [138]. As this was the definitive animal study for this project and sufficient evidence existed for the potential utility of TDPC anti-adhesive devices, spinal cord injury was performed prior to the placement of AAM prototypes to simulate the handling of tissues during microdiscectomy.

5.3.1 Materials implanted

Four materials were evaluated for peridural adhesion prevention: composite electrospun AAMs with and without cHyp delivery, composite films, and Integra LifeSciences' DuraGen PLUS[®]. Composite electrospun AAMs were electrospun using the dual spinneret device, Figure 3.23. Polymer solutions and electrospinning parameters were prepared according to Table 5-2. Note that in cHyp-loaded scaffolds, only the E1000.5(1k) solution contained cHyp octyl ester HCl; E0012(1k) was always electrospun with a 1:5 loading of tHyp butyl ester HCl : polymer. Fabricated and sterilized AAMs are pictured in Figure 3.30 b and c, and their physical properties are listed in Table 3-3. Briefly, the fiber diameter for each scaffold was 0.4 μm , the pore fraction was ~60%, average effective pore size was < 1 μm , and the thickness ranged from 80-95 μm .

Table 5-2. Electrospinning parameters for fabrication of 1:1 E1000.5(1k):E0012(1k) composite AAMs with either tHyp BE HCl or cHyp OE HCl from acetic acid. Key: polymer concentration, C; needle potential, NP; collector potential, CP; distance, D; needle gage, G; flowrate, Q

Solution	Materials	C [% wt/vol]	NP [kV]	CP [kV]	D [cm]	G	Q [mL/hr]
Solution A	1:5 tHyp BE HCl or cHyp OE HCl : E1000.5(1k)	16	24	-1	10	23	0.5
Solution B	1:5 tHyp BE HCl : E0012(1k)	20	24	-1	10	23	0.4

The composite film devices were fabricated from two E1224(1k) polymer films, which were compression molded into an electrospun fabric of E1002(1k), Figure 3.31. Both TDPC devices were packaged in foil pouches that were purged with nitrogen and then heat sealed. The packaged devices were sterilized by a 29-kGy dose of gamma-irradiation (Sterigenics, Rockaway, NJ). DuraGen PLUS[®] (lot# 1090644) and the sterilized TDPC samples were cut to size in a laminar flow hood using sterile instruments and a sterile surface. TDPC devices were trimmed to 3 mm x 6.5 mm, and the 3 mm-thick pieces of DuraGen PLUS[®] were trimmed to 3.5 mm x 8 mm. The DuraGen PLUS[®] membranes are longer because they were placed on top of the dura and lamina, rather than being tucked under the adjacent laminae.

5.3.2 Implantation and materials handling

Charlotte Hsu of the W. M. Keck Center for Collaborative Neuroscience created the laminectomy defect, executed the spinal cord injury, and implanted the experimental materials as described in section 5.2.2. Due to the improvement of material properties, the implantation of TDPC devices was completed more quickly and easily than in comparison to study #1, Figure 5.11. The flexibility and hydrophilicity of the composite film device permitted it to slide against the dura and under the lamina. Furthermore, the lack of sharp, rigid edges caused less bleeding during implantation.

The fiber fusion and reduced pore volume of composite AAMs increased their flexural stiffness. The increased stiffness and hydrophilicity (50% E0012(1k) content) enabled the membrane to be advanced under the laminae without buckling or wrinkling. Furthermore, the composite AAM devices' increased toughness and delamination

strength permitted handling with sharp instruments without the device being pierced or frayed. A rostral and caudal tuck was achieved with all TDPC devices.

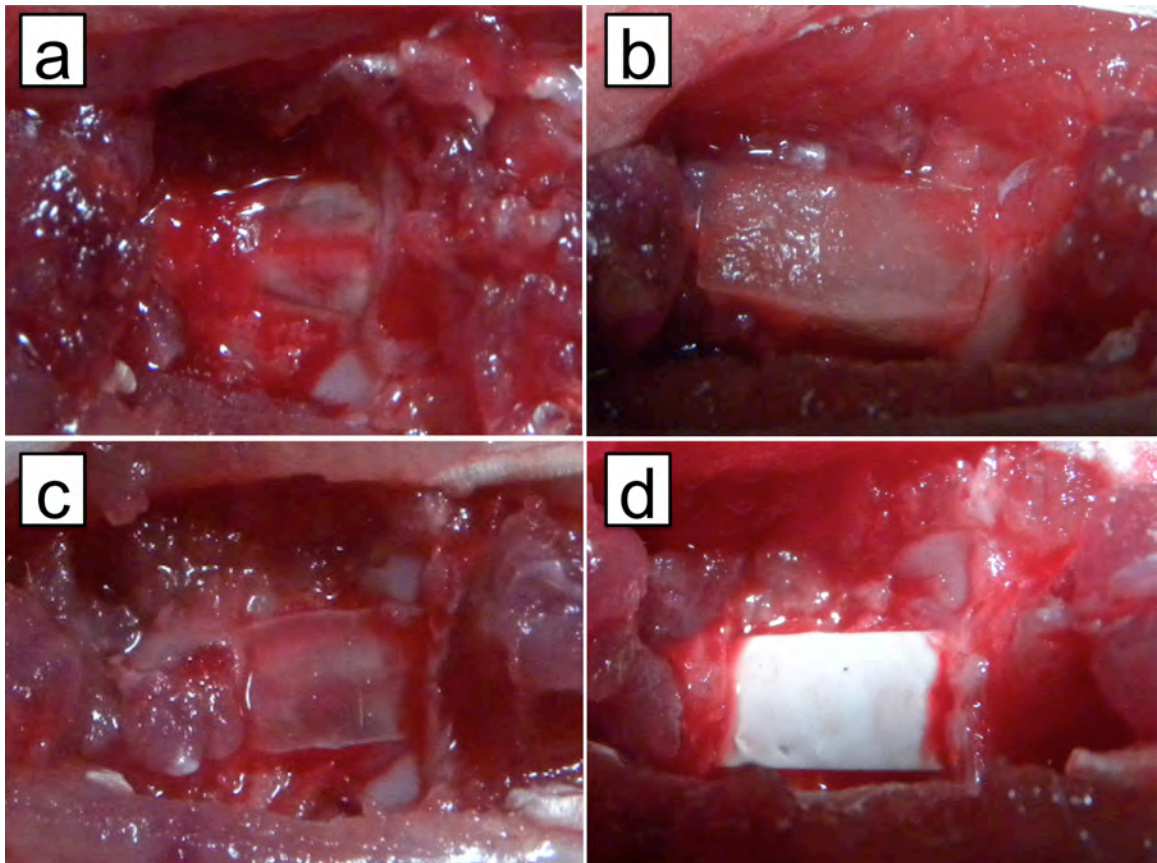


Figure 5.11. Surgical site prior to closure: (a) no intervention, (b) DuraGen PLUS[®], (c) composite film device, (d) composite AAM.

Eventhough the handling properties of the second-generation devices were far superior to the first, the onlay placement of DuraGen PLUS[®] was much quicker. Following spinal cord injury, special care was taken to achieve hemostasis. The surgical site was then rinsed with saline and dried with cotton. Dry DuraGen PLUS[®] was placed upon the dura, covering the entire laminectomy defect and a portion of the rostral and caudal lamina (1-1.5 mm per side). Saline was used to wet the collagen foam, contracting it slightly, and the surgical site was closed as in section 5.2.2.

5.3.3 Evaluation of adhesion prevention performance

At 24-hours, two trial animals were sacrificed to evaluate Charlotte Hsu's execution of the surgery. At 24-hours, fibrin matrix had either completely or partially covered the anti-adhesion devices for neurosurgery, Figure 5.12. The fibrin matrix was gently lifted from the film and membrane. Neither device was adhered to the fibrin matrix. Upon removal of the film or membrane, a clean and free dura was observed in both cases. The experimental materials remained in place, and the rostral and caudal tucks were secure. The TDPC devices prevented the advancing fibrin gel [7] from creating a provisional matrix bridge between the musculoskeletal tissues and the dura.



Figure 5.12. Sample recovery 24 hours after trial surgical placement of composite film and composite electrospun AAM devices. At left, the film device was covered with a thick fibrin matrix with some coagulated blood, which could be removed (center). At right, a fibrin gel advances from the margins of the laminectomy defect on the posterior surface of the electrospun AAM.

As measured by the primary experimental outcome, the extent of peridural adhesion at four weeks was inhibited by DuraGen PLUS® ($p = 0.003$), composite films ($p = 0.005$), and cHyp-loaded AAMs ($p = 0.048$). At eight weeks, the composite film device did not provide an inhibitory effect, while the non-drug-loaded AAM group approached significant inhibition of peridural adhesion ($p = 0.11$). At both timepoints, DuraGen PLUS® provided the greatest inhibition to adhesion formation. The performance and mechanism of each device will be discussed in the following sections.

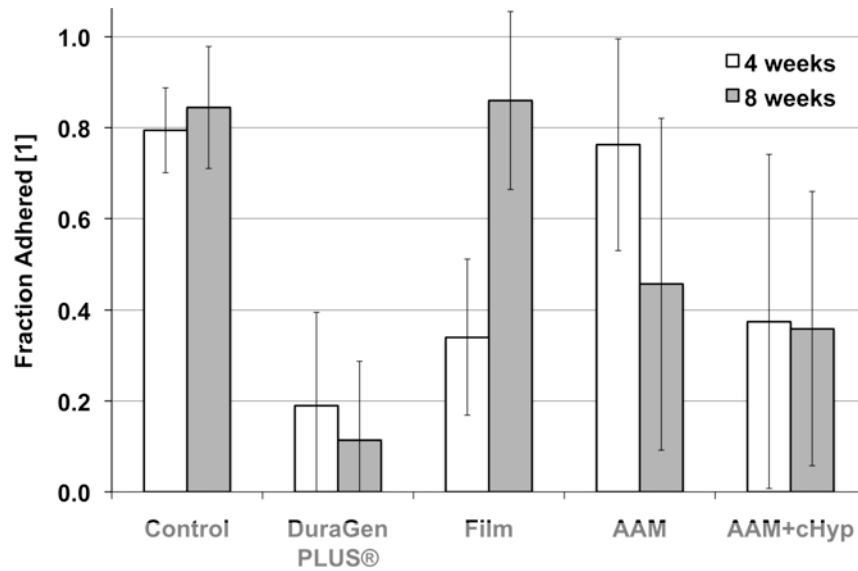


Figure 5.13. Fraction of the laminectomy defect where the dura was adhered to the laminectomy scar at weeks 4 and 8.

In control animals, collagenous granulation tissue penetrated the peridural fat and adhered the dura to the wound-healing scar at four weeks. By eight weeks, the organization and density of the collagenous tissue increased, suggesting that the tenacity of adhesion would be greater at eight weeks than at four weeks. At both timepoints, approximately 80% of the dura was tethered to the laminectomy scar, Figure 5.14.

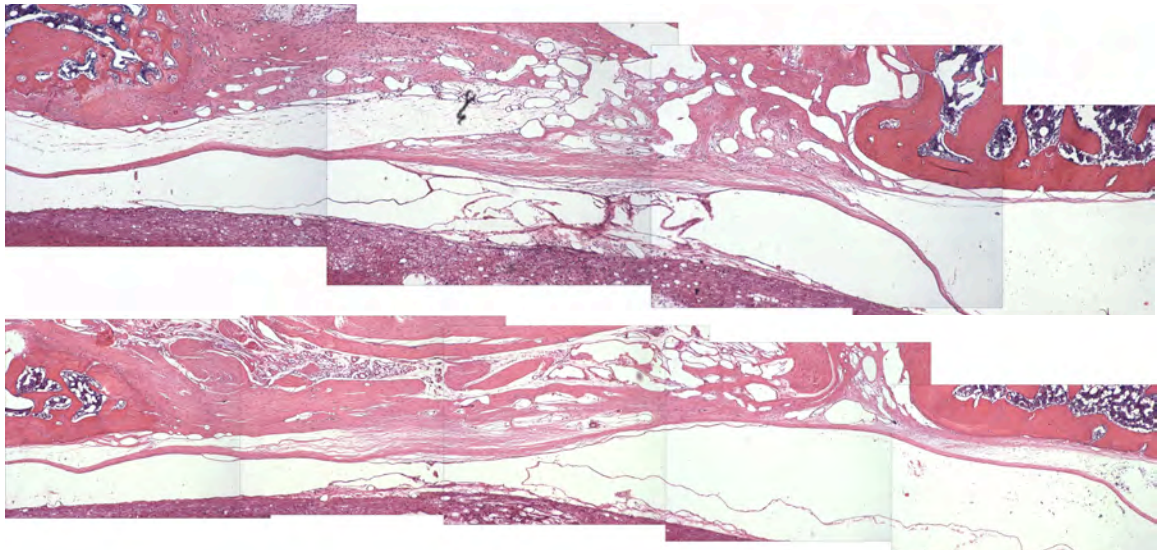


Figure 5.14. Representative 4-week (top) and 8-week (bottom) control tissue sections, where no interpositional membrane was placed between the dura and laminectomy defect. (H&E, 5x, tiled)

Composite films were able to inhibit the bridging of scar tissue to the lamina at four weeks, but fibrous tissue bridged through the fractured film at 8 weeks, Figure 5.15. In laminectomy study #1, the E0000 similarly inhibited scar progression at four weeks, but barrier function was compromised. Here, the volume and density of scar tissue increased greatly at eight weeks, and the peridural adhesion performance diminished. The high PEG-content of E1224(1k) decreased the T_g to $-4\text{ }^{\circ}\text{C}$ and increased the flexibility of the films; however, these properties did not prevent film fracture at four weeks. At 4 weeks of incubation *in vitro*, the molecular weight of E1224(1k) decreases to 16% of its initial value [158]. As the molecular weight of degradable polymers decreases, chain entanglement decreases, and the polymers become brittle. Though the composite membrane was tough upon implantation, the rapidly degrading polymer became brittle upon molecular weight loss.

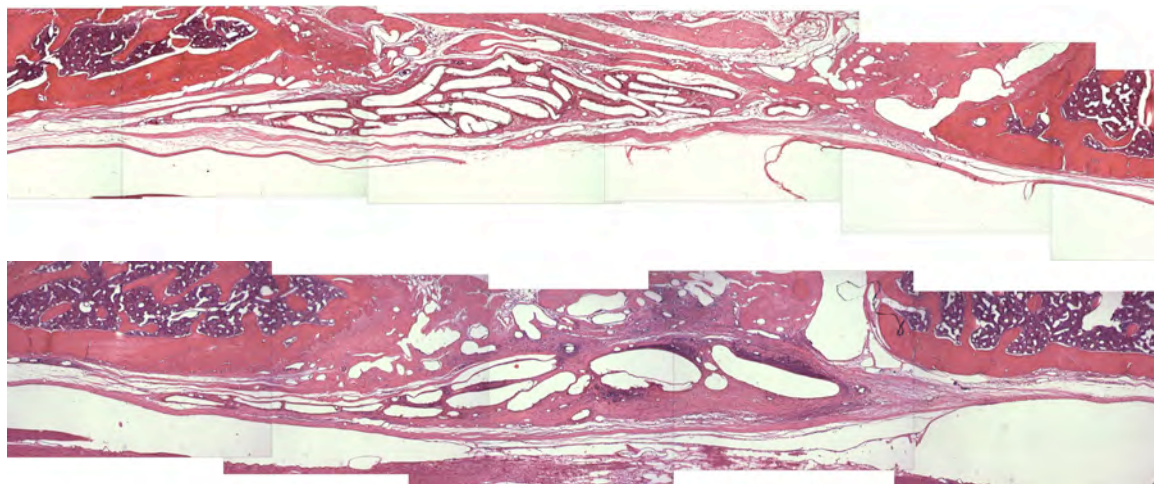


Figure 5.15. Representative 4-week (top) and 8-week (bottom) composite film tissue sections, where a film composed of E1224(1k) with E1002(1k) fibers was placed between the dura and laminectomy defect. (H&E, 5x, tiled)

As the polymer bioeroded, inflammatory cells accumulated at the device interface, especially vacuolated macrophages and FBGCs, see section 5.3.4. The growth factors released during phagocytosis encourage recruitment of additional inflammatory

cells and proliferation of fibroblasts and endothelial cells. For this reason, the space between fractured fragments of polymer became densely populated with fibrous tissue.

The performance of composite AAMs was highly variable due to instability at the caudal tuck, Figure 5.16. The composite AAMs provided a barrier to scar progression, where present. However, when the caudal tuck was released, barrier performance was no longer present at the caudal end of the implant site. In some tissue sections, that peridural fat was sufficient to prevent scar progression to the dura. However, in others the peridural fat was compromised, causing a short adhesion, while in other laminectomy sites, the scar progressed under the composite AAM, resulting in extent of adhesion as great as 0.83. Across both cHyp- and non cHyp-loaded AAMs, the extent of peridural adhesion observed was: 0.05, 0.26, 0.28, 0.50, 0.53, and 0.83.

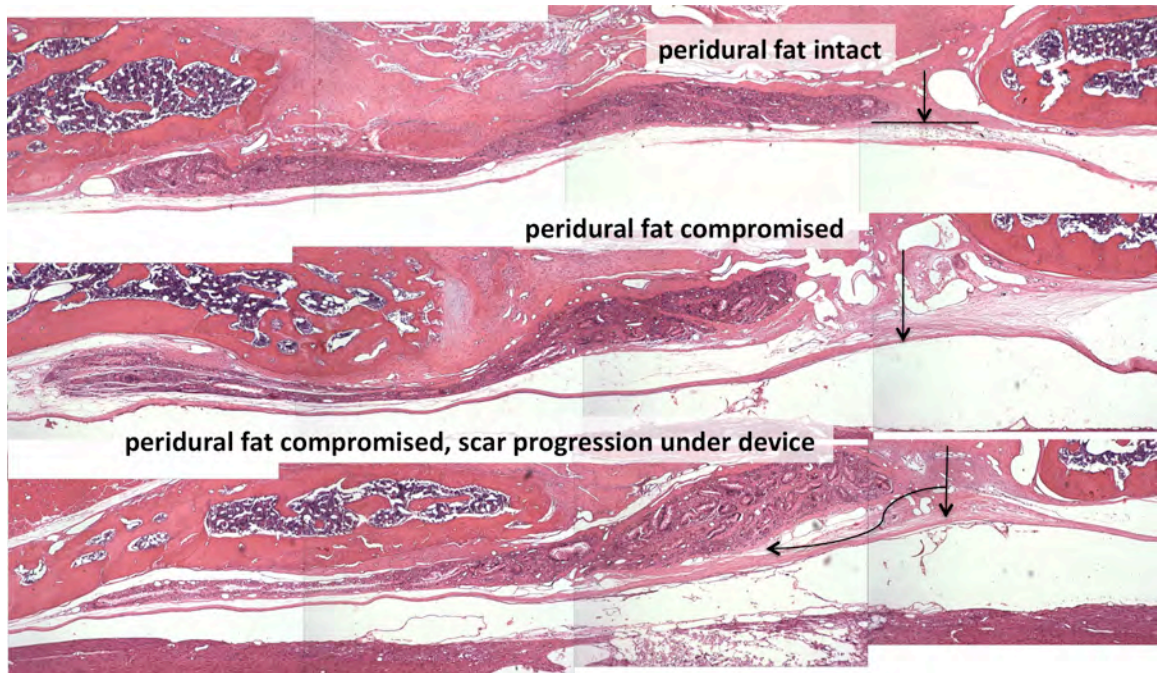


Figure 5.16. Variable adhesion prevention performance of cHyp- and non-cHyp-loaded composite AAMs at 8-weeks due to instability at caudal tuck. (H&E, 5x, tiled)

In non-cHyp-loaded AAMs, a large volume of dense scar tissue was present posterior to the implant, while varying degrees of scar progression between the implant

and dura were noted, Figure 5.17. The implant was undergoing bioerosion, with a quiescent response at the boundary between the resorbing polymeric implant and the surrounding scar tissue. The foreign body response to composite AAMs was typical of synthetic biomaterials, see section 5.3.4. In comparison to the E0000 fabrics, which inspired a chronic active response, the composite membranes resisted delamination and did not contain trace quantities of HFIP. Where present, the non-cHyp-loaded AAMs provided a barrier to scar progression across the laminectomy defect, and they incited a typical tissue reaction. At 8 weeks, an 89% certainty existed that the non-cHyp-loaded AAMs provided a true inhibition of peridural scarring compared to the control group.

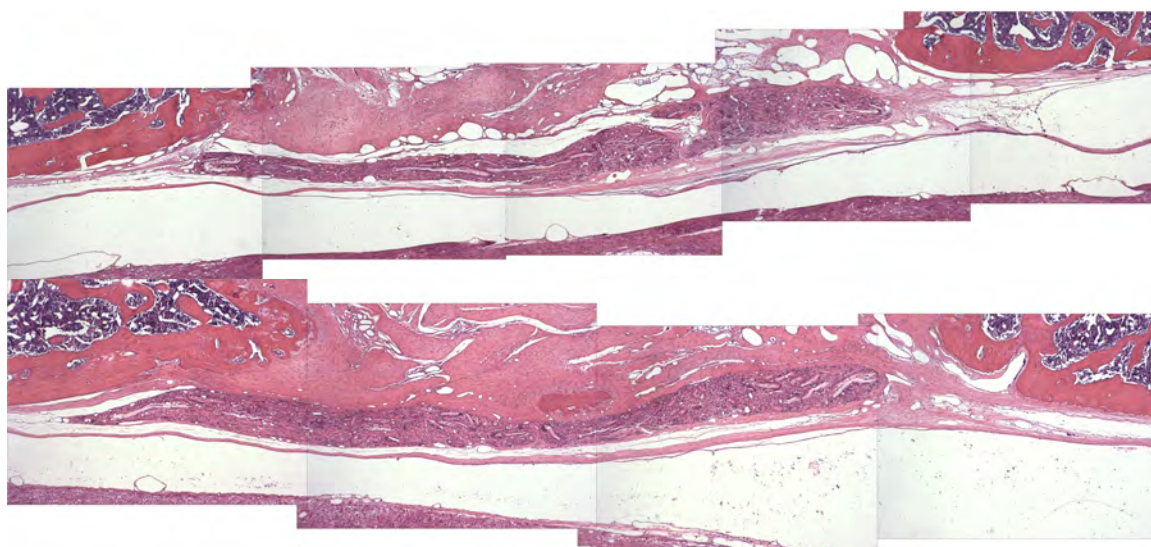


Figure 5.17. Representative 4-week (top) and 8-week (bottom) composite AAM tissue sections, where an 1:1 E1000.5(1k):E0012(1k) membrane was placed between the dura and laminectomy defect. (H&E, 5x, tiled)

The cHyp AAM group displayed similar function and performance to the AAM group without cHyp delivery. The extent of adhesions may have been reduced in cHyp-loaded scaffolds at 4 weeks ($p = 0.077$), but the high variability at the caudal tuck makes it difficult to conclude whether a true effect is present. In comparison to control animals, cHyp-loaded AAMs inhibited peridural adhesion at 4 and 8 weeks ($p = 0.048, 0.049$).

The cHyp-loaded AAMs were an effective barrier, where present, and variable adhesive scarring was observed at the caudal margin of the laminectomy defect. cHyp octyl ester HCl did not increase the severity of the tissue response to the implant, as a typical foreign body response was observed, comparable to non-cHyp-loaded AAMs.

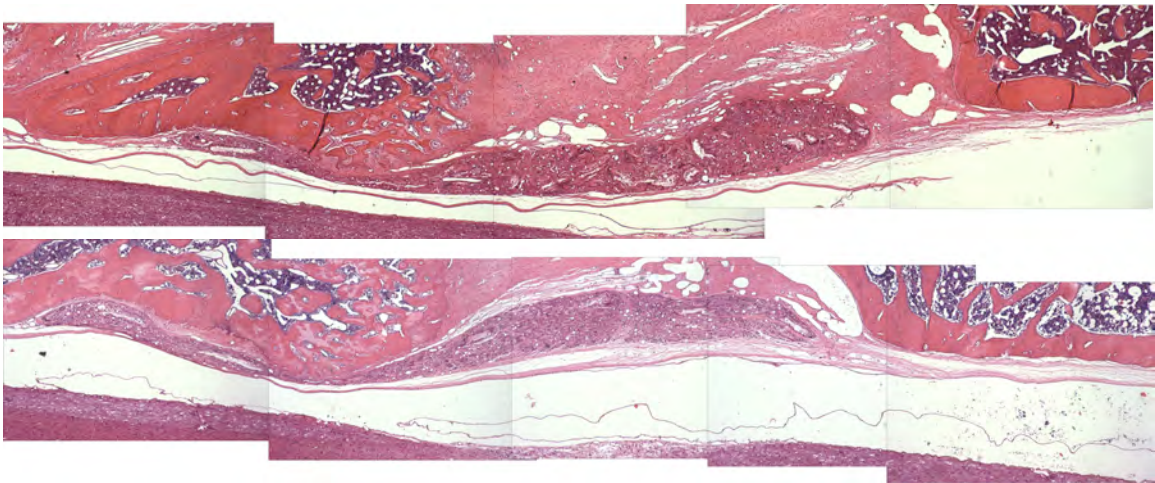


Figure 5.18. Representative 4-week (top) and 8-week (bottom) composite AAM + cHyp tissue sections, where an 1:1 E1000.5(1k):E0012(1k) membrane loaded with cHyp octyl ester HCl was placed between the dura and laminectomy defect. (H&E, 5x, tiled)

DuraGen PLUS[®] effectively inhibited scar progression to the dura at both 4 and 8 weeks ($p = 0.003, 0.005$). Though 18 and 11% of the dura had some adhesion to the laminectomy scar, the adhesions were lower in density than in film, AAM, or control groups. DuraGen PLUS[®] was incorporated into the forming scar tissue, and thus did not require degradation and phagocytosis for the implant site to resolve. The porous collagen foam does not have inherent barrier properties, so its performance requires assistance from the peridural fat. The collagen foam appears to prevent adhesions by guiding rapid synthesis of collagenous tissue by the host. This rapidly-organized scar may provide function similarly to the ligamentum flavum preservation technique [58-61], providing a collagenous barrier to scar progression. This proposed mechanism of action could only

be elucidated by observing the development and resolution of fibrin matrix and scar tissue at short timepoints.

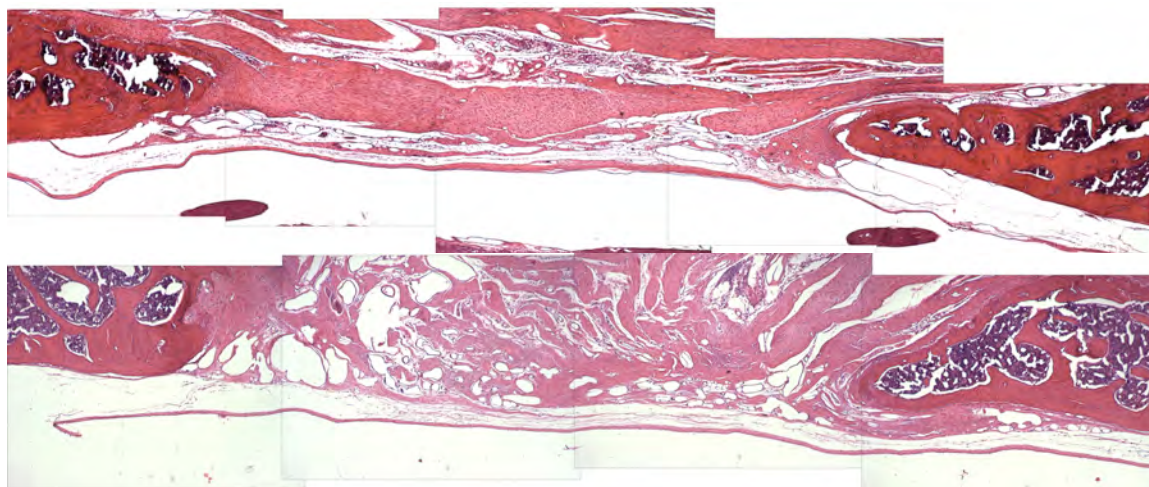


Figure 5.19. Representative 4-week (top) and 8-week (bottom) DuraGen PLUS[®] tissue sections, where an collagen foam was placed over the dura within the laminectomy defect. (H&E, 5x, tiled)

5.3.4 Biocompatibility of degradable composite devices

The biocompatibility of the degradable composite film and composite AAM devices was compared against the tissue response to 65:35 poly(D,L-lactide-co-glycolide) microspheres (typical response) and to a silk suture that was used for multiple rats (chronic active response). Detailed histological images were provided in Anderson and Shive's review [259] of Yamaguchi and Anderson's earlier work in the tissue response to PLGA microspheres [260]. In the progression of the rat laminectomy studies, Charlotte Hsu used the same suture to close the muscle tissue of multiple rats. Occasionally, this tissue layer was included in the histological sections. The tissue residue deposited on the silk suture during closure of one rat was transferred to the next rat. The chronic active response in the vicinity of the silk suture highlights the difference between the typical foreign body response to biocompatible materials, and the chronic active response that can be incited in response to non-biocompatible materials.

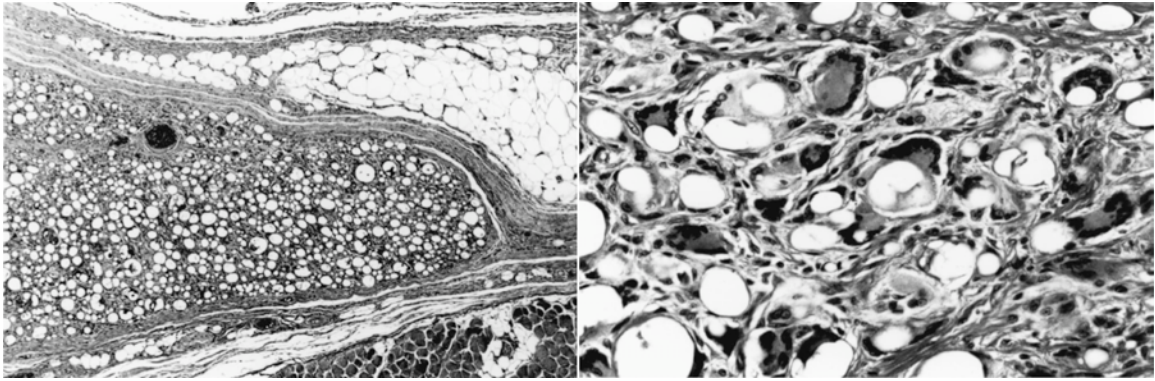


Figure 5.20. Typical foreign body response to subcutaneous injection of a bolus of poly(D,L-lactide-co-glycolide microspheres at 11 weeks (Left, H&E, 5.6x) and 13 weeks (Right, H&E, 35x) [259]

The typical foreign body response to a high surface area per volume biomaterial is depicted in Figure 5.20. The entire bolus of microspheres is encapsulated in a fibrous capsule. Within the fibrous capsule, a multitude of macrophages are present. Some have fused to form multinucleated cells, here Langhans giant cells. A light granulation tissue has formed between the microspheres. Fibroblasts, indicated by elongated nuclei, are interspersed with the macrophages in the space between the microspheres. In the original report, similar composition of the implant site was observed up to 120 days [260]. At 150 days, the volume and cellular density of the site was greatly reduced, and a small volume of mature fibrous tissue remained.

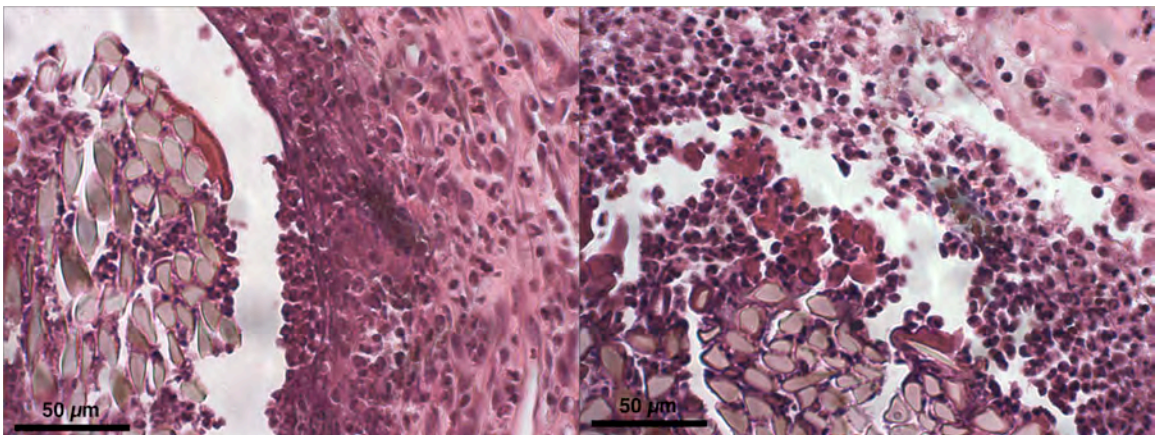


Figure 5.21. Chronic active response to a silk suture that transferred tissue from one rat to the next; histology at 4 weeks (left) and 8 weeks (right). H&E 40x

The chronic active foreign body response to a silk suture contaminated with tissue from another rat is depicted in Figure 5.21. At 4 weeks, the granulation tissue surrounding the suture is filled with a mixture of neutrophils, monocytes, macrophages, and fibroblasts. At close proximity to the silk suture, the concentration of neutrophils (indicated by lobular nuclei and low volume of cytoplasm) is greatly enhanced. At 8 weeks, the chronic active response has progressed, forming a suture abscess. Neutrophils and some lymphocytes are present at the suture interface, and a large fraction of them have died (indicated by lack of structure within the nucleus). In the granulation tissue surrounding the suture abscess, some plasma cells are identified as cells with a round, eccentrically-located nucleus. The presence of plasma cells indicates that the adaptive immune system has been recruited in response to this foreign material. The different composition of cell types at the implant site allows one to differentiate a typical foreign body response from a chronic active foreign body response.

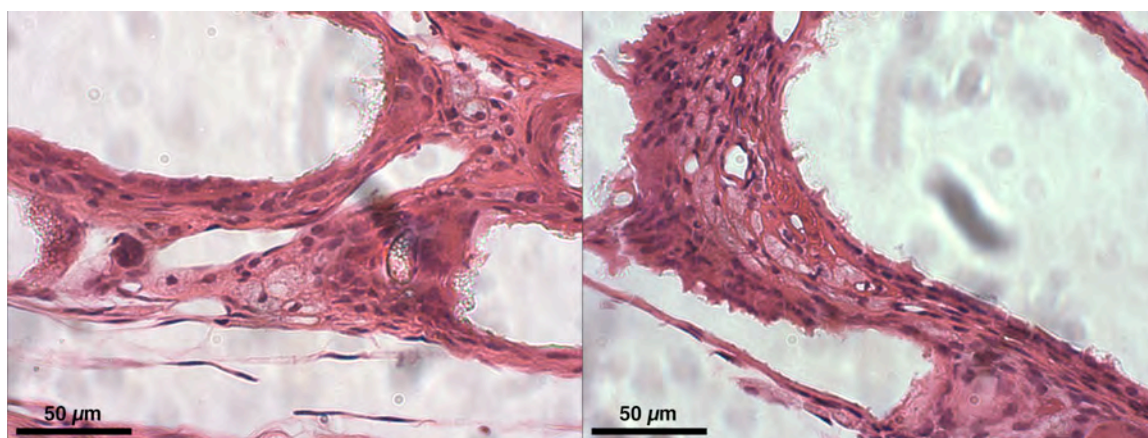


Figure 5.22. Foreign body response to a rapidly degrading E1224(1k) film reinforced with E1002(1k) fibers; histology at 4 weeks (left) and 8 weeks (right). H&E 40x

The tissue response to the composite films is comparable to a typical foreign body response. In comparison the tissue response adjacent to E0000 films, the macrophage density is much higher. The increased abundance of macrophages at the surface of the

composite films is due to the degradation of E1224(1k). At four weeks, a significant portion ($>18\%$) of the polymers' mass becomes soluble *in vitro* [158]. Bioerosion *in vivo* is expected to be higher. Because E1224(1k), but not E0000, is undergoing bioerosion at 4 and 8 weeks, more macrophages are present to phagocytose the degradation products. The cell types present in Figure 5.22 include highly vacuolated macrophages and FBGCs, with some interspersed fibroblasts. No neutrophils or plasma cells are present in the tissue sections. Though macrophage and FBGC density was high at the composite film device interface, the cell types present indicate a foreign body response typical to widely utilized biomaterials.

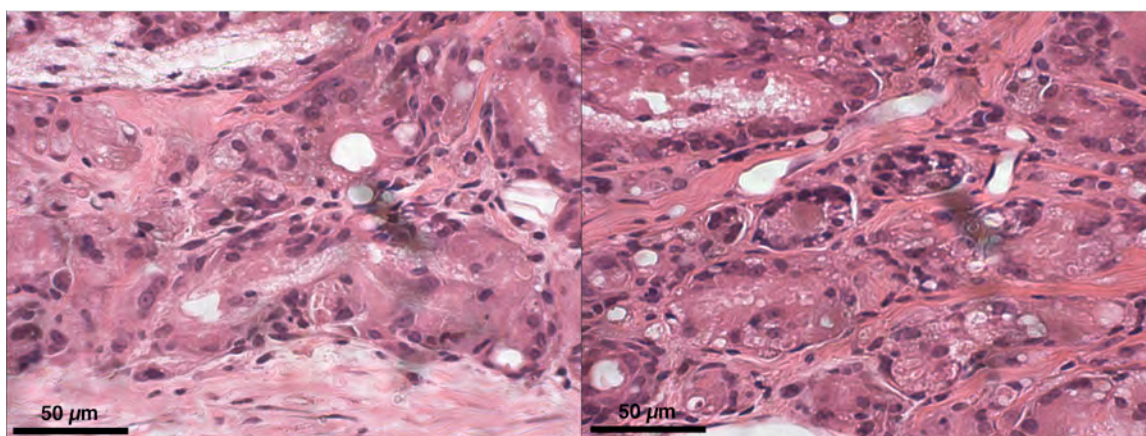


Figure 5.23. Foreign body response to degradable composite AAM; histology at 4 weeks (left) and 8 weeks (right). H&E 40x

The composite AAMs incite a foreign body response typical to high surface area biomaterials. At four weeks, vacuolated macrophages and some FBGCs were observed amongst pieces of residual implant. Light, poorly-organized interstitial fibrous tissue is observed. At eight weeks, in tact pieces of residual implant were less prominent, and macrophage fusion to FBGCs was enhanced. The interstitial fibrous tissue bands have matured and are highly organized with a lower density of fibroblasts within the extracellular matrix. If this pattern of foreign body response continues to complete

polymer resorption, the implant site should resolve to a small volume of fibrous tissue [260], likely being integrated into the fibrous scar on the posterior side of the implant.

5.3.5 Evaluation of Anti-Adhesion Device Performance

The 4- and 8-week comparator study of anti-adhesion devices for neurosurgery demonstrated that composite AAMs were competent to reduce the extent of adhesion, but the AAMs were not a synthetic alternative to DuraGen PLUS[®]. Degradable composite film devices inhibited dural adhesion to the laminectomy scar at 4 weeks despite fracturing, similar to E0000 devices. However, at 8 weeks fibrotic tissue increased in density and volume, bridging through the fractured device to the dura.

Composite electrospun AAMs greatly improved upon the performance of both composite films and E0000 electrospun AAM prototypes. Unlike the films, the composite electrospun devices did not fracture, and fibrotic tissue did not advance through the device. In comparison to E0000 electrospun AAM prototypes, the composite AAMs did not delaminate and incited a less-severe inflammatory response, which was comparable to the foreign body response to PLGA microspheres. Pooling both groups of composite AAMs, these membranes reduced the extent of adhesive scarring from 0.84 to 0.41 ($p = 0.04$) at 8 weeks. However, the consistency of peridural adhesion inhibition was poor due to instability at the caudal end of the implant site. To obtain stability at the caudal end of the laminectomy defect, the device must either be: (i) sutured to the facet capsule of adjacent vertebrae [130], (ii) fixed in place with fibrin sealant, or (iii) implanted into an animal model that would permit greater insertion length between the adjacent lamina and dura.

The high variability at the caudal margin of the laminectomy defect made it difficult to discern whether cHyp delivery had an effect on the extent of adhesion. At 4 weeks, cHyp delivery reduced the extent of adhesion from 0.76 to 0.37 ($p = 0.078$), but at the 8-week timepoint, no statistical difference in extent of adhesion was noted (0.46 without versus 0.36 with cHyp, $p = 0.35$). However, when the performance at both timepoints was considered, cHyp-delivery was able to reduce the extent of adhesion from 0.61 to 0.37 ($p = 0.082$). An effect of cHyp is suspected, but the variance caused by instability at the caudal tuck refuses the assertion that cHyp delivery enhances anti-adhesion performance.

DuraGen PLUS[®] was effective in reducing the extent of peridural adhesions to 0.19 ± 0.21 and 0.11 ± 0.17 at 4 and 8 weeks. Where adhesions were present, they were composed of light fibrous bands, Figure 5.19. Longer timepoints would be necessary to ascertain whether these bands increase in density over time or whether the bands remain at a low density. The straightforward placement of the DuraGen PLUS[®] and its demonstrated performance were not matched by the prototype synthetic AAMs in this dissertation. The collagen foam integrated into the surrounding tissue, while the synthetic devices required activation of the innate immune system to erode the implants. This integration mitigates the secretion of growth factors and cytokines in the laminectomy defect, which decreases the severity of inflammatory response, thus reducing the accumulation of fibrous tissue.

5.4 Conclusions regarding anti-adhesion performance in the laminectomy defect

Across the three laminectomy studies, the effect of device architecture was primary, while drug delivery could only provide an enhancement effect. In the

exploratory study, cHyp delivery was ineffective because there was no barrier to cell migration, and cHyp is not able to prevent the secretion of all collagen. In the first study of device architecture and drug delivery, delamination and subsequent chronic active inflammatory response obscured any effect of cHyp delivery. In the final study, AAM instability at the caudal tuck permitted scar tissue to progress around the barrier, unaffected by cHyp eluted from the AAM.

The architecture of composite electrospun AAMs permitted them to resist fracture, unlike polymer films. The fractured films inhibited adhesion at 4 weeks, but scarring progressed through the film fragments to the dura by 8 weeks. As observed in the exploratory study, cell-impermeability was required to prevent scar progression. Else, inflammatory cells infiltrated the devices, proliferated within its pores, and secreted fibrous tissue that formed a continuous scar across the device. The use of cell-permeable devices caused an additional complication through swelling, which compresses the dura against the spinal cord, involving the cord within the continuous scar. Intrusion into the spinal canal was not observed with cell-impermeable AAMs or polymer films.

Interestingly, the use of tissue-derived non-immunogenic devices permits the use of porous device architectures. DuraGen PLUS[®] encouraged the rapid synthesis of organized collagenous tissue, where a dramatically lower density of macrophages and monocytes was observed relative to porous synthetic biomaterials, Figure 3.18. Organized fibrous tissue integrated into the collagen foam by four weeks, and the scar did not progress through the peridural fat tissue. A laminectomy study with closely-spaced timepoints within the first week would be required to elucidate the mechanism through which DuraGen PLUS[®] limits the progression of the scar.

6 Conclusions

This document is concluded by evaluating the dissertation hypotheses, section 1.5, and suggesting desirable properties for an anti-adhesion device for neurosurgery.

Cell-impermeable nonwoven fabrics can be fabricated through electrospinning.

Confirmed: Cell-impermeable electrospun fabrics were demonstrated by calculation, Table 3-3, *in vitro*, Figure 3.17, and *in vivo*, Figures 3.20 and Figure 4.25.

PEG_{1k} incorporation will reduce protein adsorption to biomaterial surfaces and reduce the inflammatory response to implanted biomaterials. Not confirmed: In electrospun fabrics, attainable PEG-content was insufficient to inhibit protein adsorption. Furthermore, the E1224(1k) polymer films evaluated in rat laminectomy study #2 had an enhanced inflammatory response in comparison to the E0000 films evaluated in rat laminectomy study #1. The diverse population of granulation cells secretes a self-supporting extracellular matrix, so they are not dependent on protein adsorption to the biomaterial surface for cell viability, function, or proliferation. The heightened inflammatory response to the E1224(1k) material was due to the host cells' processing of degradation products, indicated by the abundant cytoplasm of vacuolated macrophages and FBGCs. This analysis does not refute that high PEG-content biomaterials may provide a decreased inflammatory response due to reduction in the adsorption of complement proteins.

cis-4-hydroxy-L-proline delivery from polymeric implants can be controlled through precursor molecules. Confirmed: cHyp hexyl ester HCl and cHyp octyl ester

HCl provided controlled and sustained release of cHyp for either 1 week or for 5 weeks, Figure 4.14. The alkyl chain length modulated diffusive release from polymer films and fabrics. Upon release from the polymer matrix, the ester bond hydrolyzed with a half-time of 4.9 hours, Figures 4.10 and 4.15.

Cell-impermeable nonwoven fabrics provide superior adhesion prevention, compared to polymer films. Confirmed: the greater fracture resistance of nonwoven fabrics prevented scar progression through the center of the electrospun AAMs, Figure 5.13 and Figures 5.15 versus 5.17 and 5.18. Furthermore, when the electrospun fibers became brittle and fractured, macrophages migrated and FBGCs formed throughout the device. The reduced degradation-product-releasing polymer mass per phagocyte allowed the resorption of the electrospun AAMs to occur at a lower degradant burden per cell Figure 5.23 versus Figure 5.22.

Controlled delivery of cis-4-hydroxy-L-proline enhances the adhesion prevention performance of anti-adhesion devices for neurosurgery. Inconclusive: In the electrospun AAM groups, cHyp delivery reduced the extent of adhesion 0.61 to 0.37 ($p = 0.082$) across both timepoints ($n = 6$) and from 0.76 to 0.37 ($p = 0.078$) at four weeks ($n = 3$). However, the caudal instability was the greatest predictor of adhesion formation, and the variability due to the instability obscured any potential cHyp effect. At this sample size, premature displacement of one or two non-cHyp-loaded scaffolds would greatly influence the extent of adhesion statistic. The potential enhancing effects of drug delivery should only be considered once the device architecture and stability at the implant site have been established.

Based upon these studies, further pursuit of an electrospun AAM is not recommended. Though significant inhibition of adhesion was demonstrated, the anti-adhesion performance was inferior to DuraGen PLUS[®], a material with a long history of safety in the tissues of the spine [150]. Additionally, the tissue response within the laminectomy defect was relatively quiescent by four weeks, in comparison to synthetic devices. The tissue integration capabilities of collagen-based materials are favorable for this application. The only hesitation with DuraGen PLUS[®] is that it does not possess inherent barrier properties. A device combining the stabilizing effect of DuraGen's rapid tissue integration with the barrier performance of Baxter Healthcare's TISSUDURA (Figure 1.4) may be optimal for application as an anti-adhesion device for neurosurgery.

7 References

1. Kuslich, S.D., C.L. Ulstrom, and C.J. Michael, *The tissue origin of low back pain and sciatica: A report of pain response to tissue stimulation during operations on the lumbar spine using local anesthesia*. Orthopedic Clinics of North America, 1991. **22**(2): p. 181-187.
2. Smyth, M.J. and V. Wright, *Sciatica and the intervertebral disc: An experimental study*. The Journal of Bone and Joint Surgery, 1958. **40-A**(6): p. 1401-1418.
3. Inman, T., *Foundation for a new theory and practice of medicine*. 1860, London: John Churchill.
4. Smith, C.M., *Origin and uses of primum non nocere - above all, do no harm!* Journal of Clinical Pharmacology, 2005. **45**: p. 371-377.
5. Liakakos, T., et al., *Peritoneal adhesions: Etiology, pathophysiology, and clinical significance*. Digestive Surgery, 2001. **18**: p. 260-273.
6. di Zerega, G., *Biochemical events in peritoneal tissue repair*. The European Journal of Surgery. Supplement, 1997. **577**: p. 10-16.
7. LaRocca, H., *The laminectomy membrane*. The Journal of Bone and Joint Surgery, 1974. **56B**(3): p. 545-550.
8. Anderson, J., M., *Biological responses to materials*. Annual Reviews of Materials Research, 2001. **31**: p. 81-110.
9. Silver, F.H. and D.L. Christiansen, *Biomaterials Science and Biocompatibility*. 1999, New York, NY: Springer-Verlag New York Inc.
10. Di Paolo, N. and G. Sacchi, *Atlas of Peritoneal Histology*. Peritoneal Dialysis International, 2000. **20**(S3): p. S5-S96.
11. Mutsaers, S.E., *Mesothelial cells: Their structure, function and role in serosal repair*. Respiriology, 2002. **7**: p. 171-191.
12. Becker, J.M. and A.F. Stucchi, *Intra-abdominal adhesion prevention: Are we getting any closer?* Annals of Surgery, 2004. **240**(2): p. 202-204.
13. Becker, J.M., et al., *Prevention of postoperative abdominal adhesions by a sodium hyaluronate-based bioresorbable membrane: a prospective, randomized, double-blind multicenter study*. Journal of the American College of Surgeons, 1996. **183**: p. 297-306.
14. Menzies, D., *Peritoneal adhesions: Incidence of small-bowel obstruction and adhesiolysis after open colorectal and general surgery*. Surgery Annual, 1992. **24**: p. 27-45.
15. Ward, B.C. and A. Panitch, *Abdominal adhesions: Current and novel therapies*. Journal of Surgical Research, 2009. **In Press**.
16. Ellis, H., *The clinical significance of adhesions: Focus on intestinal obstruction*. The European Journal of Surgery. Supplement, 1997. **557**: p. 5-9.
17. Herrick, S.E., et al., *Human peritoneal adhesions are highly cellular, innervated, and vascularized*. Journal of Pathology, 2000. **192**(1): p. 67-72.
18. Xu, X., et al., *Role of mast cells and myofibroblasts in human peritoneal adhesion formation*. Annals of Surgery, 2002. **236**(5): p. 593-601.

19. Saed, G.M. and D.M. P, *Molecular characterization of postoperative adhesions: The adhesion phenotype*. The Journal of the American Association of Gynecologic Laparoscopists, 2004. **11**(3): p. 307-314.
20. Liakakos, T., et al., *Peritoneal adhesions: Etiology, pathophysiology, and clinical significance - Recent advances in prevention and management*. Digestive Surgery, 2001. **18**(4): p. 260-273.
21. Monk, B.J., M.L. Berman, and F.J. Montz, *Adhesions after extensive gynecologic surgery: Clinical significance, etiology, and prevention*. American Journal of Obstetrics and Gynecology, 1994. **170**(5): p. 1396-1403.
22. Miller, G., et al., *Etiology of small bowel obstruction*. American Journal of Surgery, 2000. **180**(1): p. 33-36.
23. Fevang, B.T.S., et al., *Long-term prognosis after operation for adhesive small bowel obstruction*. Annals of Surgery, 2004. **240**(2): p. 193-201.
24. Miller, G., et al., *Natural history of patients with adhesive small bowel obstruction*. British Journal of Surgery, 2000. **87**(9): p. 1240-1247.
25. Fayez, J.A., *An assessment of the role of operative laparoscopy in tuboplasty*. Fertility and Sterility, 1987. **39**: p. 476-479.
26. Hershlag, A., M.P. Diamond, and A.H. DeCherney, *Adhesiolysis*. Clinical Obstetrics and Gynecology, 1991. **34**: p. 395-402.
27. Vrijland, W.W., et al., *Abdominal adhesions*. Surgical Endoscopy, 2003. **17**: p. 1017-1022.
28. Trimpos-Kemper, T.C., J.B. Trimpos, and E.V. van Hall, *Adhesion formation after tubal surgery: Results of the eighth-day laparoscopy in 188 patients*. Fertility and Sterility, 1985. **43**(3): p. 395-400.
29. Michalas, S., et al., *Pelvic Surgery, reproductive factors and risk of ectopic pregnancy: A case controlled study*. International Journal of Gynaecology and Obstetrics, 1992. **38**(2): p. 101-105.
30. Whitaker, D. and J. Papadimitriou, *Mesothelial healing: morphological and kinetic investigations*. The Journal of Pathology, 1985. **145**(2): p. 159-175.
31. Fotev, Z., D. Whitaker, and J.M. Papadimitriou, *Role of macrophages in mesothelial healing*. The Journal of Pathology, 1987. **151**(3): p. 209-219.
32. Alpert, S., D. Berkowitz, and S. Rhodes, *P950034 Premarket approval of Genzyme Corporation's SeprafilmTM bioresorbable membrane*, FDA, Editor. 1996, Department of Health and Human Services: Rockville, MD.
33. Beck, D.E., et al., *A prospective, randomized, multicenter, controlled study of the safety of Seprafilm(R) adhesion barrier in the abdominopelvic surgery of the intestine*. Diseases of the Colon and Rectum, 2003. **46**(10): p. 1310-1319.
34. Mais, V., et al., *Reduction of adhesion reformation after laparoscopic endometriosis surgery: a randomized trial with an oxidized regenerated cellulose absorbable barrier*. Obstetrics & Gynecology, 1995. **86**(4): p. 512-515.
35. Azziz, R., *Microsurgery alone or with INTERCEED absorbable adhesion barrier for pelvic sidewall adhesion re-formation. The INTERCEED (TC7) adhesion barrier study group II*. Surgery, Gynecology & Obstetrics, 1993. **177**(2): p. 135-139.
36. Sekiba, K., *Use of INTERCEED(TC7) absorbable adhesion barrier to reduce postoperative adhesion reformation in infertility and endometriosis surgery. The*

- obstetrics and gynecology adhesion prevention committee. Obstetrics & Gynecology*, 1992. **79**(4): p. 518-522.
37. Reid, R.L., et al., *A randomized clinical trial of oxidized regenerated cellulose adhesion barrier (INTERCEED, TC7) alone or in combination with heparin. Fertility and Sterility*, 1997. **67**(1): p. 23-29.
 38. Nordic Adhesion Prevention Study Group, *The efficacy of INTERCEED(TC7) for prevention of reformation of postoperative adhesions on ovaries, fallopian tubes, and fimbriae in microsurgical operation for fertility: a multicenter study. Fertility and Sterility*, 1995. **64**(4): p. 709-714.
 39. Franklin, R.R., *Reduction of ovarian adhesions by the use of INTERCEED. Obstetrics & Gynecology*, 1995. **86**(3): p. 335-340.
 40. Wiseman, D.M., et al., *Metaanalysis of the safety and efficacy of an adhesion barrier(Interceed TC7) in laparotomy. The Journal of Reproductive Medicine*, 1999. **44**: p. 325.
 41. Gynecare, *INTERCEED(TC7) absorbable adhesion barrier instructions for use*, in *Ethicon Inc.* 1997: Somerville, NJ.
 42. Wiseman, D.M., L. Gottlick-Larkowski, and L. Kamp, *Effect of different barriers of oxidized regenerated cellulose (ORC) on cecal and sidewall adhesions in the presence and absence of bleeding. Journal of Investigative Surgery*, 1999. **12**: p. 141-146.
 43. Wiseman, D.M., L. Gottlick, and M.P. Diamond, *Effect of thrombin-induced hemostasis on the efficacy of an absorbable adhesion barrier. The Journal of Reproductive Medicine*, 1992. **37**(9): p. 766-770.
 44. Linsky, C.B., et al., *Effect of blood on the efficacy of barrier adhesion reduction in the rabbit uterine horn model. Infertility*, 1988. **11**(4): p. 273-280.
 45. Hurst, B.S., *Permanent implantation of expanded polytetrafluoroethylene is safe for pelvic surgery. Human Reproduction*, 1999. **14**(4): p. 925-927.
 46. Monk, et al., *Expanded polytetrafluoroethylene is an effective barrier in preventing pelvic adhesions after radical surgery for ovarian cancer. International Journal of Gynecological Cancer*, 1998. **8**(5): p. 403-408.
 47. Harada, Y., et al., *Long-term results of the clinical use of expanded polytetrafluoroethylene surgical membrane as a pericardial substitute. Journal of Thoracic Cardiovascular Surgery*, 1988. **96**: p. 811-815.
 48. W.L. Gore & Associates Inc., *Instructions for use for expanded polytetrafluoroethylene GORE DUALMESH(R) biomaterials*. 2007: Flagstaff, AZ.
 49. W.L. Gore & Associates Inc., *Instructions for use for expanded polytetrafluoroethylene GORE PRECLUDE(R) pericardial membrane*. 2008: Flagstaff, AZ.
 50. Balique, J.G., et al., *Intraperitoneal treatment of incisional and umbilical hernias using an innovative composite mesh: Four-year results of a prospective multicenter clinical trial. Hernia*, 2005. **9**: p. 68-74.
 51. Ory, F.R., et al., *US Patent 6,451,032: Composite prosthesis for preventing post-surgical adhesions and method for obtaining same*, U.S.P.a.T. Office, Editor. 2002, Sofradim Production and Imedex Biomateriaux: USA.

52. Gonzalez, R., et al., *Resistance to adhesion formation: A comparative study of treated and untreated mesh products placed in the abdominal cavity*. *Hernia*, 2004. **8**: p. 213-219.
53. Jacob, B.P., et al., *Tissue ingrowth and bowel adhesion formation in an animal comparative study: polypropylene versus Proceed versus Parietex Composite*. *Surgical Endoscopy*, 2007. **21**: p. 629-633.
54. Arnaud, J.P., et al., *Ultrasound detection of visceral adhesion after intraperitoneal ventral hernia treatment: A comparative study of protected versus unprotected meshes*. *Hernia*, 2003. **7**: p. 85-88.
55. Moreno-Egea, A., et al., *Long-term results of laparoscopic repair of incisional hernias using an intraperitoneal composite mesh*. *Surgical Endoscopy*, 2010. **24**: p. 359-365.
56. Tyco Healthcare Group LP., *ParietexTM Composite dual facing mesh made of polyester and absorbable film instructions for use*. 2007.
57. Marieb, E.N., *Human Anatomy and Physiology*. 2nd ed. 1992, Redwood City: The Benjamin/Cummings Publishing Company, Inc.
58. Park, Y.-K., J.-H. Kim, and H.-S. Chung, *Outcome analysis of patients after ligament-sparing microdiscectomy for lumbar disc herniation*. *Neurosurgical Focus*, 2002. **13**(2): p. 1-4.
59. Ozer, A.F., et al., *Preserving the ligamentum flavum in lumbar discectomy: A new technique that prevents scar tissue formation in the first 6 months postsurgery*. *Operative Neurosurgery*, 2006. **59**: p. 126-132.
60. Aydin, Y., et al., *Clinical and radiological results of lumbar microdiscectomy technique with preserving of ligamentum flavum comparing to the standard microdiscectomy technique*. *Surgical Neurology*, 2002. **57**: p. 5-14.
61. Song, J.-H. and Y.-K. Park, *Ligament-sparing lumbar microdiscectomy: Technical note*. *Surgical Neurology*, 2000. **53**: p. 592-597.
62. Chou, R., et al., *Surger for low back pain*. *Spine*, 2009. **34**(10): p. 1094-1109.
63. *National neurosurgical statistics: 1999 procedural statistics*. 2000, American Association of Neurological Surgeons: Rolling Meadows, IL.
64. *National neurosurgical procedural statistics: 2006 survey*. 2008, American Association of Neurological Surgeons: Rolling Meadows, IL.
65. *Vital and health statistics: Ambulatory and inpatient procedures in the United States, 1994, Series 13*, U.S.D.o.H.a.H. Services, Editor. 1997: Washington D.C.
66. *Vital and health statistics: Ambulatory and inpatient procedures in the United States, 1995, Series 13*, U.S.D.o.H.a.H. Services, Editor. 1998: Washington D.C.
67. *Vital and health statistics: Ambulatory and inpatient procedures in the United States, 1996, Series 13*, U.S.D.o.H.a.H. Services, Editor. 1998: Washington D.C.
68. Slipman, C.W., et al., *Etiologies of failed back surgery syndrome*. *Pain Medicine*, 2002. **3**(3): p. 200-214.
69. Rodrigues, F.F., et al., *Failed back surgery syndrome: Casuistic and etiology*. *Arquivos de Neuro-Psiquiatria*, 2006. **64**(3-B): p. 757-761.
70. Fritsch, E.W., J. Heisel, and S. Rupp, *The failed back surgery syndrome: Reasons, intraoperative findings, and long-term results: A report on 182 operative treatments*. *Spine*, 1996. **21**(5): p. 626-633.

71. Robertson, J.T., *Role of peridural fibrosis in the failed back: a review*. European Spine Journal, 1996. **5**(Supplement 1): p. S2-S6.
72. Long, D.M., et al., *Clinical features of the failed-back syndrome*. Journal of Neurosurgery, 1988. **69**(1): p. 61-71.
73. North, R., et al., *Failed back surgery syndrome: 5-year follow-up in 102 patients undergoing repeated operation*. Neurosurgery, 1991. **28**(5): p. 685-691.
74. Pawl, R.P., *Arachnoiditis and epidural fibrosis: The relationship to chronic pain*. Current Review of Pain, 1998. **2**: p. 93-99.
75. Ross, J.S., et al., *Association between peridural scar and recurrent radicular pain after lumbar discectomy: magnetic resonance evaluation*. Neurosurgery, 1996. **38**(4): p. 855-863.
76. Manchikanti, L., et al., *Evidence-based practice guidelines for interventional techniques in the management of chronic spinal pain*. Pain Physician, 2003. **6**: p. 3-81.
77. Manchikanti, L., et al., *Non-endoscopic and endoscopic adhesiolysis in post lumbar laminectomy syndrome: A one-year outcome study and cost effectiveness analysis*. Pain Physician, 1999. **2**(3): p. 52-58.
78. Manchikanti, L., et al., *Role of one day epidural adhesiolysis in management of chronic low back pain: A randomized clinical trial*. Pain Physician, 2001. **4**(2): p. 153-166.
79. Manchikanti, L., et al., *A comparative effectiveness evaluation of percutaneous adhesiolysis and epidural steroid injections in managing lumbar post surgery syndrome: A randomized, equivalence controlled trial*. Pain Physician, 2009. **12**: p. E355-E368.
80. *Press Release: Integra LifeSciences announces poster presentation 'Periradicular lumbar fibrosis: What to do?' at 2007 Congress of Neurological Surgeons Annual Meeting*. 2007, Integra LifeSciences: Plainsboro, NJ.
81. Hilse, A., *Experimentelle untersuchungen uber freie fetttransplantation bei blutungen parenchymatoser bauchorgane*. Langenbecks Archiv Klinisch Chirurgie, 1914. **103**: p. 1042-1083.
82. Lexer, E., *Zwanzig jahre transplantations forschung in der chirurgie*. Langenbecks Archiv Klinisch Chirurgie, 1925. **138**: p. 294-297.
83. Rehn, E., *Die fetttransplantation*. Langenbecks Archiv Klinisch Chirurgie, 1912. **98**: p. 1-37.
84. Bryant, M., A. Bremer, and T. Nguyen, *Autogeneic fat transplants in the epidural space in routine lumbar spine surgery*. Neurosurgery, 1983. **13**(4): p. 367-370.
85. Weisz, G.M. and A. Gal, *Long-term survival of a free fat graft in the spinal canal: a 40 month postlaminectomy case report*. Clinical Orthopaedics and Related Research, 1986. **205**: p. 204-206.
86. Jacobs, R., McClain, and J. Neff, *Control of postlaminectomy scar formation: an experimental and clinical study*. Spine, 1980. **5**: p. 223-229.
87. Langenskiöld, A. and O. Kiviluoto, *Prevention of epidural scar formation after operations on the lumbar spine by means of free fat transplants*. Clinical Orthopaedics and Related Research, 1976. **115**: p. 92-95.

88. Van Akkerveeken, P., W. Van De Kraan, and J.W. Muller, *The fate of the free fat graft: a prospective clinical study using CT scanning*. Spine, 1986. **11**(5): p. 501-504.
89. Kanamori, M., et al., *The fate of autogenous free-fat grafts after posterior lumbar surgery: Part 1. A postoperative serial magnetic resonance imaging study*. Spine, 2001. **26**(20): p. 2258-2263.
90. Saunders, M.C., et al., *Survival of autologous fat grafts in humans and in mice*. Connective Tissue Research, 1981. **8**: p. 85-91.
91. Rossatti, B., *Revascularisation and phagocytosis in free fat autografts: An experimental study*. British Journal of Plastic Surgery, 1961. **13**: p. 35-41.
92. Mackay, M.A., et al., *The effect of interposition membrane on the outcome of lumbar laminectomy and discectomy*. Spine, 1995. **20**(16): p. 1793-1796.
93. Bernsmann, K., et al., *Lumbar micro disc surgery with and without autologous fat graft: A prospective randomized trial evaluated with reference to clinical and social factors*. Archives of Orthopaedic and Trauma Surgery, 2001. **121**: p. 476-480.
94. Görgülü, A., et al., *The effect of epidural free fat graft on the outcome of lumbar disc surgery*. Neurosurgical Review, 2004. **27**: p. 181-184.
95. Prusick, V.R., D.S. Lint, and W.J. Bruder, *Cauda equina syndrome as a complication of free epidural fat-grafting*. The Journal of Bone and Joint Surgery, 1988. **70-A**(8): p. 1256-1258.
96. Cabezudo, J.M., A. Lopez, and F. Bacci, *Symptomatic root compression by a free fat transplant after laminectomy*. Journal of Neurosurgery, 1985. **63**: p. 633-635.
97. Mayer, P.J. and F.S. Jacobsen, *Cauda equina syndrom after surgical treatment of lumbar spinal stenosis with application of free autogenous fat graft*. The Journal of Bone and Joint Surgery, 1989. **71-A**(7): p. 1090-1093.
98. Kanamori, M., et al., *The fate of autogenous free-fat grafts after posterior lumbar surgery: Part 2. Magnetic resonance imaging and histologic studies in repeated surgery cases*. Spine, 2001. **26**(20): p. 2264-2270.
99. Curran, R.C. and J. Crocker, *Curran's Atlas of Histopathology*. 4th ed. 2000, London: Harvey Miller Ltd. 288.
100. Martin-Ferrer, S., *Failure of autologous fat grafts to prevent postoperative epidural fibrosis in surgery of the lumbar spine*. Neurosurgery, 1989. **24**: p. 718-721.
101. Alpert, S., *P960057 Premarket approval of Adcon(R) adhesion barrier gel*, FDA, Editor. 1998, Department of Health and Human Services: Rockville, MD.
102. Frederickson, R.C.A., *ADCON-L: a review of its development, mechanism of action, and preclinical data*. European Spine Journal, 1996. **5**: p. S7-S9.
103. Einhaus, S.L., et al., *Reduction of peridural fibrosis after lumbar laminotomy and discectomy in dogs by a resorbable gel (ADCON-L)*. Spine, 1997. **22**(13): p. 1440-1446.
104. Le, A.X., et al., *Unrecognized durotomy after lumbar discectomy*. Spine, 2001. **26**(1): p. 115-118.
105. Hieb, L.D. and D.L. Stevens, *Spontaneous postoperative cerebrospinal fluid leaks following application of anti-adhesion barrier gel*. Spine, 2001. **26**(7): p. 748-751.
106. Richter, H.-P., et al., *Results of applying ADCON-L gel after lumbar discectomy: the German ADCON-L study*. Journal of Neurosurgery: Spine, 2001. **95**: p. 179-189.

107. Ross, J.S., N. Obuchowski, and R. Zepp, *The postoperative lumbar spine: Evaluation of epidural scar over a 1-year period*. American Journal of Neuroradiology, 1998. **19**: p. 183-186.
108. Ganzer, D., et al., *Two-year results after lumbar microdiscectomy with and without prophylaxis of a peridural fibrosis using Adcon-L*. Archives of Orthopaedic and Trauma Surgery, 2003. **123**: p. 17-21.
109. Rönnberg, K., et al., *Peridural scar and its relation to clinical outcome: A randomised study on surgically treated lumbar disc herniation patients*. European Spine Journal, 2008. **17**: p. 1714-1720.
110. Stanford Law School, *Gliatech, Inc. - Securities class action*, in *Securities class action clearinghouse*. 2003.
111. Gerszten, P.C., et al., *Low-dose radiotherapy for the inhibition of peridural fibrosis after reexploratory nerve root decompression for postlaminectomy syndrome*. Journal of Neurosurgery: Spine, 2003. **99**: p. 271-277.
112. Liu, L.-S. and R.A. Berg, *Adhesion barriers of carboxymethylcellulose and polyethylene oxide composite gels*. Journal of Biomedical Materials Research, 2002. **63**: p. 326-332.
113. Kim, K.D., et al., *Reduction of radiculopathy and pain with Oxiplex/SP gel after laminectomy, laminotomy, and discectomy*. Spine, 2003. **28**(10): p. 1080-1088.
114. Jose, J., et al., *FDA PMA P070023 executive summary: July 15, 2008 panel meeting of orthopaedic and rehabilitation devices panel*, F.a.D. Administration, Editor. 2008: Silver Spring, MD.
115. Kim, K.D., et al., *Reduction in leg pain and lower-extremity weakness with Oxiplex/SP gel for 1 year after laminectomy, laminotomy, and discectomy*. Neurosurgical Focus, 2004. **17**(1): p. 1-6.
116. Assietti, R., A. Mora, and M. Brayda-Bruno, *Use of barboxymethylcellulose/polyethylene oxide gel in microdiscectomy with interlaminectomy: A case series comparison with long-term follow-up*. Spine, 2008. **33**(16): p. 1762-1765.
117. Melkerson, M.N., *PMA P080013: FDA summary of safety and effectiveness data - DuraSeal spine sealant system*, FDA, Editor. 2009, Department of Health and Human Services: Division of Surgical, Orthopedic, and Restorative Devices: Silver Spring, MD.
118. Preul, M.C., et al., *A unique dual-function device: A dural sealant with adhesion prevention properties*, in *White Paper*. 2005, Confluent Surgical Inc.: Waltham, MA. p. 1-5.
119. Convidien. *The technology behind the DuraSeal™ dural sealant system*. 2010 [cited 2010 February 9, 2010]; Available from: <http://www.durasealinfo.com/DuraSealCranial/pagebuilder.aspx?topicID=177868&page=WhatIsDuraSealCranial:Detail>.
120. Preul, M.C., et al., *Application of a hydrogel sealant improves watertight closures of duraplasty onlay grafts in a canine craniotomy model*. Journal of Neurosurgery, 2007. **107**: p. 642-650.
121. Preul, M.C., et al., *Toward optimal tissue sealants for neurosurgery: use of a novel hydrogel sealant in a canine durotomy repair model*. Neurosurgery, 2003. **53**(5): p. 1189-1198.

122. Blackburn, S.L. and M.D. Smyth, *Hydrogel-induced cervicomedullary compression after posterior fossa decompression for Chiari malformation*. Journal of Neurosurgery, 2007. **106**: p. 302-304.
123. Mulder, M., J. Crosier, and R. Dunn, *Cauda equina compression by hydrogel dural sealant after a laminotomy and discectomy*. Spine, 2009. **34**(4): p. E144-E148.
124. *Clinical trial to evaluate safety and efficacy of Hyalospine(R) in lumbar laminectomy or laminotomy*. 2009; Available from: <http://clinicaltrials.gov/ct2/show/NCT00939406>.
125. Della_Valle, F. and A. Romeo, *US Patent 5,676,964: Crosslinked carboxy polysaccharides*, U.S.P.a.T. Office, Editor. 1997, Fidia, S.p.A.: USA.
126. Riccio, M., et al., *Efficiency of Hyaloglide(R) in the prevention of the recurrence of adhesions after tenolysis of flexor tendons in zone II: a randomized, controlled, multicentre clinical trial*. Journal of Hand Surgery (European Volume), 2010. **35**(2): p. 130-138.
127. Brunelli, G., et al., *Adhesion reduction after knee surgery in a rabbit model by Hyaloglide(R), a hyaluronan derivative gel*. Journal of Orthopaedic Research, 2005. **23**: p. 1377-1382.
128. Dam-Hieu, P., et al., *Reduction of postoperative perineural adhesions by hyaloglide gel: An experimental study in the rat sciatic nerve*. Neurosurgery, 2005. **56**: p. 425-433.
129. DiFazio, F.A., et al., *The use of expanded polytetrafluoroethylene as an interpositional membrane after lumbar laminectomy*. Spine, 1995. **20**(9): p. 986-991.
130. Lladó, A., et al., *Expanded polytetrafluoroethylene membrane for the prevention of peridural fibrosis after spinal surgery: a clinical study*. European Spine Journal, 1999. **8**: p. 144-150.
131. Topsakal, C., et al., *Seprafilm superior to gore-tex in the prevention of peridural fibrosis*. Journal of Neurosurgery, 2004. **101**: p. 295-302.
132. Seref, D., et al., *The effects of Seprafilm and Interceed TC7 on epidural fibrosis in a rat hemilaminectomy model*. Neurosurgery Quarterly, 2009. **19**(3): p. 190-195.
133. Welch, W.C., et al., *Use of polylactide resorbable film as an adhesion barrier*. Journal of Neurosurgery, 2002. **97**: p. 413-422.
134. Klopp, L.S., et al., *Use of polylactide resorbable film as a barrier to postoperative peridural adhesion in an ovine dorsal laminectomy model*. Neurosurgical Focus, 2004. **16**(3): p. 2.
135. *Press Release: Kensey Nash announces acquisition of assets of MacroPore Biosurgery business unit from Cytos Therapeutics*. 2007, Kensey Nash Corporation: Exton, PA.
136. Klopp, L.S., et al., *Comparison of caprolactone/Lactide film (Mesofol) to two polylactide film products as a barrier to postoperative peridural adhesion in an ovine dorsal laminectomy model*. Spine, 2008. **33**(14): p. 1518-1526.
137. Melkerson, M.N., *K062558: Mesofol(R) Surgical Sheet*, FDA, Editor. 2007, Department of Health and Human Services: Rockville, MD.
138. *Randomized controlled trial of DuraGen Plus(R) adhesion barrier matrix to minimize adhesions following lumbar discectomy*. 2009; Available from: <http://clinicaltrials.gov/ct2/show/NCT00387829>.

139. Zerris, V.A., et al., *Repair of the dura mater with processed collagen devices*. Journal of Biomedical Materials Research, 2007. **83B**: p. 580-588.
140. Integra LifeSciences Corporation, *DuraGen Plus: Spine solutions from the leader in regenerative technology*. 2004.
141. Exposito, J.-Y., et al., *Sea urchin collagen evolutionarily homologous to vertebrate pro- $\alpha 2(I)$ collagen*. The Journal of Biological Chemistry, 1992. **267**(22): p. 15559-15562.
142. Constantinou, C.D. and S.A. Jimenez, *Structure of cDNAs encoding the triple-helical domain of murine alpha e(VI) collagen chain and comparison to human and chick homologues. Use of polymerase chain reaction and partially degenerate oligonucleotide for generation of navel cDNA clones*. Matrix, 1991. **11**(1): p. 1-9.
143. Bernard, M.P., et al., *Nucleotide sequences of complimentary deoxyribonucleic acids for the Pro $\alpha 1$ chains of human type I procollagen: Statistical evaluation of structures that are conserved during evolution*. Biochemistry, 1983. **22**: p. 5213-5223.
144. Bernard, M.P., et al., *Structure of a cDNA for the Pro $\alpha 2$ chain of human type I procollagen: comparison with chick cDNA for Pro $\alpha 2(I)$ identifies structurally conserved features of the protein and the gene*. Biochemistry, 1983. **22**: p. 1139-1145.
145. Gilbert, T.w., T.L. Sellaro, and S.F. Badylak, *Decellularization of tissues and organs*. Biomaterials, 2006. **27**: p. 3675-3683.
146. Piterina, A.V., et al., *ECM-based materials in cardiovascular applications: Inherent healing potential and augmentation of native regenerative processes*. International Journal of Molecular Sciences, 2009. **10**: p. 4375-4417.
147. *Press Release: Integra LifeSciences announces CE Mark for DuraGen PlusTM Adhesion Barrier Matrix*. 2004, Integra LifeSciences: Plainsboro, NJ.
148. Arrotegui, I. and J.L. Llombart. *Dural graft matrix as an adhesion barrier*. in *54th Annual meeting of the Congress of Neurological Surgeons*. 2004. San Francisco, CA.
149. Arrotegui, I. and J.L. Llombart. *Peri-radicular lumbar fibrosis - What to do?* in *College of Neurological Surgeons Annual Meeting*. 2007. San Diego, CA.
150. Integra LifeSciences Corporation, *DuraGen Plus: Duraplasty solutions from the leader in regenerative technology*. 2006.
151. Odar, J. and R. Nistor-Gallo, *US Patent Application 20100028309: Method for directed cell in-growth and controlled tissue regeneration in spinal surgery*, U.S.P.a.T. Organization, Editor. 2010, Baxter International Inc.: USA.
152. Siegel, R.C. and G.R. Martin, *Collagen Cross-linking: Enzymatic synthesis of lysine-derived aldehydes and the produciton of cross-linked components*. The Journal of Biological Chemistry, 1970. **245**(7): p. 1653-1658.
153. Odar, J., et al., *WO 2004/108179: Compositions for repairing and regenerating human dura mater*, World_Intellectual_Property_Organization, Editor. 2004, Baxter International Inc.
154. Gazzeri, R., et al., *Transparent equine collagen biomatrix as dural repair: A prospective clinical study*. Acta Neurochir, 2009. **151**: p. 537-543.
155. Biroli, F., et al., *Novel equine collagen-only dural substitute*. Operative Neurosurgery, 2008. **62**: p. 273-274.

156. Pesnell, A.D., *A focused library of tyrosine-derived polycarbonates for the discovery of optimal polymers for use in resorbable stents*, in *Chemistry and Chemical Biology*. 2006, Rutgers University: New Brunswick, NJ.
157. Abramson, S., et al. *Small changes in polymer structure can dramatically increase degradation rates: The effect of free carboxylate groups on the properties of tyrosine-derived polycarbonates*. in *Annual Meeting of the Society for Biomaterials*. 2000. Kamuela, HI: The Society for Biomaterials.
158. Khan, I.J., *The utility of L-tyrosine based polycarbonate copolymers containing poly(ethylene glycol) as a degradable carrier for the release of a hydrophobic peptide molecule*, in *Biomedical Engineering*. 2009, Rutgers University: New Brunswick, NJ. p. 164.
159. Yu, C. and J. Kohn, *Tyrosine-PEG-derived poly(ether carbonate)s as new biomaterials - Part I: Synthesis and evaluation*. *Biomaterials*, 1999. **20**(3): p. 253-264.
160. Ertel, S. and J. Kohn, *Evaluation of a series of tyrosine-derived polycarbonates as degradable biomaterials*. *Journal of Biomedical Materials Research*, 1994. **28**(8): p. 919-930.
161. Pulapura, S. and J. Kohn, *Tyrosine-derived polycarbonates: Backbone-modified pseudo-poly(amino acids) designed for biomedical applications*. *Biopolymers*, 1992. **32**(4): p. 411-417.
162. Johnson, P.A., et al., *Interplay of anionic charge, poly(ethylene glycol), and iodinated tyrosine incorporation within tyrosine-derived polycarbonates: Effects on vascular smooth muscle cell adhesion, proliferation, and motility*. *Journal of Biomedical Materials Research*, 2010. **93A**(2): p. 505-514.
163. Macario, D.K., et al., *Iodine inhibits antiadhesive effect of PEG: Implications for tissue engineering*. *Journal of Biomedical Materials Research*, 2008. **86B**(1): p. 237-244.
164. Tziampazis, E., J. Kohn, and P.V. Moghe, *PEG-variant biomaterials as selectively adhesive protein templates: model surfaces for controlled cell adhesion and migration*. *Biomaterials*, 2000. **21**(5): p. 511-520.
165. Weber, N., H.P. Wendel, and J. Kohn, *Formation of viscoelastic protein layers on polymeric surfaces relevant to platelet adhesion*. *Journal of Biomedical Materials Research*, 2005. **72A**(4): p. 420-427.
166. James, K.S., et al., *Small changes in polymer chemistry have a large effect on the bone-implant interface: Evaluation of a series of degradable tyrosine-derived polycarbonates in bone defects*. *Biomaterials*, 1999. **20**(23-24): p. 2203-2212.
167. Stevens, M.M. and J.H. George, *Exploring and engineering the cell surface interface*. *Science*, 2005. **310**(5751): p. 1135-1138.
168. Venugopal, J. and S. Ramakrishna, *Applications of polymer nanofibers in biomedicine and biotechnology*. *Applied Biochemistry and Biotechnology*, 2005. **125**(3): p. 147-157.
169. Formhals, A., *US Patent 1,975,504: Process and apparatus for preparing artificial threads*, U.S.P.a.T. Office, Editor. 1934, Schreiber-Gastell, Richard Formhals, Anton: USA.

170. Formhals, A., *US Patent 2,116,942: Method and apparatus for the production of fibers*, U.S.P.a.T. Office, Editor. 1938, Formhals, Anton Schreiber-Gastell, Richard: USA.
171. Manning, F.W., *US Patent 2,336,745: Method and apparatus for making unwoven and composite fabrics*, U.S.P.a.T. Office, Editor. 1943, Manning, Fred W: USA.
172. Doshi, J. and D.H. Reneker, *Electrospinning process and applications of electrospun fibers*. Journal of Electrostatics, 1995. **35**: p. 151-160.
173. Reneker, D.H. and I. Chun, *Nanometre diameter fibres of polymer, produced by electrospinning*. Nanotechnology, 1996. **7**(3): p. 216-223.
174. Li, D. and Y. Xia, *Electrospinning of nanofibers: Reinventing the wheel?* Advanced Materials, 2004. **16**(14): p. 1151-1170.
175. Ushiki, T., *Collagen fibers, reticular fibers, and elastic fibers: A comprehensive understanding from a morphological viewpoint*. Archives of Histology and Cytology, 2002. **65**(2): p. 109-126.
176. Nisbet, D.R., et al., *Review paper: A review of the cellular response on electrospun nanofibers for tissue engineering*. Journal of Biomaterials Applications, 2009. **24**(1): p. 7-29.
177. Taylor, G., *Electrically driven jets*. Proceedings of the Royal Society of London: Series A, Mathematical and Physical Sciences, 1969. **313**: p. 453-475.
178. Spivak, A.F., Y.A. Dzenis, and D.H. Reneker, *A model of steady state jet in the electrospinning process*. Mechanics Research Communications, 2000. **27**(1): p. 37-42.
179. Shin, Y.M., et al., *Experimental characterization of electrospinning: the electrically forced jet and instabilities*. Polymer, 2001. **42**: p. 9955-9967.
180. Feng, J.J., *The stretching of an electrified non-Newtonian jet: A model for electrospinning*. Physics of Fluids, 2002. **14**(11): p. 3912-3926.
181. Yarin, A.L., W. Kataphinan, and D.H. Reneker, *Branching in electrospinning of nanofibers*. Journal of Applied Physics, 2005. **98**: p. 064501.
182. Gupta, P., et al., *Electrospinning of linear homopolymers of poly(methyl methacrylate): Exploring relationships between fiber formation, viscosity, molecular weight and concentration in a good solvent*. Polymer, 2005. **46**: p. 4799-4810.
183. McKee, M.G., et al., *Correlations of solution rheology with electrospun fiber formation of linear and branched polyesters*. Macromolecules, 2004. **37**: p. 1760-1767.
184. Tan, S.-H., et al., *Systematic parameter study for ultra-fine fiber fabrication via electrospinning process*. Polymer, 2005. **46**: p. 6128-6134.
185. Fong, H., I. Chun, and D.H. Reneker, *Beaded nanofibers formed during electrospinning*. Polymer, 1999. **40**: p. 4585-4592.
186. Theron, S.A., E. Zussman, and A.L. Yarin, *Experimental investigation of the governing parameters in the electrospinning of polymer solutions*. Polymer, 2004. **45**: p. 2017-2030.
187. Son, W.K., et al., *The effects of solution properties and polyelectrolyte on electrospinning of ultrafine poly(ethylene oxide) fibers*. Polymer, 2004. **45**: p. 2959-2966.

188. Wang, C., C.-H. Hsu, and J.-H. Lin, *Scaling laws in electrospinning of polystyrene solutions*. *Macromolecules*, 2006. **39**: p. 7662-7672.
189. Yang, Y., et al., *Experimental investigation of the governing parameters in the electrospinning of polyethylene oxide solution*. *IEEE Transactions on Dielectrics and Electrical Insulation*, 2006. **13**(3): p. 580-585.
190. Fridrikh, S.V., et al., *Controlling the fiber diameter during electrospinning*. *Physical Review Letters*, 2003. **90**(14): p. 144502.
191. Wang, Y.K., T. Yong, and S. Ramakrishna, *Nanofibers and their influence on cells for tissue regeneration*. *Australian Journal of Chemistry*, 2005. **58**: p. 704-712.
192. Pham, Q.P., U. Sharma, and A.G. Mikos, *Electrospinning of polymeric nanofibers for tissue engineering applications: A review*. *Tissue Engineering*, 2006. **12**(5): p. 1197-1211.
193. Burger, C., B. Hsiao, and B. Chu, *Nanofibrous materials and their applications*. *Annual Reviews of Materials Research*, 2006. **36**: p. 333-368.
194. Liang, D., B.S. Hsiao, and B. Chu, *Functional electrospun scaffolds for biomedical applications*. *Advanced Drug Delivery Reviews*, 2007. **59**: p. 1392-1412.
195. Sell, S.A., et al., *Electrospinning of collagen/biopolymers for regenerative medicine and cardiovascular tissue engineering*. *Advanced Drug Delivery Reviews*, 2009. **61**: p. 1007-1019.
196. Yoo, H.S., T.G. Kim, and T.G. Park, *Surface-functionalized electrospun nanofibers for tissue engineering and drug delivery*. *Advanced Drug Delivery Reviews*, 2009. **61**: p. 1033-1042.
197. Chakraborty, S., et al., *Electrohydrodynamics: A facile technique to fabricate drug delivery systems*. *Advanced Drug Delivery Reviews*, 2009. **61**(1043-1054).
198. Cao, H., T. Liu, and Y. Chew, *The application of nanofibrous scaffolds in neural tissue engineering*. *Advanced Drug Delivery Reviews*, 2009. **61**: p. 1055-1064.
199. Jang, J.-H., O. Castano, and H.-W. Kim, *Electrospun materials as potential platforms for bone tissue engineering*. *Advanced Drug Delivery Reviews*, 2009. **61**: p. 1065-1083.
200. Liao, S., C.K. Chan, and S. Ramakrishna, *Electrospun nanofibers: Work for medicine?* *Frontiers of Materials Science in China*, 2010. **4**(1): p. 29-33.
201. Xie, J., X. Li, and Y. Xia, *Putting electrospun nanofibers to work for biomedical research*. *Macromolecular Rapid Communications*, 2008. **29**: p. 1775-1792.
202. Sill, T.J. and H.A. von Recum, *Electrospinning: Applications in drug delivery and tissue engineering*. *Biomaterials*, 2008. **29**: p. 1989-2006.
203. Luzhansky, D.M. *Quality control in manufacturing of electrospun nanofiber composites*. in *International Nonwovens Technical Conference*. 2003. Baltimore, MD.
204. Depass, D., Donaldson, *SurModics launch product for research cell growth*, in *Star Tribune*. 2006: Minneapolis, MN.
205. Zeus_Inc., *Technical newsletter: Electrospinning - fibers at the nano-scale*. 2009: Orangeburg, SC.
206. Smith, D.J. and D.H. Reneker, *US Patent 6,737,447: Nitric oxide-modified linear poly(ethylenimine) fibers and uses thereof*, U.S.P.a.T. Office, Editor. 2004, The University of Akron: USA.

207. Smith, D.J., S. Pulfer, and M. Shabani, *US Patent 5,519,020: Polymeric wound healing accelerators*, U.S.P.a.T. Office, Editor. 1996, The University of Akron: USA.
208. Reneker, D.H. and D.J. Smith, *US Patent Application 20080286321: Polymer NO donor predrug nanofiber coating for medical devices and therapy*, U.S.P.a.T. Organization, Editor. 2008, The University of Akron: USA.
209. *Controlled nitric oxide releasing patch versus meglumine antimoniate in the treatment of cutaneous leishmaniasis*. 2009; Available from: <http://clinicaltrials.gov/ct2/show/NCT00317629>.
210. *Clinical trial for the treatment of diabetic foot ulcers using a nitric oxide releasing patch: PATHON*. 2009; Available from: <http://clinicaltrials.gov/ct2/show/NCT00428727>.
211. Chase, G.C. and D.H. Reneker. *Coalescence Filtration Nanomaterials Consortium*. [cited 2010; Available from: http://www.engineering.uakron.edu/~chem/fclty/chase/CFNC_OnePageSummary.pdf
212. Mason, J., *Biodegradable nanofiber could prevent scar tissue*, in *Small Times Correspondent*. 2002: Ann Arbor, MI.
213. Zong, X., et al., *Prevention of postsurger-induced abdominal adhesions by electrospun bioabsorbable nanofibrous poly(lactide-co-glycolide)-based membranes*. *Annals of Surgery*, 2004. **240**(5): p. 910-915.
214. Chu, B., et al., *US Patent 6,689,347: Biodegradable and/or bioabsorbable fibrous articles and methods for using the articles for medical applications*, U.S.P.a.T. Office, Editor. 2004, The Research Foundation of the State University of New York: USA.
215. Kim, K., et al., *Incorporation and controlled release of a hydrophilic antibiotic using poly(lactide-co-glycolide)-based electrospun nanofibrous scaffolds*. *Journal of Controlled Release*, 2004. **98**: p. 47-56.
216. Food and Drug Administration Health and Human Services, *International Conference on Harmonisation; Guidance on impurities: Residual solvents*, FDA, Editor. 1997, Federal Register: Rockville, MD. p. 67377-67388.
217. Kim, K., et al., *Control of degradation rate and hydrophilicity in electrospun non-woven poly(D,L-lactide) nanofiber scaffolds for biomedical applications*. *Biomaterials*, 2003. **24**: p. 4977-4985.
218. Nielsen, G.D., et al., *Sensory irritation mechanisms investigated from model compounds: Trifluoroethanol, hexafluoroisopropanol and methyl heptafluoroisopropyl ether*. *Archives of Toxicology*, 1996. **70**(6): p. 319-328.
219. Jeong, S.I., et al., *Morphology of elastic poly(L-lactide-co-ε-caprolactone) copolymers and invitro and in vivo degradation behavior of their scaffolds*. *Biomacromolecules*, 2004. **5**: p. 1303-1309.
220. Aucejo, S., C. Marco, and R. Gavara, *Water effect on the morphology of EVOH copolymers*. *Journal of applied Polymer Science*, 1999. **74**(5): p. 1201-1206.
221. Prockop, D.J., et al., *The biosynthesis of collagen and its disorders*. *New England Journal of Medicine*, 1979. **301**: p. 13-24, 77-85.
222. Kivirikko, K.I. and R. Myllylä, *Post-translational processing of procollagens*. *Annals of the New York Academy of Sciences*, 1985. **460**: p. 187-201.
223. Olson, B.R., *Collagen Biosynthesis*, in *Cell Biology of Extracellular Matrix*, E.D. Hay, Editor. 1981, Plenum Press: New York. p. 5-37.

224. Rosenbloom, J., M. Harsch, and S. Jimenez, *Hydroxyproline content determines the denaturation temperature of chick tendon collagen*. Archives of Biochemistry and Biophysics, 1973. **158**(2): p. 478-484.
225. Bretscher, L.E., et al., *Conformational stability of collagen relies on a stereoelectronic effect*. Journal of the American Chemical Society, 2001. **123**(4): p. 777-778.
226. Berisio, R., et al., *Recent progress on collagen triple helix structure, stability and assembly*. Protein and Peptide Letters, 2002. **9**(2): p. 107-116.
227. Vitagliano, L., et al., *Preferred proline puckerings in cis and trans peptide groups: Implications for collagen stability*. Protein Science, 2001. **10**: p. 2627-2632.
228. Holmgren, S.K., et al., *Code for collagen's stability deciphered*. Nature, 1998. **392**: p. 666-667.
229. Eberhardt, E.S., N. Panasik Jr, and R.T. Raines, *Inductive effects on the energetics of prolyl peptide bond isomerization: Implications for collagen folding and stability*. Journal of the American Chemical Society, 1996. **118**(49): p. 12261-12266.
230. DeRider, M.L., et al., *Collagen stability: Insights from NMR spectroscopic and hybrid density functional computational investigations of the effect of electronegative substituents on prolyl ring conformations*. Journal of the American Chemical Society, 2002. **124**(11): p. 2497-2505.
231. Brodsky, B. and A.V. Persikov, *Molecular structure of the collagen triple helix*. Advances in Protein Chemistry, 2005. **70**: p. 301-339.
232. Kao, W.W.-Y., R.A. Berg, and D.J. Prockop, *Kinetics for the secretion of procollagen by freshly isolated tendon cells*. The Journal of Biological Chemistry, 1977. **252**(23): p. 8391-8397.
233. Kao, W.W.-Y., D.J. Prockop, and R.A. Berg, *Kinetics for the secretion of nonhelical procollagen by freshly isolated tendon cells*. The Journal of Biological Chemistry, 1979. **254**(7): p. 2234-2243.
234. Uitto, J., H.-P. Hoffmann, and D.J. Prockop, *Retention of nonhelical procollagen containing cis-hydroxyproline in rough endoplasmic reticulum*. Science, 1975. **190**(4220): p. 1202-1204.
235. Berg, R.A., M.L. Schwartz, and R.G. Crystal, *Regulation of the production of secretory proteins: Intracellular degradation of newly synthesized "defective" collagen*. Proceedings of the National Academy of Sciences, 1980. **77**(8): p. 4746-4750.
236. Radtke, N.D., A.D. Weinsieder, and R.J. Ballou, *Pharmacological therapy for proliferative vitreoretinopathy*. Graefe's Archive for Clinical and Experimental Ophthalmology, 1986. **224**: p. 230-233.
237. Yasukawa, T., et al., *Sustained release of cis-hydroxyproline in the treatment of experimental proliferative vitreoretinopathy in rabbits*. Graefe's Archive for Clinical and Experimental Ophthalmology, 2002. **240**: p. 672-678.
238. Gean, K.F., et al., *New polymeric carriers of cis-hydroxy-L-proline: Potential agents for the inhibition of excess collagen synthesis*. Polymer Preprints, 1992. **33**(2): p. 51-52.
239. Gean, K.F., et al., *Polymeric carriers of cis-hydroxy-L-proline with improved antifibrotic activity*. Proceedings of the International Symposium on Controlled Release of Bioactive Materials, 1993. **20**: p. 152-153.

240. Poiani, G.J., et al., *Conjugates of cis-4-hydroxy-L-proline and poly(PEG-Lys), a water soluble poly(ether urethane): Synthesis and evaluation of antifibrotic effects in vitro and in vivo*. Bioconjugate Chemistry, 1994. **5**(6): p. 621-630.
241. Poiani, G.J., et al., *Polymeric carrier of proline analogue with antifibrotic effect in pulmonary vascular remodeling*. American Journal of Respiratory and Critical Care Medicine, 1997. **155**: p. 1384-1390.
242. Simon, P.M., et al., *Prodrug of proline analogue reduces hypoxic pulmonary hypertension in rats*. Pulmonary Pharmacology & Therapeutics, 2006. **19**: p. 242-250.
243. Dickens, H., et al., *Anticancer drug cis-4-hydroxy-L-proline: correlation of preclinical toxicology with clinical parameters of liver function*. Molecular Medicine Reports, 2008. **1**: p. 459-464.
244. Pachence, J.M., B.A. Belinka, and C.L. Putnam, *WO/2004/089311: Polymeric drug agents for the treatment of fibrotic disorders*, WIPO, Editor. 2004, VectraMed Inc.
245. Magno, M.H., et al., *Synthesis, degradation and biocompatibility of tyrosine-derived polycarbonate scaffolds*. Journal of Materials Chemistry, 2010.
246. Starcher, B., *A ninhydrin-based assay to quantitate the total protein content of tissue samples*. Analytical Biochemistry, 2001. **292**: p. 125-129.
247. Bae, Y.H., et al., *Minute changes in composition of polymer substrates produce amplified differences in cell adhesion and motility via optimal ligand conditioning*. Acta Biomaterialia, 2006. **2**(5): p. 473-482.
248. Meechaisue, C., et al., *Electrospun mat of tyrosine-derived polycarbonate fibers for potential use as tissue scaffolding material*. Journal of Biomaterials Science-Polymer Edition, 2006. **17**(9): p. 1039-1056.
249. Jarusuwannapoom, T., et al., *Effect of solvents on electro-spinnability of polystyrene solutions and morphological appearance of resulting electrospun polystyrene fibers*. European Polymer Journal, 2005. **41**: p. 409-421.
250. Lin, K., et al., *Reducing electrospun nanofiber diameter and variability using cationic amphiphiles*. Polymer, 2007. **48**: p. 6384-6394.
251. Wang, S.-Q., J.-H. He, and L. Xu, *Non-ionic surfactants for enhancing electrospinnability and for the preparation of electrospun nanofibers*. Polymer International, 2008. **57**: p. 1079-1082.
252. Yao, L., et al., *Electrospinning and stabilization of fully hydrolyzed poly(vinyl alcohol) fibers*. Chemistry of Materials, 2003. **15**(9): p. 1860-1864.
253. Sampson, W.W., *A multiplanar model for the pore radius distribution in isotropic near-planar stochastic fibre networks*. Journal of Materials Science, 2003. **38**: p. 1617-1622.
254. Kidoaki, S., K.I. Kwon, and T. Matsuda, *Mesoscopic spatial designs of nano- and microfiber meshes for tissue-engineering matrix and scaffold based on newly devised multilayering and mixing electrospinning techniques*. Biomaterials, 2005. **26**: p. 37-46.
255. Thakur, R.A., et al., *Electrospun nanofibrous polymeric scaffold with targeted drug release profiles for potential application as wound dressing*. International Journal of Pharmaceutics, 2008. **364**(1): p. 87-93.

256. Hong, Y., et al., *Generating elastic, biodegradable polyurethane/poly(lactide-co-glycolide) fibrous sheets with controlled antibiotic release via two-stream electrospinning*. *Biomacromolecules*, 2008. **9**: p. 1200-1207.
257. Hooper, K.A., J.D. Cox, and J. Kohn, *Comparison of the effect of ethylene oxide and γ -irradiation on selected tyrosine-derived polycarbonates and poly(L-lactic acid)*. *Journal of applied Polymer Science*, 1997. **63**(11): p. 1499-1510.
258. Schoenmakers, R.G., et al., *The effect of the linker on the hydrolysis rate of drug-linked ester bonds*. *Journal of Controlled Release*, 2004. **95**: p. 291-399.
259. Anderson, J.M. and M.S. Shive, *Biodegradation and biocompatibility of PLA and PLGA microspheres*. *Advanced Drug Delivery Reviews*, 1997. **28**: p. 5-24.
260. Yamaguchi, K. and J.M. Anderson, *In vivo biocompatibility studies of medisorb(R) 65/35 D,L-lactide/glycolide copolymer microspheres*. *Journal of Controlled Release*, 1993. **24**: p. 81-93.

Curriculum Vitae

Charles A. Florek

Education

Aug 1999 – Dec 2003	University of Illinois – Urbana-Champaign Mechanical Engineering, Bachelor of Science
Jan 2004 – Oct 2010	Rutgers, the State University of New Jersey Biomedical Engineering, Doctor of Philosophy

Employment

Nov 2003 – Jan 2004	Boston Scientific Inc. Technician - Taxus Operations Analytical Laboratory
May 2006 – Aug 2006	Ethicon Inc. Graduate Intern - Corporate Product Characterization

Publications

Thakur, R.A., Florek, C.A., Kohn, J., Michniak, B.B., *Electrospun nanofibrous polymeric scaffold with targeted drug release profiles for potential application as a wound dressing*. International Journal of Pharmaceutics 264:(1) 87-93 (2008)

Thakur, R.A., Florek, C.A., Kohn, J., Michniak, B.B., *Electrospun matrices for the delivery of hydrophilic and lipophilic compounds*. International Patent WO 2008/055038, published: May 08, 2008, priority date: Oct 30, 2006

Bae, Y.H., Johnson, P.A., Florek, C.A., Kohn, J., Moghe, P.V., *Minute changes in composition of polymer substrates produce amplified differences in cell adhesion and motility via optimal ligand conditioning*. Acta Biomaterialia 2:(5) 473-482 (2006)

Florek, C.A., Tucker III, C.L., *Stretching distributions in chaotic mixing of droplet dispersions with unequal viscosities*. Physics of Fluids 17:(5) 053101 (2005)

Tucker III, C.L., Florek, C.A., Pham, T, *An ellipsoidal droplet model for dilute emulsions: application to complex mixing flows*. in Computational Methods in Multiphase Flow II, Ed. Mammoli, A.A., Brebbia, C.A., WIT Press, Southampton U.K. (2003)